

Generation and use of new tools for the characterisation of gut hormone receptors

Emma Kate Biggs

August 2018

Selwyn College, University of Cambridge

This dissertation is submitted for the degree of Doctor of
Philosophy

Abstract

Enteroendocrine hormones released from the intestine following food intake have several roles in the control of metabolism, some of which are exploited therapeutically for the treatment of type 2 diabetes. Within this thesis, focus has been on the receptors of the gut hormones glucagon-like peptide-1 (GLP-1), glucose-dependent insulinotropic polypeptide (GIP) and glucagon-like peptide-2 (GLP-2).

In recent years there has been a surge of interest in the enteroendocrine hormones particularly due to the success of GLP-1 mimetics in the treatment of type 2 diabetes. GLP-1 is an incretin hormone, which enhances glucose induced insulin secretion by binding GLP-1 receptors (GLP1R) on pancreatic β -cells. Despite the therapeutic success, several extra-pancreatic clinical effects of GLP-1 remain unexplained. Here, a GLP1R monoclonal antagonistic antibody that can block GLP1R signalling *in vivo* has been developed and characterised, providing a new tool for the study of GLP1R physiology.

GIP is the second incretin hormone, initially referred to as the ‘ugly duckling’ incretin hormone due to its ineffectiveness in inducing insulin secretion in type 2 diabetic patients. Aside from the incretin actions, GIP is thought to be involved in the regulation of high-fat diet (HFD) induced obesity. A new transgenic mouse model expressing a fluorescent reporter under the control of the *Gipr* promoter has been used here to identify GIPR expressing cells. This model showed GIPR expression in the pancreas, adipose tissue, duodenum and nodose ganglia. Surprisingly GIPR expressing cells were found centrally, in areas of the hypothalamus involved in the regulation of food intake and energy expenditure. We consequently sought to investigate the function of GIPR expressing hypothalamic cells.

GLP-2, unlike GLP-1 and GIP, is not an incretin hormone. Rather, GLP-2 has been implicated in the regulation of epithelial cell proliferation and apoptosis within the intestine. Therapeutically, an analogue of GLP-2 is used for the treatment of short bowel syndrome. A common missense mutation in the GLP-2 receptor (GLP2R), D470N, has been found to be associated with type 2 diabetes, and here we sought to understand the mechanism underlying this association. The D470N mutant has decreased β -arrestin recruitment, though the significance of this finding will need further research.

Overall; the new monoclonal antagonistic GLP1R antibody will help to further understand GLP1R physiology, the new transgenic GIPR mouse model has contributed to the understanding of GIPR localisation, and cell based assays have identified functional implications of a polymorphism in the GLP2R associated with an increased risk of diabetes. It is hoped that further understanding of the physiology of these gut hormone receptors will be critical in the development of new therapeutics for diabetes and obesity.

Declaration

This dissertation is the result of my own work and includes nothing which is the outcome of work done in collaboration except as declared in the Preface and specified in the text. It is not substantially the same as any that I have submitted, or, is being concurrently submitted for a degree or diploma or other qualification at the University of Cambridge or any other University or similar institution except as declared in the Preface and specified in the text. I further state that no substantial part of my dissertation has already been submitted, or, is being concurrently submitted for any such degree, diploma or other qualification at the University of Cambridge or any other University or similar institution. It does not exceed 60,000 words.

Emma K Biggs

Publications

Development and characterisation of a novel glucagon like peptide-1 receptor antibody

Biggs EK, Liang L, Naylor J, Madalli S, Collier R, Coghlan MP, Baker DJ, Hornigold DC, Ravn P, Reimann F, Gribble FM. *Diabetologia* 2018, 61 (3): 711-721.

Scaling it down: new in vitro tools to get the balance right.

Biggs EK, Gribble FM, Reimann F. *Biochemical Journal* 2017, 474 (1): 47-50.

Table of Contents

Abstract.....	i
Declaration.....	ii
Publications.....	iii
Table of Contents.....	iv
Acknowledgements.....	ix
Abbreviations.....	x
Chapter 1. Introduction	1
1.1 Metabolic Physiology	1
1.1.1 Physiology of the Gastrointestinal Tract.....	1
1.1.2 Physiology of the gut-brain axis.....	1
1.1.3 Pancreatic Physiology	2
1.1.4 Physiology of Adipose Tissue	3
1.2 The Enteroendocrine System.....	4
1.3 Physiology of Glucagon-like peptide 1 (GLP-1).....	6
1.3.1 Production of GLP-1.....	6
1.3.2 Regulation of GLP-1 secretion	7
1.3.3 GLP-1 Receptor (GLP1R) Structure and Signalling	8
1.3.4 GLP1R Localisation.....	9
1.3.5 Actions of GLP-1.....	9
1.3.5.1 <i>Actions of GLP-1 in the pancreas</i>	10
1.3.5.2 <i>Extra-pancreatic actions of GLP-1</i>	11
1.3.5.3 <i>Centrally mediated actions of GLP-1</i>	12
1.4 Physiology of Glucose-dependent insulinotropic peptide (GIP).....	13
1.4.1 Production of GIP	13
1.4.2 Regulation of GIP secretion	14
1.4.3 GIP receptor (GIPR) Structure and Signalling.....	14
1.4.4 GIPR Localisation.....	15
1.4.5 Actions of GIP	15
1.4.5.1 <i>Pancreatic actions of GIP</i>	16
1.4.5.2 <i>Actions of GIP in adipose tissue</i>	17
1.5 Physiology of Glucagon-like peptide 2 (GLP-2).....	18
1.5.1 Production of GLP-2 and regulation of secretion	18
1.5.2 GLP-2 Receptor (GLP2R) Structure and Signalling	18
1.5.3 GLP2R Localisation.....	18

1.5.4 Actions of GLP-2.....	19
1.5.4.1 Gastrointestinal actions of GLP-2	20
1.5.4.2 Actions of GLP-2 outside of the gastrointestinal tract.....	21
1.6 Clinical Abnormalities in Metabolic Physiology	21
1.6.1 Therapeutic Targeting of the Gut Hormones GLP-1, GIP and GLP-2	22
1.7 Aims of Thesis	23
Chapter 2. Generation of a GLP1R antagonistic antibody	24
2.1 Introduction	24
2.1.1 Therapeutic Targeting of GLP1R	24
2.1.2 Use of antagonists to study the GLP1R.....	24
2.1.3 Specificity of GLP1R antibodies.....	25
2.2 Aims	26
2.3 Methods.....	27
2.3.1 Solutions and Compounds	27
2.3.2 Bacterial Strains	27
2.3.3 Cell Culture.....	27
2.3.4 Phage Display Selections.....	27
2.3.4.1 Soluble selections	27
2.3.4.2 Cell surface selections	28
2.3.4.3 Selection Rescue.....	28
2.3.4.4 Phage ELISA.....	28
2.3.4.5 Antibody expression and purification	29
2.3.5 Phage Display Library Generation.....	30
2.3.5.1 Stop template generation and production of uracil containing single stranded DNA (dU-ssDNA)	30
2.3.5.2 Kunkel mutagenesis	30
2.3.5.3 Preparation of electrocompetent TG1 cells and electroporation	31
2.3.5.4 Library Rescue	31
2.3.6 Cell Based Assays	32
2.3.6.1 cAMP Homogenous Time Resolved Fluorescence (HTRF) Accumulation Assay	32
2.4 Results.....	33
2.4.1 Naïve Phage Display Selection of GLP1R antibodies.....	33
2.4.2 Identification of ScFv's of interest	36
2.4.3 Screening of clones of interest in cAMP assays.....	38
2.4.4 Affinity maturation of Glp1R0017	40

2.4.5 Screening of Glp1R0017 affinity maturation products	44
2.5 Discussion.....	48
2.5.1 Phage Display for Antibody Production	48
2.5.2 Affinity maturation approaches using phage display	49
2.5.3 Affinity maturation approaches using alternative display platforms	51
2.5.4 Affinity maturation approaches using computational methods	51
2.5.5 Summary	52
Chapter 3. Characterisation of Glp1R0017, a GLP1R antagonistic antibody	53
3.1 Introduction	53
3.1.1 GLP1R Signalling Pathways	53
3.1.2 GLP1R Physiology.....	54
3.2 Aims	55
3.3 Methods.....	56
3.3.1 Solutions and Compounds	56
3.3.2 Cell Culture.....	56
3.3.3 Cell Based Assays	56
3.3.3.1 <i>cAMP Homogenous Time Resolved Fluorescence (HTRF) Accumulation Assay</i>	56
3.3.3.2 <i>cAMP FRET Imaging</i>	57
3.3.3.3 <i>Calcium Measurements</i>	57
3.3.3.4 <i>Insulin Secretion Assay</i>	58
3.3.3.5 <i>Receptor Ligand Binding Assay</i>	58
3.3.3.6 <i>Nano-Glo® Live Cell Assay for Beta-Arrestin Measurements</i>	58
3.3.4 Animal Studies	59
3.3.4.1 <i>Transgenic mice</i>	59
3.3.4.2 <i>Immunostaining</i>	59
3.3.4.3 <i>Single-dose pharmacokinetics study</i>	60
3.3.4.4 <i>Glucose Tolerance Tests (GTTs)</i>	60
3.4 Results.....	62
3.4.1 Glp1R0017 exhibits cross-species antagonistic activity for GLP1R.....	62
3.4.2 Glp1R0017 is a specific, competitive antagonist for GLP1R	65
3.4.3 Glp1R0017 also inhibits alternative signalling pathways downstream of the GLP1R.....	66
3.4.4 Glp1R0017 inhibits GLP1R at natural levels in the INS-1 832/3 cells	69
3.4.5 Glp1R0017 can be used to immunostain GLP1R from mouse tissue	71
3.4.6 Glp1R0017 inhibits the GLP-1 incretin effect <i>in vivo</i>	73

3.5 Discussion.....	76
3.5.1 Characterisation of Glp1R0017 using cell based assays	76
3.5.2 Use of Glp1R0017 for immunostaining.....	78
3.5.3 Characterisation of <i>in vivo</i> GLP1R inhibition using Glp1R0017	79
3.5.4 Possible future uses of Glp1R0017	80
3.5.5 Summary	82
Chapter 4. Localisation and characterisation of glucose-dependent insulinotropic polypeptide receptor (GIPR) expressing cells	83
4.1 Introduction	83
4.1.1 Therapeutic Relevance of GIPR.....	83
4.1.2 Location of GIPR.....	83
4.1.3 The role of GIPR in obesity.....	84
4.2 Aims	86
4.3 Methods.....	87
4.3.1 Animal Studies	87
4.3.2 Transgenic mice	87
4.3.3 Immunostaining	87
4.3.4 Intracerebroventricular Surgery	88
4.3.5 Mouse feeding studies.....	88
4.4 Results.....	89
4.4.1 Localisation of the GIPR in peripheral tissues.....	89
4.4.2 Localisation of GIPR within the brain.....	92
4.4.3 Ablation of hypothalamic GIPR positive cells	97
4.4.4 Activation of hypothalamic GIPR positive cells.....	102
4.5 Discussion.....	106
4.5.1 Use of Gipr-Cre mice for GIPR localisation	106
4.5.2 Central expression of GIPR	108
4.5.3 Hypothalamic GIPR ablation	110
4.5.4 Hypothalamic GIPR activation	111
4.5.5 Summary	113
Chapter 5. Characterisation of a GLP2R variant, D470N, associated with Type 2 Diabetes risk	114
5.1 Introduction	114
5.1.1 A missense variant in GLP2R is associated with citrulline levels and type 2 diabetes risk.....	114
5.1.2 Function of intestinal GLP2R.....	114
5.1.3 GLP2R signalling pathways.....	115

5.2 Aims	116
5.3 Methods.....	117
5.3.1 Molecular Biology	117
5.3.2 HitHunter® cAMP Assay.....	117
5.3.3 Nano-Glo® Live Cell Assay for Beta-Arrestin Measurements	118
5.3.4 ERK1/2 Phosphorylation Analysis by Western Blotting.....	118
5.4 Results.....	119
5.4.1 Generation of D470N GLP2R mutant expressing constructs.....	119
5.4.2 Comparison of WT and D470N GLP2R signalling via cAMP	120
5.4.3 Comparison of β-arrestin recruitment to the WT and D470N GLP2R	121
5.4.4 Comparison of WT and D470N GLP2R signalling via P-ERK	123
5.5 Discussion.....	125
5.5.1 Mutant GLP2R displays decreased β-arrestin recruitment	125
5.5.2 Consequences of decreased β-arrestin recruitment to the mutant GLP2R	125
5.5.3 Future investigations of the D470N mutant GLP2R.....	126
5.5.4 Summary	127
Chapter 6. General Discussion	128
6.1 Summary	128
6.2 Glp1R0017 enables controlled blockade of the GLP1R over several days	128
6.2.1 Future directions for Glp1R0017	129
6.3 GIPR transgenic mice reveal previously unknown central GIPR localisation.....	130
6.3.1 Future directions for understanding GIPR biology using GIPR transgenic mice	132
6.4 The common missense GLP2R mutation, D470N, has decreased β-arrestin binding	133
6.4.1 Future directions of GLP2R research	133
6.5 Overall therapeutic implications of gut hormone research	134
6.6 Conclusion.....	135
7. References	136
8. Appendix	167
Appendix 1 – Plasmid Map for pCantab6	167
Appendix 2– Primer Details	168
Appendix 3 – Cell Seeding Densities for cAMP HTRF Assay.....	169
Appendix 4 – Antibody Details.....	169
Appendix 5 – AAV-flex-taCasp3-TEVp plasmid map	170
Appendix 6 – AAV-hSyn-DIO-hM3D(Gq)-mCherry plasmid map	170

Acknowledgements

This PhD was funded by MedImmune and the Cambridge Biomedical Research Centre.

I would like to thank my supervisors Frank Reimann and Fiona Gribble at the University of Cambridge, along with my industrial supervisors Peter Ravn and David Hornigold at MedImmune for their support, guidance and feedback throughout my PhD.

I have been fortunate enough to learn from many colleagues across both the department of Antibody Development & Protein Engineering and department of Cardiovascular & Metabolic Diseases at MedImmune, I would like to thank each individual who has shown me new techniques. I would also like to thank colleagues within the university who have generously shared time to guide me in experimental design, help with imaging, and provide core services. Particular thanks go to my colleagues in the Gribble and Reimann group, both past and present, who have helped day to day and made my PhD an enjoyable experience.

My upmost thanks go to my husband, parents, sister and friends for believing in me and providing encouragement when I needed it most.

Abbreviations

12N	Hypoglossal nucleus
5-HT	Serotonin
AAV	Adeno-associated virus
AgRP	Agouti-related peptide
AP	Area postrema
aP2	Adipocyte protein 2
ARC	Arcuate nucleus
ARRIVE	Animal Research: Reporting of In Vivo Experiments
ASBT	Apical sodium-dependent bile acid transporter
ATP	Adenosine triphosphate
AUC	Area under curve
AVPe	Anteroventral periventricular nucleus
Bcl-2	B-cell lymphoma-2
BMV	Bone marrow vault
BOAT	Sodium-coupled neutral amino acid transporter
BSA	Bovine serum albumin
BST	Nucleus of stria terminalis
CA1	Field CA1 of the hippocampus
cAMP	Cyclic adenosine monophosphate
CART	Cocaine- and amphetamine-regulated transcript
CASR	Calcium-sensing receptor
CCK	Cholecystokinin
CDR	Complementarity determining region
CFP	Cyan fluorescent protein
cfu	Colony forming units
CHO	Chinese hamster ovary
C _{max}	Maximal concentration
CNO	Clozapine N-oxide
CNS	Central Nervous System
CREB	cAMP response element binding protein
CS	Combined spleen
DAB	3,3'-diaminobenzidine
DAG	Diacylglycerol

DEXA	Dual-energy X-ray absorptiometry
DG	Dentate gyrus
Dgat1	Acyl CoA:diacylglycerol transferase
DMD	Dorsomedial hypothalamic nucleus
dNTP	Deoxynucleotide triphosphate
DPP-4	Dipeptidyl peptidase-4
DREADD	Designer receptors exclusively activated by designer drugs
DTT	Dithiothreitol
dU-ssDNA	Uracil containing single stranded DNA
EC	Enterochromaffin
ECD	Extracellular domain
ECL1	Extracellular loop 1
Epac	Exchange protein directly activated by cAMP
EPI	External plexiform layer
ERK	Extracellular signal-regulated kinase
EYFP	Enhanced yellow fluorescent protein
FA	Fatty acid
FABP4	Fatty-acid binding protein 4
FFAR	Free fatty acid receptors
FrA	Frontal association cortex
FRET	Fluorescence resonance energy transfer
GCG	Glucagon
GCGR	Glucagon receptor
GIP	Glucose-dependent insulinotropic polypeptide
GIPR	Glucose-dependent insulinotropic polypeptide receptor
GLP-1	Glucagon like peptide-1
GLP1R	Glucagon like peptide-1 receptor
GLP-2	Glucagon like peptide-2
GLP2R	Glucagon like peptide-2 receptor
GLUT4	Glucose transporter 4
GPBAR1	G-protein-coupled bile acid receptor 1
GPCR	G protein coupled receptor
GPR119	G-protein coupled receptor 119
GPRC6A	G protein-coupled receptor family C group 6 member A

GRPP	Glicentin related pancreatic polypeptide
GSIS	Glucose stimulated insulin secretion
GTT	Glucose tolerance test
GWAS	Genome wide association study
HEK	Human embryonic kidney
HFD	High fat diet
hGLP1R	Human GLP1R
HRP	Horseradish peroxidase
HTRF	Homogenous time-resolved fluorescence
IBMX	3-isobutyl-1-methylxanthine
ICV	Intracerebroventricular
IgG	Immunoglobulin G
InsL5	Insulin-like peptide 5
IP ₃	Inositol-1,4,5-triphosphate
IPGTT	Intraperitoneal glucose tolerance test
IRES	Internal ribosome entry site
K _{ATP}	ATP sensitive potassium channel
KRB	Krebs-Ringer Buffer
K _v	Voltage-gated K ⁺ channels
LB	Luria-Bertani
LH3	Long V _H CDR3
LO	Lateral orbital cortex
LPL	Lipoprotein lipase
LSD	Dorsal part of the lateral septal nucleus
MAPK	Mitogen-activated protein kinase
mGLP1R	Mouse GLP1R
mRNA	Messenger ribonucleic acid
Mi	Mitral cell layer
MnPO	Median preoptic nucleus
MOI	Multiplicity of infection
MPA	Medial preoptic area
MPBS	PBS containing milk
MS	Medial septal nucleus
MSX	L-methionine sulfoximine

NHE3	Sodium-hydrogen exchanger 3
NMR	Nuclear magnetic resonance
OGTT	Oral glucose tolerance test
PaAP	Anterior parvicellular part of the paraventricular hypothalamic nucleus
PBS	Phosphate buffered saline
PC	Prohormone convertase
Pdx1	Pancreatic duodenal homeobox 1
Pe	Periventricular hypothalamic nucleus
PEI	Polyethylenimine
PEPT1	Proton-coupled peptide transporter
PFA	Paraformaldehyde
PI3K	Phosphoinositide 3-kinase
PIP ₂	Phosphatidylinositol-4,5-bisphosphate
PKA	Protein kinase A
PKC	Protein kinase C
PLC	Phospholipase C
POMC	Proopiomelanocortin
PV	Paraventricular thalamic nucleus
PPY	Peptide-YY
Rfx6	Regulatory factor X6
rtTA	Reverse tetracycline transactivator
SBS	Short bowel syndrome
ScFv	Single chain variable fragment
SChDM	Dorsomedial part of the suprachiasmatic nucleus
SD	Standard deviation
SEM	Standard error of the mean
SFO	Subfornical organ
SGLT1	Sodium-dependent glucose transporter 1
SNP	Single nucleotide polymorphism
SolM	Nucleus of the solitary tract
Sst	Somatostatin
T2D	Type 2 diabetes
TAG	Triacylglycerol
TAS1R2/3	Taste receptor type 1 member 2/3

TBS	Tris-buffered saline
TBS-T	TBS + 0.1% (v/v) Tween-20
TCF-4	Transcription factor-4
Tcf7	Transcription factor-7
TD-NMR	Time domain nuclear magnetic resonance
tdRFP	Tandem red fluorescent protein
TEVp	Tobacco Etch Virus protease
TG	Triglyceride
TM2	Transmembrane domain 2
TMB	Tetramethylbenzidine
TORC2	cAMP-responsive CREB coactivator 2
Tre	Tetracycline responsive element
TRL	TG rich proteins
TRPA1	Transient receptor potential cation channel subfamily A member 1
TYAG	TY media, 100 µg/ml ampicillin, 2% (w/v) glucose
TYAGC	TY media, 100 µg/ml ampicillin, 2% (w/v) glucose, 10 µg/ml chloramphenicol
TYAK	TY media, 100 µg/ml ampicillin, 50 µg/ml kanamycin
TYAKU	TY media, 100 µg/ml ampicillin, 50 µg/ml kanamycin, 0.25 µg/ml uridine
TYG	TY media, 2% (w/v) glucose
VDCC	Voltage-dependent calcium channel
VIP	Vasoactive intestinal polypeptide
YFP	Yellow Fluorescent Protein
α-SMA	Alpha-smooth muscle actin

Chapter 1. Introduction

1.1 Metabolic Physiology

Metabolism is defined as the chemical reactions which occur within cells of all living organisms essential for maintaining normal function. In this section, the metabolic physiology of key organs involved in nutrient digestion and energy storage have been described separately, however it is important to point out that metabolic physiology is an integrated whole-body process.

1.1.1 Physiology of the Gastrointestinal Tract

When considering nutrient metabolism following food intake, the gastrointestinal tract is the first organ which nutrients reach. The acidic environment of the stomach, together with the presence of digestive enzymes such as gastric lipases and pepsin lead to initial digestion of food into the composite nutrients, which is aided by trituration driven by circular contractions of the gastric antrum. The rate at which these nutrients are absorbed is then determined by a range of factors which govern the nutrient delivery rate to the proximal small intestine via gastric emptying [1]. The process of gastric emptying is highly regulated, with the caloric delivery rate to the duodenum remaining almost constant at ~200 kcal/hour [2]. However, it appears that this rate is not affected by the macronutrient composition of food [2-4]. The vagus nerve is important for controlling the rate of gastric emptying; with bilateral truncal vagotomy (surgical resection of the vagus nerve) causing delayed gastric emptying [5], and vagus nerve stimulation promoting gastric emptying [6]. Blood glucose concentrations also have a small effect on the regulation of gastric emptying, with hyperglycaemia delaying gastric emptying, and hypoglycaemia accelerating gastric emptying [1].

Following gastric emptying, once nutrients reach the small intestine they can begin to be absorbed as they traverse the intestine. Additionally, these nutrients stimulate gut hormone secretion which is a function of particular interest. These gut hormones have a range of downstream actions, including the regulation of glucose homeostasis and gastric emptying. Research within this thesis has focused upon a handful of these gut hormones, and as such the enteroendocrine system will be detailed in more depth in Section 1.2.

1.1.2 Physiology of the gut-brain axis

The gastrointestinal tract alone is not solely responsible for regulating appetite, rather signals sent from the gastrointestinal tract to the brain via the vagus nerve are important for appetite regulation. There are two main regions within the brain that are involved in the control of food intake and energy expenditure; the brainstem and the hypothalamus [7].

The vagus nerve predominantly terminates in the thoracic and abdominal cavities, with the gastrointestinal tract being of particular interest when considering metabolic physiology. Within the gastrointestinal tract, the vagus nerve terminals are found in three distinct locations; the external muscle layers, the myenteric plexus, and the mucosal lamina propria. The neuronal cell bodies are located within the nodose ganglia, and the central neuronal projections innervate the nucleus of the solitary tract (NTS) [8].

The NTS within the caudal brainstem, is essential for co-ordinating peripheral and central appetite regulation signals. Projections from the hypothalamus extend to this region and vice versa, meaning neuronal signals can be transmitted from the NTS to the hypothalamus, the second main brain region involved in appetite regulation [9]. The area postrema (AP) is located within the caudal brainstem, which is a circumventricular organ, meaning peripheral factors can also cross the blood-brain barrier here, and signal within the NTS [10]. The main function of the brainstem in appetite regulation appears to be negative-feedback control of ingestion [11].

Within the hypothalamus, the arcuate nucleus (Arc) is particularly important for regulating appetite [12]. This nucleus of cells is located directly next to the median eminence, which is a circumventricular organ with a highly fenestrated capillary network, providing an incomplete blood-brain barrier [13, 14]. Consequently, this means that peripheral factors, such as circulating gut hormones, have access to this area of the central nervous system. Within the Arc there are two main populations of neurons which are involved in appetite regulation; the agouti-related peptide (AgRP) neurons and the pro-opiomelanocortin (POMC) neurons. Activation of the AgRP neurons leads to an orexigenic response (the stimulation of appetite), whereas activation of the POMC neurons gives an anorexigenic response (inhibition of food intake/loss of appetite) [15]. These neuronal populations do not act independently, rather the neurons project and signal to other hypothalamic nuclei including the paraventricular nucleus, dorsomedial nucleus, lateral hypothalamus and ventromedial nucleus [16, 17].

1.1.3 Pancreatic Physiology

Aside from the gastrointestinal tract, pancreas function is also important to consider in metabolic physiology, with roles in digestion and glucose homeostasis. The pancreas can be divided into two physiological components; the exocrine and the endocrine pancreas. The acinar tissue, which makes up the majority of the pancreas, is exocrine in nature and responsible for secreting digestive enzymes such as amylase and pancreatic lipase into pancreatic ducts [18].

The endocrine cells are located in clusters, named the islets of Langerhans. These cells respond to a range of signals and regulate the release of pancreatic hormones [19, 20]. There are at least five different endocrine cell types within the pancreas: α -cells which secrete glucagon [21], β -cells which

secrete insulin [22], δ -cells which secrete somatostatin [23], γ -cells which secrete pancreatic polypeptide [24], and ϵ -cells which are a small population of cells which secrete ghrelin [25]. Together, these hormones are responsible for the regulation of glucose homeostasis. Glucagon increases blood glucose, insulin decreases blood glucose, somatostatin inhibits the secretion of both glucagon and insulin, with pancreatic polypeptide also regulating hormone secretion [20].

The β -cells make up the highest proportion of endocrine cells within the islets of Langerhans. β -cells secrete insulin in response to glucose via a canonical glucose sensing mechanism. GLUT transporters on the surface of pancreatic β -cells are responsible for glucose uptake into the cell. Upon entering the cell glucose is phosphorylated by glucokinase, a hexokinase which controls the flux of glucose in glycolysis [26]. The metabolism of glucose leads to increased ATP, together with decreased ADP, giving an overall increased ATP:MgADP ratio. This increased ATP:MgADP ratio closes the K_{ATP} channels on the β -cell membrane, leading to membrane depolarisation. Consequently, voltage-gated calcium channels are opened, and the resultant increased calcium influx stimulates exocytosis of insulin-containing vesicles [27, 28]. Following secretion, insulin increases glucose absorbance from the bloodstream into insulin-sensitive tissues, such as muscle and fat, via increasing translocation of the glucose transporter GLUT4 onto the plasma membrane of these cells [29].

1.1.4 Physiology of Adipose Tissue

For a more complete understanding of metabolic physiology, one must also consider the storage of nutrients following digestion. Adipose tissue is a depot for storage of lipids, which is split into 3 subsets: white, brown and beige adipose tissue.

White adipose tissue is the main tissue in which lipids are stored as triacylglycerols (TAG), in unilocular adipocytes [30]. Two processes are involved in controlling the amount of TAG stored in the white adipocytes; lipogenesis which is the synthesis and storage of TAG, and lipolysis which is the hydrolysis of TAG using enzymes such as lipoprotein lipase (LPL) [31, 32]. When food is scarce, or there is a high energy demand, lipolysis is increased to provide fatty acids and glycerol as alternative energy substrates. On the other hand, when food intake outweighs energy demand, lipogenesis leads to increased storage of lipids in adipocytes, increasing adiposity [30].

In contrast to white adipose tissue, brown adipose tissue contains brown adipocytes which are multilocular, and dissipate the energy in lipids as heat in non-shivering thermogenesis [33, 34]. The process underlying this non-shivering thermogenesis is uncoupled respiration, which is mediated by uncoupling protein 1 (UCP1) expressed specifically within brown adipose tissue. This results in increased fatty acid oxidation and heat production [33, 35, 36].

The white adipose depots and brown adipose depots are normally located in distinct regions. However, ‘beige adipose tissue’ is the presence of brown adipocytes within white adipose tissue depots [36]. One stimulus of this ‘beiging’ process is prolonged cold exposure [37-39]. The ‘beige’ adipocytes have variable characteristics dependent upon the stimulus and are able to adopt either white or brown adipocyte functions [36].

1.2 The Enteroendocrine System

The enteroendocrine system responsible for secretion of gut hormones is essential for maintaining metabolic physiology. The gut has been described as ‘the largest endocrine organ in the body’ [40], hence research into this enteroendocrine system is vital for understanding the control of metabolism. 1902 marked the discovery of the first gut hormone, secretin, a chemical substance released from the duodenum in acidic conditions causing pancreatic exocrine secretions [41]. Closely following this, it was hypothesised that chemical substances or ‘hormones’ in the gut can regulate endocrine secretions from the pancreas, and could be used to treat patients with diabetes [42]. These hormones were later described as incretins, however their function wasn’t defined until 1964 when two groups showed oral glucose elevates insulin secretion substantially more than an equivalent dose of intravenous glucose [43, 44]. This effect has been coined the ‘incretin effect’ and can be explained by the secretion of incretin hormones following nutrient ingestion, which enhance glucose stimulated insulin secretion from pancreatic beta cells.

Two incretin hormones have been described; glucagon-like peptide 1 (GLP-1) and glucose-dependent insulinotropic peptide (GIP) [45, 46]. Since their discovery, interest in this field has increased due to the therapeutic relevance of targeting incretin hormones for treatment of type 2 diabetes. Analogues/mimetics of GLP-1 are now used for the treatment of type 2 diabetes, and new drugs are being designed which target both incretin hormones simultaneously [47, 48].

Aside from incretin hormones, there are a plethora of different enteroendocrine hormones produced and secreted from specialised enteroendocrine cells in the gut [49] (Figure 1.1). These enteroendocrine hormones have a wide range of roles involved in regulation of metabolism. For example; somatostatin (Sst) is secreted from D-cells in the stomach and intestine, where it functions to inhibit gastric acid secretion, gastric emptying and intestinal motility [50, 51]. Enteroendocrine L-cells secrete both glucagon-like peptides (GLP-1 and GLP-2), peptide-YY (PYY), and insulin-like peptide 5 (InsL5), each of which has differing roles in the regulation of metabolism [52]. GLP-1 and GLP-2 will be described in detail in further sections, PYY is thought to inhibit food intake and insulin secretion [53, 54]. InsL5 is a relatively newly defined gut hormone, in contrast to GLP-1 and PYY, production of InsL5 is increased by calorie restriction and the peptide has orexigenic effects [55]. I-cells primarily

secrete cholecystokinin (CCK) which reduces appetite and slows gastric emptying [56-58]. K-cells secrete the incretin hormone GIP, to be described in detail in a later section. Enterochromaffin (EC) cells secrete serotonin (5-HT), a multifunctional bioamine which is involved in peristalsis, nausea and possibly the regulation of metabolism [59-62]. These metabolic effects include, regulation of glucose homeostasis, hepatic gluconeogenesis, mobilisation of hepatic free fatty acids, and browning of white adipose tissue [63]. Other gut hormones include motilin which is secreted from D₁ cells and regulates interdigestive migrating contractions which are the fasted motor pattern in the gastrointestinal tract [64], and secretin which is secreted from S cells and stimulates secretions from the exocrine pancreas [65]. Initially this classification of hormones and cell-types was thought to be strictly defined, however recent research has indicated there is more hormonal overlap than that originally described [66, 67].

Within this thesis, research has been performed on the GLP-1 receptor (GLP1R), GIP receptor (GIPR), and GLP-2 receptor (GLP2R), consequently the comprehensive literature review will focus on GLP-1, GIP and GLP-2.

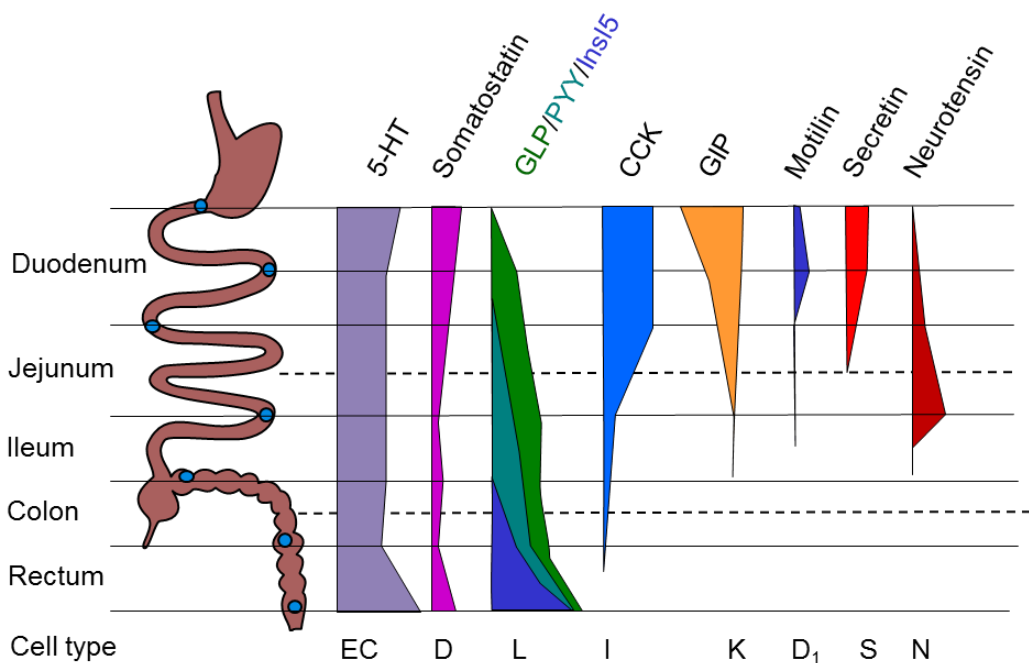


Figure 1.1 Schematic representation of enteroendocrine hormone distribution and cell-type.
Enteroendocrine hormones are secreted from specialised cell-types, with varying densities along the intestine as indicated. Figure was adapted by F. Reimann, based on an immunohistochemical study by Sjolund *et al.* (1983)[68] and updated to include Insl5 using data from Grosse *et al.* (2014)[55].

1.3 Physiology of Glucagon-like peptide 1 (GLP-1)

1.3.1 Production of GLP-1

GLP-1 is derived from the proglucagon gene, expressed in small intestinal and colonic enteroendocrine L-cells, pancreatic α -cells and specific subsets of neurons within the brainstem [69]. Transcription of proglucagon is activated by the transcription factor Pax6 in rodent intestinal endocrine cells [70]. In human intestinal cells, this transcription is regulated by factors including β -catenin and transcription factor-4 (TCF-4) [71].

Following transcription and translation of the proglucagon gene, the proglucagon product is cleaved by prohormone convertases (PC) to yield a number of peptides. In pancreatic α -cells PC2 is expressed, leading to the cleavage of proglucagon into glucagon, glicentin related pancreatic polypeptide (GRPP), and the larger major proglucagon fragment [72]. In contrast, the intestinal L-cells and proglucagon expressing cells in the central nervous system (CNS) express PC1/3, leading to differential processing of proglucagon. PC1/3 cleavage of proglucagon leads to the production of GLP-1, GLP-2, glicentin and oxyntomodulin (Figure 1.2) [73].

Biologically active GLP-1 exists in two isoforms, GLP-1_{7-36 amide} and GLP-1₇₋₃₇, with the main circulating form in humans being GLP-1_{7-36 amide} [74, 75]. The circulating levels of biologically active GLP-1 are only within the picomolar range, due to rapid degradation by dipeptidyl peptidase 4 (DPP-4) giving GLP-1 an extremely short half-life of 1-2 minutes, together with rapid clearance of both DPP-4 cleaved and full-length GLP-1 [76-78].

DPP-4 cleaves the agonistic GLP-1_{7-36 amide} to GLP-1_{9-36 amide} which is often thought to be inactive. However, GLP-1_{9-36 amide} binding to the GLP1R has been observed, with a much lower binding affinity than GLP-1_{7-36 amide} [79]. In addition to this, some studies suggest that GLP-1_{9-36 amide} has antagonistic, inhibitory properties, inhibiting hepatic glucose production in obese mice [80].

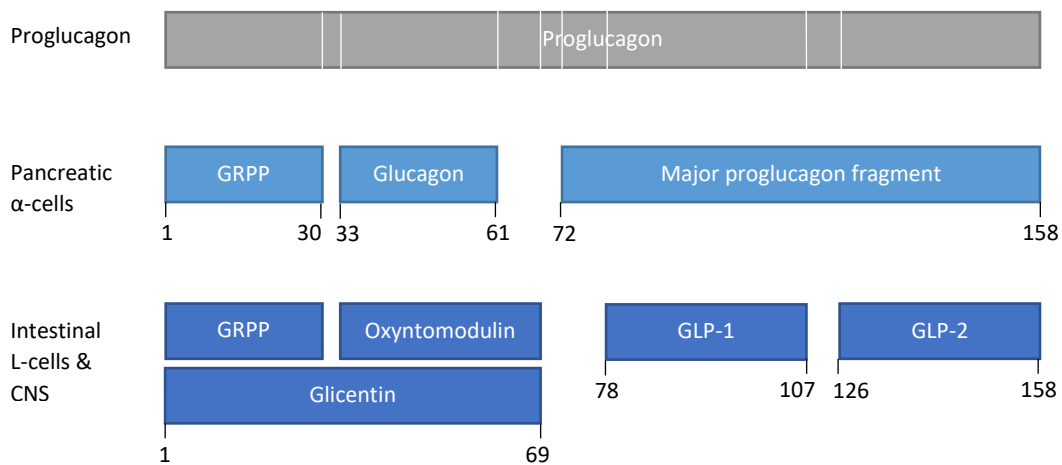


Figure 1.2 Differential processing of proglucagon. Prohormone convertase (PC) isoforms PC1/3 and PC2 differentially cleave proglucagon in the intestinal L-cells/CNS and pancreatic α -cells respectively. Figure based upon Holst (2007) review [73].

1.3.2 Regulation of GLP-1 secretion

GLP-1 is secreted from enteroendocrine L-cells distributed along the epithelial layer of the intestine, increasing in density towards the ileum and colon [73]. These enteroendocrine cells are often ‘open-type’, with microvilli covered apical surfaces, and the base residing on the basal lamina. Following consumption of a meal, the enteroendocrine L-cells ‘sense’ nutrients which stimulate secretion of GLP-1. A wide-range of nutrients and metabolites lead to the secretion of GLP-1, including derivatives from carbohydrates, protein and fat in the forms of glucose, amino acids, bile acids, fatty acids and monoacylglycerols [81]. Briefly, the underlying molecular mechanism for secretion relies either upon stimulation of membrane depolarisation, increased concentrations of cyclic adenosine monophosphate (cAMP), or increased concentrations of intracellular Ca^{2+} (Figure 1.3).

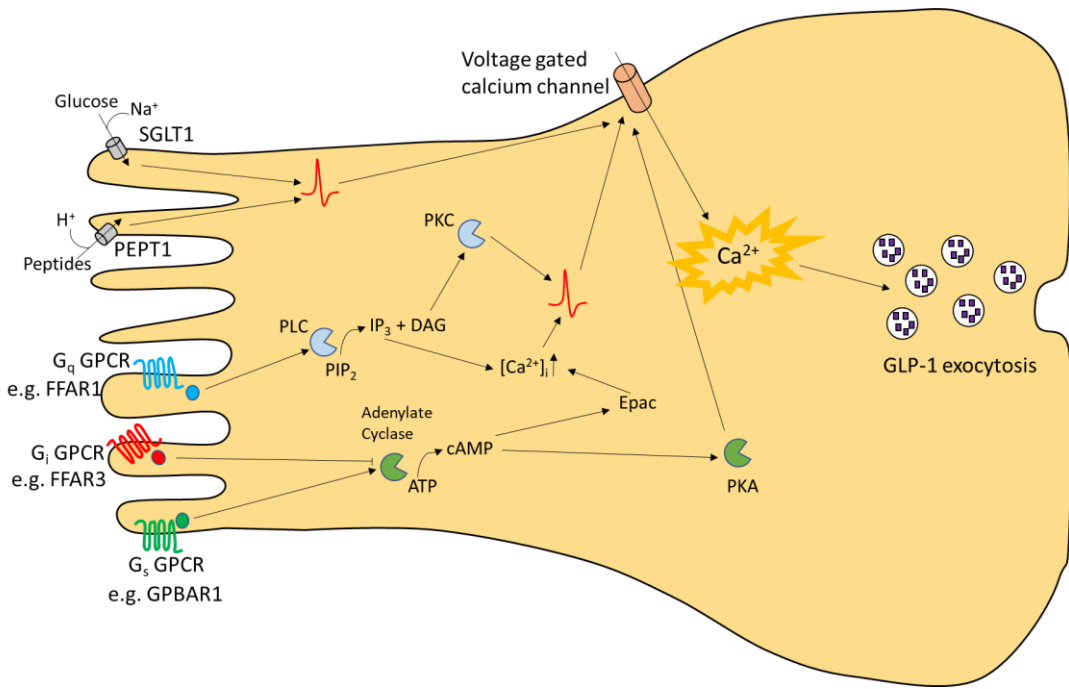


Figure 1.3 Overview of nutrient sensing for GLP-1 secretion. A wide-range of nutrients and metabolites stimulate GLP-1 secretion through a variety of mechanisms. A selection of transporters, channels and GPCRs involved in ‘sensing’ these metabolites are depicted [81]. Abbreviations: sodium-dependent glucose transporter 1 (SGLT1), proton-coupled peptide transporter (PEPT1), free fatty acid receptors 1 and 3 (FFAR1, FFAR3), G-protein-coupled bile acid receptor 1 (GPBAR1), phospholipase C (PLC), phosphatidylinositol-4,5-bisphosphate (PIP_2), inositol-1,4,5-triphosphate (IP_3), diacylglycerol (DAG), protein kinase C (PKC), exchange protein directly activated by cAMP (Epac) and protein kinase A (PKA).

1.3.3 GLP-1 Receptor (GLP1R) Structure and Signalling

Following secretion of GLP-1, the biologically active circulating form binds to and activates the GLP1R located in a number of distinct cell-types throughout the body. When considering the mechanism of how GLP-1 binds to and activates the GLP1R, the structure of GLP1R has revealed where GLP-1 binds.

The GLP1R is a G protein coupled receptor (GPCR) with a large N terminal extracellular domain, in the ‘Class B’ or ‘secretin’ family of GPCRs [82]. Up until recently, only the X-ray crystal structure of the extracellular domain (ECD) was available, showing the ECD is responsible for binding the C-terminal part of GLP-1 [83, 84]. Now, X-ray crystal structures and structures derived from cryo-electron microscopy are available for the full GLP1R in complex with agonist peptides or $\text{G}_{\alpha s}$ proteins [85-87]. Overall, this structural data has revealed that the seven transmembrane domains of the GLP1R are arranged in a similar manner to that of other ‘Class B’ GPCR’s, with a V-shaped central cavity. In contrast to the structure of the glucagon receptor, no helical stalk is found linking the transmembrane domains to the ECD, rather the extracellular loop 1 (ECL1) and second transmembrane domain (TM2) extend well beyond the membrane plane, and contact the ECD [85]. Despite this, evidence suggests

that the ECD is flexible in the absence of ligand, aiding the initial binding of the ECD to GLP-1 [88]. Aside from ECL1 which has a short helix-turn-helix secondary structure, all other connecting loops lack a secondary structure and are flexible in their nature. From the X-ray crystallography structural data, a simulation model of the molecular dynamics of GLP-1 binding has been made [86]. This is in line with what was previously known regarding the 2-domain binding mechanism, and matches the mechanistic proposals of GLP1R activation made from cryo-electron microscopy [87]. Briefly, agonist binding appears to cause a conformational change within helix V and VI of the GLP1R transmembrane domain, which then disrupts an intracellular ionic lock, opening a cavity for G-protein interactions [86, 87].

The GLP1R signals primarily via $G_{\alpha s}$ coupling leading to increased cAMP [89]. Downstream of cAMP, protein kinase A (PKA) is activated along with ‘exchange protein directly activated by cAMP’ (Epac). PKA and Epac have several downstream effects in the cell [90]. Both signalling proteins increase the ATP sensitivity of ATP sensitive potassium channels (K_{ATP}) leading to membrane depolarisation and Ca^{2+} influx. In pancreatic β -cells, this triggers insulin granule exocytosis. PKA and Epac also alter the dynamics of proteins that regulate insulin secretion, and in part increase insulin gene expression. Overall, this results in increased glucose stimulated insulin secretion (GSIS) from the pancreatic β -cells [91]. Aside from the main $G_{\alpha s}$ coupled signalling pathway, there are also indications that GLP1R may signal via $G_{\alpha q}$ and β -arrestin (described further in chapter 3).

1.3.4 GLP1R Localisation

The GLP1R is not solely located within pancreatic islets; expression is much more widespread. Studies using antibodies to determine GLP1R localisation have been limited due to the lack of antibodies that specifically detect GLP1R [92].

Use of a transgenic mouse model, expressing Cre downstream of the *glp1r* promoter and crossed with fluorescent reporters, has enabled detailed characterisation of GLP1R localisation, without the use of GLP1R antibodies with limited specificity. This *glp1r*-Cre mouse model revealed GLP1R expression in the pancreatic β - and δ -cells, vascular smooth muscle, cardiac atrium, gastric antrum/pylorus, enteric neurons and vagal/dorsal root ganglia [93]. A subsequent study has also used this model to reveal GLP1R expression in a number of distinct areas in the central nervous system [94], which has since been confirmed using *in situ* hybridisation with a newly generated GLP1R antibody specific for mouse tissue [95].

1.3.5 Actions of GLP-1

The widespread localisation of the GLP1R results in GLP-1 having a wide range of actions. As described earlier, the main role of GLP-1 exploited therapeutically is the ability to enhance glucose stimulated insulin secretion, known as the ‘incretin effect’. This effect is clearly mediated by GLP1R in the

pancreas, however functions of GLP-1 mediated by extra-pancreatic GLP1R are also important in the regulation of metabolism (Figure 1.4).

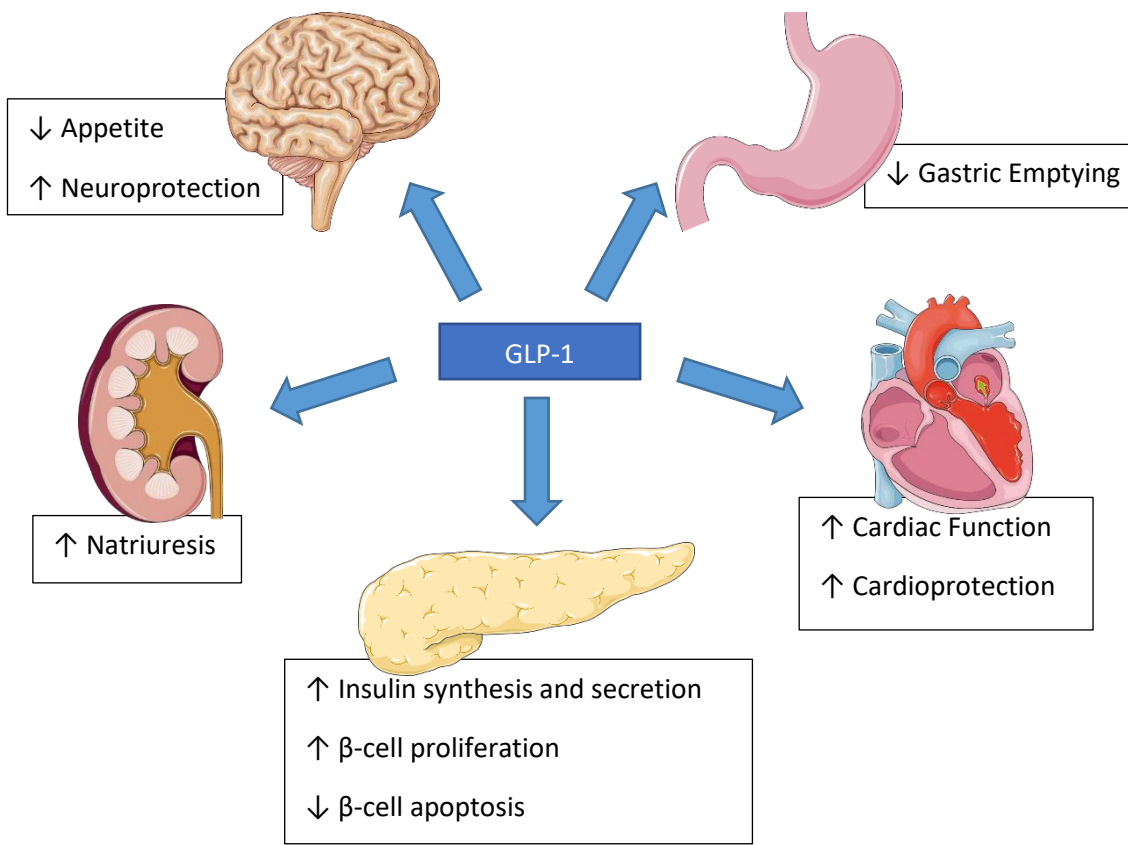


Figure 1.4 Schematic representation of GLP-1 functions. Aside from the well-known incretin actions of GLP-1 on insulin secretion, GLP-1 also exerts a wide-range of other functions depicted above. Figure is based on review from Meier (2012)[47]. Images downloaded from Servier Medical Art.

1.3.5.1 Actions of GLP-1 in the pancreas

Aside from GLP1R in pancreatic β-cells mediating insulin secretion, GLP-1 also increases β-cell proliferation possibly involving the epidermal growth factor receptor [96] and decreases β-cell apoptosis, in part due to protein kinase C (PKC) activation [97, 98]. Together, this results in GLP-1 increasing total β-cell mass, leading to further increased insulin secretion. Additionally, GLP-1 has been shown to effect the biosynthesis of insulin; increasing insulin gene transcription, and enhancing insulin mRNA stability via interactions with pancreatic duodenal homeobox 1 (Pdx1) transcription factor [89, 99].

In the pancreatic α-cells GLP-1 inhibits glucagon secretion, therefore regulating glucose control via two complementary mechanisms. Whether this inhibition is a direct or indirect effect is unknown. As GLP1R is found in a subset of α-cells this indicates the possibility of a direct GLP-1 effect [93], which

has been demonstrated by GLP-1 inhibition of voltage gated Ca^{2+} channels in α -cells [100]. On the other hand, GLP-1 stimulation of somatostatin secretion from δ -cells has been observed, which would have an indirect effect on the inhibition of glucagon secretion [101].

1.3.5.2 Extra-pancreatic actions of GLP-1

Locally, following GLP-1 secretion from the enteroendocrine L-cells, GLP-1 reduces gastric emptying [102]. This has been observed in both humans and rodents, the slowing or reduction of gastric emptying means decreased nutrient absorption in the intestine, and consequently decreased post-prandial glucose excursions [102, 103]. This regulation of gastrointestinal motility by GLP-1 is thought to be mediated by GLP1R expressing vagal afferents, as both the denervation of vagal afferents in rats, and truncal vagotomy in humans abolishes the GLP-1 induced effects [103, 104]. Other local effects of GLP-1 include decreasing gut motility [105] and decreasing gastric acid secretion [106].

GLP-1 has several effects in extra-pancreatic tissue, not limited to the location of GLP-1 secretion. For example, renal effects of GLP-1 include increased natriuresis and diuresis [107], along with increased glomerular filtration rate [108]. Although the mechanism of these renal effects are not fully characterised, direct mechanisms involving the inhibition of sodium-hydrogen exchanger isoform 3 (NHE3) have been proposed [109-111]. On the other hand, there are also suggestions that the renal effects are indirect effects of GLP-1 influencing feeding and drinking behaviour [112]. GLP-1 regulation of food intake is thought to be mediated by central GLP1R, and will be described in section 1.2.5.3.

GLP-1 also has a range of actions in the cardiovascular system which were brought to light in the use of GLP-1 mimetics for the treatment of type 2 diabetic patients. To name a few physiological effects; GLP-1 modulates heart rate and blood pressure, and protects the heart from ischemia and reperfusion injury. With regards to clinical studies using GLP-1 mimetics, the cardiovascular beneficial effects appear to differ dependent on the agonist used [113-115]. As GLP-1 mimetics are now widely used for the treatment of type 2 diabetes, the long-term effects of GLP-1 mimetics on cardiovascular parameters will be critical to define any additional beneficial cardiovascular effects.

The exact location of GLP1R in the cardiovascular system remains uncertain. The glp1r-cre reporter mice found GLP1R in the aorta, arteries, arterioles and atrium myocardium however not in the ventricular myocardium [93]. Within the primate heart, GLP1R is detected within myocytes in the sinoatrial node, and smooth muscle cells or arteries and arterioles [116]. Most recently, analysis of human cardiovascular tissue has detected GLP1R mRNA in the heart, however the exact location within the heart remains to be determined by immunostaining [117].

The molecular mechanisms of GLP-1 induced cardiovascular effects remain fairly unclear, with debate surrounding whether the effects are direct or indirect. Regarding possible direct mechanisms, there are several studies that suggest effects are mediated directly via GLP1R mediated signalling in the affected tissue. For example, experiments with cardiomyocytes demonstrated Epac2 translocation to the cell membrane, and downstream secretion of vasodilatory atrial natriuretic peptide in response to a GLP1R agonist [118]. Further supporting evidence for a direct GLP1R mediated effect, is that GLP1R knock-out mice have altered cardiovascular properties compared to wild-type mice [119]. On the other hand, GLP-1 administration to GLP1R knock-out mice still exerts many of its cardiovascular effects [120]. There are also a number of studies which show the ‘inactive’ form of GLP-1, GLP-₁₉₋₃₆_{amide} has similar cardiovascular effects to the biologically active form GLP-₁₇₋₃₆_{amide} [120-122]. Together, this supports the theory that GLP-1 exerts its cardiovascular actions independently of the GLP1R. A further proposal is that GLP-1 indirectly causes changes in cardiovascular parameters via the autonomic nervous system. Supporting evidence for this hypothesis is that intracerebroventricular administration of GLP-1 alters heart rate and blood pressure in rodents, which is blocked by antagonism of central cholinergic receptors [123]. Additionally, *ex vivo* studies using isolated perfused mouse hearts show GLP1R agonists cannot induce the chronotropic effects showing these effects require the neural inputs [124]. Most likely, both direct and indirect effects mediate the GLP-1 induced effects on cardiovascular parameters, however more research is required to clearly define the molecular mechanism.

1.3.5.3 Centrally mediated actions of GLP-1

Aside from the peripheral extra-pancreatic actions of GLP-1, GLP-1 also controls appetite partly via centrally expressed GLP1R in the hypothalamus. Early studies showed that intracerebroventricular injection of GLP-1 reduced acute food and water intake in fasted rats in a dose-dependent fashion [107, 125]. Central injection of the small molecule GLP1R antagonist, exendin 9-39, prevented this GLP-1 mediated inhibition, thus showing central GLP1R is involved in the GLP-1 control of appetite [125]. Daily central administration of GLP-1 to rats even reduces body weight alongside food intake, suggesting GLP-1 may play a physiological role in regulating body weight [126]. This activity makes GLP-1 mimetics particularly attractive for treatment of type 2 diabetes, which often occurs in overweight patients.

GLP1R activating therapeutic peptides, such as liraglutide, are also able to control appetite alongside glucose levels, even when given peripherally. Whether centrally expressed GLP1R is necessary or sufficient for these anorectic effects of GLP1R agonists has recently been investigated. A number of studies, including the early intracerebroventricular GLP-1 injection experiments show that central GLP1R is sufficient for GLP-1 mediated effects on appetite control [107, 125]. Indeed, subsets of

neurons such as the paraventricular nucleus of the hypothalamus, nucleus of the solitary tract, and central amygdala are activated following peripheral injection of GLP1R agonists [125, 127]. Knock-out of central GLP1R using *nestin-Cre* reduced the effects of liraglutide on food intake both acutely and chronically, showing these effects are mediated primarily via the central nervous system [128]. Other studies, using fluorescently labelled liraglutide have shown that it is specifically neurons within the arcuate nucleus (ARC) which are involved in centrally regulating liraglutide effects on appetite. In particular, neurons expressing the proopiomelanocortin (POMC) peptide and cocaine- and amphetamine-regulated transcript (CART) were stimulated by liraglutide, which have an impact on inhibiting food intake [129]. These studies suggest that GLP1R agonists require hypothalamic GLP1R for the appetite regulating effects, however experiments using hypothalamic specific knock-out and knock-down mouse models suggest the hypothalamic GLP1R is in fact not required for appetite regulation. Both GLP1R agonists, exendin-4 and liraglutide, retain anorectic actions in hypothalamic GLP1R knock-down mice, paraventricular nucleus GLP1R knock-out mice, and POMC specific GLP1R knock-out mice [130]. If the central GLP1R is not necessary for GLP1R agonist effects on regulating appetite, one would suggest these effects are mediated either via alternative GLP1R neurons in other locations such as the area postrema, or the GLP1R on vagal afferents which can transmit signals centrally via the nodose ganglia terminating in the nucleus of the solitary tract[131, 132].

1.4 Physiology of Glucose-dependent insulinotropic peptide (GIP)

1.4.1 Production of GIP

GIP is encoded by the ProGIP gene, comprising 6 exons, with exon 3 encoding the majority of the active GIP sequence [133]. Unlike GLP-1, GIP-expressing cells are the enteroendocrine K-cells predominantly found in the proximal small intestine, with expression also found in the submandibular salivary gland of rats [134, 135]. The factors which regulate transcription of GIP have not been defined, however binding sites exist for several transcription factors [136, 137]. Translation produces the proGIP prohormone precursor, which is subsequently cleaved at single arginine residues by PC1/3 to yield the incretin hormone, GIP [138]. The other peptides encoded by the proGIP precursor seem to have no known function.

Similar to GLP-1, GIP is inactivated by DPP-4 mediated cleavage at position 2 [139, 140]. This means GIP also has a short half-life, of 7 minutes in healthy human subjects, and the maximal circulating levels are in the range of 100 picomolar following meal consumption [141, 142]. Although this half-life is short, it is not equivalent to the GLP-1 half-life, and there are suggestions that GIP is less susceptible to DPP-4 cleavage *in vivo* when compared to GLP-1 [139, 140].

1.4.2 Regulation of GIP secretion

GIP is secreted from enteroendocrine K cells lining the intestinal wall, with increased density at the proximal end of the intestine in the duodenum and jejunum. This secretion is nutrient-dependent, primarily driven by the ingestion of dietary fat and carbohydrates [143-145]. The cellular structure of K-cells is similar to that of L-cells, with the apical surface being covered in microvilli at the luminal wall, meaning K-cells can directly sense the presence of nutrients. When considering the molecular mechanism responsible for this sensing, it is thought that the sodium-dependent sugar uptake pathway is involved in detection of luminal carbohydrates [146, 147], and free fatty-acid receptors are involved in the detection of fat in the form of fatty acids [147, 148].

1.4.3 GIP receptor (GIPR) Structure and Signalling

GIP binds to and activates the GIPR on a number of cell-types throughout the body. The GIPR, like the GLP1R is a member of the ‘Class B’ family of GPCRs [82], with a large extracellular N terminal domain, a core domain consisting of seven transmembrane helices, and an intracellular C terminal tail which interacts with associated G proteins [149-151]. Although the complete structure of the GIPR is not yet available, a crystal structure of the N terminal ECD responsible for binding GIP has been produced. This structure indicates that GIP binds to the N terminal ECD within a surface groove using mainly hydrophobic interactions, with the N terminal residues of GIP being free from interactions [152]. This suggests that GIP interacts both with the ECD, and the core domain which fits with the proposed 2-step mechanism for ‘Class B’ GPCR activation. Briefly, within this mechanism of activation the ligand first binds the N terminal domain of the receptor locking the ligand in place, and bringing it into contact with the core transmembrane domain of the receptor for a second interaction, resulting in a conformational change of the receptor which causes activation [153].

As with the GLP1R, and other members of the ‘Class B’ GPCR family, the GIPR signals primarily via the $G_{\alpha s}$ coupled protein which causes accumulation of cAMP, and downstream activation of PKA and Epac [154, 155]. Molecularly, in the pancreatic β -cell, these signalling molecules lead to a variety of downstream effects such as closure of K_{ATP} channels, opening of voltage-dependent calcium channels (VDCC) leading to Ca^{2+} influx, and possible direct actions on granule movement and exocytosis [155]. In comparison to GLP-1, the GIP effects on insulin secretion appear to be more dependent upon K_{ATP} channel closure [156]. A further comparison using transfected cell lines has suggested that the GIPR has a higher basal activity than the GLP1R, which may be because unlike the GLP1R, the GIPR shows decreased β -arrestin 2 binding which could be extrapolated to the other β -arrestins which regulate receptor desensitisation [157].

GIP activation of the GIPR also leads to signalling via alternative downstream pathways. For example, extracellular signal-regulated kinase (ERK) phosphorylation is stimulated in a PKA-dependent manner [158]. Downstream of this, it has been observed that GIP promotes expression of transcription factor-7 (*Tcf7*) gene in pancreatic β-cells, which is thought to be important for the cytoprotective effects of GIP [159]. Additionally, GIP mediates anti-apoptotic signalling, reducing the effects of B-cell lymphoma-2 (Bcl-2) family members on pancreatic β-cell apoptosis [160].

1.4.4 GIPR Localisation

Similar to the GLP1R, when considering GIPR localisation, it is not limited to pancreatic β-cells where GIP exerts its insulinotropic actions. Rather GIPR localisation is more widespread; early *in situ* hybridisation studies showed that the GIPR is also found in adipose tissue, the heart, gut, pituitary glands, and inner layers of the adrenal cortex [149]. There are also indications that the GIPR is found in the central nervous system in addition to these peripheral organs [149, 161]. However, the data from these studies has limited resolution. Very little further work has been completed in the study of GIPR localisation due to a lack of antibodies verified for use in immunostaining [162-164].

1.4.5 Actions of GIP

The main described actions of GIP, of interest therapeutically, are its ability to stimulate insulin secretion from pancreatic β-cells in the presence of glucose, and to increase nutrient storage and therefore lipogenesis in adipose tissue. These actions will be described in detail below. Other functions also include a role in bone formation [165], inhibition of gastric acid secretion from the stomach at supraphysiological concentrations [166], and possibly a role in memory formation [167, 168] (Figure 1.5).

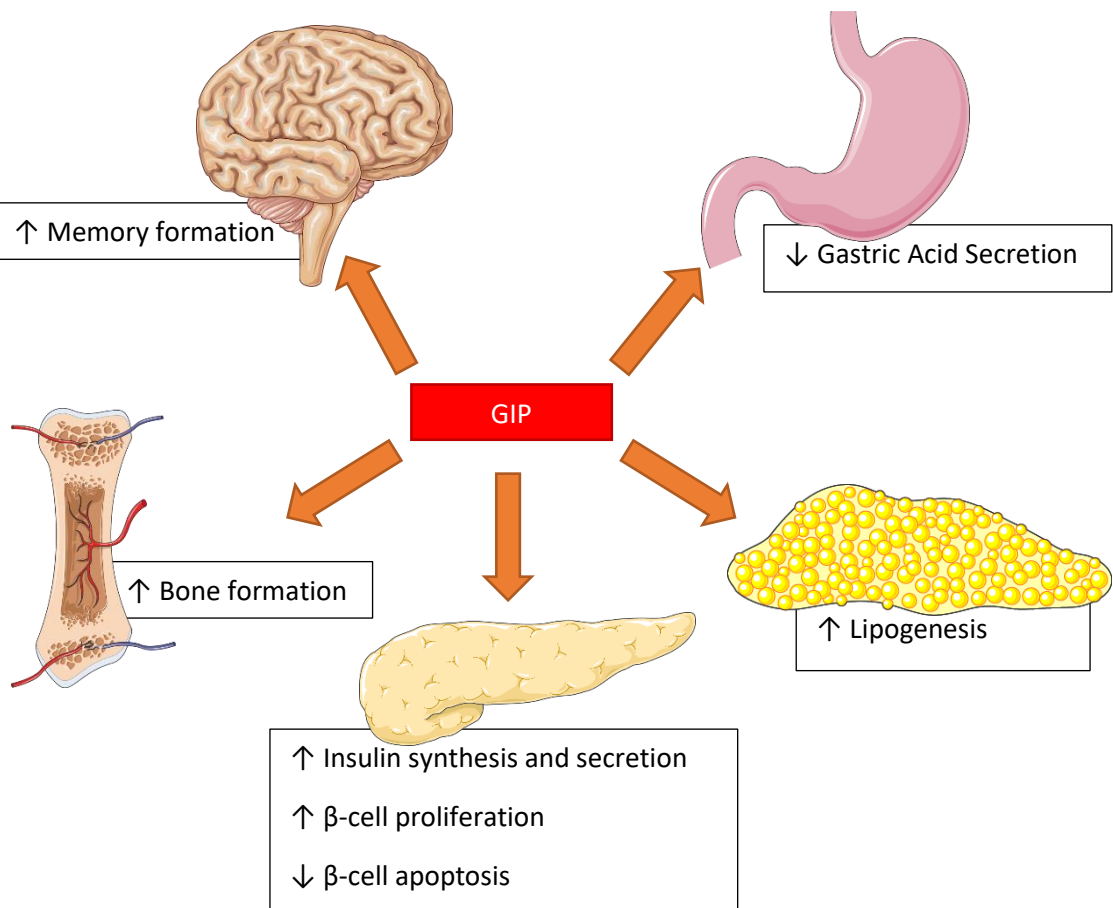


Figure 1.5 Schematic representation of GIP functions. GIP also has a number of roles aside from stimulating insulin secretion from the pancreas, these are depicted above. Figure is based on review from Baggio and Drucker (2007) [78]. Images downloaded from Servier Medical Art.

1.4.5.1 Pancreatic actions of GIP

The insulinotropic actions of GIP on pancreatic β -cells are analogous to those of GLP-1. However, targeting of the GIPR for treatment of type 2 diabetic patients has not yet been successfully exploited therapeutically without also targeting the GLP1R [48, 169].

Aside from the insulinotropic effect of GIP, there are also indications that GIP exerts anti-apoptotic and proliferative actions on the pancreatic β -cells. Regarding the anti-apoptotic actions at a molecular level, PKA activated upon GIPR stimulation causes phosphorylation of cAMP response element binding protein (CREB), which in the nucleus promotes transcription of the anti-apoptotic factor Bcl2 [170]. Regarding the proliferative actions, GIP causes signalling via ERK phosphorylation which leads to proliferation [158]. Additionally, in terms of cell-cycle regulating proteins, GIP causes transcription of cyclin D1 which is essential for cells to progress through the G1 phase [171].

In contrast to GLP-1, there are suggestions that GIP is able to enhance glucagon secretion from pancreatic α -cells [172]. This would appear to counteract its glucose lowering actions induced by stimulation of insulin secretion, and may be an explanation for the lack of GIPR agonists in the clinic for treatment of type 2 diabetes.

1.4.5.2 Actions of GIP in adipose tissue

The second aspect of GIP physiology most described is the ability to increase nutrient storage in the adipose tissue. Early indications that GIP may play a role in nutrient uptake to adipose tissue came from studies using rat epididymal fat pads. GIP in the presence of insulin increased fatty acid incorporation into these fat pads [173]. Additionally, *in vivo* studies demonstrated a role of GIP in clearing chylomicron-associated triglycerides from circulation in rats and dogs [174, 175].

One of the direct roles of GIP on adipocytes is the enhancement of lipoprotein lipase (LPL) activity [176-179], which is involved in the hydrolysis of triacylglycerols [180]. Regarding the mechanism responsible for this, GIP has been shown to alter the transcription of LPL. In human adipocytes, a GIP dependent increase in LPL gene expression is observed in the presence of insulin. This appears to be due to GIP inducing phosphorylation of CREB, together with nuclear localisation of cAMP-responsive CREB coactivator 2 (TORC2) which both bind to the LPL promoter and increase transcription [181]. This may not be the only way in which GIP increases LPL activity, post-transcriptional events could also contribute. For example, the time-dependent manner in which GIP increases LPL activity suggests GIP may mediate its actions on LPL via an intermediate signalling molecule. One suggestion is that GIP increases secretion of adipokine resistin which then signals to increase LPL activity [177].

A further role of GIP in adipose tissue is the regulation of adipocyte glucose metabolism. Although in the past there has been controversy surrounding this function of GIP, there is some evidence to suggest GIP potentiates adipocyte insulin sensitivity, increasing glucose uptake [182, 183]. At the intracellular level, GIP in the presence of insulin increases the membrane translocation of the Glut4 glucose transporter, and increases nuclear exclusion of the FoxO1 transcription factor. Molecularly, this relies upon activation of CREB and the p110 β isoform of phosphoinositide 3-kinase (PI3K), however the complete molecular mechanism remains to be elucidated [184].

GIPR knock-out mouse models also show the importance of adipose tissue GIPR. Both a global GIPR knock-out, and GIPR knock-out restricted to adipose tissue using a *mouse adipocyte protein 2 (aP2)*-Cre line, provide protection from HFD induced obesity [182, 185]. The reason for this protection is not fully understood. In the global GIPR knock-out model, the investigators suggested the explanation was due to decreased triglyceride in adipocytes resulting in less nutrient storage [182]. Whereas the adipose specific GIPR knock-out investigators showed the differences in body weight were due to

decreased lean mass rather than fat mass [185]. Clearly more investigation is required to fully understand the role of GIP in adipose tissue.

1.5 Physiology of Glucagon-like peptide 2 (GLP-2)

1.5.1 Production of GLP-2 and regulation of secretion

GLP-2, along with GLP-1 described earlier, is derived from the proglucagon gene [69]. For the production of GLP-2, PC1 cleaves the proglucagon product in intestinal L cells and proglucagon expressing cells in the central nervous system, yielding the 33 amino-acid peptide (Figure 1.2) [73, 186].

The secretion of GLP-2 from the enteroendocrine L-cells occurs simultaneously with GLP-1, thus as described earlier a wide range of nutrients and metabolites stimulate secretion. In addition to nutrient sensing being responsible for GLP-2 secretion, intestinal injury also causes GLP-2 secretion [187]. Again, like GLP-1 and GIP, GLP-2 is a target for degradation by DPP-4. Within minutes of GLP-2 secretion, intact biologically active GLP-2₁₋₃₃ is cleaved to GLP-2₃₋₃₃ [188].

1.5.2 GLP-2 Receptor (GLP2R) Structure and Signalling

As with the GLP1R and GIPR, the GLP2R is a member of the ‘Class B’ GPCR’s primarily coupled to G_{αs}. In contrast to the previously described receptors, structural data for the GLP2R does not exist. Rather, structural models have been generated computationally for the human GLP2R extracellular domain (ECD) based upon the GLP1R, with which the GLP2R shares the highest sequence similarity [189, 190]. Nuclear magnetic resonance (NMR) studies have revealed the GLP-2 structure containing a central α-helical region along with a loose helical region at the C-terminal end. This has enabled the modelling of GLP2 binding to the GLP2R ECD; only the C-terminal portion of GLP-2 binds to the GLP2R ECD, sitting within the hydrophobic binding cavity of the ECD [189].

Studies using primary cultures and transfected cell lines have shown GLP-2 binding to the GLP2R leads to signalling primarily via G_{αs} and the generation of cAMP [191]. Aside from this, GLP-2 activation of the GLP2R leads to phosphorylation of protein kinase B (known as Akt) and phosphorylation of ERK1/2 in a PI3K dependent manner, as observed in primary cultures of enteric neurons [192]. There is also evidence indicating that β-arrestin 2 is recruited to the GLP2R upon activation, which may then cause downstream signalling [193].

1.5.3 GLP2R Localisation

Unlike the GLP1R and GIPR, the main described location of the GLP2R is the gastrointestinal tract, encompassing the stomach, small and large intestine. However, the precise cellular location of the GLP2R in these areas is debatable, with two main schools of thought. On one hand,

immunocytochemistry studies using human, rat or pig tissue have observed the GLP2R in enteroendocrine cells within the epithelial lining of the intestine [194-196]. On the other hand, a number of studies using a combination of *in situ* hybridisation, immunocytochemistry and receptor autoradiography localise the GLP2R to cells outside of the epithelial layer including enteric neurons, subepithelial myofibroblasts and submucosal glial cells neurons [192, 197-200]. One likely reason for the debate surrounding GLP2R localisation is a low abundance of GLP2R positive cells, combined with the available GLP2R antibodies lacking sensitivity and specificity [201].

1.5.4 Actions of GLP-2

GLP-2 is known to be an intestinotrophic factor, initially found to increase small bowel weight due to increased length of the intestinal villi, when injected into mice twice daily for 10 days [202]. Other gastrointestinal functions of GLP-2 include the increase of nutrient absorption [203-205], a possible inhibitory effect on gut motility [206], decreased gut permeability and increased intestinal barrier function [207, 208]. Aside from the intestinal effects, GLP-2 also increases visceral blood flow [209, 210], inhibits bone resorption [211, 212] and may stimulate glucagon secretion from pancreatic α -cells [205, 213] (Figure 1.6).

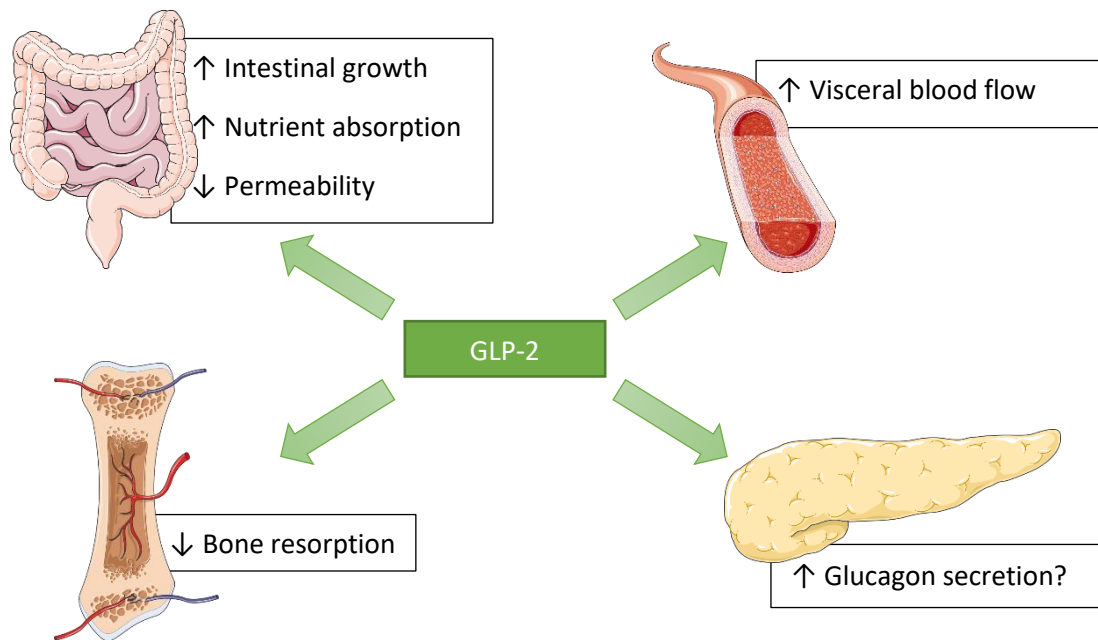


Figure 1.6 Schematic representation of GLP-2 functions. The main functions of GLP-2 are in the gastrointestinal tract, with some functions in other tissues depicted above. Images downloaded from Servier Medical Art.

1.5.4.1 Gastrointestinal actions of GLP-2

The intestinotrophic actions of GLP-2 are due to an increase in crypt cell proliferation together with a decrease in epithelial cell apoptosis, however the molecular mechanism resulting in these changes are not completely explained. Morphologically, electron microscopy has shown GLP-2 treatment in mice makes epithelial cells narrower and longer, with longer microvilli [207]. The increased length of intestinal villi is linked to a change in nutrient transport, and changes in gut permeability.

The effects of GLP-2 on nutrient transport were first detected in 1997 when it was observed that the intestinal growth stimulated by GLP-2 also leads to increased intestinal RNA and protein content, which is synonymous with an increase in brush border disaccharidase and peptidase enzymes. To assess nutrient transport and absorbance of carbohydrates, amino acids, or triglycerides respectively either glucose, maltose or a mixture of leucine and triolein were administered by oral gavage or directly to the duodenum. No GLP-2 mediated effects on nutrient absorbance were detected when nutrients were administered orally, possibly due to GLP-2 effects on gastric emptying. In contrast, GLP-2 increased absorbance of leucine and triolein in the duodenal nutrient tolerance test. However, GLP-2 did not increase carbohydrate absorbance in this setting [214]. In a separate set of experiments using *in vivo* perfusions in the rat, fructose absorbance was increased in the presence of GLP-2, however whether this represents a physiological setting is debatable [215].

The GLP-2 mediated increase in lipid absorption is associated with increased triglyceride (TG) incorporation into TG rich lipoproteins (TRL) also known as chylomicrons, which upon secretion lead to increased plasma TG. An increase in secretion of chylomicrons has been observed upon GLP-2 treatment in mice and hamsters. It is thought that CD36 glycosylation is required for this process, as CD36 knock-out animals fail to show GLP-2 mediated increases in lipid absorption [204]. It should be noted that these effects on lipid absorption have also been observed in humans [205, 216].

The GLP-2 mediated effects on amino acid absorbance have recently been confirmed in mice. The use of GLP2R knock-out mice gave confidence that the GLP-2 mediated increase in basal amino acid absorbance was dependent upon the GLP2R. Mechanistically, GLP-2 appears to increase the expression of the cationic amino acid transporter *slc7a9* and increase 4F2hc which is required for the function of light-chain amino acid transporters [217].

Regarding gut permeability, GLP-2 administration to mice reduces paracellular transport of Na⁺ ions and small molecules in the intercellular space. GLP-2 also reduces transcellular transport of larger molecules through the epithelial cells. These decreases in flux were observed at as little as 4 hours after GLP-2 treatment, suggesting that the GLP-2 mediated effects on flux are not completely dependent upon changes in morphology. Overall, the increased epithelial barrier function indicates

therapeutics based on GLP-2 may be useful for treating enteropathies related to increased epithelial permeability and resultant inflammatory responses [207]. Molecularly, there are some observations indicating that GLP-2 increases expression of the tight junction proteins zonula occludens-1, occudin, and claudin-1 in pig jejunal tissue, which is reduced by inhibition of mitogen-activated protein kinase (MAPK) [218]. However, this does not provide a full molecular explanation for how GLP-2 reduces gut permeability.

1.5.4.2 Actions of GLP-2 outside of the gastrointestinal tract

Aside from the direct gastrointestinal effects, GLP-2 also increases mesenteric blood flow in humans, as measured in the superior mesenteric artery which supplies the gastrointestinal tract with oxygenated blood [210]. The mechanism by which GLP-2 exerts this action is not understood, though studies in pigs suggest nitric oxide is essential for the increased intestinal blood flow as demonstrated by the use of a nitric oxide synthase inhibitor [209].

In the pancreas, there is debate surrounding whether GLP-2 can stimulate glucagon secretion. Infusion of supra-physiological concentrations GLP-2 to humans increases plasma glucagon levels, however there are no effects on plasma glucose [205]. Additionally, the perfused rat pancreas secretes glucagon in response to high concentrations of GLP-2. In pancreas tissue from human and rat the GLP2R is colocalised with glucagon in islet α -cells, suggesting effects on glucagon secretion are mediated directly by the GLP2R [213]. However, there are inter-species differences, in the mouse no effects of GLP-2 on glucagon have been found, nor is there expression of GLP2R in the pancreatic α -cells [194, 219].

1.6 Clinical Abnormalities in Metabolic Physiology

Defects in metabolic physiology cause a whole range of diseases; two of which that are increasing in prevalence are obesity and type 2 diabetes. Patients with obesity are extremely overweight with excessive body fat. Patients with type 2 diabetes have insufficient insulin secretion for their level of insulin resistance, meaning blood glucose levels are not controlled, and patients have high levels of blood glucose, known as hyperglycaemia [220]. Increased insulin resistance associated obesity results in a high risk of type 2 diabetes in obese people [221-223].

Severe obesity is increasingly managed by surgical approaches, most commonly either by roux-en-Y gastric bypass surgery or sleeve gastrectomy. Briefly, roux-en-Y gastric bypass surgery is a procedure whereby the stomach is divided; a small pouch of the proximal stomach is connected to the distal portion of the jejunum, the other part of the stomach remains connected to the duodenum, and is anastomosed lower down the jejunum [224]. Sleeve gastrectomy on the other hand is a procedure whereby approximately 75% of the stomach is removed, leaving a tubularised stomach with reduced

capacity [224]. These metabolic surgeries are highly efficacious in treating obesity and are also the single most effective treatment for type 2 diabetes, however the reason for this is not clear [220, 225].

A further clinical abnormality in metabolic physiology, of relevance for this thesis, is short bowel syndrome (SBS). This syndrome is often caused by extensive intestinal resection surgery, resulting in a short small intestinal length which is inadequate for optimal absorption. This insufficient intestinal function means that patients on a normal diet are unable to maintain protein-energy, fluid, electrolyte and micronutrient balances [226]. The consequences of this mean that patients are often using parenteral nutrition, being fed intravenously, giving a reduced quality of life. Not only this, but SBS is also associated with significant morbidity and mortality [227, 228].

1.6.1 Therapeutic Targeting of the Gut Hormones GLP-1, GIP and GLP-2

Studies on the physiology of the gut hormones GLP-1, GIP and GLP-2 revealed possibilities for targeting these hormones therapeutically; either using the incretin properties of GLP-1 and GIP for the treatment of type 2 diabetes, or using the intestinotrophic properties of GLP-2 for the treatment of short bowel syndrome (SBS).

Patients with type 2 diabetes suffer from hyperglycaemia due to ineffective regulation of blood glucose levels, this results in a number of symptoms including increased risk of developing cardiovascular disease [229]. For the treatment of type 2 diabetes there are two main therapeutic strategies focused on gut hormones; the use of GLP-1 mimetics which are resistant to degradation by DPP-4 [47], and the use of DPP-4 inhibitors which prevent the degradation of incretin hormones [230]. More recently, focus has shifted to the development of unimolecular agonists that target multiple gut hormone pathways simultaneously. This arose from the observation that upon comparison of all treatments for type 2 diabetes, gastric bypass surgery is the most effective [225]. Clearly, this efficacy is not the result of targeting one molecular pathway, rather a whole host of metabolic and physical changes are induced after surgery, one of which is a differing pattern of gut hormone secretion leading to increased levels of several gut hormones [231]. This new therapeutic strategy of targeting multiple gut hormones simultaneously with a unimolecular agonist aims to mimic the effects of gastric bypass surgery. Many of these agonists are centred on GLP-1, which is already known to exert beneficial therapeutic effects of patients with type 2 diabetes [232]. One such dual agonist is the GLP-1/GIP dual peptide, targeting both axes of the incretin effect which allows for a lower dose of GLP-1 to be used reducing gastrointestinal side effects [48].

Patients with SBS have decreased capacity to absorb nutrients via the intestine, and thus can suffer from malabsorption, dehydration and malnutrition [233]. For the treatment of SBS, the intestinotrophic activity of GLP-2 makes it an attractive therapeutic target [234]. Indeed, teduglutide,

a GLP2R agonist with an extended half-life compared to GLP-2, improves intestinal absorption in these patients likely due to increasing intestinal mucosal growth [235, 236].

1.7 Aims of Thesis

As described above, enteroendocrine hormones have a wide range of roles in the control of metabolism, and can be targeted therapeutically. A detailed understanding of the physiology of these gut hormones and their receptors is therefore particularly useful for further development of therapeutics. With this in mind, the aims of this thesis were three-fold.

Firstly, I focused on the receptor to GLP-1, the incretin hormone which is the most widely targeted gut hormone for the treatment of type 2 diabetes. However, therapeutic targeting of GLP-1 also leads to a number of extra-pancreatic effects which have not yet been fully explained at the molecular level. For the study of GLP1R physiology, antibodies to the GLP1R are limited. The first aim of my thesis was to generate a GLP1R monoclonal antagonistic antibody using naïve phage display (Chapter 2). Subsequently the specificity of this antibody was assessed, along with the ability to block GLP1R mediated signalling pathways and downstream effects in a range of in vitro and in vivo experiments (Chapter 3).

Secondly, I focused on GIPR, the receptor for the second incretin hormone (GIP) which also regulates nutrient storage in adipose tissue. Due to a lack of GIPR antibodies for use in immunostaining there is limited information surrounding GIPR localisation. The second aim of my thesis was to identify and characterise cells containing the GIPR using a newly generated mouse model expressing fluorescent reporters downstream of the *Gipr* promoter (generated by F. Reimann). I used immunohistochemistry to identify GIPR expressing cells in peripheral organs and the central nervous system. The function of hypothalamic GIPR expressing cells in the regulation of food intake was then investigated (Chapter 4).

Finally, I focused on the GLP2R, the receptor for GLP-2 which is an intestinotrophic gut hormone secreted simultaneously with GLP-1. Collaborators raised interest in a common missense mutation in the GLP2R (D470N) which they found to be associated with increased citrulline levels, and increased risk of type 2 diabetes (L. Lotta, C. Langenberg and colleagues). As the final aim of my thesis I sought to characterise the effects of this GLP2R polymorphism on GLP-2 signalling pathways, including cAMP stimulation, β-arrestin recruitment and phosphorylation of ERK1/2 (Chapter 5).

Chapter 2. Generation of a GLP1R antagonistic antibody

2.1 Introduction

2.1.1 Therapeutic Targeting of GLP1R

The endogenous incretin actions of GLP-1, as described in chapter 1, are now utilised for the treatment of type 2 diabetes. Two forms of therapeutics are available; long-lasting GLP-1 mimetics such as liraglutide, and DPP-4 inhibitors such as sitagliptin which prevent the degradation of endogenous GLP-1 [237]. The success of these treatments is primarily due to the regulation of glycaemic control, however other beneficial effects are also observed including weight loss, and decreased cardiovascular risk.

It should be noted that the beneficial effects of GLP-1 mimetics appear to differ between studies, and may depend on the agonist used. For example, the LEADER trial showed liraglutide reduced the number of major cardiovascular events in patients with a high risk of a cardiovascular event. A time-to-event analysis showed the occurrence of cardiovascular death, nonfatal myocardial infarction, or nonfatal stroke was less in type 2 diabetes patients treated with liraglutide [113]. A similar result was seen in the SUSTAIN-6 trial, in which semaglutide also decreased these major cardiovascular events in type 2 diabetes patients with a high risk of cardiovascular disease [114]. In contrast, the ELIXA trial showed lixisenatide, the shorter-acting GLP-1 mimetic, had no beneficial effects on these major cardiovascular events in type 2 diabetic patients who had recently had an acute coronary event [115].

Combined, these trials have increased interest of GLP-1 actions in the cardiovascular system. At a mechanistic level, uncertainty surrounds whether the effects are mediated directly via GLP1R in the affected tissue, indirectly via GLP1R activation in neurons, or via alternative receptors in GLP1R-independent pathways [238]. Further research is required to underpin the cardiovascular and other extra-pancreatic effects of GLP-1. Pharmacologically this could be investigated using GLP1R selective antagonists.

2.1.2 Use of antagonists to study the GLP1R

Antagonism of GLP1R is widely achieved using the peptide antagonist exendin 9-39, a truncated form of exendin-4, originally derived from *Heloderma suspectum* [239]. Recently, ¹⁸F-labeled derivatives of exendin9-39 have been developed for imaging and downstream quantification of beta-cell mass, showing an alternative use of the antagonist [240]. Interestingly, the use of exendin9-39 for treatment of congenital hyperinsulinism and post-bariatric hypoglycaemia is being investigated, raising the potential to use GLP1R antagonists therapeutically [241, 242].

However, exendin 9-39 off-target effects have been observed in preclinical studies using cardiomyocytes from $\text{Glp1r}^{-/-}$ mice [121]. Alongside this, exendin 9-39 has also been shown to inhibit the other incretin receptor, GIPR [243, 244]. Combined, these studies raise questions about the specificity of exendin 9-39. One solution that we propose is the use of an antagonistic antibody that specifically targets GLP1R, which would also provide the advantage of having an extended half-life when compared to exendin 9-39.

2.1.3 Specificity of GLP1R antibodies

Although some GLP1R antibodies were available at the start of this PhD project, their usefulness and specificity were questionable. In 2013, the specificity of commercially available antibodies was investigated by immunoprecipitation and western blot of $\text{Glp1r}^{+/+}$ and $\text{Glp1r}^{-/-}$ tissue extract. All of the tested antibodies reacted unspecifically with both tissue extracts [92]. As a result, alternative methods have since been sought for studying receptor expression, including the generation of a transgenic mouse model expressing fluorescent reporters downstream of the *Glp1r* promoter [93].

As described in chapter 1, the GLP1R is a GPCR, and as such the generation of antibodies to the receptor is inherently difficult for several reasons. For example, the extracellular exposed domains within GPCRs provide limited epitopes, the extracellular region of GPCRs is often highly variable, and it is difficult to prepare functional GPCR antigens [245]. Despite these difficulties, at the beginning of this PhD, a new antibody with specificity for the human and monkey GLP1R, mAb3F52, had just been produced by Novo Nordisk using a hybridoma strategy, and extensively validated for use in immunostaining [116].

The most straight forward strategy for production of GPCR antibodies is to generate antibodies targeting the extracellular domain (ECD), which gives the added benefit of modifying ligand binding. No GLP1R antibodies targeting the mouse GLP1R were available at the outset of this project, thus we sought to produce a new GLP1R antibody targeting both the mouse and human GLP1R. Antagonistic activity of the antibody was also desired to provide an alternative tool to exendin 9-39 for studying GLP1R pharmacology.

2.2 Aims

To generate a novel monoclonal antagonistic antibody for GLP1R with cross-reactivity for the mouse and human GLP1R by:

- a) Naïve phage display using the biotinylated human GLP1R ECD and CHO cells overexpressing mouse GLP1R.
- b) Screening the clones of interest in agonistic and antagonistic cAMP assays in GLP1R overexpressing cell lines.
- c) Affinity maturation of the lead clone of interest to improve affinity for GLP1R.

2.3 Methods

2.3.1 Solutions and Compounds

Assay buffer for the cAMP homogenous time-resolved fluorescence (HTRF) assay was Hanks' balanced salt solution supplemented with 25 mmol/l HEPES, 0.1% (w/v) bovine serum albumin (BSA) (pH 7.4) and 0.5 mmol/l 3-isobutyl-1-methylxanthine (IBMX).

The GLP1R extracellular domain (ECD) was produced in *Escherichia coli*, purified as described previously [246], and biotinylated in-house at MedImmune using EZ-link Sulfo-NHS-LC-Biotin (ThermoFisher Scientific, Loughborough, UK). Unless stated otherwise, chemicals were obtained from Sigma-Aldrich (Poole, UK), and peptides were purchased from Bachem (Bubendorf, Switzerland). The exendin (9-39) acetate salt stock was dissolved in dimethyl sulfoxide (DMSO) to 136 µmol/l. GLP-1 (7-36) was diluted in water to 100 µmol/l.

2.3.2 Bacterial Strains

TG1 cells, CJ236 cells, and DH5 α cells were cultured in 2xTY media (Bactotryptone 16 g/L, Bactoyeast extract 10 g/L, NaCl 5g/L, pH adjusted to 7.0), supplemented according to experimental requirements. pCantab6 was used as the expression vector for single chain variable fragments (Appendix 1).

2.3.3 Cell Culture

All cell lines were maintained at 37°C with 5% CO₂. G22 cells (MedImmune) were maintained in CCM8 media (SAFC) supplemented with 100 mg/l hygromycin B, and 25 mg/l L-methionine sulfoximine (MSX).

Chinese Hamster Ovary (CHO) K1 cells were maintained in Nutrient Mixture F-12 Ham supplemented with 10% FBS, 0.1 units/l penicillin, 0.1 µg/l streptomycin and 2 mmol/l L-glutamine. Stably transfected cell lines overexpressing GPCRs of interest were generated at AstraZeneca (Gothenburg, Sweden) or MedImmune (Cambridge, UK). For experimental use these overexpressing cell lines were thawed from liquid nitrogen stocks directly into assay buffer.

2.3.4 Phage Display Selections

2.3.4.1 Soluble selections

Selections were performed against biotinylated human GLP1R extracellular domain (ECD). For each round of selection, input and output titres of phage were calculated. Phage and magnetic streptavidin beads were blocked for 1 hour in 3% (w/v) skimmed milk powder in PBS (MPBS), rotating at 20 rpm at room temperature. The phage libraries were then deselected against streptavidin beads, following which biotinylated GLP1R ECD was incubated with the phage library for 1 hour. 50 µl of blocked beads

were then mixed with the selection, and equilibrated in a deep well 96 well plate. Beads were washed in 0.1% (v/v) PBS-Tween using the Kingfisher 96, and released into 10 µg/ml trypsin in 0.1 M sodium phosphate buffer. The plates were then incubated for 30 minutes at 37°C, 300 rpm. Eluted phage was used to infect 1-5 ml of TG1 cells in the logarithmic phase of growth, at 37°C and 150 rpm for 1 hour. Selection outputs were plated onto 2xTYAG (100 µg/ml ampicillin, 2% (w/v) glucose) bioassay plates, and incubated overnight at 30°C. Finally, TG1 cells were harvested in 2xTY with 17% (w/v) glycerol, and stored at -80°C.

2.3.4.2 Cell surface selections

Selections were performed on Chinese Hamster Ovary (CHO) cells overexpressing mouse GLP1R (mGLP1R), using 1×10^7 cells per selection blocked in 3% (w/v) MPBS, and 50 µl phage also blocked in 3% (w/v) MPBS. In the washing stage cells were pelleted at 400 g for 1 minute, supernatant removed, and resuspended in 1 ml PBS. This was repeated 8 times. Phage were eluted in 200 µl of 100 µg/ml trypsin in 0.1 M sodium phosphate buffer. Eluted phage were used to infect TG1 cells, as described above. 88 colonies from each selection output were picked for sequencing.

2.3.4.3 Selection Rescue

2xTYAG (100 µg/ml ampicillin, 2% (w/v) glucose) media was inoculated with TG1 cells from selection outputs to a starting OD₆₀₀ of 0.1. Cells were then grown to logarithmic phase, and infected with WT K07 M13 helper phage using a multiplicity of infection (m.o.i) of 10, for one hour at 37°C, 150 rpm. After infection, media was changed to 2xTYAK (100 µg/ml ampicillin, 50 µg/ml kanamycin), and cells were cultured overnight at 25°C, 280rpm. To prepare bacteriophage for further rounds of selection, 1 ml of overnight cultures was centrifuged at max g in a table top centrifuge, and supernatant containing bacteriophage was kept on ice until use.

2.3.4.4 Phage ELISA

Bacteriophage was prepared from 88 individual colonies of selection output, according to the selection rescue protocol, in 96 deep-well plates containing 500 µl appropriate media. In addition, nunc maxisorp plates were coated with 50 µl GLP1R ECD either at 1µg/ml or 10µg/ml overnight at 4°C.

The following day plates were rinsed 3 x in PBS, the plates and phage were then blocked in 3% (w/v) MPBS at room temperature for 1 hour. After a further 3 x wash of antigen plates in PBS, 50 µl phage was added per well for 1 hour. Plates were then washed 3 x with PBS + 0.1% (v/v) Tween20, and phage binding was detected by addition of 50 µl anti-M13-HRP (1:5000 dilution in 3% MPBS) incubated at room temperature for 1 hour. Finally, the plate was washed 3 x with PBS + 0.1% (v/v) Tween20, and developed by addition of 50 µl 3,3',5,5'-tetramethylbenzidine (TMB) substrate. The reaction was

stopped after 20 minutes by addition of 50 µl 0.5 M H₂SO₄. Absorbance at 450nm was measured on the 2104 EnVision® Multilabel Reader.

For the cell based ELISA assays, cells were seeded into 96 well flat bottom plates (Costar), and incubated overnight at 37°C with 5% CO₂. CHO K1, and CHO human GLP1R (hGLP1R) cells were seeded at 10,000 cells/well. CHO mGLP1R cells were seeded at 7,500 cells/well. Prior to use in the ELISA, cells were centrifuged at 485 g for 5 minutes, then washed with PBS, and blocked for 1 hour with 3% (w/v) MPBS. Following blocking, cells were washed once with PBS, and 100 µl of phage also blocked in 3% (w/v) MPBS was added for 1 hour. The plates were then washed twice with PBS, and anti-M13-horseradish peroxidase (HRP) was added to wells as described above. The final wash step was 3 x PBS washes, and the reaction was developed as above.

2.3.4.5 Antibody expression and purification

Variable genes from antibodies of interest were amplified using PCR (primers defined in Appendix 2) and cloned into pEU expression vectors. The heavy chain variable genes were digested with *BssHII* and *BstEII*, then inserted into pEU1.4. Light chain variable genes were digested with *ApaL1* and *Pac1*, then inserted into pEU4.4. DNA quick ligase (New England Biolabs, Hitchin, UK) was used for ligation reactions, and Z competent DH5α cells were transformed. Successful cloning was confirmed using PCR with primers in the pEU backbone, products were loaded in a 1% agarose gel, which was ran at 120V for 30 minutes to check for the presence of an insertion. The insert sequence was then checked using DNA sequencing, and DNA was harvested from successful clones using the QIAGen Midi Prep Plus Kit.

For antibody expression, DNA from the heavy and light chain variable genes was transfected into G22 cells using polyethylenimine (PEI) Max (Polysciences Inc, Warrington, USA). The transfected cells were then incubated for 5-16 hours at 37°C with shaking at 140 rpm, 5% CO₂ and 65% humidity. 30% (v/v) M20a feed media was then added to the cells, and cells were incubated for 1 week at 34°C with shaking at 140 rpm, 5% CO₂ and 70% humidity. Antibody was harvested by centrifugation at 500 g for 30 minutes at 4°C, and filtered using a 0.22 µm steriflip filter. MabSelect SuRe resin (GE Healthcare Bio-sciences, Marlborough, USA) was used for purification, and antibody was eluted either with glycine buffer or 0.1 M sodium citrate (pH3) in the high throughput method. Desalting was then performed using either PD10 columns (GE Healthcare Bio-sciences) or Zeba Spin plates (ThermoFisher Scientific). To confirm successful purification, samples were ran on an SDS PAGE and the gels stained with InstantBlue™ to visualise protein bands. This process was carried out with the help of MedImmune protein expression team.

2.3.5 Phage Display Library Generation

2.3.5.1 Stop template generation and production of uracil containing single stranded DNA (dU-ssDNA)

Mutagenic primers were designed to insert stop templates into the complementarity determining regions (CDRs) of Glp1R0017. Mutagenesis was carried out using the QuikChange II Site-Directed Mutagenesis Kit (Agilent Technologies, Santa Clara, USA) according to the standard protocol. Mutant DNA was used to transform Z competent CJ236 cells, which were plated onto 2xTYAGC (100 µg/ml ampicillin, 2% (w/v) glucose, 10 µg/ml chloramphenicol) petri dishes and incubated overnight at 37°C. Successful mutagenesis was confirmed by Sanger sequencing.

Successful mutant CJ236 colonies were grown to logarithmic phase in 30 ml 2xTYAGC and infected with wild-type M13 KO7 helper phage using an multiplicity of infection (MOI) of 10. To allow infection cells were incubated at 37°C, 300 rpm for 30 minutes. After infection, media was changed to 2xTYAKU (100 µg/ml ampicillin, 50 µg/ml kanamycin, 0.25 µg/ml uridine), and cells were cultured overnight at 37°C, 300 rpm. Cells were pelleted by centrifugation at 26,890 g and 2°C. 1/5 volume 20% (v/v) PEG8000/2.5M NaCl was added to the supernatant and incubated at room temperature for 30 minutes to precipitate phage. Phage were pelleted by centrifugation at 11,950 g and 2°C for 10 mins, supernatant was decanted, before a second centrifugation at 11,950 g and 2°C for 2 mins. The resulting phage pellet was resuspended in 0.5 ml PBS, and any debris was pelleted in a final centrifugation step at 16,200 g for 5 minutes.

dU-ssDNA was harvested from the supernatant using the E.Z.N.A® M13 DNA MiniKit (Omega Biotek, Norcross, USA), and eluted in 50 µl dH₂O. DNA concentration was determined by measuring absorbance at 260nm, and the quality of dU-ssDNA harvested was examined on a 1% (w/v) TAE agarose gel. This process was carried out with the help of R. Fertin.

2.3.5.2 Kunkel mutagenesis

Kunkel mutagenesis relies upon the use of dU-ssDNA as a template, following mutagenesis, the product is transformed into bacteria (TG1) which contain uracil N-glycosidase which will destroy the template DNA, which will then be replaced by replication the mutant strand template.

For each library a single mutagenic primer was designed to randomise blocks of up to 6 consecutive amino acids using NNS codons (where N = A/G/C/T, S = C/G) within degenerate oligonucleotides. 0.7 µg of each mutagenic oligonucleotide was phosphorylated using 20 units of T4 polynucleotide kinase. Each reaction used 1 x TM buffer, 1 mM ATP, 5 mM DTT. Reactions were incubated at 37°C for 1 hour. Phosphorylation products were annealed to 20 µg template dU-ssDNA by incubation at 90°C for 2

minutes, 50°C for 3 minutes and 20°C for 5 minutes. Following this, 30 units T4 DNA ligase, 30 units T4 DNA polymerase, 0.33 mM ATP, 0.83 mM dNTPs and 5 mM DTT were added to the reaction for incubation at 20°C for 3 hours. Reaction products were affinity purified using either the Roche High PCR Product Purification Kit or Machery-Nagel Nucleospin Gel and PCR clean up kit according to manufacturer's instructions.

2.3.5.3 Preparation of electrocompetent TG1 cells and electroporation

TG1 cells were grown to logarithmic phase in 400 ml 2xTY media, then chilled on ice for 30 minutes prior to centrifugation at 2,700 g for 15 minutes at 2°C. The cell pellet was resuspended in 300 ml ice-cold Milli-Q water. Cells were then pelleted by centrifugation at 2,700 g for 15 minutes at 2°C. The wash and centrifugation steps were repeated, cells were then resuspended in 50 ml Milli-Q water, and centrifuged in 50 ml falcon tubes at 2,210 g for 10 minutes at 4°C. The supernatant was then discarded, and a further 50 ml wash was completed. Cells were resuspended in the remaining liquid, to yield 2 ml electrocompetent cells per library. Cells were kept on ice, and electroporated immediately.

5 x 400 µl of cells were electroporated per library in electroporation cuvettes with a 0.2 cm electrode gap width. Electroporation settings of 2.5 kV field strength, 200 Ω resistance, 25 µF capacitance were used. The time constant was approximately 5 ms. Immediately after electroporation, 1 ml 2xTYG (2% (w/v) glucose) was added to each cuvette, and cells were transferred to a 50 ml falcon tube, cuvettes then further rinsed with 1 ml 2xTYG. Cells were then incubated at 37°C, 150 rpm for 1 hour.

The total library size was determined by plating a dilution series on 2xTYAG petri dishes. The remaining cells were plated on a 2xTYAG bioassay plate. Following overnight incubation at 30°C, libraries were scraped into 10 ml 2xTY with 17% (w/v) glycerol, and stored at -80°C.

2.3.5.4 Library Rescue

For each library, cells were grown to logarithmic phase in 400 ml 2xTYAG, and then infected with M13KO7^{trp} helper phage at an m.o.i of 10, for 1 hour at 37°C, 150 rpm. The cells were then centrifuged at 2,643 g for 15 minutes at room temperature and resuspended in 400 ml 2xTYAK for overnight culture at 25°C, 280 rpm.

The cells were collected by centrifugation at 10,820 g for 20 minutes at 4°C. 120 ml of chilled 20% (v/v) PEG8000 / 2.5 M NaCl was then added to the supernatant and incubated on ice for 1 hour. The bacteriophage was pelleted by centrifugation at 10,820 g for 20 minutes at 4°C, resuspended in 10 ml TE buffer (pH 8.0) and centrifuged at 14,460 g for 15 min at 4 °C. 3 ml chilled 20% (v/v) PEG8000 / 2.5 M NaCl was added to the supernatant, then incubated on ice for 1 hour. The bacteriophage was pelleted by centrifugation at 14,460 g for 20 minutes at 4°C, then resuspended in 2 ml PBS. A final

centrifugation of 14,460 g for 10 minutes at 4°C was used to pellet bacterial debris. The bacteriophage in supernatant was stored at 4°C until used.

2.3.6 Cell Based Assays

2.3.6.1 cAMP Homogenous Time Resolved Fluorescence (HTRF) Accumulation Assay

Control peptides and antibody were serially diluted in assay buffer, and plated using an ECHO525 acoustic liquid handler (Labcyte, Sunnyvale, CA, USA) to give 11-point dose response curves in 384 well plates. Overexpressing cell lines resuspended in assay buffer, at a density dependent on the cell line (Appendix 3), were then combined with the test compounds. For agonism experiments, cAMP was measured after 30 minutes of incubation at room temperature. For antagonism experiments, an agonist challenge was given after 15 minutes using the ECHO550 acoustic liquid handler (Labcyte), and samples were mixed by centrifugation at 150 g for 1 minute. After a further 30 minute incubation at room temperature, cAMP was measured. Cellular cAMP levels were measured using the cAMP dynamic 2 HTRF kit (Cisbio, Codolet, France) according to the manufacturer's recommendations. Plates were read on an EnVision plate reader (PerkinElmer, Waltham, MA, USA) after 1 hour. Non-linear regression was used to calculate EC₅₀ and IC₅₀ values.

2.4 Results

2.4.1 Naïve Phage Display Selection of GLP1R antibodies

Antibodies targeting GLP1R were generated using a naïve antibody phage display selection approach. M13 bacteriophage provide an excellent system for antibody development as the surface proteins are directly encoded by genes which are packaged within the bacteriophage. This attribute means that genes can be cloned and packaged in bacteriophage with the expressed proteins displayed on the surface of the phage, enabling the selection of desired genes based on the binding properties of the respective proteins [247]. For antibody phage display, single chain variable fragment (ScFv) recombinant genes are packaged into the bacteriophage. In comparison to an IgG structure, a ScFv is composed of V_H and V_L antibody domain connected by a flexible linker (Figure 2.1).

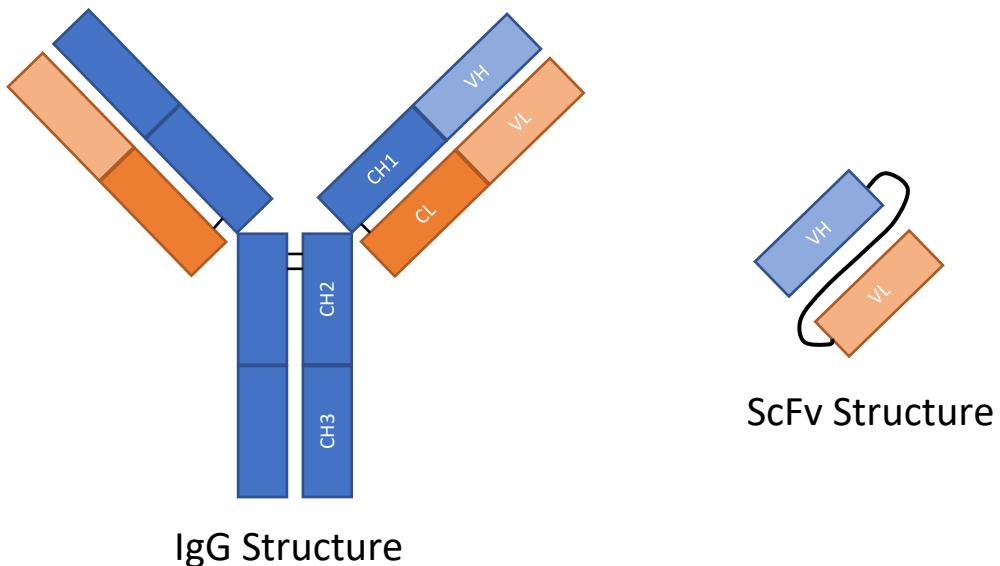


Figure 2.1 Schematic diagram of IgG and ScFv structure. The variable domains from the IgG structure (V_H and V_L) are connected by a flexible linker to form a ScFv used for antibody phage display.

For antibody phage display, bacteriophage have been engineered using phage display vectors (e.g. pCantab6) to contain the recombinant ScFv gene upstream of gene 3, meaning the ScFv fragment is fused to the pIII coat protein on the surface of bacteriophage. Large libraries of ScFv's have been created by manipulating DNA, which enables selection of antibodies to 'all' targets [248]. ScFv's that bind to the target antigen are isolated by antigen-guided selection, followed by collection and propagation of bound phage then repeated rounds of antigen-guided selections [247, 249] (Figure 2.2).

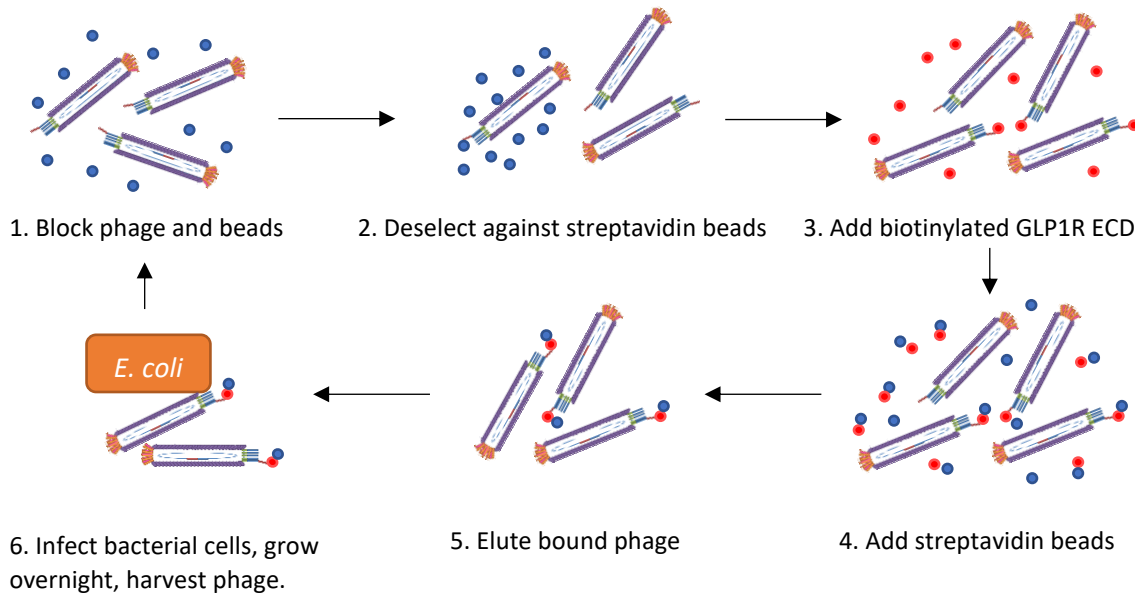


Figure 2.2 Summary of bacteriophage display process. Bacteriophage display utilises engineered bacteriophage, which express ScFv's fused to the PIII coat protein of M13 filamentous bacteriophage. Each bacteriophage expresses a singular ScFv determined by the phagemid sequence. Bacteriophage bound to the target biotinylated antigen are separated out using magnetic streptavidin beads, then used to infect the *E. coli* bacterial strain TG1. Transformed bacteria, containing the phagemids of interest, are then used to produce a fresh pool of bacteriophage for further rounds of selection.

For the generation of cross-reactive human and mouse GLP1R antibodies, four naïve bacteriophage libraries were used; BoneMarrowVault_{trp} (BMV_{trp}) which contains variable genes isolated from bone marrow, CombinedSpleen_{trp} (CS_{trp}) which contains variable genes isolated from a combined spleen library, and two semi-synthetic libraries, DP47_{trp} based on the V_H3 framework of the DP-47 gene segment also known as immunoglobulin heavy variable 3-23, and Long V_H CDR3_{trp} (LH3_{trp}) library, composed of ScFv's with long CDR3 regions.

Each of these libraries was used in a series of selections; first on 100 nmol/l biotinylated human GLP1R ECD, then 50 nmol/l biotinylated human GLP1R ECD, followed by cell surface selections on mouse GLP1R overexpressing CHO cells (Figure 2.3). Output titres were calculated at each round of selection, and at the third round of selection clone diversity and enrichment was assessed by sequencing (Table 2.1).

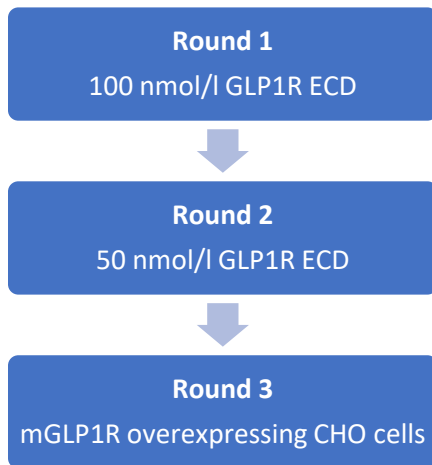


Figure 2.3 Schematic representation of selection strategy used for naïve phage display. Selections were performed using four naïve phage display libraries: BMV_{trp}, CS_{trp}, DP47_{trp}, and LH3_{trp}.

Round of selection	Output Titre (cfu/ml)				Sequence Diversity (%)
	BMV _{trp}	CS _{trp}	DP47 _{trp}	LH3 _{trp}	
1	~10 ⁴	~10 ⁴	~10 ⁴	~10 ⁴	N/A
2	10 ⁴	2.4 × 10 ⁴	1.7 × 10 ⁴	2.3 × 10 ⁴	N/A
3	3.1 × 10 ³			N/A	23%

Tables 2.1 Output titres and sequence diversity of initial phage display selection strategy. Round 1 of selection used 100 nmol/l biotinylated human GLP1R ECD, round 2 used 50 nmol/l biotinylated human GLP1R ECD, and round 3 used CHO cells overexpressing the mouse GLP1R. The % sequence diversity was calculated from the number of different HCDR3 sequences within 88 clones.

The output titre at each round of selection is expected to be between 10³ – 10⁶ colony forming units (cfu) per ml. An increase in the output titre may suggest an enrichment of binders. In contrast, when the output titre drops below 10³ cfu/ml this indicates that the selection pressure has been too harsh, and the selection should be assessed. Initially following round 2 of selection (Figure 2.3), the BMV_{trp}, CS_{trp}, and DP47_{trp} selection outputs were pooled to save resource in selections. However, this resulted in a low diversity in sequencing at round 3 of selection (Table 2.1).

To increase the chance of isolating unique clones that specifically bind to the mouse GLP1R, further selections were performed using the CHO mGLP1R cells. Each selection output from round 2 was used individually in the additional round 3 selections. Again, output titre and sequencing diversity was assessed for each output. Overall, sequencing diversity of clones that bind mGLP1R was increased (Table 2.2).

	BMV_{trp}	CS_{trp}	DP47_{trp}	LH3_{trp}
CHO mGLP1R selection. Output titre (cfu/ml)	4.3×10^5	4.4×10^4	3.6×10^5	2.6×10^5
Parental CHO selection. Output titre (cfu/ml)	4×10^4	3.3×10^3	9.0×10^3	3.2×10^4
Fold difference	10.75	13.33	40	8.13
Sequence diversity (%)	11%	20.5%	13%	30%

Tables 2.2 Output titres and sequence diversity of further phage display selections on CHO mGLP1R cells. As a negative control, selections were also performed on the parental CHO cell line. The fold difference displays the difference in output titres between parental CHO and CHO mGLP1R selections.

2.4.2 Identification of ScFv's of interest

To determine the clones of interest for functional screening, binding properties of ScFv's were assessed and sequencing was analysed. Binding properties of the round 3 pooled selection output were assessed using phage ELISA, with either hGLP1R ECD, mGLP1R overexpressing cells or hGLP1R overexpressing cells. Antigen-bound phage was detected with an anti-M13 antibody conjugated to horseradish peroxidase (HRP). A number of weak binders were detected in the cell based phage ELISAs, with a small signal window over the parental CHO K1 cell line. In comparison, several of the clones showed a robust signal with the human GLP1R ECD, indicating binding (Figure 2.4).

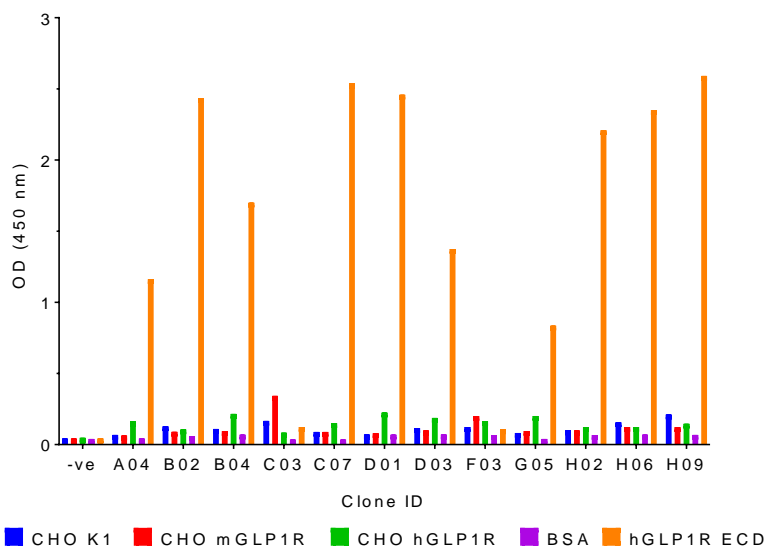


Figure 2.4 Clones of interest determined by phage ELISA. Binding of the pooled round 3 CHO mGLP1R cell selection outputs to hGLP1R and mGLP1R was assessed using phage ELISA. OD (450 nm) is displayed for the clones which were taken forward for ScFv production.

Analysis of sequencing from the round 3 pooled selection output revealed three dominant clones (C03, A04 and B04), all of which were positive in the phage ELISA, and consequently selected for functional analysis. In addition, clones with specific sequences that produced a signal in the phage ELISA were selected for functional analysis (Table 2.3 and Figure 2.4).

Selection description	Sequencing ID	No. of Sequence Copies	ScFv Nickname
R3, libraries pooled	ZZ1LSB-A04	12	Glp1R0001
R3, libraries pooled	ZZ1LSB-B02	2	Glp1R0002
R3, libraries pooled	ZZ1LSB-B04	12	Glp1R0003
R3, libraries pooled	ZZ1LSB-C03	42	Glp1R0004
R3, libraries pooled	ZZ1LSB-C07	1	Glp1R0005
R3, libraries pooled	ZZ1LSB-D01	1	Glp1R0006
R3, libraries pooled	ZZ1LSB-D03	1	Glp1R0007
R3, libraries pooled	ZZ1LSB-F03	1	Glp1R0008
R3, libraries pooled	ZZ1LSB-G05	1	Glp1R0009
R3, libraries pooled	ZZ1LSB-H02	1	Glp1R0010
R3, libraries pooled	ZZ1LSB-H06	1	Glp1R0011
R3, libraries pooled	ZZ1LSB-H09	1	Glp1R0012
R3, BMV _{trp}	ZZ1LUF-D07	5	Glp1R0016
R3, BMV _{trp}	ZZ1LUF-B08	7	Glp1R0015
R3, BMV _{trp}	ZZ1LUF-B02	3	Glp1R0014
R3, CS _{trp}	ZZ1LUE-B09	3	Glp1R0019
R3, CS _{trp}	ZZ1LUE-G10	17	Glp1R0022
R3, CS _{trp}	ZZ1LUE-D10	18	Glp1R0021
R3, CS _{trp}	ZZ1LUE-B02	3	Glp1R0018
R3, CS _{trp}	ZZ1LUE-A11	12	Glp1R0017
R3, CS _{trp}	ZZ1LUE-D08	5	Glp1R0020
R3, LH3 _{trp}	ZZ1LUC-E06	6	Glp1R0025
R3, LH3 _{trp}	ZZ1LUC-H03	3	Glp1R0027
R3, LH3 _{trp}	ZZ1LUC-B06	27	Glp1R0024
R3, LH3 _{trp}	ZZ1LUC-A07	8	Glp1R0023
R3, LH3 _{trp}	ZZ1LUC-H06	3	Glp1R0028

Table 2.3 Details of clones selected for ScFv purification based on ELISA and sequencing data.
88 clones were sequenced per selection output, therefore number of sequence copies is out of a total of 88 possible sequences. From now on, clones will be referred to by the ScFv nickname.

As the phage ELISA assay had several limitations (detailed in discussion), clones of interest from the extra mGLP1R cell selections were determined solely by sequencing analysis. Sequences with more than three replicates in the selection outputs were selected for functional analysis, with the hypothesis that replicated sequences have improved binding compared to unique sequences (Table 2.3). Overall 26 ScFv clones were selected for functional analysis, and each was purified using immobilised metal ion affinity chromatography by the BET Team at MedImmune.

2.4.3 Screening of clones of interest in cAMP assays

The ability of ScFv's to agonise the mGLP1R and thus stimulate cAMP signalling was assessed in a cell-based homogenous time resolved fluorescence (HTRF) assay. None of the selected ScFv's displayed agonistic activity on the mGLP1R (Figure 2.5a).

The ability of ScFv's to antagonise GLP-1 stimulated cAMP production was also assessed. Seven unique ScFv's were identified as antagonistic for the mGLP1R upon screening, of which Glp1R0017 had the lowest IC₅₀ value of 238 nmol/l (Figure 2.5b, 2.5c). Based on reproducibility of cAMP antagonistic activity Glp1R0017, Glp1R0020, Glp1R0025 and Glp1R0015 were selected for conversion into humanised IgG's (hIgG1.TM format) by the BET Team at MedImmune. Upon conversion of Glp1R0015, a glycosylation site was identified within the antibody framework therefore Glp1R0015 was discarded.

Following conversion into the IgG1 format, cAMP agonistic and antagonistic activity was determined in the mGLP1R cell line. Again, none of the antibodies exhibited agonistic activity (Figure 2.6a). All three antibodies retained antagonistic activity, and increased in potency. Glp1R0017 was the most potent IgG, with an IC₅₀ of 5.2 nmol/l (Figure 2.6b), and was selected as the lead antibody for further characterisation and lead optimisation.

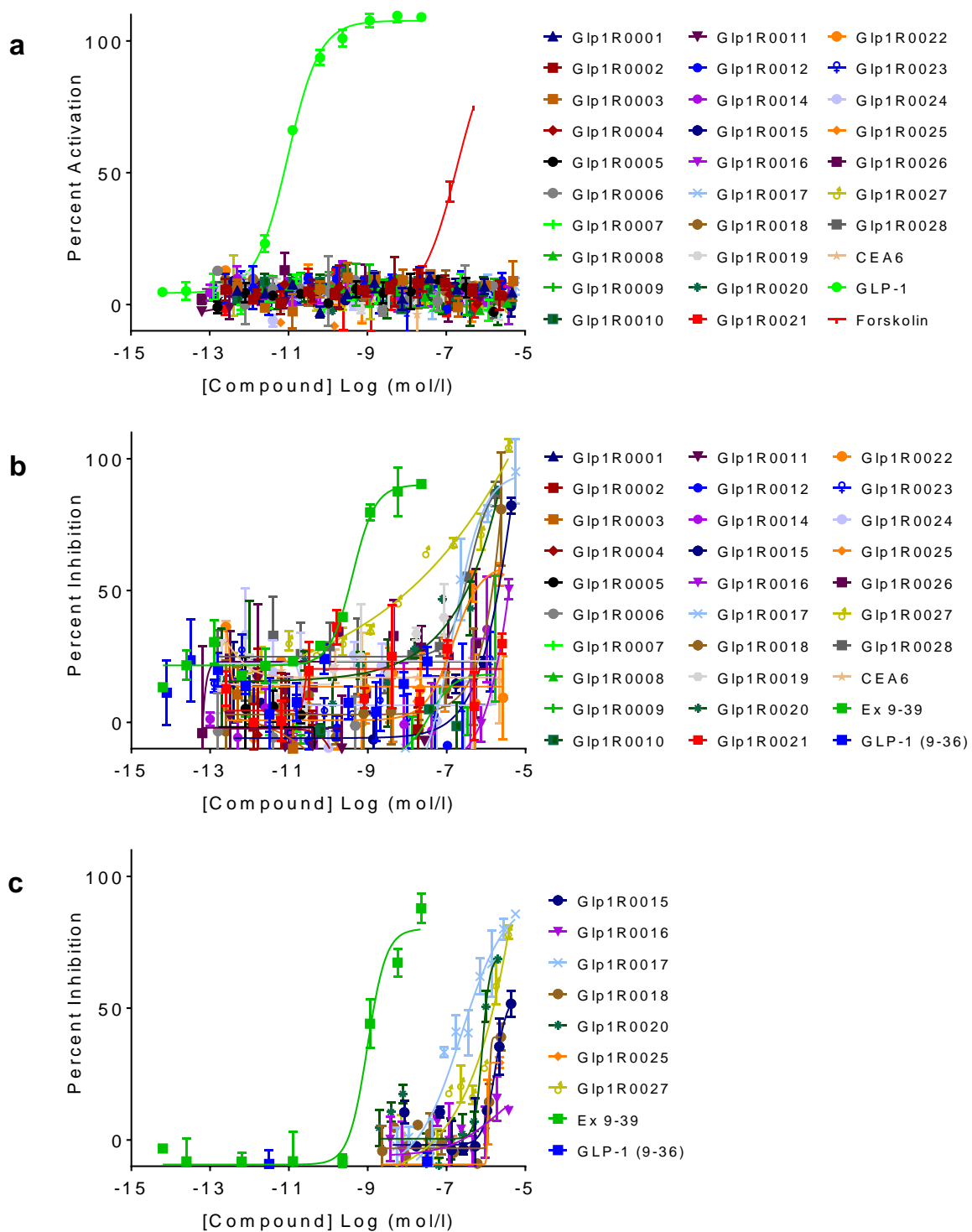


Figure 2.5 ScFv screening in CHO mGLP1R cells reveals four clones of interest for conversion into IgG format. (a) Agonism activity of ScFvs is displayed as % activation of the maximal GLP-1 response. No agonistic activity was observed for the ScFvs screened. (b) Antagonism activity of ScFvs in initial screening. Antagonistic activity is displayed as % inhibition of the GLP-1 EC₈₀ response. (c) Antagonism activity of selected ScFvs in second round of antagonism screening. Data are mean ± SD from duplicate wells.

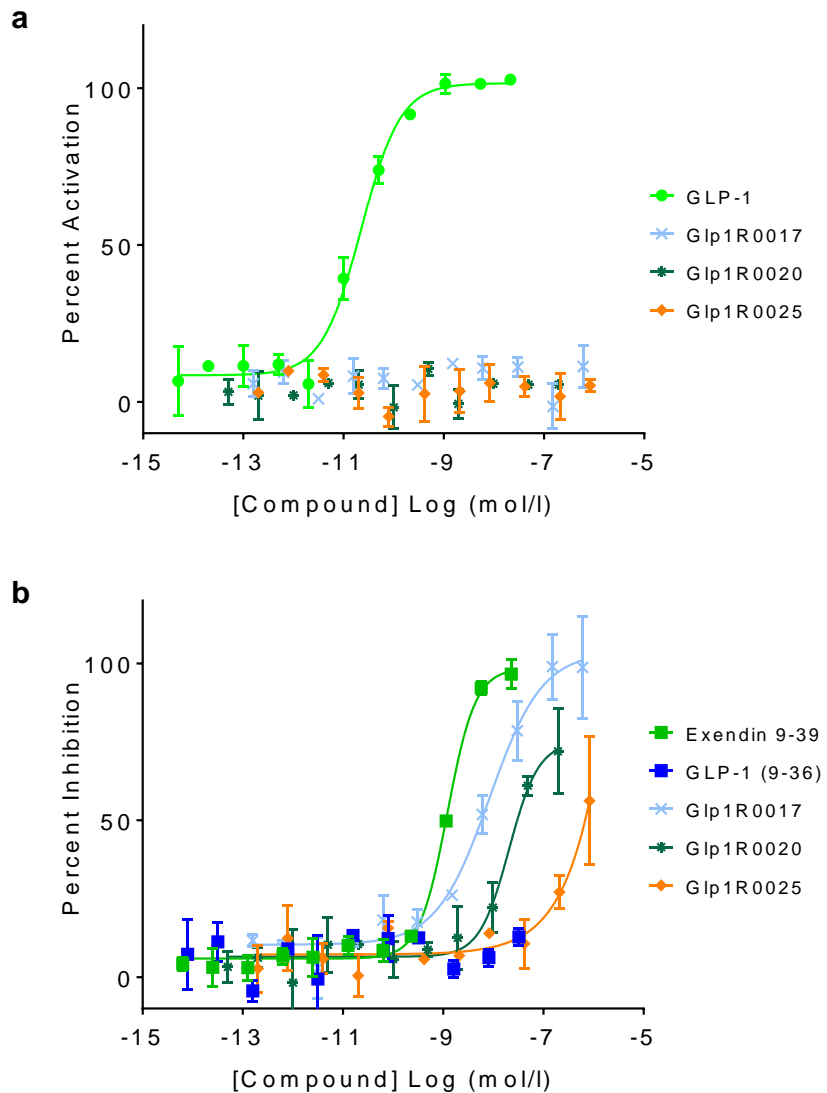


Figure 2.6 IgG screening in CHO mGLP1R cells. (a) Agonism activity of IgGs displayed as % activation of the maximal GLP-1 response. (b) Antagonism activity of IgGs displayed as % inhibition of the GLP-1 EC₈₀ response. Data are mean \pm SD from duplicate wells, and the data shown are representative of at least three separate experiments.

2.4.4 Affinity maturation of Glp1R0017

In an attempt to improve the affinity of Glp1R0017 for the GLP1R, mutant libraries were made in the complementarity determining regions (CDRs) which are responsible for antigen binding. IgG's have three CDR regions in both the heavy and light chain, with the CDR3 regions often being responsible for stabilisation of antigen binding [250, 251]. For this reason, both CDR3 regions were targeted in our affinity maturation approach. Upon comparison of the remaining CDR regions, the HCDR2 region of Glp1R0017 is the longest, containing 17 amino acids. This provides the highest possibility for mutations, and was therefore also chosen for affinity maturation.

In total 8 ScFv phage display libraries targeting HCDR2, HCDR3 and LCDR3 were generated. Four overlapping libraries were constructed in HCDR3, and two overlapping libraries were constructed in LCDR3 to ensure full coverage. As HCDR2 is predicted to be less critical for antigen binding, only two libraries were constructed in the central region of this CDR. Kunkel mutagenesis readily generates mutant libraries of 10^9 clones, which covers the theoretical diversity of randomising 6 codons. For each library, Kunkel mutagenesis was used to replace 6 consecutive codons with NNS codons (where N = A/C/G/T, S = C/G), allowing for inclusion of any amino acid at the targeted positions. Prior to use in phage display selections, the size and quality of each library was assessed (Table 2.4). All libraries were larger than 10^8 , and therefore each library was taken forward for phage display selections.

Each library was used in a series of selections (Figure 2.7); the first three rounds were against biotinylated human GLP1R ECD at 20 nmol/l, then 5 nmol/l and 1 nmol/l. Output titres were calculated for each round of selection (Table 2.5). Sequencing assessment at round 3 showed all the clones in library HCDR3.3 were the parental Glp1R0017, consequently this library was discarded. For the fourth round of selection, using mGLP1R overexpressing CHO cells, the HCDR2 libraries were pooled due to the lower sequence diversity. The HCDR3.1 and HCDR3.2 libraries were also pooled.

Library	Total size (from counting)	No. of stop templates	No. of poor sequences	No. of frameshifts	No. of uniques	Actual Library Size
HCDR2.1	5.2×10^9	20/88	4/88	2/88	58/88	3.4×10^9
HCDR2.2	1.7×10^{10}	24/88	1/88	7/88	53/88	1×10^{10}
HCDR3.1	3.6×10^9	50/88	4/88	18/88	16/88	6.6×10^8
HCDR3.2	9.3×10^8	54/88	2/88	12/88	19/88	2×10^8
HCDR3.3	6.3×10^9	22/88	6/88	13/88	47/88	3.4×10^9
HCDR3.4	8.3×10^9	36/88	3/88	22/88	25/88	2.4×10^9
LCDR3.1	3.8×10^9	35/88	14/88	7/88	21/88	9×10^8
LCDR3.2	1.4×10^9	26/88	12/88	9/88	38/88	6×10^8

Table 2.4 Diversity of phage display libraries generated for affinity maturation of Glp1R0017. To assess the quality of libraries generated for affinity maturation, the size was determined by counting, and then 88 colonies from each library were picked for sequencing to assess diversity. The column displaying the number of stop templates shows the number of sequences that contained a stop codon within the CDR. The actual library size was calculated using the proportion of unique sequences within the total library size.

	Output Titre (cfu/ml)					Sequence Diversity (%)	
	R1	R2	R3	R4	R5	R3	R5
HCDR2.1	7.9×10^5	4.0×10^5	4.5×10^5	6.6×10^4	1.2×10^5	36%	25%
HCDR2.2	5.6×10^7	1.1×10^6	4.4×10^5			27%	
HCDR3.1	5.6×10^6	1.4×10^6	5.6×10^5	7.4×10^4	7.4×10^5	39%	/
HCDR3.2	3.3×10^5	4.8×10^5	2.0×10^5			20%	
HCDR3.3	1.9×10^6	5.5×10^5	2.5×10^5	/	/	0%	/
HCDR3.4	1.7×10^6	2.6×10^5	2.9×10^5	4.2×10^4	8.0×10^4	73%	61%
LCDR3.1	5.1×10^7	2.6×10^6	9.9×10^5	6.6×10^4	4.2×10^5	36%	68%
LCDR3.2	9.4×10^6	3.2×10^5	1.4×10^5	3.3×10^4	4.9×10^4	84%	93%

Tables 2.5 Output titres and sequence diversity of selections from affinity maturation of Glp1R0017. Rounds 1, 2 and 3 of selection used 20 nmol/l, 5 nmol/l and 1 nmol/l of biotinylated human GLP1R ECD respectively. Round 4 of selection was performed on mGLP1R overexpressing CHO cells. In the fifth round of selection 100 pmol/l biotinylated human GLP1R ECD was used. The % sequence diversity was calculated from the number of unique sequences within 44 clones. The sequencing diversity of the HCDR3.1/HCDR3.2 pooled library was not assessed at round 5 due to a lack of signal window over the negative control selection.

To further push the selections, a fifth round of selection was performed against biotinylated human GLP1R ECD at 100 pmol/l. Finally, for the sixth round of selection, all libraries were pooled, and used in ‘competitive’ phage display selections with 50 pmol/l biotinylated human GLP1R ECD (Figure 2.7). To describe briefly, antigen-bound phage were competed off by overnight incubation with a $10 - 10^5$ molar excess of Glp1R0017. Output titres for these ‘competitive’ selections ranged from 7×10^3 to 5×10^4 , and sequencing diversity was assessed.

Sequencing data from round 3, 5 and 6 selection outputs were combined, and potential clones of interest were selected based either on the number of copies within different rounds of selection, or observation of a shorter recurring sequence between different clones (Table 2.6). The amino acid sequence has not been shown due to MedImmune confidentiality. Seventeen clones of interest were identified (Glp1R0037 – Glp1R0054), and then converted into the IgG1 format for functional screening.

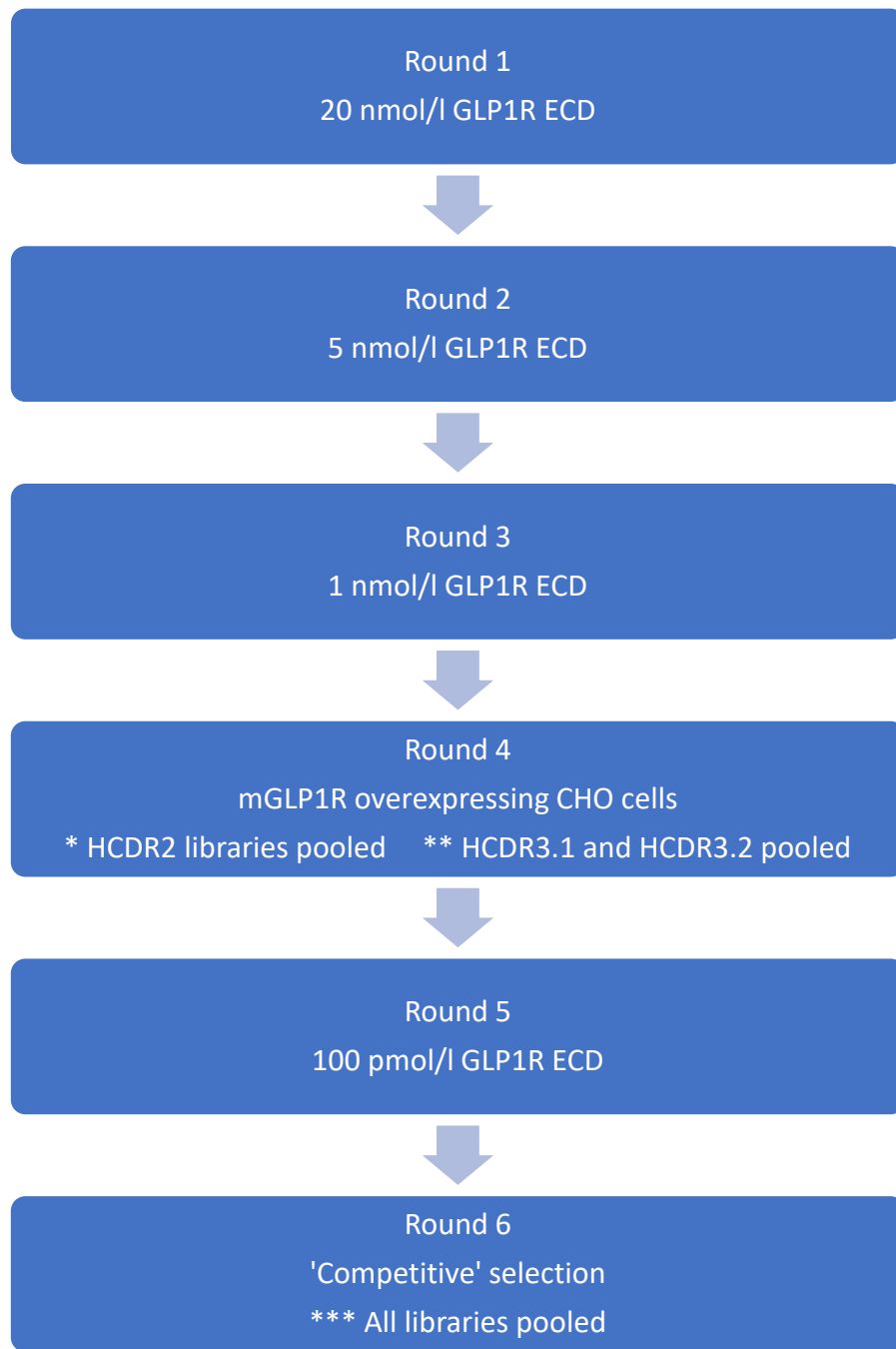


Figure 2.7 Schematic representation of selection strategy used for Glp1R0017 affinity maturation. Selections were performed using libraries over HCDR2, HCDR3 and LCDR3. Libraries were pooled at the stages indicated. The 'competitive' selection used 50 pmol/l biotinylated human GLP1R ECD, and antigen-bound phage were competed off by overnight incubation with a $10 - 10^5$ molar excess of Glp1R0017.

Sequencing ID	CDR region	Reason for selection	IgG Nickname
ZZ1YAG-F08	LCDR3.1	2 copies in round 5 output	Glp1R0052
ZZ1YAG-A06	LCDR3.2	2 copies in round 5 output	Glp1R0050
ZZ1YAG-A04	LCDR3.2	EDL replicated	Glp1R0049
ZZ1YAG-G04	LCDR3.2	HLHV replicated	Glp1R0054
ZZ1YAG-B11	LCDR3.1	RDLRT duplicated	Glp1R0039
ZZ1YAG-G06	LCDR3.1	4 copies of SWSD	Glp1R0040
ZZ1YAG-G10	LCDR3.1	QELD duplicated	Glp1R0053
ZZ1YAH-G04	HCDR2	2 copies in round 3 output 3 copies in round 5 output 1 copy in round 6 output	Glp1R0044
ZZ1YAH-E05	HCDR2	2 copies in round 3 output 4 copies in round 5 output	Glp1R0042
ZZ1YAH-H02	HCDR2	1 copy in round 3 output 1 copy in round 5 output	Glp1R0046
ZZ1YAH-F06	HCDR3	2 copies in round 5 output (4 copies of VGPL)	Glp1R0043
ZZ1YAH-C08	HCDR3	2 copies in round 5 output (3 copies of GYPRD)	Glp1R0041
ZZ1YAH-H08	HCDR3	2 copies in round 5 output (3 copies of SEI)	Glp1R0048
ZZ1YAH-H06	HCDR3	2 copies in round 5 output (4 copies of MGFP)	Glp1R0047
ZZ1YA9-G11	HCDR3	11 copies in round 6 output	Glp1R0045
ZZ1YA9-A04	HCDR2	3 copies in round 6 output	Glp1R0037
ZZ1YA9-A08	HCDR3	2 copies in round 6 output	Glp1R0038

Table 2.6 Details of clones selected for IgG purification from Glp1R0017 affinity maturation. 44 clones were sequenced per selection output, therefore number of sequence copies is out of a total of 44 possible sequences. From now on, clones will be referred to by the IgG nickname.

2.4.5 Screening of Glp1R0017 affinity maturation products

Glp1R0039 failed to convert into the IgG1 format, therefore only sixteen of the seventeen affinity maturation products were screened for functional activity on both the mGLP1R and hGLP1R. Firstly it was confirmed that none of the affinity maturation products showed agonism in the mGLP1R or hGLP1R cell line (data not shown).

When antagonistic activity was assessed on mGLP1R, all of the affinity maturation productions displayed antagonistic activity (Figure 2.8a), with all of the IC₅₀ values being within 2-fold of Glp1R0017 activity (Table 2.7). This suggests that affinity maturation was unsuccessful. However, when antagonistic activity was assessed in the hGLP1R cell line, the majority of affinity maturation products showed a greater than 2-fold improvement in IC₅₀ (Figure 2.8b and Table 2.7). The two antibodies with the largest improvement in affinity were Glp1R0047 (hGLP1R IC₅₀ = 7.9 nmol/l) and Glp1R0048 (hGLP1R IC₅₀ = 7.2 nmol/l). It should be noted that Glp1R0017 has approximately a 10-fold lower IC₅₀ value on the human GLP1R compared to the mouse GLP1R, therefore the affinity improved antibodies remain in the nanomolar affinity range.

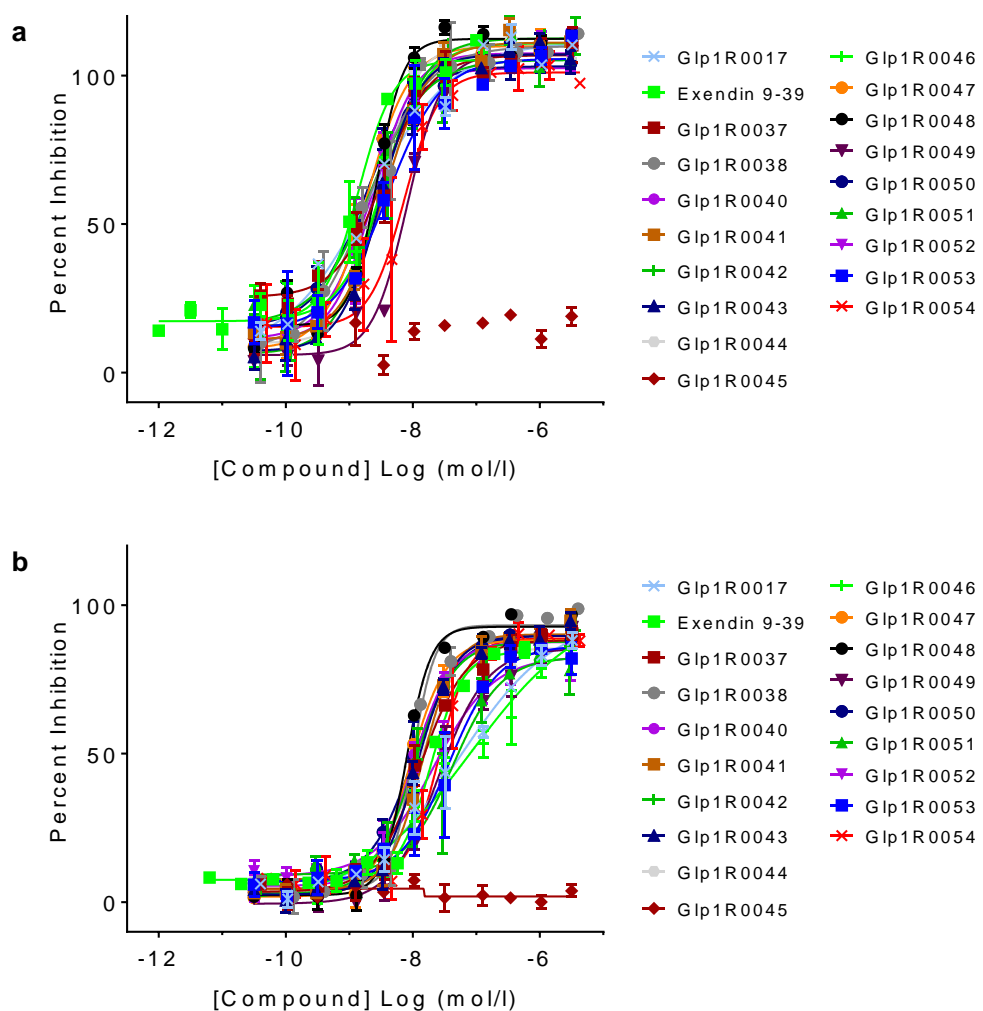


Figure 2.8 Antagonistic activity of Glp1R0017 affinity maturation products in mGLP1R and hGLP1R expressing cells. (a) Antagonism activity of IgGs in mGLP1R expressing cells displayed as % inhibition of the GLP-1 EC₈₀ response. (b) Antagonism activity of IgGs in hGLP1R expressing cells displayed as % inhibition of the GLP-1 EC₈₀ response. Data are mean ± SD from duplicate wells, and the data shown are representative of at least two independent experiments.

	Average IC ₅₀ (mol/l)		Fold improvement over Glp1R0017	
	Mouse GLP1R	Human GLP1R	Mouse GLP1R	Human GLP1R
Glp1R0017	2.15E-09	4.97E-08	1.00	1.00
Glp1R0037	2.43E-09	1.14E-08	0.89	4.35
Glp1R0038	1.33E-09	8.9E-09	1.62	5.59
Glp1R0040	2.08E-09	1.13E-08	1.04	4.40
Glp1R0041	3.31E-09	1.31E-08	0.65	3.81
Glp1R0042	2.14E-09	1.04E-08	1.01	4.78
Glp1R0043	2.77E-09	1.07E-08	0.78	4.64
Glp1R0044	2.30E-09	1.15E-08	0.94	4.34
Glp1R0045	/	/	/	/
Glp1R0046	2.68E-09	6.68E-08	0.80	0.74
Glp1R0047	1.60E-09	7.88E-09	1.35	6.31
Glp1R0048	2.09E-09	7.23E-09	1.03	6.87
Glp1R0049	5.02E-09	2.15E-08	0.43	2.32
Glp1R0050	1.92E-09	9.22E-09	1.12	5.39
Glp1R0051	1.82E-09	3.01E-08	1.18	1.65
Glp1R0052	2.03E-09	2.51E-08	1.06	1.98
Glp1R0053	4.59E-09	2.98E-08	0.47	1.67
Glp1R0054	7.42E-09	2.35E-08	0.29	2.12

Table 2.7 Average IC₅₀ values of affinity maturation products on mouse and human GLP1R, together with fold improvement over the Glp1R0017 IC₅₀. The average IC₅₀ value was determined from n=3 for the mouse GLP1R cell line, and n=2 for the human GLP1R cell line.

To increase the chance of isolating an antibody with increased potency for both the mGLP1R and hGLP1R, more clones were selected for screening from the fifth round of phage display selection. The round 5 selection outputs were chosen as the output titre window at this round, when using 100 pmol/l of the biotinylated human GLP1R ECD, remained high. This demonstrates that ScFv's were binding to 100 pmol/l of the antigen. In comparison, the lowest concentration of the ECD used in naïve phage display to select Glp1R0017 was 50 nmol/l. This observed binding to 100 pmol/l of antigen suggested that antibodies would be present in the round 5 output that bind to the antigen with a higher affinity than Glp1R0017.

To screen clones from the round 5 output, the heavy and light chain variable fragments from each library were cloned into IgG expression vectors. Sequences of the cloning products were then determined, 44 new unique clones were found with mutations in the heavy chain, and 65 unique clones were found with mutations in the light chain. A high-throughput expression and purification method was then used to harvest a total of 109 new antibodies in the IgG1 format for screening (in collaboration with the BET Team, MedImmune).

Screening was performed for antagonism of both the mGLP1R and hGLP1R. The mean IC₅₀ values were calculated, followed by the fold improvement over Glp1R0017 IC₅₀. Within this set of screening, the antagonistic activity of the affinity maturation products clustered around a 2-fold improvement on the hGLP1R when compared to Glp1R0017 (Figure 2.9). On the mGLP1R, antagonistic activity showed little improvement compared to Glp1R0017 with the maximal fold improvement being 2.1-fold.

Overall this affinity maturation approach was not able to significantly improve the potency of Glp1R0017 for mGLP1R, therefore Glp1R0017 was scaled up and taken forward for further characterisation (Chapter 3).

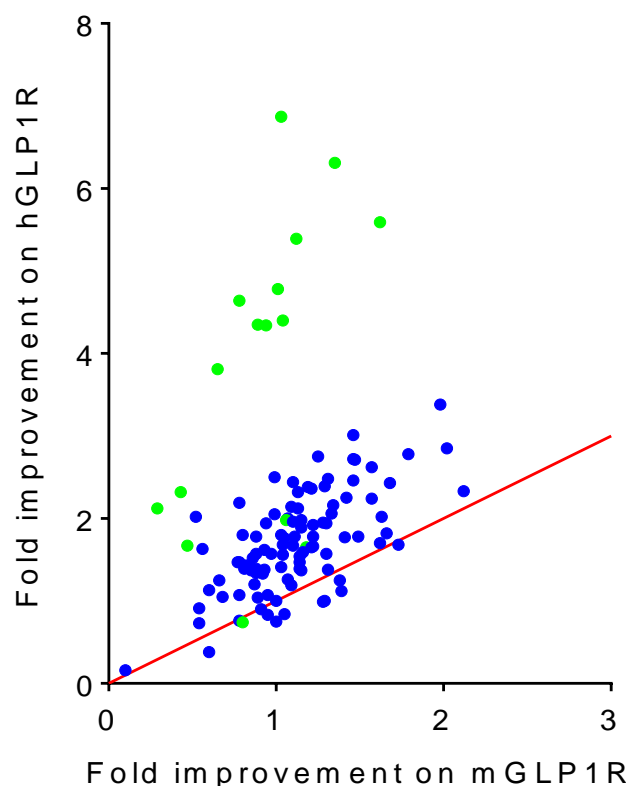


Figure 2.9 Summary of affinity maturation fold improvements in antagonistic activity. IC₅₀ values from at least two independent experiments were averaged, and the fold improvement over Glp1R0017 calculated. Green points display summary data from the initial round of screening, blue points display summary data from the second round of screening. Overall the affinity maturation products showed a greater improvement in antagonism of hGLP1R compared to mGLP1R.

2.5 Discussion

2.5.1 Phage Display for Antibody Production

In this study, a monoclonal antibody to GLP1R with antagonistic activity has been developed using naïve phage display. Within the phage display selection process, human GLP1R ECD and mouse GLP1R expressing CHO cells were used as antigen in subsequent rounds of selection. This has enabled the production of an antibody with antagonistic activity on both the human and mouse GLP1R (Figure 2.8 and Table 2.7).

Whilst this work was being completed, Novo Nordisk published a mouse GLP1R selective antibody (7F38A2), complementing the human/monkey GLP1R antibody (mAb3F52) [252]. The ability of mAb3F52 to block activation of the human GLP1R *in vitro* was also demonstrated during the course of this study [253]. In contrast, antagonistic activity of the mouse GLP1R specific antibody (7F38A2) has not yet been shown, the main use of 7F38A2 is immunostaining.

When Glp1R0017 is compared to the alternative GLP1R antibodies, mAb3F52 and 7F38A2 [116, 252, 253], the cross-species reactivity is the main advantage. This is likely due to the use of phage display selection strategy used for antibody generation, which made use of both human GLP1R ECD and mouse GLP1R overexpressing cells. The use of different antigens in subsequent rounds of phage display selection, offers the possibility of yielding cross-reactive antibodies which would be impossible to achieve by hybridoma [254]. Several other comparisons can be made between phage display and the hybridoma approach for antibody generation. One key benefit of phage display is that antibodies of similar affinity to hybridoma antibodies can be produced, without the use of animals. This also means that antibodies can be produced for toxins and non-immunogenic molecules [255-258]. In comparison with the hybridoma approach, the recombinant nature of phage display means the antibody-encoding gene sequence is readily accessible, and can be cloned into a human IgG backbone reducing any immunogenicity effects when used therapeutically. A further benefit is that phage display can be more easily automated than hybridoma work, and the time-frame for producing a panel of antibodies of interest is much shorter. After Glp1R0017 selection via phage display, the ScFv was converted into an IgG1 format, and has subsequently been characterised (Chapter 3).

Selections using phage display can lead to the production of large panels of antibodies, meaning there is a need for high throughput screening techniques to be in place alongside phage display to select clones of interest. In this study, clones of interest were determined based on phage ELISA activity (Figure 2.4), and assessment of sequencing (Tables 2.3 and 2.6). The signal windows observed in the cell based phage ELISA were small (Figure 2.4), indicating that this technique requires further optimisation before being used routinely as an initial screen for binding. Possible suggestions for

improvement of the assay include; a change in culturing conditions of the cells or an increase in cell plating density, allowing cells to become confluent prior to use in the assay, alternatively a change in blocking solution to bovine serum albumin may help decrease cell death.

In this study, sequencing assessment was successful in isolating clones of interest, with Glp1R0017 originally being isolated due to having 12 copies of the sequence within 88 clones from the round 3 selection output (Table 2.3). However, an initial optimised screen to confirm ScFv binding to the GLP1R would have been useful to give confidence in the choice of selection products for functional screening. As the phage ELISA using the human GLP1R ECD gave a larger signal window, a phage ELISA on both the mouse and human GLP1R ECD could be considered for initial screening.

2.5.2 Affinity maturation approaches using phage display

The nanomolar potency of Glp1R0017 was surprising considering this antibody was isolated directly from naïve phage display. However, affinity maturation approaches have the capability to improve affinity to the picomolar and even femtomolar range [259-261]. This is another advantage when comparing phage display to hybridoma, as the affinity gained in a hybridoma approach is limited to approximately 100 picomolar due to B cell physiology [262].

With the aim of improving the affinity, and thereby potency of Glp1R0017 for both the human and mouse GLP1R, Glp1R0017 mutant libraries were generated in which the CDR's were targeted by Kunkel mutagenesis (Table 2.4). The resultant libraries were used in a selection strategy with increased stringency, using lower concentrations of human GLP1R ECD at each round (Figure 2.7 and Table 2.5). To improve affinity on the mouse GLP1R, mGLP1R overexpressing cells were used at round 4 of selection (Figure 2.7), however availability of biotinylated mouse GLP1R ECD could have improved the affinity maturation strategy used.

The maximal improvement in potency was observed on the human GLP1R, with Glp1R0048 showing a 6.9-fold improvement in potency when compared to Glp1R0017 (Table 2.7). This could be explained by the dominance of human GLP1R ECD within our affinity maturation approach giving a bias towards increased affinity for the human GLP1R. As this improvement in potency was less than 10-fold, the characterisation of Glp1R0048 as an alternative GLP1R antibody was not pursued. Of note, Glp1R0048 was produced by affinity maturation of HCDR3, which is thought to be the most important in determining antibody binding [250, 251]. In comparison, only a minor improvement in potency was observed on the mouse GLP1R. This lack of improvement in potency meant that the affinity of improved clones was not measured by kinetics.

When considering future affinity maturation of Glp1R0017, it will be important to have a target potency in mind. An increase in potency for both the human and mouse GLP1R is desired, for *in vitro* signalling experiments, and pre-clinical studies in mice. A picomolar affinity is regularly achievable using phage display for affinity maturation, which would hopefully give a potency in line with the range of exendin 9-39 in our cAMP assays (Human GLP1R IC₅₀ = 16.2 nmol/l; Mouse GLP1R IC₅₀ = 1.09 nmol/l). Exendin 9-39 is currently being investigated clinically for the therapeutic treatment of congenital hyperinsulinemia, and post-bariatric hypoglycaemia [241, 242]. Should a GLP1R antagonistic antibody be developed into a clinically relevant agent, for example to provide an improved alternative to exendin 9-39 in the treatment of post-bariatric hypoglycaemia, increased affinity for the human GLP1R would be desirable.

A number of approaches can be used for further affinity maturation, which will be discussed and described below. One potential strategy could be to combine Glp1R0048 with the most improved HCDR2 mutant sequence and most improved LCDR3 mutant sequence. Alternatively, a new panel of antibodies for screening could be generated from our selection outputs, by combining a selection of the highest affinity mutant heavy chains with a selection of the highest affinity mutant light chains, and vice versa. These combination approaches provide the potential to generate new antibodies that have the additive or synergistic affinities of the contributing heavy and light chains.

In this study, the affinity maturation approach was to target the CDR regions independently of each other. One other approach involving the CDR's is CDR walking, in which CDRs are optimised sequentially [260]. This method has the potential to give a better result, however due to the staggered approach of sequential library generation and phage display, it would take longer to produce a final affinity improved antibody.

Often affinity maturation strategies target the CDR regions, which is beneficial because the framework remains unaffected, meaning the antibody stability should be unchanged [263]. Other affinity maturation approaches do exist, for example chain shuffling in which the V_H or V_L gene is replaced with a repertoire of V genes [259, 264]. Another approach is the use of focused mutagenesis then recombination of the best mutants. In this approach, each residue within the CDR's is mutated one at a time, creating libraries in which each clone has a single amino acid change in one of the CDR positions. Following initial screening, the recombination of the best mutants enables the production of affinity matured clones without the use of large libraries which are generated when complete CDRs are randomised [265].

2.5.3 Affinity maturation approaches using alternative display platforms

Alternative platforms are available for affinity maturation of antibodies including yeast display and ribosome display, both of which could be utilised for Glp1R0017 affinity maturation.

Yeast display is analogous to phage display in ways, and can be used in affinity maturation. One limitation of phage display, is the unpredictable expression bias of *Escherichia coli* for eukaryotic proteins which may explain why a single amino acid change within a CDR can eliminate expression [266]. A further limitation of phage display is that clones may appear in the output due to factors other than antigen binding, such as increased infectivity of phage or reduced host toxicity [259, 267]. Yeast display overcomes some of these limitations, as the endoplasmic reticulum within *Saccharomyces cerevisiae* is very similar to that in mammalian cells overcoming any library bias which may be observed in phage display, and enabling post-translational modifications. When considering the number of displayed ScFv's, each yeast cell is able to display large numbers of ScFvs fused to cell surface anchor proteins such as adhesion receptors, whereas bacteriophage express a single ScFv per bacteriophage [268]. Yeast display is also compatible with flow cytometry for cell sorting, which allows for the easy isolation of mutants with increased binding affinity [269]. This technique has been used successfully to generate antibodies with femtomolar affinity [261].

Ribosome display has also been developed as a technique to generate and affinity mature antibodies. In comparison to phage display, ribosome display is performed entirely *in vitro* without the use of any cells. In principle, the encoding gene sequence (mRNA) and ScFv peptide are linked together in a ribosomal complex. The ScFv library is translated and transcribed *in vitro*, and as the mRNA does not contain a stop codon, mRNA-ribosome-ScFv complexes are formed. These are the complexes used in selection against the immobilised target. Following ScFv binding, the mRNA is isolated, purified and used in subsequent rounds of selection. In error prone ribosome display libraries, prior to subsequent rounds of selection, mutations are introduced into the mRNA using low-fidelity DNA polymerase for amplification resulting in error prone PCR. This gives the advantage of directed evolution at each round of ribosome display. In the case of optimising insulin antibodies, ribosome display was used to improve affinity by up to 40-fold [270]. Thus, this approach to affinity maturation could be helpful in optimising Glp1R0017.

2.5.4 Affinity maturation approaches using computational methods

Aside from the alternative display platforms discussed above, the advent of bioinformatics means that *in silico* modelling can be used to assist the process of affinity maturation. For example, structural knowledge of the lead antibody could be used to give a more informed approach to affinity maturation.

Indeed, crystal structures of antibody:antigen or ScFv:antigen complexes can be used to reveal the residues within the CDR that appear to be important for binding, then phage display libraries can be made around these residues [271]. A more *in silico* based approach is to first identify residues important for binding using structural data, then use computational protein design to alter the residue type and conformations at the selected positions. Computational power allows all possible combinations of mutations to be modelled, and binding properties to be predicted. A selection of the best mutants can then be constructed to determine the actual binding properties [272].

When 3D structures are not available for the antibody of interest, a combination of phage display and computational approaches can be sought. For example, one could first target the CDR3 regions for affinity maturation using phage display, and screen the outputs for affinity. Those with the best improvement in affinity can then be modelled computationally for binding to the epitope, again mutations in the ScFv can be made, and the effect predicted [251].

These approaches rely on some level of structural knowledge about the epitope. As there are now structures available for the GLP1R [85, 86, 273], computational modelling could be used for epitope mapping of Glp1R0017, and subsequent determination of the residues important for binding. This could be extremely helpful in providing a more targeted approach to affinity maturation of Glp1R0017. It would also be helpful to determine the structure of Glp1R0017.

2.5.5 Summary

Overall in this chapter, a GLP1R antagonistic antibody with nanomolar potency has been generated using naïve phage display. We have demonstrated that Glp1R0017 has cross-species reactivity, with antagonism of both the mouse and human GLP1R being observed. Attempts were made to improve the affinity of Glp1R0017 by randomising sections of the CDR regions, and using the resulting libraries in phage display. However, within the time frame of this study only a slight improvement in Glp1R0017 potency for the human GLP1R was observed, with no improvement in potency on the mouse GLP1R. Alternative affinity maturation approaches have been discussed which may be considered for future affinity maturation of Glp1R0017. Glp1R0017 has since been scaled up, and characterised in more depth, which will be detailed in chapter 3.

Chapter 3. Characterisation of Glp1R0017, a GLP1R antagonistic antibody

3.1 Introduction

3.1.1 GLP1R Signalling Pathways

To characterise the monoclonal GLP1R antagonistic antibody generated in Chapter 3, several GLP1R signalling pathways have been assessed including cAMP, Ca^{2+} , and β -arrestin signalling. It is well known that the GLP1R is a $G_{\alpha s}$ coupled GPCR within the secretin (class B) family of GPCRs, thus the canonical signalling pathway leads to generation of cyclic AMP (cAMP) via adenylate cyclase [89, 274]. Downstream, cAMP leads to activation of protein kinase A (PKA) and exchange protein directly activated by cAMP (Epac), which together have several downstream effects in cells, including the triggering of insulin granule exocytosis from pancreatic beta cells [90, 91].

There are also suggestions that GLP1R can couple to $G_{\alpha q}$ resulting in elevation of cytosolic $[\text{Ca}^{2+}]$. The binding of $G_{\alpha q}$ to GLP-1 activated GLP1R was first observed by western blotting of CHO cells overexpressing the GLP1R, and led to the suggestion that GLP1R may also signal via the $G_{\alpha q}$ coupled pathway [275]. $G_{\alpha q}$ signalling leads to activation of phospholipase C (PLC) which breaks down phosphatidylinositol-4,5-bisphosphate (PIP_2) into inositol-1,4,5-triphosphate (IP_3) and diacylglycerol (DAG) [276]. Downstream, IP_3 causes an increase in cytosolic calcium, which together with DAG activates protein kinase C which then phosphorylates extracellular signal-regulated kinase (ERK) [277, 278]. Dose-dependent increases in intracellular calcium following GLP1R stimulation have indeed been observed using both GLP-1 and GLP-1 mimetics in GLP1R overexpressing cell lines, indicating that the GLP1R signals via $G_{\alpha q}$ in addition to $G_{\alpha s}$ [279, 280]. It has even been proposed that this $G_{\alpha q}$ signalling is responsible for agonist induced internalisation of the GLP1R [279].

Further evidence suggests the GLP1R can signal using G protein independent pathways, including β -arrestin signalling. Historically it was thought that β -arrestin binding was solely responsible for mediating receptor internalisation via endocytosis, however more recently β -arrestin induced signalling pathways have been described, such as phosphorylation of ERK1/2 and other kinases [281, 282]. A direct interaction of β -arrestin 1 with the GLP1R has been observed in the rat INS-1 pancreatic beta cell line, and an interaction of GLP1R with β -arrestin 2 has also been demonstrated [283, 284].

The functional role of β -arrestin recruitment to the GLP1R is unclear. In terms of GLP1R internalisation; β -arrestin 1 depletion does not affect GLP1R endocytosis, whereas enhancement of β -arrestin 2 action increases GLP1R endocytosis [283, 284]. When considering signalling pathways, β -arrestin 1 signalling upon acute GLP1R stimulation potentiates glucose stimulated insulin secretion, and regulates beta-

cell apoptosis [283, 285]. However, prolonged GLP1R exposure to agonist, leads to β-arrestin induced receptor endocytosis and desensitisation of the GLP1R, reducing insulin secretion [286].

Interest surrounds the field of GLP1R signalling bias due to the desire for development of new treatments for T2D. As mentioned previously, GLP-1 mimetics are available for treatment of T2D, but there is always a need for drugs with improved therapeutic efficacy. One strategy for this is to develop drugs that exploit the GLP1R signalling bias in a differing fashion to those drugs already on the market. For example, a biased agonist with reduced β-arrestin1 recruitment and signalling has recently been described, which when tested *in vivo* was more effective at correcting hyperglycaemia when used at sub-maximal concentrations compared to exendin-4 [280].

3.1.2 GLP1R Physiology

The downstream effects of GLP-1 signalling vary dependent upon the cell type in which GLP1R is expressed. As described in chapter 1, GLP1R is expressed in many different tissues. In the pancreas, GLP-1 modulates insulin, glucagon and somatostatin secretion from the islets of Langerhans. GLP1R activation in the β-cell leads to increased glucose stimulated insulin secretion, decreased apoptosis, and increased proliferation [98]. A subset of α cells express GLP1R [93], and GLP-1 inhibits glucagon secretion from the α cells. However, whether this is a direct or an indirect mechanism remains controversial [101, 287, 288]. In the δ cells, GLP-1 causes somatostatin secretion which in turn inhibits glucagon secretion from α cells [101, 289]. Together, GLP-1 actions on the pancreas are responsible for regulating glucose levels in the ‘incretin effect’.

In extra-pancreatic tissue, GLP-1 has several other effects [47]. In the kidney, GLP-1 stimulates natriuresis, however whether this is a direct or indirect effect is unknown [290]. GLP1R activation in the central nervous system and brain leads to decreased food intake, increased neuroprotection and increased neurogenesis [98].

GLP-1 also has a range of actions in the cardiovascular system, some of which include modulation of heart rate, and cardio-protection in myocardial ischaemia. Considerable uncertainty surrounds whether these cardiac effects are mediated via a direct or indirect mechanism, most likely both direct and indirect signalling are involved [124, 238]. The exact location of cardiac GLP1R remains to be elucidated, mRNA transcripts of GLP1R have been detected in human hearts however location of the GLP1R protein by immunostaining remains unclear, with further research required to determine the GLP1R positive cell-type [117].

For the characterisation of Glp1R0017 *in vivo*, the effect on GLP-1 regulated glucose levels were determined, which is mainly controlled by pancreatic actions of GLP-1.

3.2 Aims

To characterise the newly developed GLP1R antibody, Glp1R0017, by:

- a) Determining the specificity for GLP1R, and any cross-species reactivity.
- b) Assessing inhibition of GLP1R alternative signalling pathways.
- c) Assessing inhibition of endogenous levels of GLP1R in INS-1 832/3 cells.
- d) Assessing the use in immunostaining of GLP1R.
- e) Assessing inhibition of GLP1R *in vivo* using glucose tolerance tests to monitor incretin effects on glucose regulation.

3.3 Methods

3.3.1 Solutions and Compounds

Standard saline solution contained (mmol/l) 138 NaCl, 4.5 KCl, 4.2 NaHCO₃, 1.2 NaH₂PO₄, 2.6 CaCl₂, 1.2 MgCl₂, 10 HEPES. Krebs-Ringer Buffer (KRB) contained (mmol/l) 120 NaCl, 3.5 KCl, 1.2 KH₂PO₄, 1.2 MgSO₄, 2.5 CaCl₂, 25 NaHCO₃ (pH 7.2). Assay buffer for calcium measurements and ligand-binding assays was Hanks' balanced salt solution supplemented with 25 mmol/l HEPES and 0.1% (w/v) bovine serum albumin (BSA) (pH 7.4); for the cAMP homogenous time-resolved fluorescence (HTRF) assay, the buffer was supplemented with 0.5 mmol/l 3-isobutyl-1-methylxanthine (IBMX).

Unless stated otherwise, chemicals were obtained from Sigma-Aldrich (Poole, UK), and peptides were purchased from Bachem (Bubendorf, Switzerland). The following stocks were dissolved in dimethyl sulfoxide (DMSO): 10 mmol/l forskolin, 100 mmol/l IBMX, 136 µmol/l exendin (9-39) acetate salt, 150 µmol/l GIP (1-42), and 285 µmol/l glucagon (1-29). GLP-1 (7-36) was diluted in water to 100 µmol/l.

3.3.2 Cell Culture

All cell lines were maintained at 37°C with 5% CO₂. Chinese Hamster Ovary (CHO) K1 cells were maintained in Nutrient Mixture F-12 Ham, and Human embryonic kidney (HEK) 293 cells were maintained in DMEM with 1000 mg/ml glucose; both of these medias were supplemented with 10% FBS, 0.1 units/l penicillin, 0.1 µg/l streptomycin and 2 mmol/l L-glutamine.

INS-1 832/3 cells were cultured in RPMI 1640 Media with GlutaMAX supplement (ThermoFisher Scientific), 10% FBS, 10 mmol/l HEPES, 50 µmol/l β-mercaptoethanol, 1 mmol/l sodium pyruvate and penicillin/streptomycin [291].

Stably transfected cell lines overexpressing GPCRs of interest were generated at AstraZeneca (Gothenburg, Sweden) or MedImmune (Cambridge, UK). For experimental use these overexpressing cell lines were thawed from liquid nitrogen stocks directly into assay buffer.

3.3.3 Cell Based Assays

3.3.3.1 cAMP Homogenous Time Resolved Fluorescence (HTRF) Accumulation Assay

Control peptides and antibody were serially diluted in assay buffer, and plated using an ECHO525 acoustic liquid handler (Labcyte, Sunnyvale, CA, USA) to give 11-point dose response curves in 384 well plates. Overexpressing cell lines resuspended in assay buffer, at a density dependent on the cell line (Appendix 3), were then combined with the test compounds. For agonism experiments, cAMP was measured after 30 minutes of incubation at room temperature. For antagonism experiments, an agonist challenge was given after 15 minutes using the ECHO550 acoustic liquid

handler (Labcyte), and samples were mixed by centrifugation at 150 g for 1 minute. After a further 30 minute incubation at room temperature, cAMP was measured. Cellular cAMP levels were measured using the cAMP dynamic 2 HTRF kit (Cisbio, Codolet, France) according to the manufacturer's recommendations. Plates were read on an EnVision plate reader (PerkinElmer, Waltham, MA, USA) after 1 hour. Non-linear regression was used to calculate EC₅₀ and IC₅₀ values.

3.3.3.2 cAMP FRET Imaging

A fluorescence resonance energy transfer (FRET)-based sensor, Epac2-camps, was used for single cell measurements of cAMP in INS-1 832/3 cells. Cells were seeded into 35 mm plastic dishes, after 24 hours cells were transfected with 3 µg Epac2-camps DNA probe using 3 µl lipofectamine 2000. Following 24 hours cells were trypsinised, and re-seeded onto matrigel-coated 35 mm glass bottomed dishes for imaging 24 – 48 hours later. During imaging, solutions were continually perfused at approximately 1 ml/minute. For experiments to determine antagonism, cells were pre-incubated with 100 µmol/l Glp1R0017 for 15 minutes prior to imaging.

An inverted microscope (IX71; Olympus, Southend on Sea, UK) with a x40 oil immersion objective was used to visualise cells. Cells were excited at 435 nm (200 – 225 ms excitations) every 5 seconds using a Xenon arc lamp coupled to a monochromator (Cairn Research, Faversham, UK) and controlled by MetaFluor software (Molecular Devices). Cyan fluorescent protein (CFP) emission (470 nm) and yellow fluorescent protein (YFP) emission (535 nm) were monitored using an Optosplit II beam splitter (Cairn Research) and an Orca-ER digital camera (Hamamatsu, Welwyn Garden City, UK). Emissions were expressed as CFP/YFP fluorescence ratio, and a sliding average across 30 seconds was used for smoothening data. Responses were calculated as maximum ratio during test reagent application minus maximum ratio at baseline immediately prior to reagent application. Overall changes in CFP/YFP emission ratio was calculated as mean ± SEM. Statistical significance was assessed by one-way ANOVA with a post-hoc Bonferroni test.

3.3.3.3 Calcium Measurements

CHO cells overexpressing human GLP1R were seeded into black poly-D-lysine coated 384 well plates (Greiner Bio-One, Stonehouse, UK) at 15,000 cells/well. The following day, cells were washed with assay buffer then loaded with Fluo-4 NW containing 2.5 mmol/l probenecid (Thermo Fisher Scientific) for 30 minutes at 37°C then 15 minutes at room temperature. After loading, antibody was added to cells for 15 minutes at room temperature, prior to adding GLP-1. The FLIPR Tetra (Molecular Devices, Wokingham, UK) was used to record fluorescence every 0.5 seconds for 1 minute after agonist addition, then every 3 seconds for 4 minutes. Responses were normalised to the vehicle control, and average responses were calculated by subtracting basal fluorescence from peak intensity.

3.3.3.4 Insulin Secretion Assay

INS-1 832/3 cells were seeded in 24-well plates at 500,000 cells/well, and used for insulin secretion after 24 hours. Cells were washed thoroughly in PBS before being incubated in KRB containing 0.2% BSA with or without Glp1R0017 for 1 hour at 37°C in 5% CO₂. Test reagents diluted in KRB were then added to cells, and incubated for a further 2 hours. After incubation the supernatant fractions were collected and centrifuged at 4°C to remove cell debris. Insulin was then measured in the supernatant fractions by the Core Biochemical Assay Laboratory (Cambridge Biomedical Campus, Cambridge, UK), using a rat insulin assay (Meso Scale Discovery, Gaithersburg, MD, USA).

3.3.3.5 Receptor Ligand Binding Assay

AlexaFluor647 tagged GLP-1 (Cambridge Research Biochemicals, Billingham, UK) was serially diluted and combined with GLP1R overexpressing CHO cell lines seeded in black clear bottomed 384 well plates at 1000 cells/well. The cells were then incubated +/- 0.5 µmol/l Exendin-4 overnight at 4°C in the dark. The following morning, fluorescence was measured using the FL3 (650-690 nm) emission channel on a mirrorball system (TTP Labtech, Melbourn, UK). FL3 total readings (median fluorescence per event x count) were plotted.

3.3.3.6 Nano-Glo® Live Cell Assay for Beta-Arrestin Measurements

NanoBiT® technology was used to measure protein-protein interactions between beta-arrestin 1 or 2 and GPCRs of interest. Firstly, GPCRs of interest were cloned into the pBiT1.1-C[TK/LgBiT] vector using *Xho*1 and *Eco*R1 as the restriction enzymes. The pBiT2.1-N[TK/SmBiT] vector was used to express SmBiT at the N terminal of beta-arrestin 1 and beta-arrestin 2. Successful cloning was verified by Sanger sequencing prior to using the constructs in the assay.

HEK293 cells were seeded into 96 well plates at 20,000 cells/well. The following day, cells were transfected with NanoBiT constructs using 50 ng of each relevant construct per well with 0.5 – 1 µL Lipofectamine 2000. After overnight incubation, media was replaced with 100 µL OptiMEM Reduced Serum Media, and cells were incubated at 37°C for 30 minutes prior to the start of the assay. The Nano-Glo® Live Cell Substrate was then diluted 20-fold with Nano-Glo® LCS Dilution Buffer to make the Nano-Glo® Live Cell Reagent. Luminescence measurements were made on the Tecan Spark™ 10M multimode microplate reader, at 37°C with 5% CO₂. After the first 5 minutes, 25 µL of Nano-Glo® Live Cell Reagent was added to cells and luminescence was monitored for 10 minutes prior to ligand addition. Luminescence was then measured every 30 seconds for 1 hour.

For antagonist experiments, the antagonist or control antibodies were diluted in OptiMEM and incubated with cells for the 30 minutes prior to luminescence measurement. To check that antagonists

had no effect on beta-arrestin recruitment, the antagonist was also added to wells at the point of ligand addition.

3.3.4 Animal Studies

All experimental procedures were approved by local ethical review bodies and were performed in accordance with the Animal (Scientific Procedures) Act 1986, Home Office guidelines, local establishment guidelines and Animal Research: Reporting of In Vivo Experiments (ARRIVE) guidelines. Experiments performed using my personal licence (I290CEFFE), under a number of Home Office Project Licenses. C57/Bl6 mice were purchased from Charles River UK. Mice were group-housed in individually ventilated cages, with ad libitum access to chow diet and water unless otherwise stated. Animals were euthanized by cervical dislocation, unless otherwise stated.

3.3.4.1 Transgenic mice

Transgenic mice were generated by F. Reimann, in which the expression of cre-recombinase is driven by the *glp1r* promoter [93]. Expression of cre-recombinase is responsible for reporter gene activation. The cre-recombinase recognises loxP sites surrounding a stop codon in front of the reporter gene, then deletes the ‘floxed’ stop codon. Consequently, the reporter protein is only produced in cells which express the gene of interest. However, once the reporter gene is expressed it is under the control of a constitutively active *rosa26* promoter, meaning after initial activation each cell will continue to produce the reporter protein independent of cre-recombinase. The fluorescent reporter proteins used in this study are enhanced yellow fluorescent protein (EYFP), tandem red fluorescent protein (tdRFP) [292] and the fluorescent calcium indicator GCaMP3 [293].

GLP1R knockout mice were kindly provided under license from D.Drucker (Lunenfeld-Tanenbaum Research Institute, Toronto, ON, Canada). Briefly, these mice have a deletion of the two exons encoding the first and third transmembrane domain of GLP1R, resulting in an absence of the GLP1R [294].

3.3.4.2 Immunostaining

Tissue for immunostaining was fixed in 4% (w/v) paraformaldehyde (PFA) overnight, and subsequently dehydrated using a gradient of 15% then 30% (w/v) sucrose. For processing, tissue was frozen in optimal cutting temperature embedding media (VWR Chemicals, Radnor, PA, USA). 6-10 µm sections were sliced on the cryostat, and mounted onto Superfrost Plus glass slides (Thermo Fisher Scientific).

Slides were incubated for 1 hour in blocking solution containing 5% (v/v) donkey or goat serum, 0.05% (v/v) Tween-20 and 1% (w/v) BSA. Slides were then stained overnight with primary antisera of interest

in the same blocking solution (Appendix 4). After washing in blocking solution, slides were incubated with appropriate secondary antisera diluted 1:300 and Hoescht diluted 1:1300 for 1 hour. Negative control slides were stained in parallel with only secondary antisera. Finally, coverslips were mounted with hydromount (National Diagnostics, Atlanta, GA, USA) and DABCO.

Brain tissue was collected from mice perfused *in situ* with 4% (w/v) PFA and stored in 4% PFA, 30% (w/v) sucrose prior to sectioning on a freezing microtome (Leica) into 5 subsets of 25 µm slices. Following slicing, slides were stored in ethylene glycol based cryoprotectant. For immunofluorescent staining, antigen retrieval was performed using sodium citrate buffer, and sections were stained in suspension using a method similar to that described above, however blocking solution did not contain BSA.

Slides were imaged using confocal microscopy (TCS SP8; Leica, Wetzlar, Germany) or automated widefield microscopy (Axio Scan.Z1, Zeiss, Oberkochen, Germany). Images displayed are either confocal slices or Z-stacks, quantification of cell number and co-localisation was performed using either Image J or HALO software (Indica Labs, Corrales, USA).

3.3.4.3 Single-dose pharmacokinetics study

The pharmacokinetic profile of Glp1R0017, administered via intraperitoneal or subcutaneous injection, was assessed in two groups of six male C57/Bl6 mice randomised according to body weight (13 weeks old, mean weight 29.1 ± 0.2 g). Blood samples were collected in EDTA capillary tubes, using a sparse sampling approach, at 0.5, 1, 2, 4 and 7 hours after injection, then every 24 hours for 5 days. At the 120 hour endpoint, animals were terminally anaesthetised by isoflurane inhalation, blood samples were collected via cardiac puncture, and death was confirmed using cervical dislocation. Plasma samples were obtained by centrifugation, and the plasma antibody concentration was assessed using a Gyrolab assay, according to manufacturer's instructions (Gyros, Uppsala, Sweden). Briefly, this procedure is based on a sequential flow-through sandwich method. Firstly, the analyte was captured using a biotinylated idiotype antibody against IgG1 (MedImmune, Cambridge, UK). An Alexa-labelled sheep anti-human IgG (The Binding Site, Birmingham, UK) was then added to detect the bound captured analyte. Fluorescence was measured using the Gyrolab Workstation, which is directly proportional to the amount of analyte in the plasma sample. This work was carried out with the help of L. Liang and S. Madalli.

3.3.4.4 Glucose Tolerance Tests (GTTs)

Antibody effect on glucose tolerance was assessed by either intraperitoneal glucose tolerance tests (IPGTTs) or oral glucose tolerance tests (OGTTs). All GTTs were performed in 10 week old male C57/Bl6

mice randomised according to body weight, after a 6 hour fast. Groups of eight mice were used, which was pre-determined by power analysis where the effect size set at 15%, with 80% power and significance <0.05. Animals were dosed subcutaneously either with antibody or saline 24 hours prior to the GTTs.

In the IPGTT, 0.1 mg/kg liraglutide (Victoza; Novo Nordisk, Gatwick, UK) or vehicle was dosed by subcutaneous injection 2 hours prior to intraperitoneal glucose administration (2 g/kg). Blood glucose was measured using a hand-held glucometer (AlphaTrak; Zoetis, London, UK) in tail-prick blood samples at -120, 0, 15, 30, 45, 60, 90 and 120 minutes relative to the glucose challenge. In the OGTT the same glucose challenge (2 g/kg) was administered via oral gavage, and blood glucose was measured at 0, 15, 30, 45, 60, 90 and 120 minutes relative to the glucose challenge. The area under the curve (AUC) between 0 and 120 minutes was calculated, and used for analysis. Statistical significance was assessed by one-way ANOVA with post-hoc Bonferroni test. This work was carried out with the help of L. Liang and the core team at the MedImmune animal facility.

3.4 Results

3.4.1 Glp1R0017 exhibits cross-species antagonistic activity for GLP1R

As the GLP1R is primarily recognised as a G_{αs} coupled GPCR, the antagonistic ability of Glp1R0017 was initially assessed in cAMP based HTRF assays.

For assessment of cross-species reactivity, CHO cells overexpressing mouse, rat, human, dog or cynomolgus monkey GLP1R were used. To find an appropriate agonist challenge for use in the antagonistic assays, GLP-1 agonist activity was first investigated in each of these cell lines (in collaboration with J. Naylor at MedImmune). Dose-response curves of GLP-1 revealed the EC₅₀ values ranged from 0.7 pmol/l to 6.07 pmol/l in the cynomolgus monkey and dog GLP1R cell lines respectively (Figure 3.1, Table 3.1). The concentration of agonist challenge used in the antagonistic assays ranged between EC₅₅ to EC₈₀ (Figure 3.1). Glp1R0017 antagonism of the GLP1R was observed in each species assessed, and IC₅₀ values were calculated (Figure 3.2a). The IC₅₀ values ranged from 5.2 to 43 nmol/l in the mouse and human GLP1R cell lines respectively (Table 3.1).

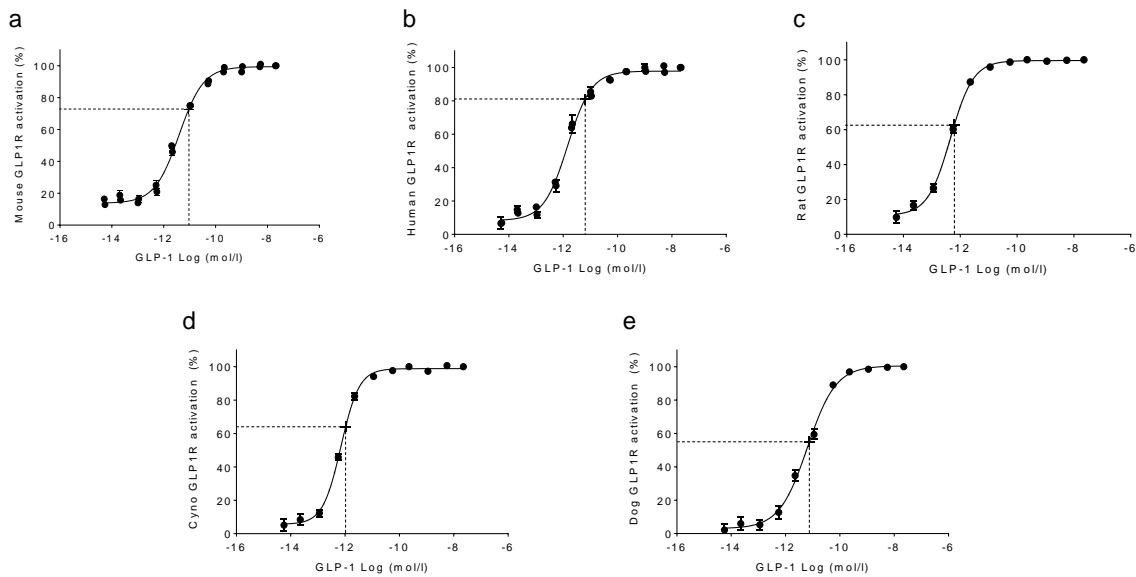


Figure 3.1 Agonistic activity of GLP-1 in GLP1R overexpressing cell lines. The dose response curves of cAMP stimulation by GLP-1 in CHO cells overexpressing mouse GLP1R (a), human GLP1R (b), rat GLP1R (c), cyno GLP1R (d), and dog GLP1R (e) are displayed. For each cell line, the concentration of GLP-1 used as the agonist challenge in antagonistic cAMP assays is marked by a dotted line. Data displayed are n3 for each cell line.

	Mouse GLP1R	Human GLP1R	Rat GLP1R	Cyno GLP1R	Dog GLP1R
GLP-1 EC ₅₀ (mol/l)	3.92E-12	1.45E-12	4.51E-12	7.05E-13	6.07E-12
Glp1R0017 IC ₅₀ (mol/l)	5.21E-09	4.33E-08	5.3E-09	8.99E-09	11.7E-09

Table 3.1 Summary of GLP-1 and Glp1R0017 activity in each of the GLP1R overexpressing CHO cell lines. The mean EC₅₀ values are displayed for GLP-1, along with the mean IC₅₀ values for Glp1R0017.

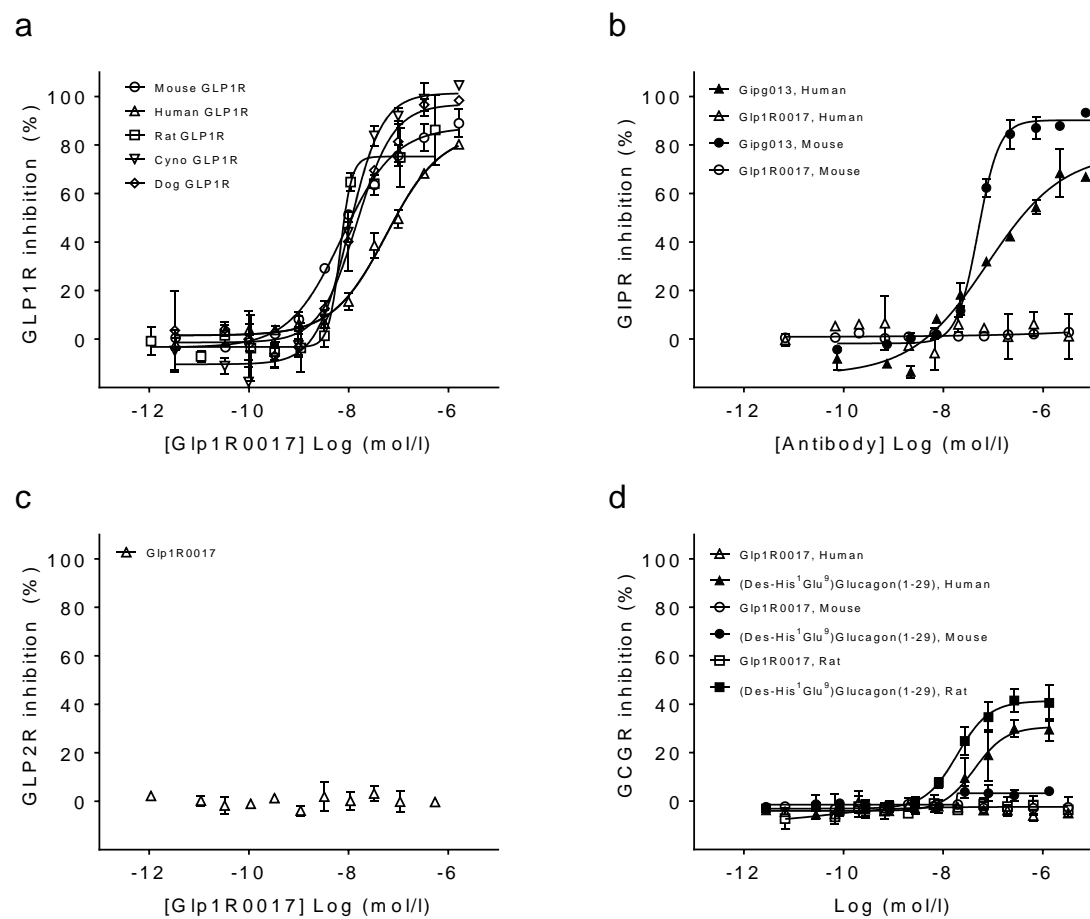


Figure 3.2 Antagonistic activity of Glp1R0017 in GLP1R, GIPR, GLP2R and GCGR overexpressing cell lines. (a) Antagonistic profiles of Glp1R0017 in CHO cells overexpressing mouse, human, rat, cynomolgus monkey, or dog GLP1R. (b) Antagonistic profiles of Glp1R0017 and the antagonistic GIPR antibody Gipg013 in CHO cells overexpressing human GIPR, and HEK293 cells overexpressing mouse GIPR. (c) Antagonistic profile of Glp1R0017 in HEK293 cells overexpressing human GLP2R. (d) Antagonistic profiles of Glp1R0017 and the glucagon receptor partial antagonist des-His¹-[Glu⁹]-glucagon (1–29) amide in CHO cells overexpressing human, mouse or rat GCGR. Values have been normalised to the maximum activity of each receptor, defined by the total cellular cAMP production in the absence of peptide/IgG. Data are mean ± SE from duplicate wells, and the data shown are representative of at least three separate experiments.

The observed differences in IC₅₀ values of Glp1R0017 and EC₅₀ values of GLP-1 between different cell lines may be affected by differing levels of GLP1R overexpression. This was investigated by monitoring AlexaFluor647 tagged GLP-1 binding to each of the overexpressing cell lines. Measurements of the fluorescent max for each cell line suggested that the rat GLP1R cell line most highly expressed GLP1R, whereas the mouse GLP1R expresses very low levels of GLP1R which were undetectable in this receptor ligand binding assay (Figure 3.3).

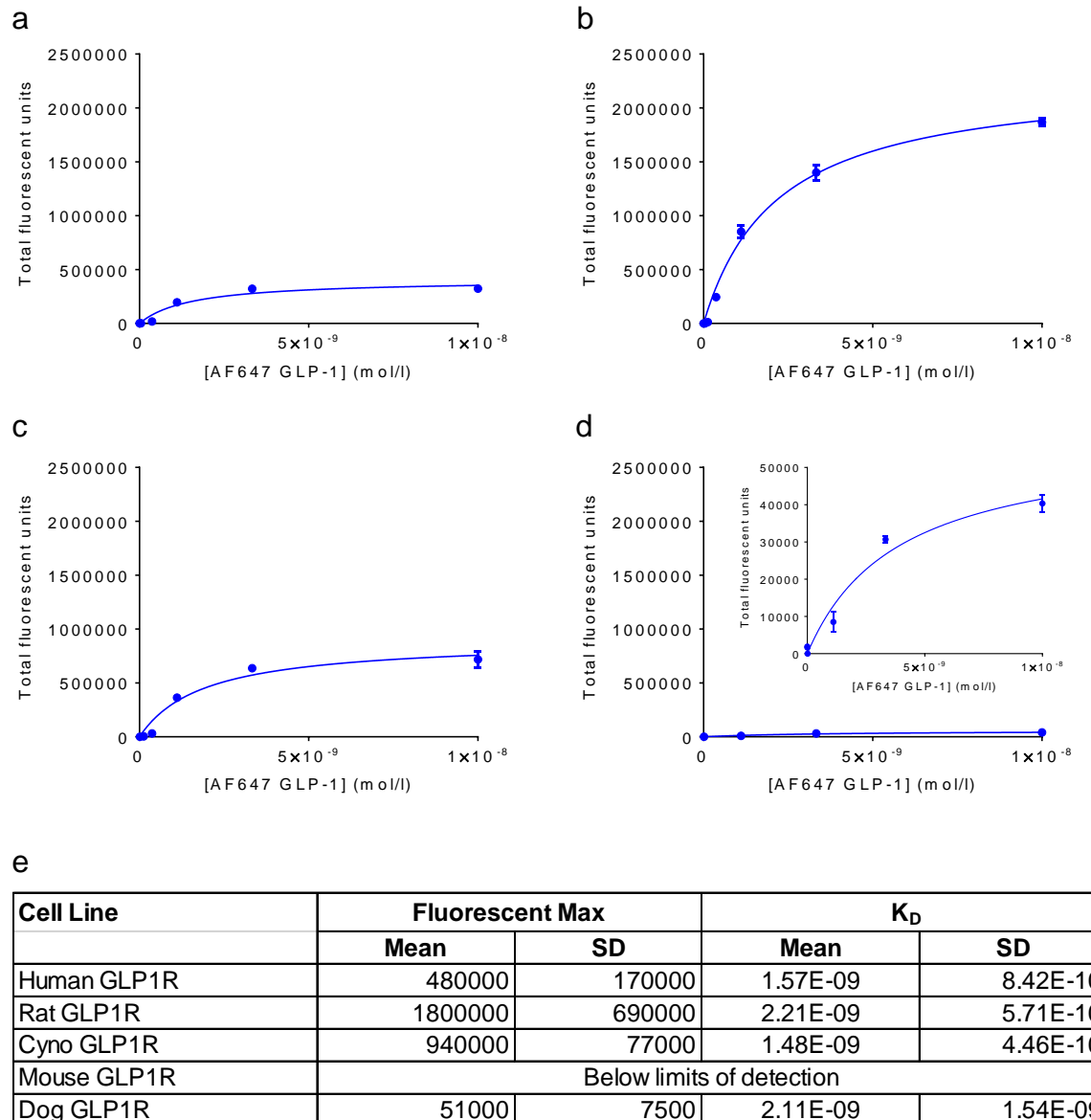


Figure 3.3 AlexaFluor647 tagged GLP-1 binding to GLP1R overexpressing CHO cells indicates level of GLP1R overexpression. Representative AlexaFluor647 GLP-1 binding curves ($n=3$) are displayed for CHO cells overexpressing human GLP1R (a), rat GLP1R (b), cyno GLP1R (c), and dog GLP1R with zoom inset (d). The mean fluorescent max (FL max) and K_D for each cell line are tabulated (e). Non-linear binding curves were plotted with non-specific binding and background constrained to 0.

3.4.2 Glp1R0017 is a specific, competitive antagonist for GLP1R

To determine the specificity of Glp1R0017 for GLP1R, the ability to antagonise related class B GPCR's was measured in the cAMP based HTRF assays. No antagonistic activity was observed in cells overexpressing the GIPR, GLP2R or glucagon receptor (GCGR) (Figure 3.2b-d). This suggested that Glp1R0017 displays specificity for antagonism of the GLP1R.

For downstream application, Glp1R0017 was likely to be used in the mouse to investigate GLP1R function in more detail. Therefore, the *in vitro* pharmacology of Glp1R0017 antagonistic activity was investigated in more detail on the mouse GLP1R. Schild regression analysis was used to determine whether Glp1R0017 displays competitive antagonism for the GLP1R. The effect of increasing concentrations of Glp1R0017 on GLP-1 dose response curves was assessed, and revealed the maximal cAMP response to GLP-1 was not reduced by increasing Glp1R0017 concentrations (Figure 3.4a). This suggested that Glp1R0017 antagonism is not insurmountable. The same was observed for the small peptide antagonist, exendin 9-39 (Figure 3.4b). When the Schild regression line was plotted, the slope gradient for Glp1R0017 was 0.56, and the calculated dissociation constant was 466 pmol/l. Exendin 9-39 had a slope gradient of 0.89 and a calculated dissociation constant of 315 pmol/l (Figure 3.4c).

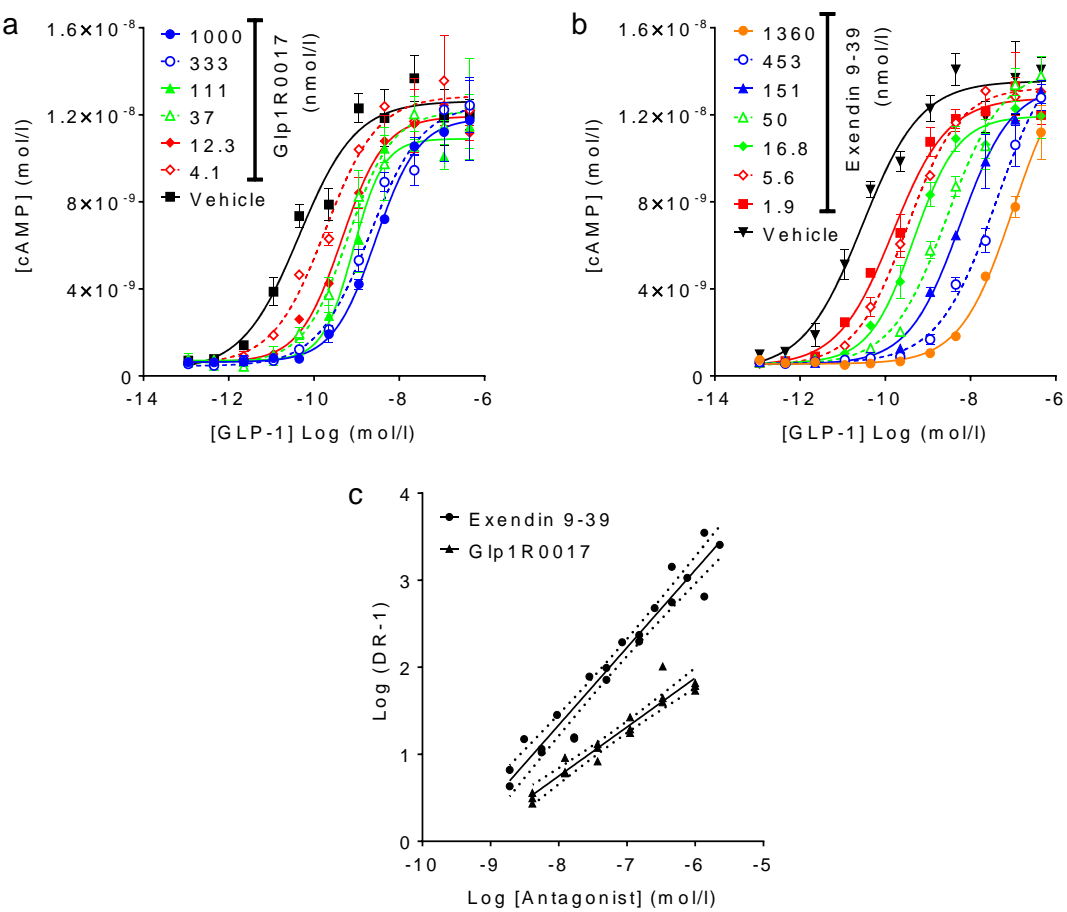


Figure 3.4 Schild Regression Analysis of Glp1R0017 and exendin 9-39 antagonism of the mouse GLP1R. (a) GLP-1 dose response curves in the presence of varying concentrations of Glp1R0017. (b) GLP-1 dose response curves in the presence of varying concentration of exendin9-39. Data are mean \pm SE from duplicate wells, and are representative of at least three independent experiments. (c) Schild regression analysis of GLP-1 dose response curves in the presence of Glp1R0017 or exendin9-39. Dose ratio (DR) is the ratio of apparent GLP-1 EC₅₀ in the presence of the antagonist at a set concentration, over the GLP-1 EC₅₀ in the absence of antagonist. Points from three independent experiments are plotted with the 95% confidence interval band for each line. Dissociation constants of 466 pmol/l for Glp1R0017, and 315 pmol/l for exendin 9-39 are yielded from the x-axis intersect of the lines.

3.4.3 Glp1R0017 also inhibits alternative signalling pathways downstream of the GLP1R

In addition to signalling via cAMP, GLP1R has also been shown to stimulate G_{αq} coupled pathways, leading to increases in cytosolic Ca²⁺. The ability of GLP-1 to stimulate intracellular Ca²⁺ in CHO cells overexpressing mouse GLP1R or human GLP1R was first assessed. No Ca²⁺ response was observed in the mouse GLP1R overexpressing cell line (data not shown). The dose response curve of GLP-1 in human GLP1R cells showed GLP-1 stimulates an increase in intracellular Ca²⁺ at concentrations greater

than 556 nmol/l. The dose-response curve was significantly right shifted when compared to the dose-response seen in the cAMP assays, even at the maximal GLP-1 concentration of 5 μ mol/l the dose-response curve had not reached plateau (Figure 3.5a).

Glp1R0017 at 1 μ mol/l successfully inhibited the 5 μ mol/l GLP-1 induced intracellular calcium response in the human GLP1R overexpressing CHO cells (Figure 3.5b, c). In contrast, an isotype control antibody (R347) had no effect on the calcium response (Figure 3.5b, c). This suggested the Glp1R0017 inhibitory effect was specifically due to GLP1R binding.

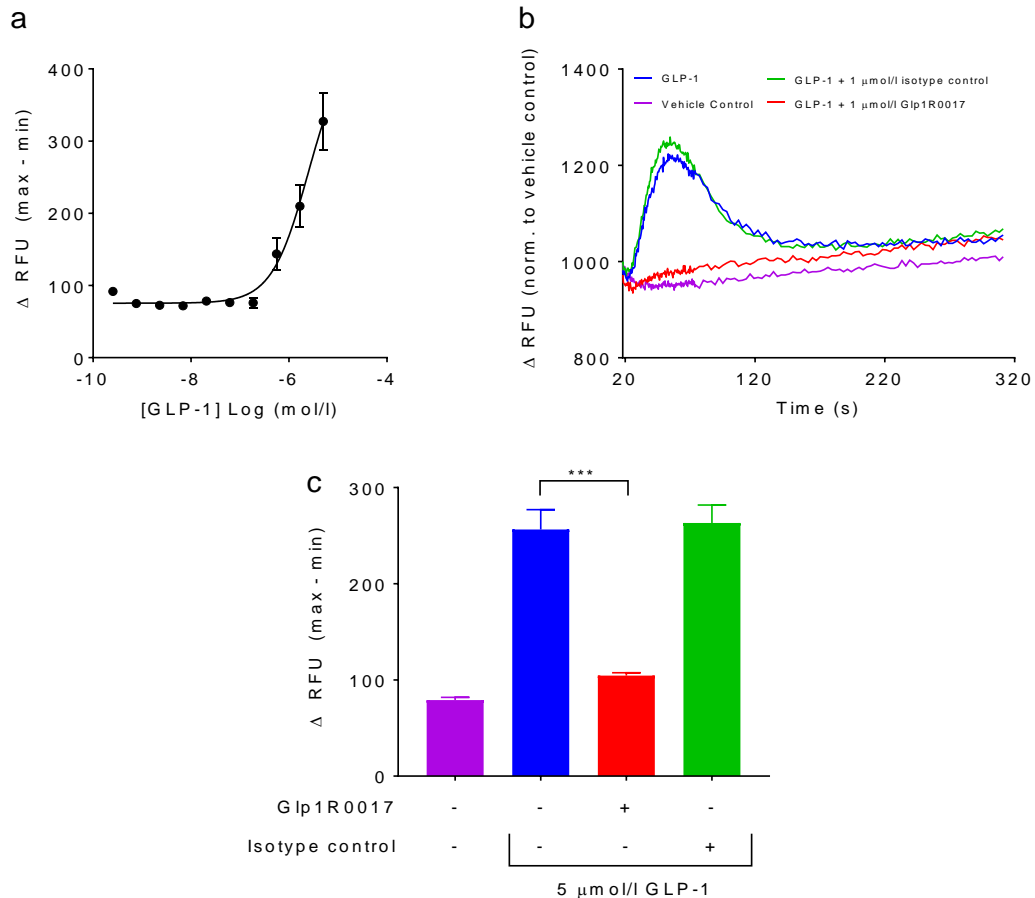


Figure 3.5 Glp1R0017 inhibits GLP-1 induced intracellular calcium responses from the human GLP1R. (a) GLP-1 dose response curve showing intracellular calcium responses, calculated by subtracting basal fluorescence at 19 s from peak intensity. Data are mean \pm SEM, n=2. (b) Representative intracellular calcium responses of CHO cells overexpressing human GLP1R, measured in relative fluorescent units (RFU). All traces have been normalised (norm.) to the vehicle control response. (c) Mean intracellular calcium responses were calculated as in (a). Data are mean \pm SD, n=16 wells (eight wells from each of two independent experiments). Statistical significance was assessed by one-way ANOVA with post hoc Bonferroni test. ***p<0.001

GLP1R signalling via the β -arrestins has also been observed in the literature. Therefore, the recruitment of β -arrestin 1 and β -arrestin 2 to the human GLP1R was determined, followed by the

ability of Glp1R0017 to inhibit β -arrestin recruitment. This was investigated using the Nano-Glo® live cell assay system in transiently transfected HEK293 cells, with an increase in luciferase activity indicating β -arrestin binding to the GLP1R. A pilot dose-response curve of GLP-1 showed that at concentrations greater than 10 nmol/l GLP-1 stimulates β -arrestin 1 and β -arrestin 2 recruitment to the GLP1R (Figure 3.6).

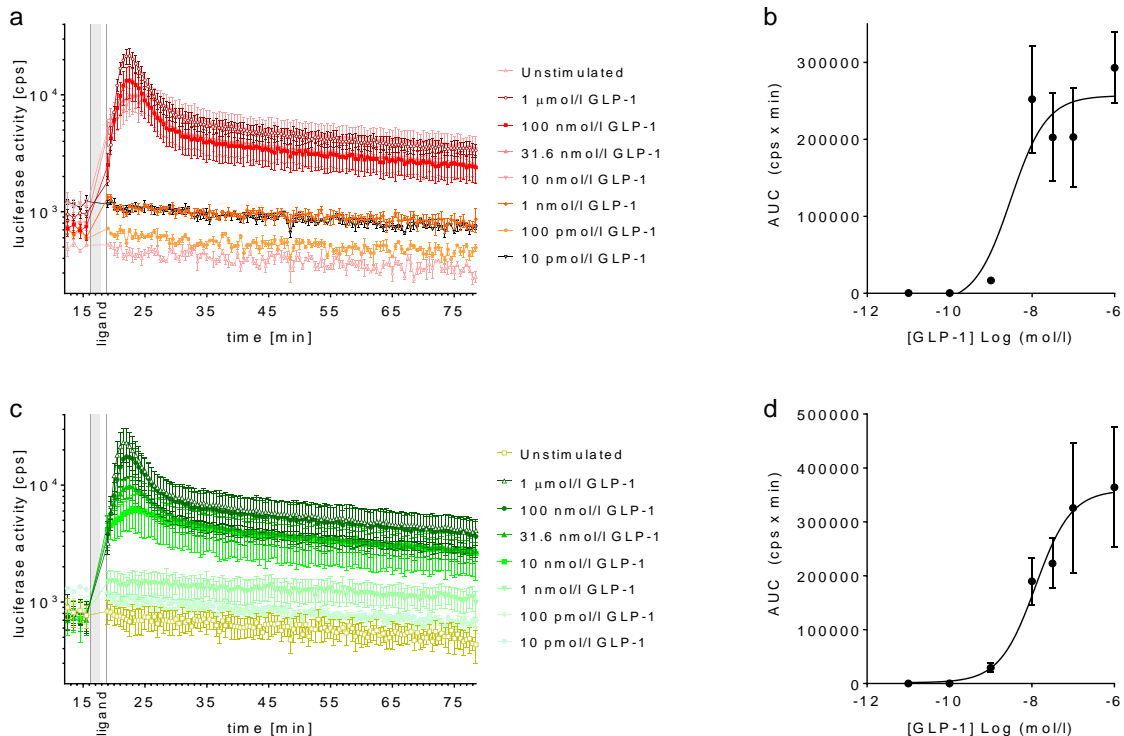


Figure 3.6 GLP1R signalling via beta-arrestin 1 and beta-arrestin 2. (a) Real-time beta arrestin 1 responses to a dose titration of GLP-1. The beta-arrestin is tagged with the small part of nanoluciferase, and GLP1R is tagged with the large part of nanoluciferase, an increase in luciferase activity represents recruitment of beta-arrestin to the GLP1R. (b) Area under curve (AUC) summary data displays GLP-1 dose response curve for beta-arrestin 1 recruitment. (c) Real-time beta arrestin 2 responses to a dose titration of GLP-1. (d) Area under curve (AUC) summary data displays GLP-1 dose response curve for beta-arrestin 2 recruitment. This was a pilot experiment to determine the dose of GLP-1 required for beta-arrestin recruitment, data are mean \pm SEM ($n=1$ from 3 wells).

Pre-incubation of cells with 1 μ mol/l Glp1R0017 prior to use in the assay had varying effects on GLP-1 induced β -arrestin 1 and β -arrestin 2 recruitment, dependent on the GLP-1 concentration. When Glp1R0017 and GLP-1 were used at equimolar concentrations, no effect was seen on recruitment of the β -arrestins. 10-fold excess of Glp1R0017 slightly reduced recruitment of both β -arrestins, however when the area under the curve (AUC) was calculated, the Glp1R0017 effect was not significant. When Glp1R0017 was used at 100-fold excess, GLP-1 stimulated β -arrestin recruitment was inhibited (Figure 3.7a-d). Use of an isotype control antibody (NIP228) showed that the inhibitory effect was specific for

Glp1R0017 (Figure 3.7e, f). When either Glp1R0017 or the isotype control antibody was added at the time of ligand addition, no β -arrestin recruitment was observed (data not shown).

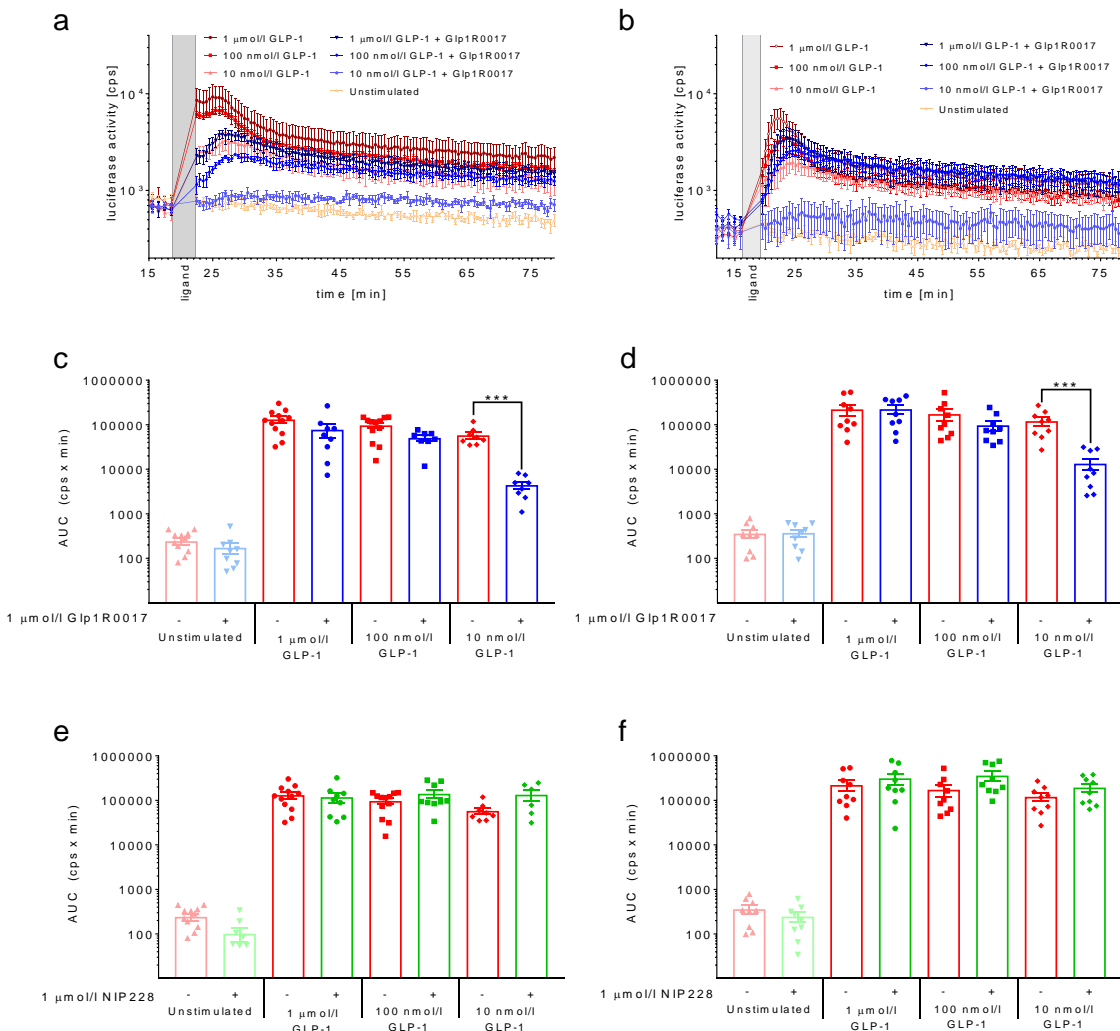


Figure 3.7 GLP1R signalling via beta-arrestin 1 and beta-arrestin 2 is inhibited by Glp1R0017 pre-incubation. Example real-time beta arrestin responses to a dose titration of GLP-1 +/- 1 $\mu\text{mol/l}$ Glp1R0017 are displayed for beta-arrestin 1 (a) and beta-arrestin 2 (b). Area under curve (AUC) summary data +/- 1 $\mu\text{mol/l}$ Glp1R0017 ($n=3$) displayed for beta-arrestin 1 recruitment (c) and beta-arrestin 2 recruitment (d). AUC summary data +/- 1 $\mu\text{mol/l}$ NIP228 ($n=3$) displayed for beta-arrestin 1 recruitment (e) and beta-arrestin 2 recruitment (f). AUC has been calculated using the 5 minutes prior to ligand addition as the baseline value. Data are mean \pm SEM. Data was \log_{10} transformed for normality. Following this statistical significance was assessed by one-way ANOVA with post hoc Bonferroni test, *** $p<0.001$.

3.4.4 Glp1R0017 inhibits GLP1R at natural levels in the INS-1 832/3 cells

To determine whether Glp1R0017 could inhibit the GLP1R when expressed at natural levels, the rat pancreatic beta cell line INS-1 832/3 was used. Firstly, the antagonism of GLP-1 induced cAMP responses was measured by live cell imaging. Briefly, INS-1 832/3 cells were transfected with Epac2-

camps, a FRET-based cAMP sensor [295], and then the CFP/YFP ratio was recorded over time. GLP-1 at 100 nmol/l stimulated an increase in cAMP (Figure 3.8a). However, when 1 μ mol/l Glp1R0017 was incubated with cells prior to live-cell imaging, the cAMP response was reduced (Figure 3.8b). Overall, the cAMP response was reduced by 64%. In contrast, Glp1R0017 pre-incubation had no effect on the responses to forskolin/IBMX (Figure 3.8c).

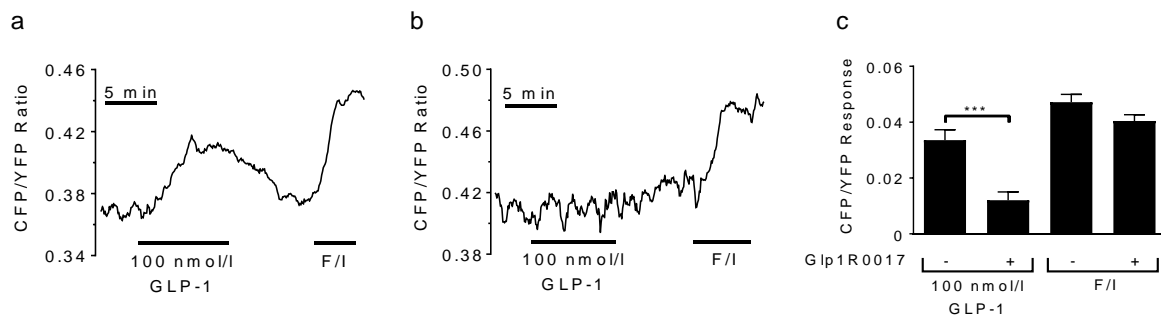


Figure 3.8 Glp1R0017 reduces GLP-1-stimulated cAMP in INS-1 832/3 cells. (a) Example trace of changes in cAMP concentration in response to GLP-1 receptor activation. INS-1 832/3 cells were transfected with Epac2-camps, to enable measurement of cAMP by FRET. Cells were then perfused with GLP-1 (100 nmol/l) followed by forskolin/IBMX (F/I; 10 μ mol/l or 100 μ mol/l), as indicated. (b) Example trace demonstrating the effect of 15 minute pre-incubation of cells with 1 μ mol/l Glp1R0017 (c) Mean changes in the CFP/YFP emission ratio. Data are mean \pm SEM; $n=19$ for antibody-treated cells, and $n=26$ for cells without antibody (monitored in 9–11 independent experiments per condition). Statistical significance was assessed by one-way ANOVA with post hoc Bonferroni test. *** $p<0.001$.

As the INS-1 832/3 cells are a pancreatic beta cell line, this enabled the Glp1R0017 effect on insulin secretion to be investigated. The potentiation of insulin secretion by GLP-1 requires the presence of glucose, therefore the concentration of basal glucose to use was first assessed. Insulin secretion in the presence of 8.3 mmol/l glucose or 16.7 mmol/l glucose was compared. 16.7 mmol/l glucose increased basal insulin secretion, and GLP-1 potentiated insulin secretion was only observed at a significant level with 100 nmol/l GLP-1. In comparison, when 8.3 mmol/l glucose was used as basal glucose, significant increases in insulin secretion were observed with both 10 and 100 nmol/l GLP-1 (Figure 3.9a).

Glp1R0017 reduced GLP-1 stimulated insulin secretion, but had no effect on GIP stimulated insulin secretion (Figure 3.9b). Interestingly, Glp1R0017 was only able to reduce GLP-1 stimulated insulin secretion to basal levels when used at a 10-fold excess. When used at equimolar concentrations, the insulin secretion was only partially reduced. Of note, Glp1R0017 also significantly reduced the 8.3 mmol/l glucose induced insulin secretion. Upon further investigation, 8.3 mmol/l glucose was shown to stimulate GLP-1 secretion from INS-1 832/3 cells (Figure 3.9c). This basal level of GLP-1 secretion

likely explains why Glp1R0017 reduced insulin secretion at 8.3 mmol/l glucose without the addition of exogenous GLP-1.

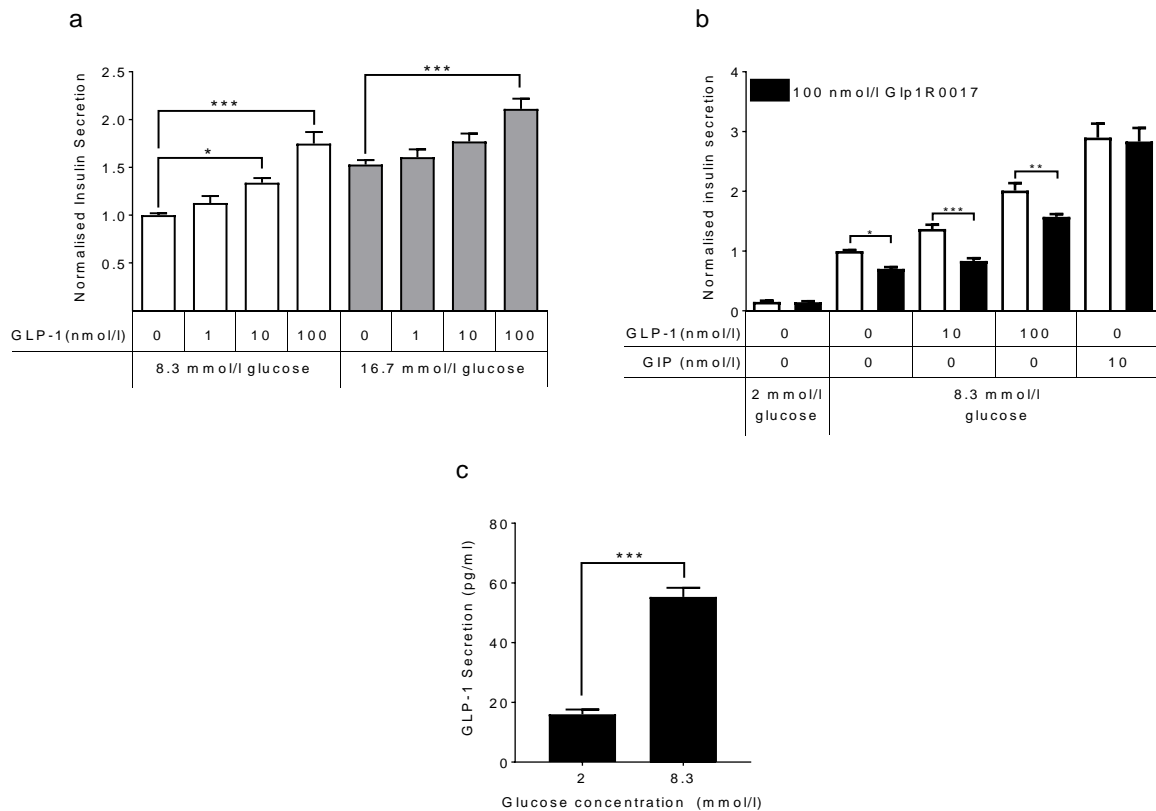


Figure 3.9 Glp1R0017 reduces GLP-1 induced insulin secretion in INS-1 832/3 cells. Insulin secretion is expressed relative to secretion in 8.3 mmol/l glucose, all data are mean \pm SEM. (a) 8.3 mmol/l glucose and 16.7 mmol/l glucose were assessed as basal glucose concentrations for investigating GLP-1 induced insulin secretion. $n=6$ wells (from 2 independent experiments). Statistical significance was assessed by one-way ANOVA with post hoc Bonferroni test. (b) Effect of Glp1R0017 on GLP-1 and GIP stimulated insulin secretion. $n=9-18$ wells (from 3–6 independent experiments). Statistical significance was assessed by one-way ANOVA with post hoc Bonferroni test. (c) GLP-1 secretion from INS-1 832/2 cells stimulated by glucose. $n=9$ wells (from 3 independent experiments). A two-tailed unpaired t-test was used to assess statistical significance. * $p<0.05$, ** $p<0.01$, *** $p<0.001$.

3.4.5 Glp1R0017 can be used to immunostain GLP1R from mouse tissue

In addition to the use of Glp1R0017 as a GLP1R antagonist, the ability of Glp1R0017 to immunostain GLP1R in mouse tissue was also investigated. Initially, pancreas tissue was used to test the antibody, due to the high levels of GLP1R expression within pancreatic islets. Tissue was collected from *Glp1r-Cre/ROSA26-tdRFP* mice [93] so that colocalisation of Glp1R0017 with GLP1R could be determined. Tissue from *Glp1r^{-/-}* mice [294] was also used as a negative control.

Immunostaining of *Glp1r-Cre/ROSA26-tdRFP* tissue revealed that Glp1R0017 bound to cells expressing the tandem red fluorescent protein (tdRFP) (Figure 3.10a). In contrast, no immunostaining with

Glp1R0017 was observed in the *Glp1r*^{-/-} (Figure 3.10b). This again suggested that Glp1R0017 is specific for the GLP1R.

The ability of Glp1R0017 to immunostain GLP1R was further assessed in the arcuate nucleus region of the hypothalamus, where GLP1R expression is thought to play a role in controlling food intake [94, 107, 125]. Similar to staining in the pancreas tissue, Glp1R0017 immunostaining overlapped with tdRFP staining for the GLP1R (Figure 3.10c). Overall, these immunostaining results gave confidence that administration of Glp1R0017 to mice would lead to GLP1R binding *in vivo*.

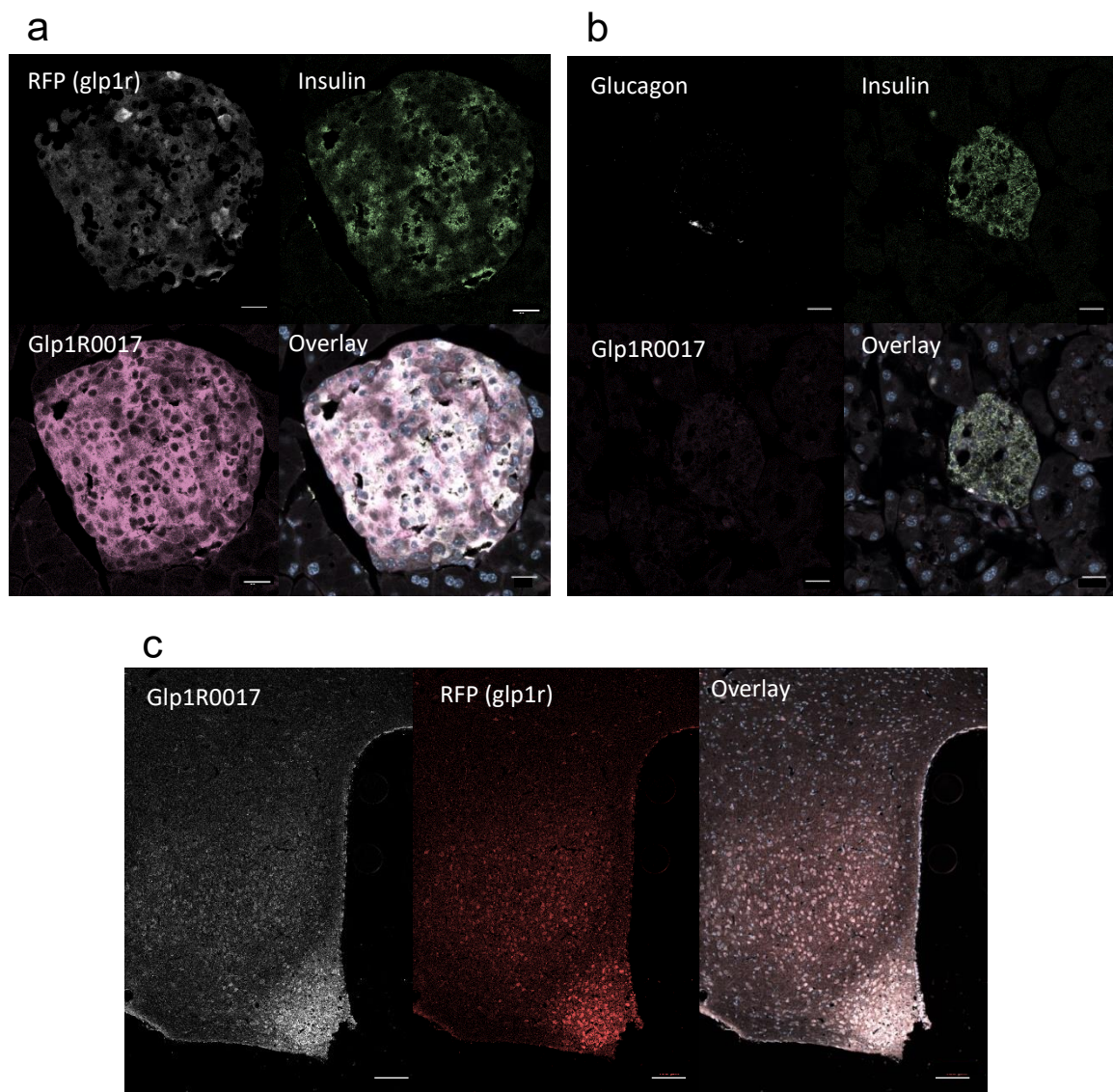


Figure 3.10 Glp1R0017 immunostains GLP1R in mouse pancreas and brain tissue. (a) Representative pancreas islet section from *Glp1r*-Cre/ROSA26-tdRFP tissue immunostained for RFP (white), insulin (green) and GLP1R using Glp1R0017 (pink). Overlay is seen in bottom right panel. Nuclei were visualised with Hoechst stain. Scale bars, 20 μ m. (b) Representative pancreas islet section from *Glp1r*^{-/-} tissue immunostained for glucagon (white), insulin (green) and GLP1R (pink). Scale bars, 20 μ m. Overlay is seen in bottom right panel. (c) Representative hypothalamic section from *Glp1r*-Cre/ROSA26-tdRFP tissue immunostained for RFP (red) and GLP1R (white). Nuclei were visualised with Hoechst stain (blue). Scale bars, 100 μ m. Overlay is seen in right hand-side panel.

3.4.6 Glp1R0017 inhibits the GLP-1 incretin effect *in vivo*

Prior to use in any functional studies *in vivo*, the pharmacokinetic profile of Glp1R0017 was determined. Glp1R0017 was dosed to mice at 19.2 mg/kg either using an intraperitoneal route or subcutaneous route, following which the pharmacokinetic profile of Glp1R0017 was compared between the different administration routes, over a period of 5 days.

The intraperitoneal dosing of Glp1R0017 reached maximal concentration (C_{max}) 4 hours after dosing, whereas Glp1R0017 dosed via subcutaneous injection reached C_{max} 24 hours post-dosing. The values of C_{max} were similar in both groups; 2.1 $\mu\text{mol/l}$ for the intraperitoneal dosing, and 1.7 $\mu\text{mol/l}$ for the subcutaneous dosing. By 120 hours post-injection, the plasma concentration of Glp1R0017 was 0.9 $\mu\text{mol/l}$ for the intraperitoneally dosed group, and 1 $\mu\text{mol/l}$ for the subcutaneously dosed group (Figure 3.11). This indicated that Glp1R0017 is relatively stable when dosed to mice, and consequently could be used for sub-chronic studies of GLP1R blockade. For functional experiments performed within this study, subcutaneous dosing was used 24 hours prior to the start of experiments.

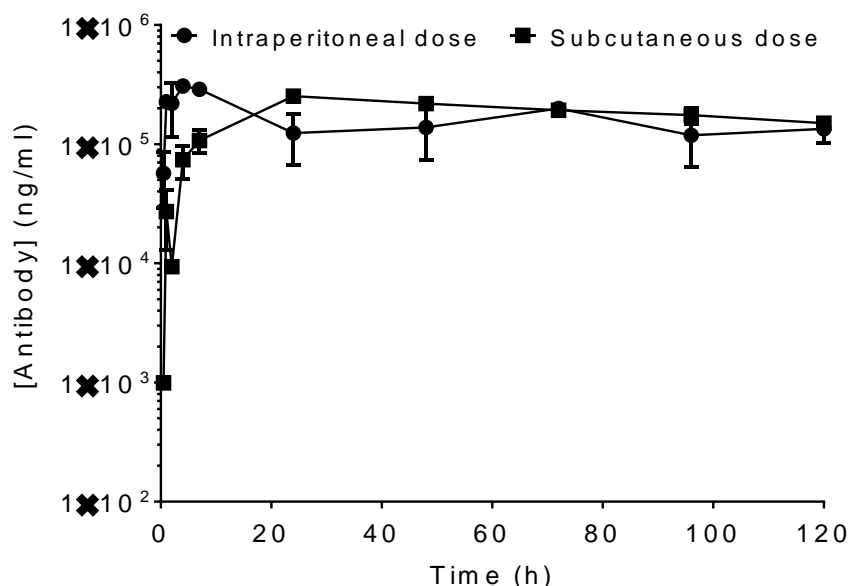


Figure 3.11 Pharmacokinetic analysis of Glp1R0017 over a 5 day timecourse. Glp1R0017 was dosed at 19.2 mg/kg to two groups ($n=6$) either intraperitoneally or subcutaneously, and antibody concentration was measured in the plasma ($n=3$ per timepoint). One sample is missing at 0.5 hours in the subcutaneous group, and one sample at 72 hours in the intraperitoneal group is also missing.

To investigate the effects of Glp1R0017 *in vivo*, glucose tolerance tests (GTTs) were used. Firstly, the ability of Glp1R0017 to block the glucose lowering effects of liraglutide, a GLP-1 mimetic, was assessed

using intraperitoneal GTTs (IPGTTs). Subsequently, the ability of Glp1R0017 to block the incretin actions of endogenous GLP-1 was determined using oral GTTs (OGTTs).

Results from the IPGTT showed that Glp1R0017 dose-dependently reversed the actions of liraglutide on glucose tolerance (Figure 3.12a, b). When the AUC of the vehicle control group was compared with the AUC of the highest concentration of Glp1R0017 group, no significant difference was found (Figure 3.12b). This indicates that at 19.2 mg/kg Glp1R0017 completely abolishes the effect of liraglutide on glucose tolerance. This set of data provided the first indication that Glp1R0017 can inhibit the GLP1R *in vivo*.

To assess possible compensation of one incretin for the other within OGTTs, Glp1R0017 was dosed alone (9.6 mg/kg) or in combination with Gipg013 (100 mg/kg), which is a GIPR antagonistic antibody, previously produced at MedImmune [164]. When Gipg013 was dosed alone, no difference in glucose tolerance was observed. In contrast, individual dosing of Glp1R0017 slightly reduced glucose tolerance when compared to the isotype antibody control group. When Glp1R0017 was dosed together with Gipg013, the glucose tolerance was even further reduced (Figure 3.12c, d). This demonstrated that both antibodies could inhibit the glucose lowering actions of their respective endogenous incretin hormones, most probably via inhibition of glucose stimulated insulin secretion.

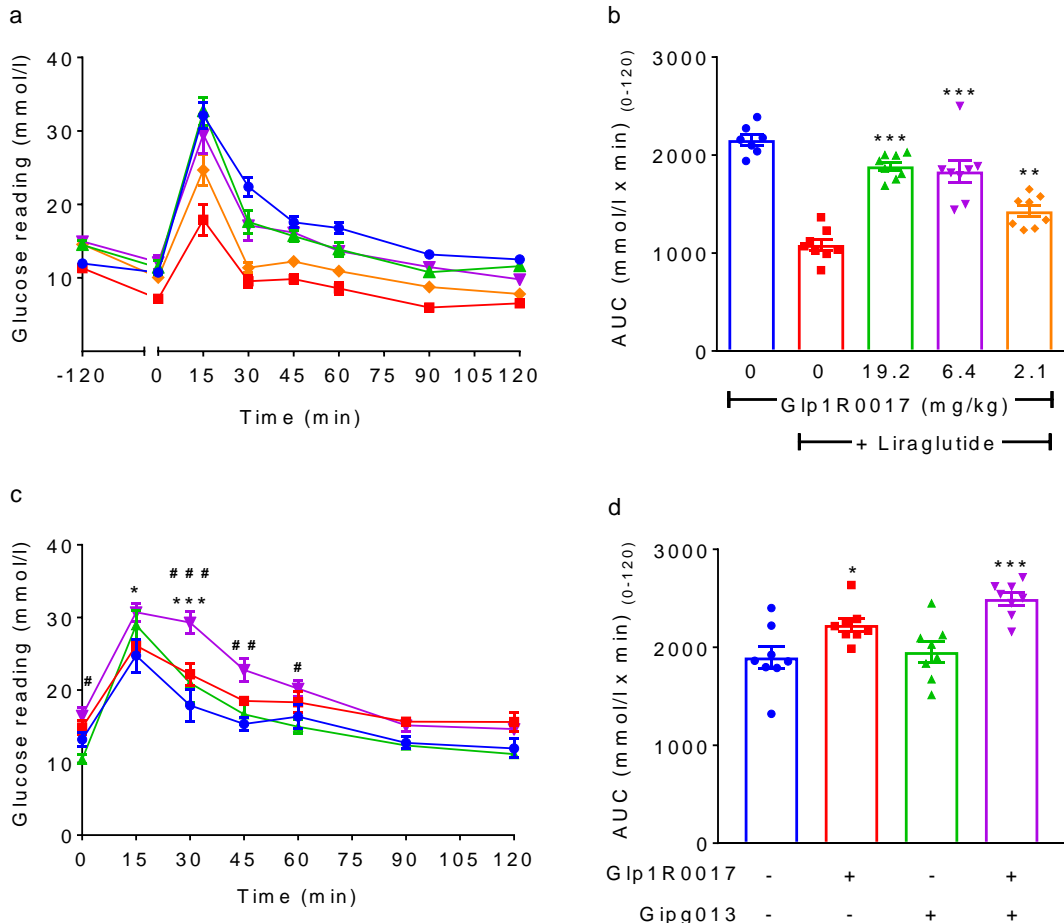


Figure 3.12 Glp1R0017 blocks the effect of liraglutide and endogenous GLP-1 on glucose tolerance. All data displayed are mean \pm SEM ($n=8$). (a) 24 hours after antibody dosing, and 2 hours after liraglutide treatment (0.1 mg/kg) intraperitoneal glucose tolerance tests (2 g/kg) were performed. The groups were; vehicle only (blue), liraglutide only (red) and liraglutide plus 19.2 mg/kg (green), 6.4 mg/kg (purple) and 3.1 mg/kg (orange) Glp1R0017. (b) AUC of glucose concentration between 0 and 120 minutes is displayed. Comparisons were made with the liraglutide-only group, and statistical significance was assessed by one-way ANOVA with post hoc Dunnett's test. (c) Oral glucose tolerance tests (2 g/kg) performed 24 hours after antibody dosing. The groups were; isotype control (blue), Glp1R0017 at 9.6 mg/kg (red), Gipg013 at 100 mg/kg (green), Glp1R0017 and Gipg013 (purple). The double-treatment group was compared with single-treatment groups, and statistical significance assessed by two-way ANOVA with post hoc Dunnett's test. *'s indicate significant differences with the Glp1R0017 only group, #'s indicate significant differences with the Gipg013 group. (d) AUC of glucose concentration between 0 and 120 minutes is displayed. Comparisons were made with the isotype control group, and statistical significance assessed by one-way ANOVA with post hoc Dunnett's test. $*p<0.05$, $**p<0.01$, $***p<0.001$

3.5 Discussion

3.5.1 Characterisation of Glp1R0017 using cell based assays

Glp1R0017 was characterised in this study using a range of *in vitro* assays, both with overexpressing cell lines and the INS-1 832/3 cell line modelling endogenously expressed GLP1R. These experiments served as a pre-requisite to *in vivo* work, and were used to show the specific inhibition of GLP1R caused by Glp1R0017. In future studies, it will be possible to use Glp1R0017 as a tool for *in vitro* inhibition of the GLP1R.

The use of cAMP HTRF based assays allowed for cross-species reactivity, and cross-receptor reactivity to be assessed. Glp1R0017 is specific for the GLP1R (Figure 3.2b-d), and has antagonistic activity across the multiple species characterised (Figure 3.2a). In comparison to the GLP1R antibodies recently produced by Novo Nordisk [116, 252, 253] (described in Chapter 2), Glp1R0017 produced here is advantageous in terms of cross-species reactivity, and the ability to block GLP1R *in vivo*. The specificity observed provides a major advantage when Glp1R0017 is compared to the peptide antagonist exendin 9-39 which has been shown to have some off-target effects [121, 243, 244]. However, it must be noted that a limited range of GPCR's were investigated here for off-target responses, meaning potential interactions with unknown targets cannot be excluded.

Schild regression analysis of Glp1R0017 in the mouse GLP1R overexpressing cell line allowed for the investigation of Glp1R0017 mode of antagonism. Antagonism of the GLP1R by Glp1R0017 was found to be surmountable, in that the maximal cAMP response was still achieved with increased competing concentrations of GLP-1 (Figure 3.4a). This led to the suggestion that Glp1R0017 is a competitive antagonist for the GLP1R. However, for this to be true it is expected that the slope of the Schild regression plot would be equal to one. In this case, the slope of the Schild plots for both Glp1R0017 and exendin 9-39 was not equal to one (Figure 3.4c). One possible reason for this is a disequilibrium between agonist and antagonist at the time of cell lysis and measurement of cAMP. Alternatively, the inhibition may not be as simple as a competition for the same binding site on the receptor. The calculated dissociation constant should therefore only be taken as an estimate.

For further investigation, structural studies would be incredibly helpful in determining whether the Glp1R0017 epitope is the same as the GLP-1 binding site. Recent structural studies have shown GLP-1 binding within the transmembrane domain and in the large N terminal extracellular domain of GLP1R [85-87]. As Glp1R0017 is larger in size than GLP-1, and was selected via binding to the extracellular domain of GLP1R, it is unlikely that Glp1R0017 shares the exact same binding site as GLP-1. Rather than binding to the transmembrane domain and extracellular domain, it is predicted that Glp1R0017 binds only to the extracellular domain of GLP1R.

When the alternative signalling pathways downstream of GLP1R were investigated, increased intracellular Ca^{2+} was observed in GLP-1 stimulated human GLP1R overexpressing cells (Figure 3.5a) but not in mouse GLP1R overexpressing cells. This increase in intracellular Ca^{2+} was abolished by pre-incubation of cells with Glp1R0017 (Figure 3.5b, c). Within published data, GLP1R signalling via intracellular Ca^{2+} has been investigated in most detail in human GLP1R overexpressing cells [279, 280], although coupling to $\text{G}_{\alpha q}$ has also been observed in cells overexpressing the rat GLP1R [275]. The lack of signalling in the mouse GLP1R overexpressing cell line observed here, may be due to the much lower levels of mouse GLP1R overexpression when compared to human GLP1R overexpression. When levels of GLP1R overexpression were measured using fluorescently tagged GLP-1, the levels of mouse GLP1R in the overexpressed cell line were below the limits of detection (Figure 3.3e). Despite this, the mouse GLP1R overexpressing cell line was successfully used in the cAMP assays.

A comparison of the GLP-1 dose response curves for intracellular Ca^{2+} and cAMP in the human GLP1R overexpressing cell line shows that the GLP-1 dose response for intracellular Ca^{2+} is right shifted compared to the cAMP response which had an EC_{50} in the nanomolar range. As the Ca^{2+} response was not saturated at the top concentration of GLP-1, an EC_{50} cannot be accurately defined, but appears to be in the micromolar range. This suggests that although some GLP1R signalling is via intracellular Ca^{2+} , the main signalling pathway is $\text{G}_{\alpha s}$ coupled with cAMP as the main signalling molecule. The *in vivo* role of GLP1R signalling via Ca^{2+} is debatable as GLP-1 is only found within the picomolar range in plasma [296]. Glp1R0017 was able to inhibit intracellular Ca^{2+} signalling without being in molar excess (Figure 3.5b, c).

Within literature, it has also been proposed that GLP1R signals via β -arrestin, therefore recruitment of β -arrestin was investigated in cells transiently transfected with the human GLP1R. GLP-1 dose response curves from a pilot study showed that both β -arrestins are recruited to the GLP1R (Figure 3.6). The GLP-1 dose response curves for β -arrestin recruitment gave an EC_{50} of 3 nmol/l for β -arrestin1, and 120 pmol/l for β -arrestin2. This assay used transiently transfected cells, whereas the cAMP assay used stable cell lines, therefore the EC_{50} values should not be directly compared. The importance of GLP1R signalling via β -arrestin *in vivo* is interesting to consider from a drug development point of view, as it is thought that GLP-1 mimetics that exhibit biased agonism have differing therapeutic efficiency [280, 286]. Glp1R0017 inhibited GLP-1 stimulated recruitment of both β -arrestins, however only when used at 100-fold excess of the GLP-1 concentration (Figure 3.7a-d).

Before moving on to *in vivo* work, the INS-1 832/3 cell line was used to study Glp1R0017 inhibition of endogenous expression levels of GLP1R. Glp1R0017 inhibited both GLP-1 stimulated cAMP signalling, and insulin secretion from this cell line (Figure 3.8, 3.9). However, Glp1R0017 also reduced insulin

secretion stimulated from 8.3 mmol/l glucose alone (Figure 3.9b). This led to the incidental finding that 8.3 mmol/l glucose stimulated GLP-1 secretion from the INS-1 832/3 cells (Figure 3.9c), which probably explains why Glp1R0017 reduces the insulin secretion when cells are stimulated with 8.3 mmol/l glucose alone. Glp1R0017 had no effect on insulin secretion stimulated with 10 nmol/l GIP (Figure 3.9b). However due to the glucose stimulated GLP-1 secretion, antibody off-target effects could not be investigated using submaximal concentrations of GIP or other $G_{\alpha s}$ coupled stimuli.

The observation of GLP-1 secretion from the INS-1 832/3 cells was surprising as the cell line is described as a pancreatic beta cell line [291, 297]. The INS-1 832/3 cells were created by transfecting INS-1 cells with the human insulin gene, and isolating the clones of interest which were highly responsive to a change in glucose concentration [297]. Originally the INS-1 cells were isolated from a radiation induced insulinoma tumour, raising the possibility that the parental INS-1 cells may not have been clonal pancreatic beta cells, and instead a mixture of pancreatic endocrine cells [298]. As GLP-1 secretion from pancreatic alpha cells has been observed elsewhere [299, 300], the hypothesis that the INS-1 832/3 cells are not clonal could explain why GLP-1 secretion was observed upon stimulation with 8.3 mmol/l glucose. Alternatively, genetic drift observed in all cell lines over time [301], may contribute to the explanation for GLP-1 secretion in 8.3 mmol/l glucose.

Overall, the combination of *in vitro* signalling data suggested that Glp1R0017 is a competitive antagonist that specifically targets the GLP1R, across multiple species.

3.5.2 Use of Glp1R0017 for immunostaining

Alongside the characterisation of Glp1R0017 in cell based assays, the antibody was successfully used for immunostaining of mouse tissue highly expressing the GLP1R in the pancreas and arcuate nucleus. Due to the limited availability of tissue from *Glp1r^{-/-}* mice, only pancreas staining was used as a negative control to show that Glp1R0017 immunostaining was specific for the GLP1R (Figure 3.10).

The staining of pancreatic tissue can be compared with staining using 7F38A2; both antibodies specifically immunostained GLP1R on the beta cells within the islets of Langerhans [252]. As described earlier, GLP1R expression is not limited to the pancreas, and is widely distributed in a number of different tissues, likely at varying levels [93, 98]. Therefore, in future work with Glp1R0017 it will be important to assess immunostaining in areas such as the kidney and heart, where GLP1R is expressed at lower levels. Due to the lower expression of antigen, it is expected that optimisation of the immunostaining procedure will be necessary, perhaps using antigen retrieval methods or increased concentrations of antibody.

The cross-species reactivity of Glp1R0017, demonstrated in a range of species-specific GLP1R overexpressing cell lines (Figure 3.2a), suggests that Glp1R0017 will be suitable for immunostaining GLP1R tissue from a range of species. It is hoped that this would complement human and monkey GLP1R immunostaining observed with the previously published GLP1R antibody, MAb 3F52, which has been used to map GLP1R expression in the primate brain [116, 302]. Compared with both MAb 3F52 and 7F38A2, Glp1R0017 produced and characterised in this study has the main advantage of cross-species reactivity. Glp1R0017 provides an additional tool for the field of GLP1R research, and the study of GLP1R physiology in rodents and other species (cynomolgus monkey, dog and human).

3.5.3 Characterisation of *in vivo* GLP1R inhibition using Glp1R0017

The pharmacokinetic study of Glp1R0017 showed stability over a 5-day period, by 120 hours post administration the concentration of Glp1R0017 in the plasma had approximately halved (Figure 3.11), leading to the estimation that Glp1R0017 half-life in mice is around 120 hours. To determine the actual biological half-life of Glp1R0017, an extended pharmacokinetic study of Glp1R0017 is required. The expected half-life for antibodies in the human IgG1 format is approximately 10 days [164, 303]. This extended stability when compared to the peptide antagonist, exendin 9-39, gives Glp1R0017 a competitive advantage. With repeated doses, Glp1R0017 could be used to study the effects of chronic GLP1R inhibition.

In this study, rather than using long term studies, the effects of acute administration of Glp1R0017 to mice were investigated. Glp1R0017 when dosed 24 hours prior to an IPGTT, dose dependently reversed the effects of liraglutide on glucose tolerance (Figure 3.12a, b). The ability of Glp1R0017 to inhibit GLP1R *in vivo* could give rise to a range of further studies. For example, GLP-1 containing dual or triple agonists could be characterised in more detail, alternatively GLP1R physiology could be studied in more depth.

OGTTs were used to assess whether Glp1R0017 could inhibit the endogenous GLP-1 effects on glucose tolerance. The availability of both Glp1R0017, along with Gipg013 as a GIPR antagonistic antibody meant that the actions of both incretin hormones could be inhibited [164]. The OGTT results produced here can be compared with glucose tolerance of *Glp1r*^{-/-} and *Gipr*^{-/-} mice. The results are comparable, as both the single antibody treated groups had mild effects on glucose tolerance (Figure 3.12c,d), similar to the glucose tolerance of individual receptor knockouts [294, 304]. In contrast, the combination of Glp1R0017 and Gipg013 had a significant effect on oral glucose tolerance. This supports the hypothesis that the incretin hormones are able to compensate for each other, as was proposed in studies using both single and double incretin receptor knockout mice [305].

Gipg013 dosed independently had no significant effect on oral glucose tolerance, whereas Glp1R0017 caused a small but significant increase in plasma glucose levels in the OGTT (Figure 3.12c, d). This suggests that the role of GLP-1 in insulin secretion is potentially more important than GIP in the C57/Bl6 mouse model. This contrasts with other studies using the single and double incretin hormone receptor knockout mouse models, which concluded GIP was more important than GLP-1 for the incretin effect [305].

Overall, cohesive conclusions cannot be made regarding which incretin hormone is the most important. However, the data confirms there is a compensatory effect upon inhibition of either of the incretin hormones, and demonstrates Glp1R0017 can be used to inhibit GLP1R *in vivo*.

3.5.4 Possible future uses of Glp1R0017

As Glp1R0017 can be used to inhibit both the actions of exogenously added GLP-1 mimetics, along with endogenously secreted GLP-1, the possible applications of Glp1R0017 are broad. Firstly, Glp1R0017 could be used to investigate GLP-1 mimetics, and GLP-1 containing dual or triple agonists in more depth. Secondly, Glp1R0017 could be used to study GLP1R physiology, such as the importance of the GLP1R after gastric bypass surgery. Finally, there is also the possibility of using Glp1R0017 therapeutically for the treatment of patients with hypoglycaemia.

GLP-1 mimetics within the clinic for type 2 diabetes treatment have varying beneficial effects within the cardiovascular system, such as reducing the number of cardiovascular events observed in high risk patients [113-115]. Despite this, the molecular mechanism for cardio-protection remains unclear [288]. As Glp1R0017 is a specific antagonist of the GLP1R, there is the possibility of using Glp1R0017 to study whether the cardiac effects of GLP-1 mimetics are directly dependent on the GLP1R or independent. Both *in vivo* and *ex vivo* experiments could be used, for example cardiac telemetry could be used to monitor cardiovascular parameters such as heart rate and blood pressure in rodents, alternatively *ex vivo* experiments using langendorff perfusion set-ups could also be useful.

GLP-1 containing dual and triple agonists are an emerging therapeutic for the treatment of type 2 diabetes, with several molecules currently being tested in clinical trials [232]. The concept for these unimolecular dual or triple agonists is based upon the observation that gastric bypass surgery is the most effective single treatment for type 2 diabetes [225]. Clearly gastric bypass surgery alters a number of molecular pathways, thus the multi-agonists are trying to mimic the effects of gastric bypass [231]. In development of these unimolecular multi-agonists, the balance of the different components is particularly important [291, 306]. For this purpose, Glp1R0017 could be useful for investigating the importance of GLP-1 within the GLP-1 containing dual or triple agonists.

When considering the use of Glp1R0017 for studying physiology, Glp1R0017 may be used for the pharmacological inhibition of GLP1R in studies looking at the molecular mechanisms of GLP-1. Additionally, Glp1R0017 could be used to confirm the location of the GLP1R in extra-pancreatic tissues [93]. Of particular interest is determining the importance of GLP-1 signalling for the metabolic effects of gastric bypass surgery. Following gastric bypass, secretion of enteroendocrine hormones is vastly different to pre-surgery. Increased secretion of GLP-1, along with anorexic peptides oxyntomodulin, and peptide YY is observed [307, 308]. On the other hand, there is reduced secretion of GIP and ghrelin [307, 309]. There is debate surrounding whether the remission of type 2 diabetes is solely due to a change in gastrointestinal factors or due to caloric restriction [231]. The use of Glp1R0017 in rodent studies could complement studies performed with exendin 9-39 [310, 311], and shed more light on the importance of increased GLP-1 signalling for the beneficial metabolic effects of gastric bypass surgery.

Surgery on the gastrointestinal tract is not only used for the treatment of obesity and type 2 diabetes, lean patients can also undergo gastrectomy as a means for treating cancer. For the lean population of patients, significant deleterious effects are observed in the long term, with a high prevalence of “dumping syndrome” [312]. This leads to a poor quality of life, symptoms for early dumping syndrome occur within 30 minutes of eating a meal, and include diarrhoea, abdominal cramping and nausea. Late dumping syndrome occurs 2-3 hours after a meal, with patients showing signs of hypoglycaemia such as faintness, hunger and dizziness [312]. One possible cause of this is increased levels of GLP-1 post-prandially [313, 314]. Clinical studies using infusions of exendin 9-39 are in progress, and may reveal that antagonism of the GLP1R is a potential therapeutic strategy for treatment of patients with “dumping syndrome” (unpublished, Gribble lab).

Bariatric surgery can occasionally give rise to the metabolic disorder post-bariatric hypoglycaemia, which is characterised by symptomatic post-prandial hypoglycaemia. Blockade of the GLP1R by infusion of exendin 9-39 prevents this hypoglycaemia, suggesting that GLP1R antagonism may be beneficial therapeutically for treatment of patients with post-bariatric hypoglycaemia [242]. A further cause of hypoglycaemia is congenital hyperinsulinism, this is the most common cause of hypoglycaemia in children. Briefly, congenital hyperinsulinism is defined by the pancreatic beta cells secreting insulin even when plasma glucose concentrations are low [315]. Pre-clinical and clinical data supports GLP1R antagonism as a therapeutic strategy for treating this group [241, 316, 317].

Together, this collection of studies shows there is a small but significant population of people for which a GLP1R antagonistic antibody could be used therapeutically to inhibit the GLP1R, and prevent hypoglycaemia.

3.5.5 Summary

In summary, Glp1R0017 has been characterised in considerable detail within this chapter. Glp1R0017 specifically antagonises all GLP1R signalling pathways investigated, and has cross-species reactivity across a range of species. In addition to this, Glp1R0017 can be used to stain GLP1R in mouse tissue, and holds the possibility of being used for immunostaining tissue from other species. Glp1R0017 also has the ability to inhibit GLP1R *in vivo* in mouse models.

Glp1R0017 provides a new method for blockade of GLP1R over several days in a range of species. Transient and/or age-restricted GLP1R blockade can be achieved using Glp1R0017, complementing studies using *Glp1r^{-/-}* mice. Glp1R0017 may also have advantages when compared to exendin 9-39, particularly in terms of the longer half-life, and when it is important to exclude cross-reactivity with related GPCRs.

Glp1R0017 provides a novel tool for investigating the GLP-1 component of emerging unimolecular dual agonists for type 2 diabetes treatment, and for further understanding GLP1R physiology. Aside from acting as a tool, there is also prospect for using a GLP1R antagonistic antibody therapeutically for the treatment of patients with postprandial hypoglycaemia.

Chapter 4. Localisation and characterisation of glucose-dependent insulinotropic polypeptide receptor (GIPR) expressing cells

4.1 Introduction

4.1.1 Therapeutic Relevance of GIPR

The GIPR is an incretin hormone receptor, similar to GLP1R, with specificity for the ‘ugly duckling’ incretin hormone GIP (described in detail in chapter 1). However, unlike the GLP1R, agonism of the GIPR has not been successfully exploited therapeutically for the treatment of type 2 diabetes [169]. When the incretin effects of GLP-1 and GIP were compared in patients with type 2 diabetes during a hyperglycaemic clamp, GIP failed to induce insulin secretion [318]. Consequently, in comparison to the GLP1R, less research has been performed to date on the GIPR.

Recently, the combination of GIPR agonism with GLP1R agonism has been described as beneficial. In pre-clinical studies, unimolecular dual agonists for GIPR and GLP1R have increased efficacy when compared to GLP-1 agonists [48].

Contrary to the initial ideas surrounding therapeutic targeting of the GIPR, the idea of GIPR antagonism for therapeutic treatment of type 2 diabetes has also been postulated [169]. This is because insulin secretion is not the only therapeutically relevant function of the GIPR. Other functions of GIPR agonism include increased glucagon secretion in euglycaemia and hypoglycaemia [319, 320], along with effects on adiposity such as stimulation of lipoprotein lipase (LPL) activity and increased triacylglycerol (TAG) uptake [176]. The suggestion of using GIPR antagonism therapeutically is centred around the hypothesis that GIPR antagonism could reduce body fat, and limit hyperglucagonemia in patients [169]. Safety of GIP(3-30)NH₂ as a GIPR antagonist has recently been demonstrated in healthy humans, along with an observation of decreased GIP-induced insulin, and block of GIP induced increases in adipose tissue blood flow [321, 322]. Whether GIPR antagonism is a practical therapeutic strategy for type 2 diabetes remains to be elucidated.

4.1.2 Location of GIPR

As described in chapter 1, GIPR expression is not limited to the pancreas; peripherally mRNA expression has been detected by *in situ* hybridisation in the gut, adipose tissue, heart, pituitary gland and inner layers of the adrenal cortex [149]. A combination of *in situ* hybridisation and radioligand binding studies have also shown central expression of the GIPR, with expression in a number of areas including the cerebral cortex, hippocampus, lateral septal nucleus and olfactory bulb [149, 161]. Aside

from these early studies, there has been very little investigation into the actions and location of central GIPR.

GIPR antibody availability is a limiting factor for the investigation of GIPR protein localisation. Limited antibodies are available for immunostaining, and the resulting images are varying in quality [162, 163]. Although GIPR antagonistic antibodies have been produced, these do not appear to work in immunostaining [164].

To circumvent this problem, we have produced a lineage tracing transgenic mouse model to identify GIPR containing cells. This approach is comparable to that previously used within our lab to identify the location of GLP1R expressing cells [93].

4.1.3 The role of GIPR in obesity

Dietary fat is one of the main stimulants for GIP secretion [323, 324]. In addition to this, it has been observed that high fat diet (HFD) and obesity are linked with hypersecretion of GIP, and increased fasting levels of GIP [182, 323, 325-327]. The underlying mechanism for this GIP hypersecretion in the obese state is unclear; hyperplasia of the GIP-secretory K cells may form a partial explanation [327], other suggestions include decreased feedback inhibition of the K cells due to insulin sensitivity [325]. More recently, increased expression of the transcription factors regulatory factor X6 (Rfx6) and pancreatic and duodenal homeobox 1 (Pdx1) have been observed in the K cells of HFD induced obese mice, leading to the suggestion that these transcription factors are important for GIP hypersecretion in obesity [137].

In humans, an elevated level of GIP in the plasma appears to be associated with an unhealthy fat distribution in men [328]. Not only does HFD induce hypersecretion of GIP, GIPR sensitivity also appears to be improved in islets from HFD fed mice. Isolated islets from HFD fed mice have significantly improved GIP induced insulin secretion compared with islets from mice fed with chow diet, while there is no difference in GIPR expression [329]. Together, the above data suggests that GIP may have a physiologically important role in obesity.

Further evidence pointing to the importance of GIP in obesity has been found using global and tissue-specific GIPR knock out mouse models. To model obesity in mouse models, mice are either fed with HFD, or Lep^{ob/ob} mice are used which have a mutation in the leptin gene, meaning hunger is not inhibited, and mice become obese with increased adipose tissue [330].

Global knockout of the GIPR gives protection from HFD induced obesity. When the GIPR^{-/-} mice were crossed with Lep^{ob/ob} mice, a decrease in body weight and fat mass was observed in comparison with the single mutant Lep^{ob/ob} mice. Thus, the GIPR is clearly important in the control of obesity, with GIP

being a ‘key molecule linking overnutrition to obesity’. Upon further investigation it was found that the GIPR^{-/-} resistance to obesity was due to increased energy expenditure. The underlying mechanism was investigated using a peripheral based approach, focusing on the adipocyte effects of GIP. The GIPR^{-/-} mice display decreased acyl CoA:diacylglycerol transferase (Dgat1) expression in the adipocytes. As Dgat1 is involved in triglyceride synthesis, a decrease in Dgat1 suggests decreased triglyceride synthesis, meaning the GIPR^{-/-} adipocytes store less nutrients than WT mice fed with the same HFD [182].

GIPR knockout restricted to the adipose tissue (GIPR^{adipo-/-}) also leads to reduced body weight gain on HFD compared with WT mice. In contrast to the global GIPR^{-/-} mouse, no significant differences in energy expenditure were observed in GIPR^{adipo-/-} mice compared to WT mice. The differences observed in body weight corresponded to a change in lean mass rather than fat mass, with a reduction in liver volume and fat content [185].

As GIPR is expressed in the brain, it is thought that there may also be some central effects of GIP that regulate energy expenditure or food intake in obesity. Central administration of GIP to rats for 4 days (2 nmol/day) decreases body weight gain compared to control groups, and alters expression of hypothalamic genes involved in energy regulation [331]. In mice, a intracerebroventricular (ICV) single high dose (6nmol) of GIP was found to decrease food intake, without any change in body weight over 24 hours [332].

The role of GIPR in obesity still requires some further investigation. To add to the field, we have used the newly developed GIPR transgenic mouse model in combination with adeno-associated virus (AAV) technology to study the acute effects of both hypothalamic GIPR ablation and GIPR activation.

4.2 Aims

To identify and characterise cells expressing the GIPR by:

- a) Immunostaining of peripheral tissues including the pancreas, adipose tissue, duodenum and nodose ganglia from Gipr-Cre x Rosa26-EYFP/RFP mice.
- b) Immunostaining of coronal sections from perfuse fixed brains from Gipr-Cre x Rosa26-EYFP/GCamp3 mice.
- c) Ablating hypothalamic GIPR positive neurons using AAV-flex-taCasp3-TEVp and characterising the effects on food intake.
- d) Activating hypothalamic GIPR positive neurons using AAV-hSyn-DIO-hM3D(Gq)-mCherry in combination with clozapine-N-oxide (CNO) and characterising the effects on food intake.

4.3 Methods

4.3.1 Animal Studies

All experimental procedures were approved by local ethical review bodies and were performed in accordance with the Animal (Scientific Procedures) Act 1986, Home Office guidelines, local establishment guidelines and Animal Research: Reporting of In Vivo Experiments (ARRIVE) guidelines. Experiments performed using my personal licence (I290CEFFE), under a number of Home Office Project Licenses. C57/Bl6 mice were purchased from Charles River UK. Mice were group-housed in individually ventilated cages, with ad libitum access to chow diet and water unless otherwise stated. Animals were euthanized by cervical dislocation, unless otherwise stated.

4.3.2 Transgenic mice

Transgenic mice were generated by F. Reimann, in which the expression of cre-recombinase is driven by the *gipr* promoter (unpublished). Expression of cre-recombinase is responsible for reporter gene activation. The cre-recombinase recognises loxP sites surrounding a stop codon in front of the reporter gene, then deletes the ‘floxed’ stop codon. Consequently, the reporter protein is only produced in cells which express the gene of interest. However, once the reporter gene is expressed it is under the control of a constitutively active *rosa26* promoter, meaning after initial activation each cell will continue to produce the reporter protein independent of cre-recombinase. The fluorescent reporter proteins used in this study are enhanced yellow fluorescent protein (EYFP), tandem red fluorescent protein (tdRFP) [292] and the fluorescent calcium indicator GCaMP3 [293].

4.3.3 Immunostaining

Immunostaining was performed as described in chapter 3. For 3,3'-diaminobenzidine (DAB) immunohistochemistry of brain tissue, slices were washed in PBS, then incubated with 0.5% (v/v) hydrogen peroxide for 15 minutes to block endogenous peroxidase activity. Following further washing, slices were blocked for 1 hour in 5% donkey serum, 0.3% (v/v) Tween-20, then incubated with primary antibody overnight at 4°C with gentle agitation. The sections were then washed with 0.1% (v/v) PBS-Tween20, and incubated with biotinylated donkey anti-goat IgG (1:400) in 0.3% (v/v) PBS-Tween20. After a further washing, sections were incubated with avidin-biotin complex (Vector Laboratories Inc., Burlingame, USA), washed a final time, then staining was developed using DAB as the substrate (Abcam). Slides were incubated for up to 10 minutes with DAB, then washed in PBS before mounting onto Superfrost Plus glass slides (VWR). Finally, slides were dried and dehydrated using an ethanol gradient, and coverslips applied with pertex mounting media (CellPath).

Slides were imaged using confocal microscopy (TCS SP8; Leica, Wetzlar, Germany) or automated widefield microscopy (Axio Scan.Z1, Zeiss, Oberkochen, Germany). Images displayed are either confocal slices or Z-stacks, quantification of cell number and co-localisation was performed using either Image J or HALO software (Indica Labs, Corrales, USA).

4.3.4 Intracerebroventricular Surgery

All surgery, and subsequent feeding studies were performed under a Home Office Project License held by C. Blouet (PC02F3663), and surgery was kindly completed by C. Blouet as a Personal Licensee (I3AC7C9CD).

Surgery was carried out in 6-10 week old male mice under isofluorane anaesthesia, and all animals received Metacam prior to the surgery and 24 hours after surgery. A bilateral steel guide cannulae (Plastics One) was stereotactically implanted as previously described [333], and positioned 1 mm above the arcuate region of the hypothalamus (ARH) (A/P: -1.1 mm, D/V: -5.9 mm, lateral: +0.4 mm from Bregma). Beveled stainless steel injectors (33 gauge) that extended 1 mm from the tip of the guide were used for injections of viruses at 100 nl/min, 500 nl/side. AAV-hSyn-DIO-hM3D(Gq)-mCherry was used to study GIPR activation, and AAV-flex-taCasp3-TEVp was used to study GIPR ablation. All animals were given at least a 3 week recovery period, during which they were acclimatized to handling and body weight was monitored.

4.3.5 Mouse feeding studies

Feeding studies were run together with T. Darwish (I562DDDF), under the Home Office Project License held by C. Blouet (PC02F3663). To monitor food intake, mice were single housed for up to 48 hours, then returned to their group housing conditions. Aggressive behaviour was monitored, and no problems were encountered with re-grouping animals. Food intake was measured over 24 hours, either with ad lib feeding, or following a 24 hour fast. Acute food intake was also measured after intraperitoneal injection of clozapine N-oxide (1 mg/kg), this was either with ad lib feeding or following a fast of up to 10 hours. Mice were fed with either standard chow, or 45% high fat diet (D12451, Research Diets).

4.4 Results

Identification and characterisation of GIPR expressing cells has been enabled by the generation of a novel transgenic mouse by F. Reimann and I. Zvetkova. A lineage tracing approach has been utilised whereby GIPR expressing cells are labelled with a fluorescent reporter protein (Figure 4.1). A number of different fluorescent reporter lines were utilised in this study; Gipr-Cre x Rosa26-EYFP, Gipr-Cre x Rosa26-tdRFP, and Gipr-Cre x Rosa26-GCamp3.

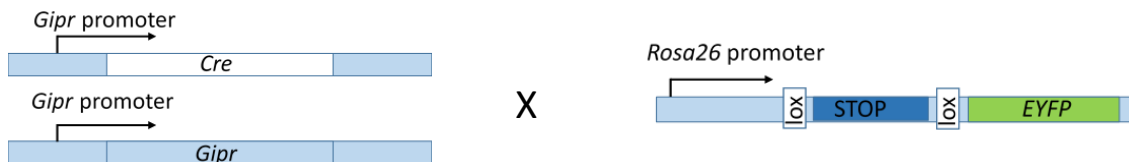


Figure 4.1 Schematic representation of transgenic mouse line used to identify cells which have expressed Gipr. The mouse model is a ‘knock-in’ model whereby on one copy of the *Gipr* gene, cre recombinase is expressed downstream of the *Gipr* promoter. Upon expression, cre recombinase removes the floxed ‘stop’ codon, enabling expression of the fluorescent reporter protein (e.g. EYFP). The fluorescent reporter is under the control of a constitutive promoter, *Rosa26*.

4.4.1 Localisation of the GIPR in peripheral tissues

For characterisation of the Gipr-Cre x Rosa26-reporter mice, pancreas tissue was the initial focus. Pancreas was collected, fixed, cryosectioned and immunostained with antibodies raised against GFP or RFP dependent upon the reporter protein used. The sections were costained for insulin as a marker for pancreatic β cells, or glucagon as a marker for pancreatic α cells (Figure 4.2). All pancreatic islets expressed the GIPR as expected for the incretin hormone receptor, with expression in both the β cells (Figure 4.2b) and α cells (Figure 4.2c). The surrounding exocrine acinar tissue also showed GIPR expression, in a heterogenous pattern (Figure 4.2a). This immunostaining provided confidence that the Gipr-Cre x Rosa26-reporter mice were successfully labelling cells which had expressed the GIPR. Secondary antibody only control slides were also imaged, and displayed no fluorescence.

Following the pancreas immunostaining, other peripheral tissues were collected and assessed for GIPR localisation. In line with the GIPR having functions in adipose tissue, expression was observed in adipose tissue from both brown and white adipose tissue depots (Figure 4.3 a, b). Within interscapular brown adipose tissue, several multilocular adipocytes scattered throughout the tissue were stained with the GFP antibody, thus suggesting GIPR expression (Figure 4.3a). GIPR positive adipocytes were also immunostained within inguinal white adipose tissue, at what appeared to be a lower density. A mixture of both multilocular and unilocular adipocytes were positively stained (Figure 4.3b). Again, no immunostaining was observed in secondary antibody only control slides.

GIP is secreted from enteroendocrine K cells within the small intestine, with a higher density of K cells in the duodenum, where GIPR expression has been reported previously [149]. We therefore examined GIPR expression in the duodenum of the Gipr-Cre x Rosa26-EYFP mouse model. Very few cells were GIPR positive within the epithelial cell layer, of interest some cells in the centre of the villus also appeared to stain with the GFP antibody (Figure 4.3c). In comparison, no cells were stained in the secondary antibody only control slides. To identify the cell-type of these GIPR positive cells co-staining experiments were performed using antibodies for glucagon, 5-hydroxy tryptamine (5-HT), vimentin and α -smooth muscle actin (α -SMA).

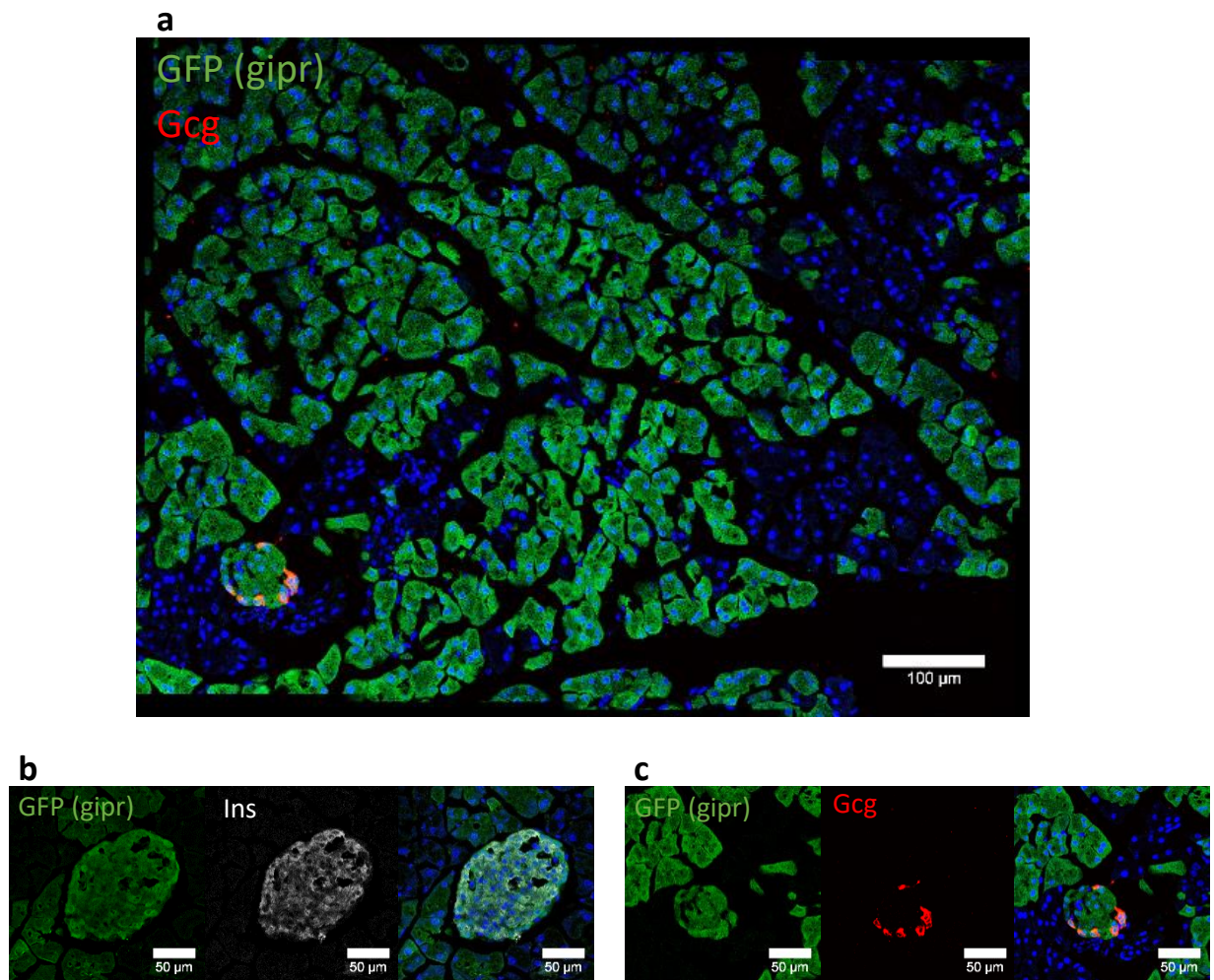


Figure 4.2 GIPR in the pancreas. Pancreas tissue from Gipr-Cre x Rosa26-EYFP mice (n=3) was assessed by immunohistochemistry. (a) Tile-scan of pancreatic tissue stained for GFP (green) and glucagon (Gcg, red) showing staining in islets and acinar tissue. (b and c) Representative pancreatic islet sections stained for GFP (green) and either insulin (Ins, white, (b)) or glucagon (Gcg, red, (c)).

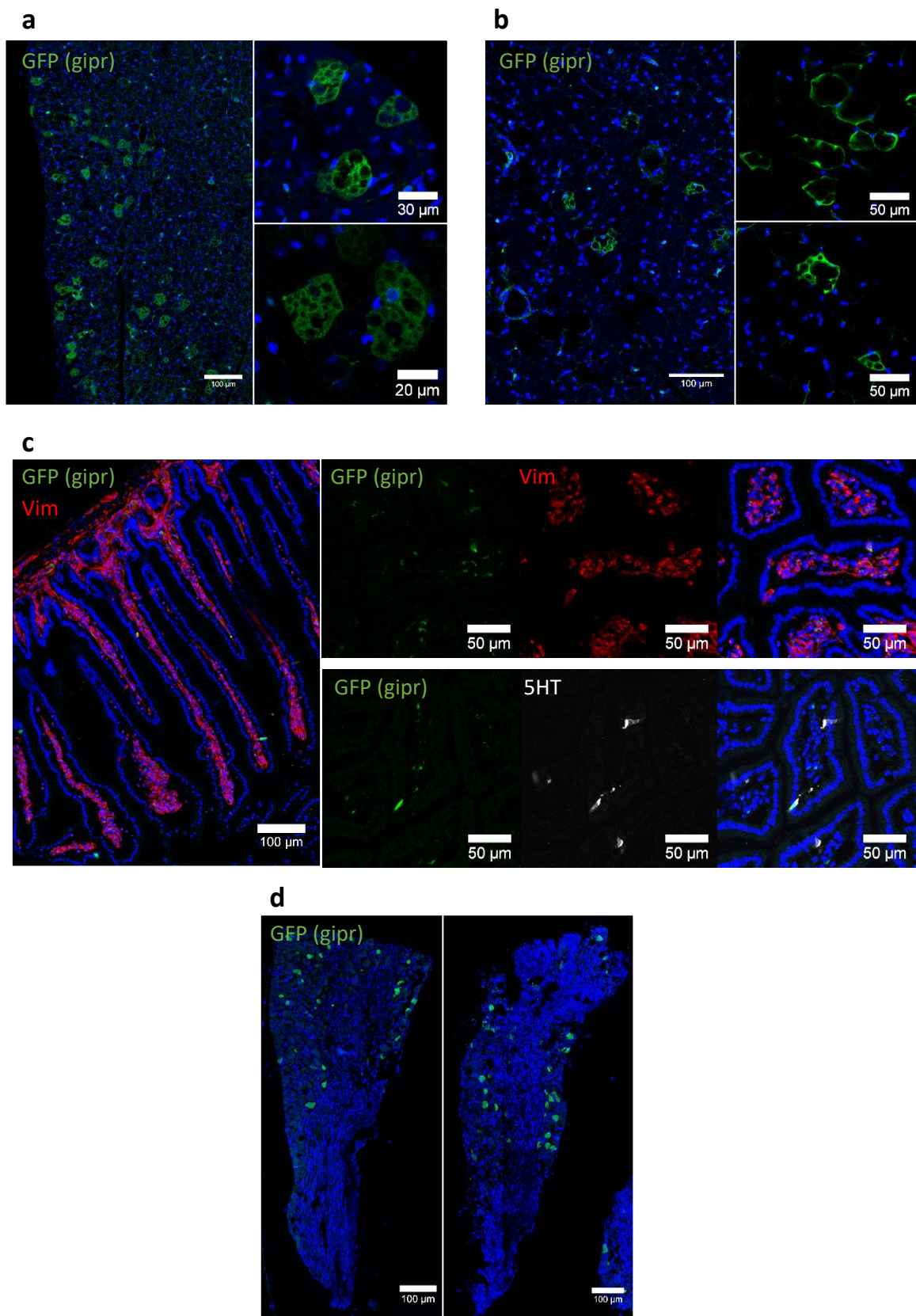


Figure 4.3 GIPR in extra-pancreatic tissue. Extra-pancreatic tissue from Gipr-Cre x Rosa26-EYFP mice was also assessed by immunohistochemistry. Sections of interscapular brown adipose tissue (a), inguinal white adipose tissue (b) duodenum (c) and nodose ganglia (d) were co-immunostained for GFP (representing *gipr* expression), and vimentin (vim) or serotonin (5HT) as indicated.

Of the GIPR positive cells within the epithelial cell layer, a minority colocalised with glucagon stained cells, indicating some GIPR expression in enteroendocrine L-cells (data not shown). 5-HT staining revealed a higher degree of colocalisation between GIPR positive cells and 5-HT producing enterochromaffin cells (Figure 4.3c). To determine the identity of the GIPR positive cells within the centre of the villi, co-staining was performed with vimentin and α-SMA to look at cells of mesenchymal origin [334, 335]. Vimentin and GFP colocalisation was observed, suggesting the GIPR positive cells within the centre of the villi are of mesenchymal origin (Figure 4.3c). The role of the GIPR within mesenchymal cells, and the specific mesenchymal cell-type in which GIPR is expressed remains to be determined.

The final peripheral tissue in which GIPR localisation was assessed was the nodose ganglia. Neurons from the nodose ganglia innervate the small intestine, as GLP1R has been identified in this tissue [93] expression of the GIPR was of interest. Indeed, immunostaining of tissue isolated from Gipr-Cre x Rosa26-EYFP mice revealed GIPR expression is found in the nodose ganglia (Figure 4.3d). No staining was found in the secondary antibody only control slides.

4.4.2 Localisation of GIPR within the brain

The GIPR is thought to play a role in regulating energy expenditure in an obese setting, and expression of the GIPR has previously been demonstrated in the brain. Expression of the GIPR within the hypothalamus would be of particular interest, as this region is known to have a role in controlling energy expenditure [336]. To add to the previous *in situ* hybridisation data set, Gipr-Cre x Rosa26-EYFP and Gipr-Cre x Rosa26-GCamp3 mice were used to further characterise the localisation of central GIPR.

To gain an overview of GIPR expression throughout the mouse brain, reporter mice were perfuse fixed with paraformaldehyde (by E. Roth) to allow complete fixation of the brain, and then coronal sections were made every 25 µm. GFP was stained, and detected by DAB immunohistochemistry, representing GIPR expression. Secondary antibody only controls were also used, and showed no immunostaining.

GIPR expressing neurons were examined from the olfactory bulb to the spinomedullary junction of the mouse brain. As described previously, GIPR expression was detected in the olfactory bulb [149, 161]. More specifically, GIPR expression was observed in the frontal association cortex (FrA), lateral orbital cortex (LO), external plexiform layer (EPI) and the mitral cell layer (Mi) of the olfactory bulb, as depicted schematically (Figure 4.4).

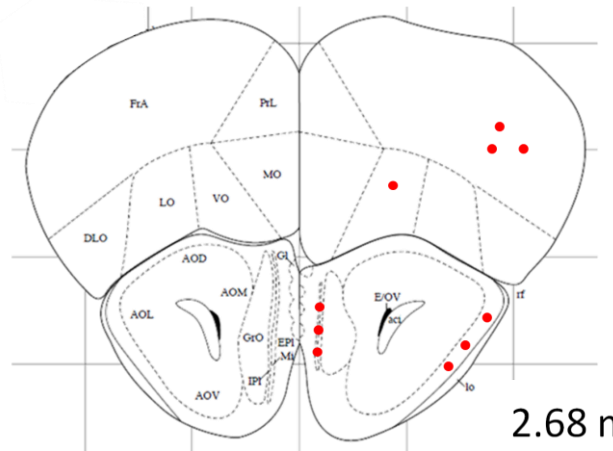
Within the nucleus of stria terminalis (BST) region of the brain GIPR expression was detected in cortex regions, in line with that previously published [149, 161] (Figure 4.4 and 4.5a). GIPR expression was also found in the medial preoptic area (MPA), medial septal nucleus (MS), dorsal part of the lateral

septal nucleus (LSD), and median preoptic nucleus (MnPO). It should be noted that staining in the LSD is similar to that observed previously [149, 161]. Surrounding the ventricle, GIPR expression was observed in the periventricular hypothalamic nucleus (Pe), anteroventral periventricular nucleus (AVPe), the anterior parvicellular part of the paraventricular hypothalamic nucleus (PaAP) and the dorsomedial part of the suprachiasmatic nucleus (SChDM). Additionally, within the BST region, densely grouped GIPR neurons were found in the subfornical organ (SFO). Of note, this expression in the SFO is similar to the GLP1R pattern of expression [94].

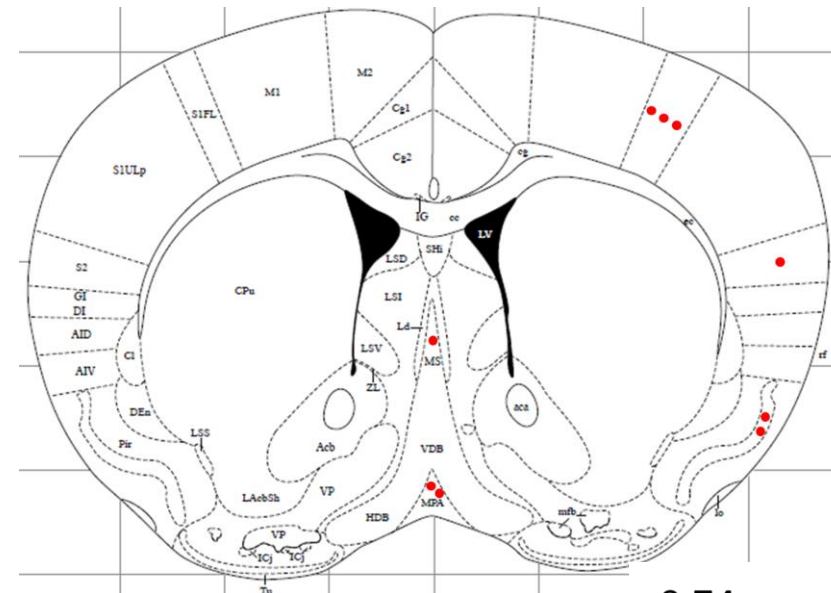
It was particularly interesting to find GIPR expression within the hypothalamic nuclei, which has not previously been described. Neuronal bodies expressing the GIPR densely populated the arcuate nucleus (Arc) region (Figure 4.4, 4.5b). In the more caudal sections of the hypothalamus GIPR positive neurons were identified in the dorsal part of the dorsomedial hypothalamic nucleus (DMD) (Figure 4.4, 4.5c). Within these sections, GIPR expression was also observed in the paraventricular thalamic nucleus (PV), field CA1 of the hippocampus (CA1), and the dentate gyrus (DG). The observation of GIPR within the hippocampus was again in line with previously published data, and gave confidence that the GIPR reporter mice were successfully reporting GIPR expressing cells [149].

Finally, upon examination of the hind brain region, GIPR positive neurons were detected at high density within the area postrema (AP), a circumventricular part of the brain that is extensively vascularised, and also expresses the other incretin hormone receptor, the GLP1R [94]. GIPR expression was also found in the medial part of the nucleus of the solitary tract (SolM) and the hypoglossal nucleus (12N) (Figure 4.4, 4.5d).

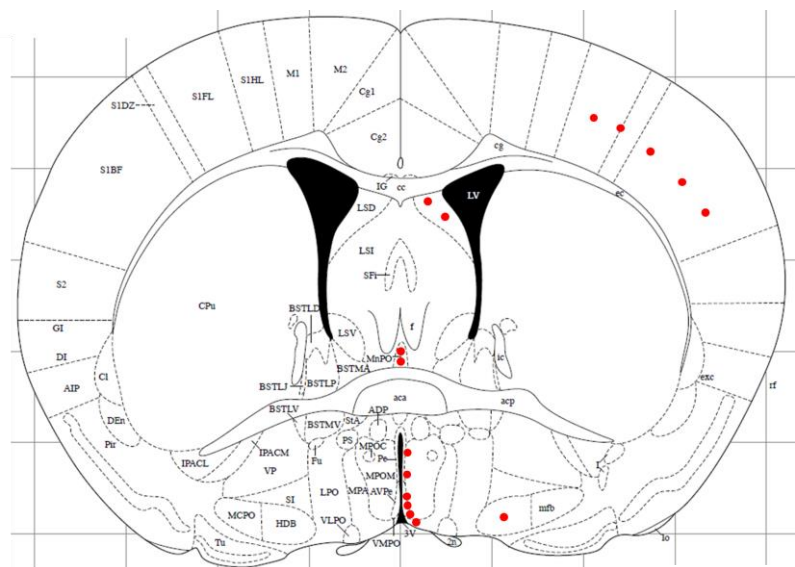
Overall, the GIPR appears to be widely distributed throughout the brain. This identification of central GIPR raises questions surrounding the function of GIPR in the brain. Initially we sought to find out whether GIP, the ligand for the GIPR, was produced centrally. Gip-Cre x Rosa26-GCamp3 transgenic mice were used for this purpose, which have a lineage tracing approach to label cells that produce GIP. Upon immunostaining of the brains from this mouse line, no expression of GFP positive cells were found within the brain (data not shown), thus suggesting GIP is not produced centrally. However, one should note that the Gip-cre model labels only 60% of GIP positive K cells in the upper small intestine [337]. This penetrance may mean that GIP positive cells in the brain were missed. With caution, from this data one would hypothesise peripheral GIP rather than centrally produced GIP acts on the central GIPR.



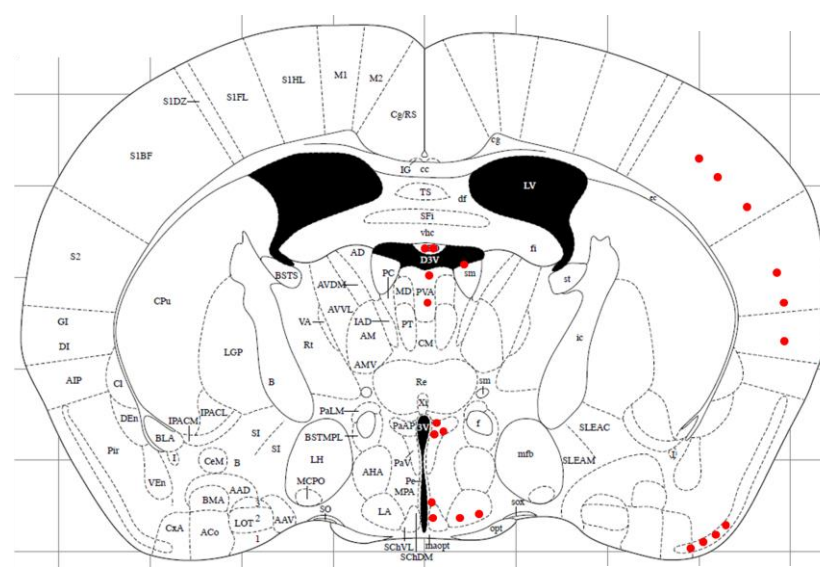
2.68 mm



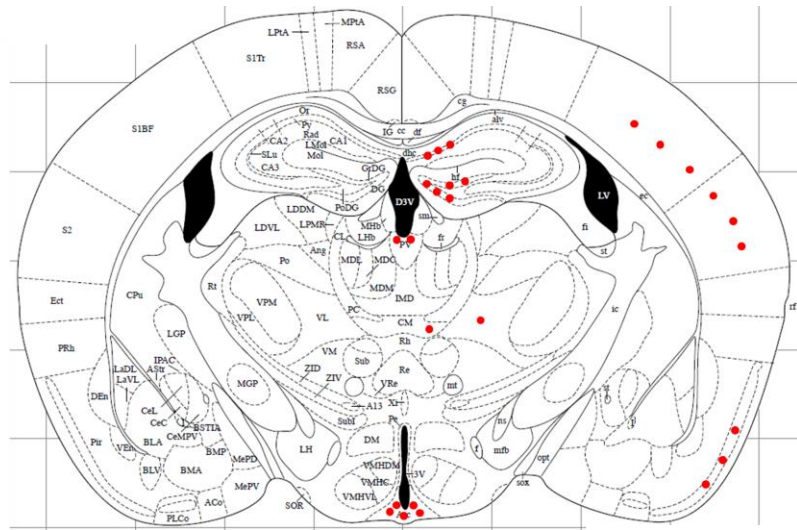
0.74 mm



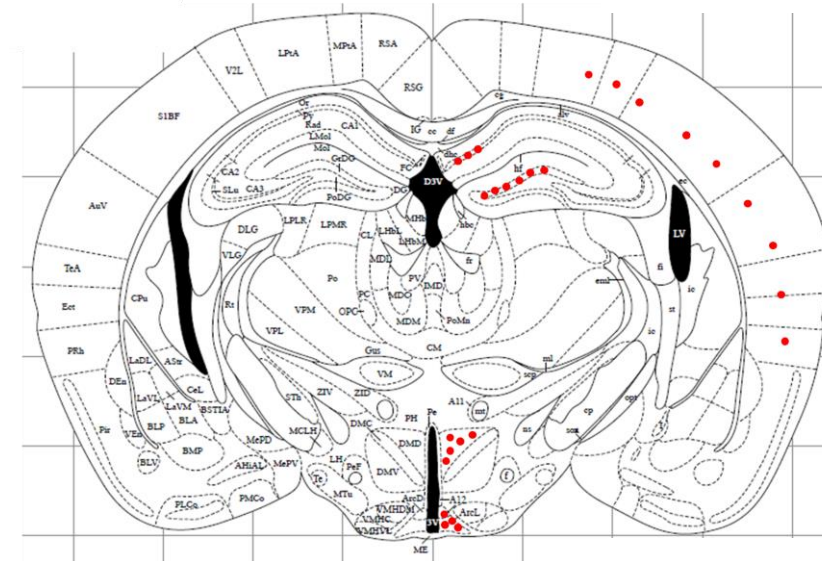
0.14 mm



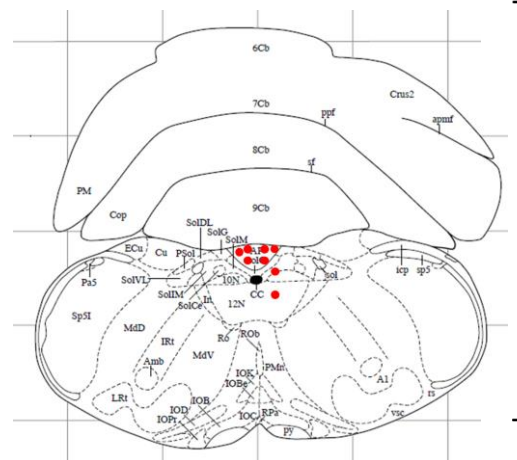
-0.58 mm



-1.46 mm



-1.94 mm



-7.48 mm

Figure 4.4 Schematic representation of GIPR expression throughout the brain. Filled red circles indicate GIPR expression, with the density indicating relative density of GFP-positive cells. Images are adapted from the Paxinos Mouse Brain Atlas, and the numerical values at the bottom right of each section shows the rostro-caudal position relative to Bregma.

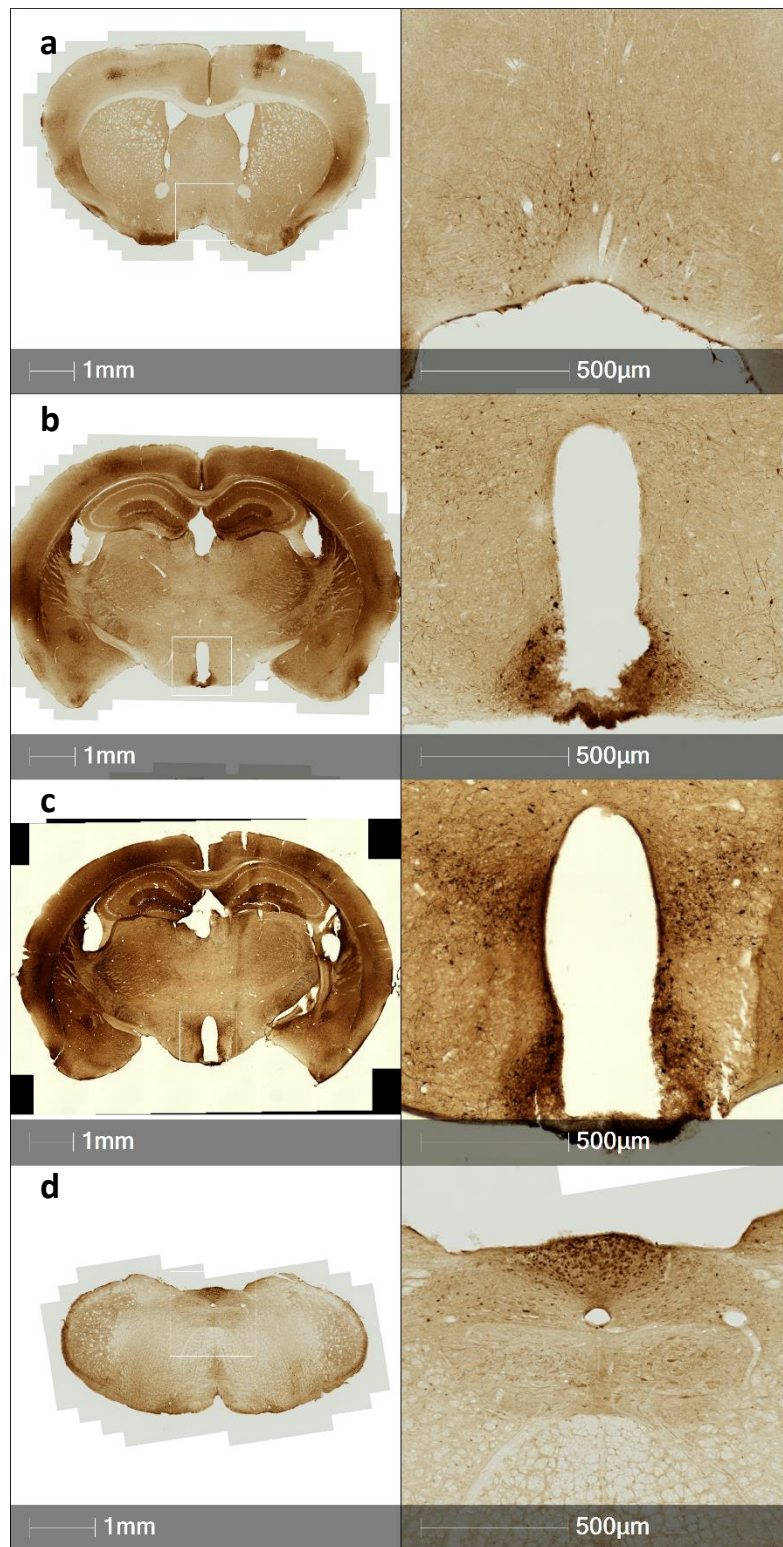


Figure 4.5 GIPR expression in the brain. Immunostaining of Gipr-Cre x Rosa26-EYFP and Gipr-Cre x Rosa26-GCamp3 brain tissue showed GIPR expression throughout the brain. Example images of a BST section (Bregma 0.74 mm) (a), a rostral (Bregma -1.46 mm) and caudal (Bregma -1.94 mm) section of the hypothalamus (b and c respectively), and a hind brain section (Bregma -7.48 mm) (d) are displayed. Areas of interest highlights in the left hand column are magnified in the right hand column.

4.4.3 Ablation of hypothalamic GIPR positive cells

Both global knockout of the GIPR, and GIPR knockout in the adipose tissue alone protect mice from HFD induced obesity [182, 185]. Following the identification of GIPR within the hypothalamus, we were interested in whether GIPR ablation in the hypothalamus had any effect on body weight or food intake.

The combination of our transgenic Gipr-Cre mouse model with Cre-dependent AAV technology allowed for the acute manipulation of Gipr-Cre positive cells. To study the function of the GIPR positive cells, hypothalamic GIPR cells were ablated by ICV injection of AAV-flex-taCasp3-TEVp (Appendix 5) (by C. Blouet). Briefly, this virus encodes a genetically engineered caspase-3, which upon activation causes apoptosis, thus removing the Cre-positive neurons expressing Gipr [338]. In more detail, the genetically engineered caspase-3, pro-taCasp3, is activated by cleavage with Tobacco Etch Virus protease (TEVp) which is co-delivered by the AAV-virus. Both pro-taCasp3 and TEVp require Cre-dependent activation [339, 340]. For the negative control group, AAV-flex-taCasp3-TEVp was injected into mice that were genotypically negative for Cre.

Within this pilot study, body weight was monitored 3 times per week, while mice were fed with standard chow diet and subsequently 45% HFD (Figure 4.6a). 24-hour food intake was assessed in the GIPR ablation and control cohort of mice, along with sensitivity to leptin. At the end of the study, adipose tissue was collected to determine whether hypothalamic GIPR ablation had any effect on adipose tissue weight. Finally, brains from three of the ablation mice with the EYFP reporter were perfuse fixed, and immunostained with a GFP antibody to confirm GIPR ablation.

When fed chow diet, both the GIPR ablation and control cohort gained body weight at the same rate (Figure 4.6b). Upon switching the diet to 45% HFD, the average increase in body weight was also the same between the two groups. However, when looking at the body weights of the individual mice, three of the ablation mice gained less body weight than the rest of the group (Figure 4.6c). No significant differences were observed between the ablation and control group when 24 hour food intake was assessed on either the chow diet and 45% HFD (Figure 4.6d, e). When mice on chow diet were injected with leptin, food intake was slightly decreased for both the ablation and control group, again with no significant difference between the two groups (Figure 4.6f). The same pattern was observed when mice were fed with 45% HFD; the net effect of leptin injection was a slight reduction in 24 hour food intake, with no significant difference in food intake between the GIPR ablation and control cohort (Figure 4.6g).

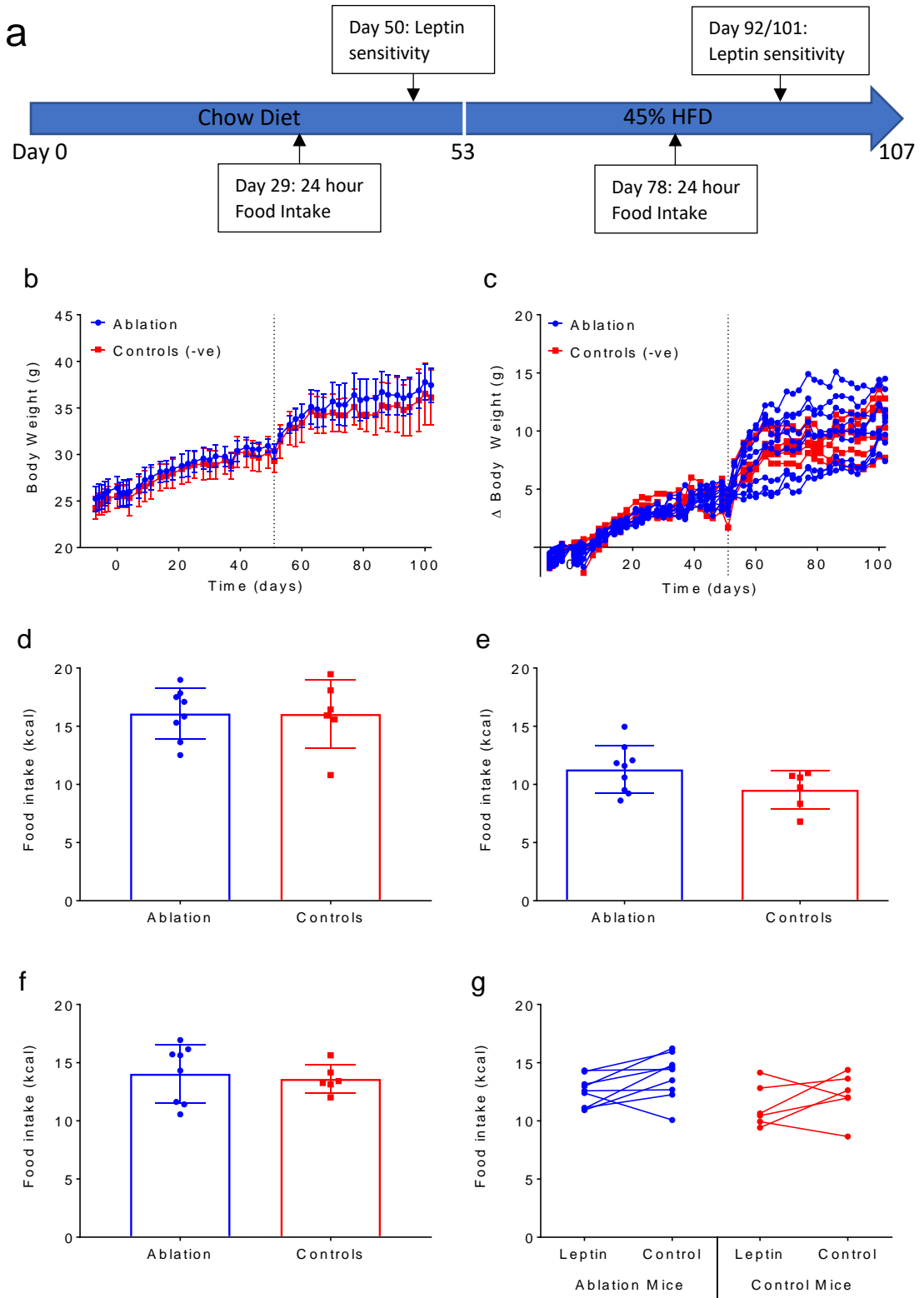


Figure 4.6 Effect of hypothalamic GIPR ablation on body weight and feeding behaviour. (a) Schematic representation of GIPR ablation study timeline. (b) Body weight monitored throughout GIPR ablation study, with a change of diet to 45% HFD indicated by the dotted line. Surgery was performed at day 0. (c) Changes in body weight throughout GIPR ablation study. (d) 24 hour food intake assessed on chow diet. (e) 24 hour food intake assessed on 45% HFD. (f) Effect of leptin injection on 24 hour food intake on chow diet. (g) Leptin sensitivity on 24 hour food intake on 45% HFD.

Despite seeing no clear differences in food intake or body weight between the GIPR ablation and control cohort of mice, at the end of the experiment adipose tissue was collected and weighed to investigate whether body fat distribution was different between the groups. Epididymal and inguinal white adipose tissue was collected along with interscapular brown adipose tissue. For each adipose tissue depot no difference in weight was observed between the GIPR ablation and control group, meaning the total adipose tissue mass was also the same in both groups (Figure 4.7).

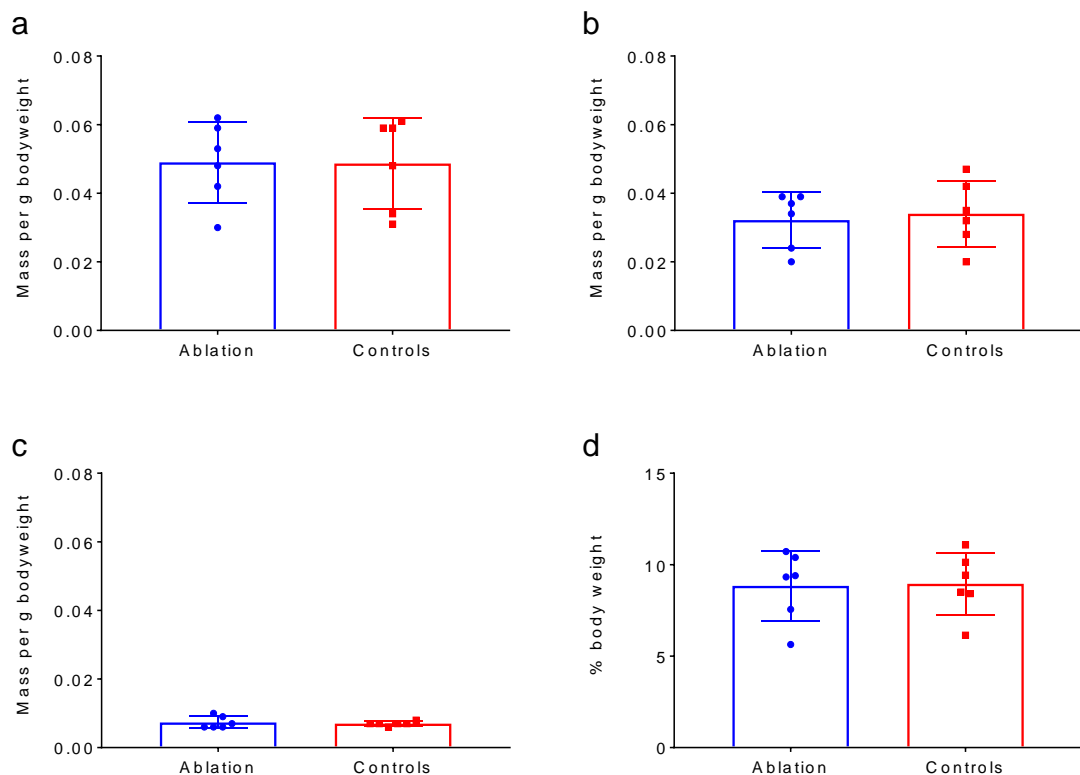


Figure 4.7 Effect of hypothalamic GIPR ablation on adipose tissue weights. Adipose tissue mass expressed per gram of body for (a) epididymal white adipose tissue (b) inguinal white adipose tissue and (c) interscapular brown adipose tissue. (d) Total adipose tissue mass expressed as percentage of body weight.

Immunostaining of hypothalamic sections confirmed two of the three GIPR ablation brains stained had successful ablation of GIPR positive cells, with fewer GFP positive cells than observed in an age-matched positive control which had not undergone surgery (Figure 4.8). To ensure this observation was correct, immunostaining was performed on two different days using either DAB immunohistochemistry, or immunofluorescent staining. For analysis, a bregma level was assigned to each section stained, then GIPR positive cells were counted within the arcuate nucleus. Per bregma level, counts have been calculated as a percentage of the total GIPR positive count in positive control tissue. Both methods of immunostaining indicated that ablation was successful for the mice with ID's

9716 and 9797. However, ablation was not successful for the third mouse with ID 9793 (Table 4.1). Of the successful GIPR ablation mice, 9716 was one of the mice which gained less body weight on 45% HFD. The remaining six mice within the GIPR ablation cohort did not have a fluorescent reporter, therefore confirmation of GIPR ablation was not possible in the rest of the cohort.

Overall, this pilot study suggests that ablation of the GIPR within the hypothalamus has no phenotypic effect on mice in terms of body weight, food intake, and fat mass distribution.

a

Percentage of cells in positive control	Bregma Level				
	-1.23	-1.31	-1.43	-1.55	-1.79
9716	37.1	10.3	42.6		71.3
9793	51.7			180.4	240.0
9797	45.7	93.1	35.5	25.5	52.5

b

Percentage of cells in positive control	Bregma Level				
	-1.22	-1.46	-1.58	-1.7	-1.94
9716		36.8		14.3	27.9
9793	28.9	62.1	91.6	281.6	
9797	83.1		24.1	18.4	

Table 4.1 Quantification of GIPR Ablation by GFP immunostaining. The three Gipr-Cre x Rosa26-EYFP mice used for GIPR ablation were used for confirmation of ablation by immunostaining for GFP (representing *gipr* expression). For each bregma level, the GFP cell count has been expressed as a percentage of total GFP cells found in control Gipr-Cre x Rosa26-EYFP brain tissue. Cells were stained using DAB staining (a) and immunofluorescent staining (b).

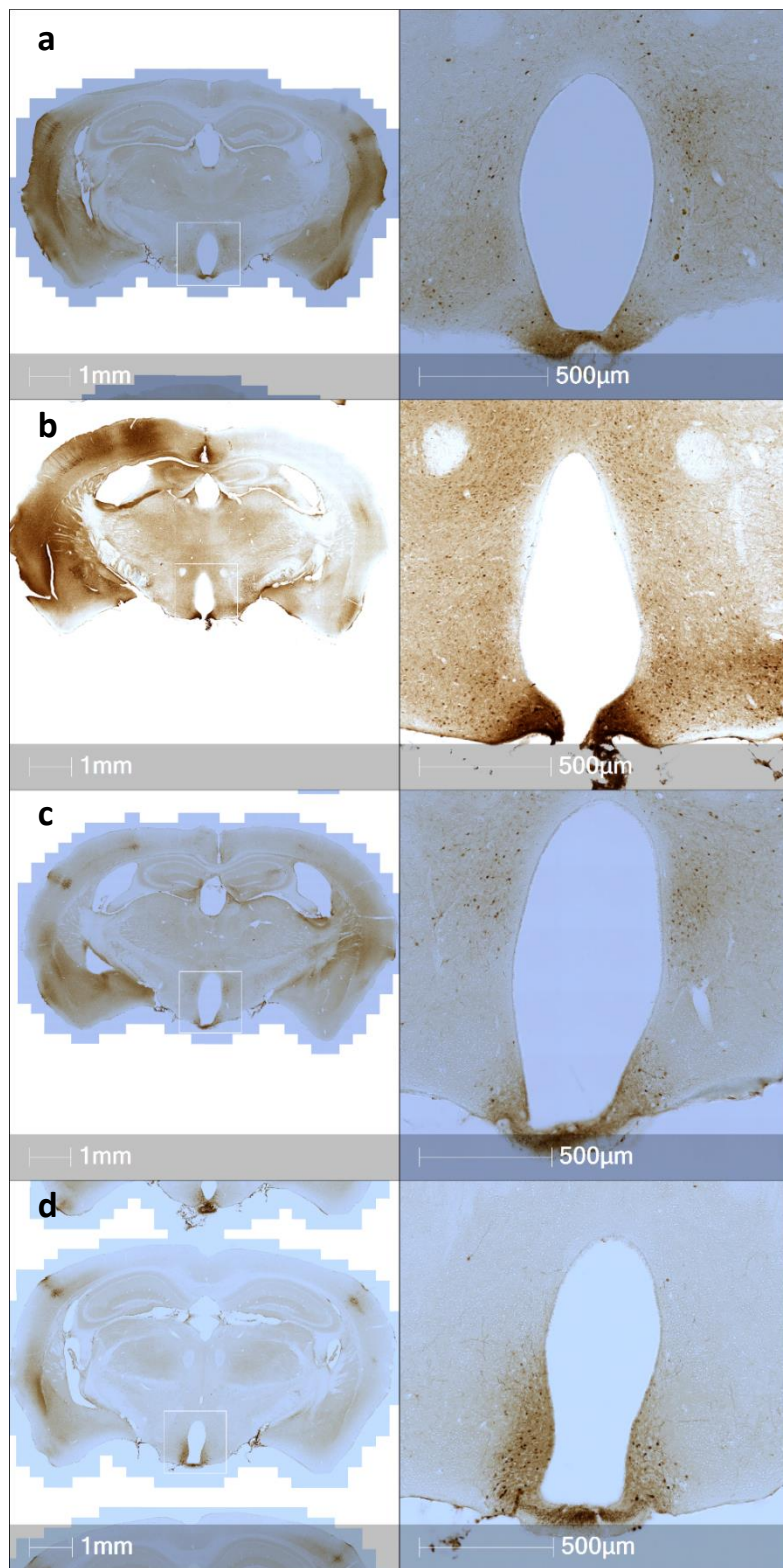


Figure 4.8 GIPR ablation in the arcuate nucleus. Immunostaining of Gipr-Cre x Rosa26-EYFP brain tissue from GIPR ablation animals (a-c), and an age matched positive control (d) showed the degree of GIPR ablation within the hypothalamus. Example images from bregma level -1.79 mm are displayed for 9716 (a), 9793 (b), 9798 (c), and the positive control which had not undergone surgery, 456 (d). The area surrounding the third ventricle is magnified in the right hand column.

4.4.4 Activation of hypothalamic GIPR positive cells

An alternative strategy for investigating the effect of GIPR positive cells in the brain is to specifically and acutely activate the GIPR neurons. Previously it has been seen that central administration of GIP can alter hypothalamic gene expression, and affect body weight gain [331]. Though these effects only seem to be observed when a high concentration of GIP is administered [332].

To directly activate hypothalamic GIPR populations, without central administration of GIP, designer receptors exclusively activated by designer drugs (DREADD) technology was used in combination with the Gipr-Cre transgenic mouse model. ICV injection of AAV-hSyn-DIO-hM3D(Gq)-mCherry (Appendix 6) meant that acute effects of GIPR activation could be monitored. Briefly, the DREADD technology uses mutant muscarinic GPCRs which are activated solely by CNO, an otherwise inert ligand [341]. The stimulatory DREADD used here, hM3D(Gq), is coupled to a $G_{\alpha q}$ pathway which consequently depolarises neurons upon activation. The AAV is cre-dependent meaning only cells expressing cre will express hM3D(Gq), hence theoretically only cells expressing GIPR will be targeted. The fusion of hM3D(Gq) to mCherry means that once the receptor is incorporated into a cell, expression can be detected by fluorescence microscopy [342-344].

Within this pilot study, GIPR was activated by intraperitoneal injection of CNO, and the acute effects on food intake were measured over the following 2 hours. Food intake was monitored when mice were fed with standard chow diet or 45% HFD, either ad libitum or following a day time fast of up to 10 hours (Figure 4.9a). The experiments were performed in a blinded fashion.

When mice were fed ad libitum, CNO had no significant effect on 2-hour food intake of standard chow diet or 45% HFD (Figure 4.9b, d). In contrast, following a day time fast of up to 10 hours, injection of CNO significantly reduced the 2-hour food intake of standard chow diet (Figure 4.9c). The same experiment, using 45% HFD fed mice after a day time fast, showed that CNO injection had no significant effect on food intake, however a trend of decreased food intake upon CNO injection seems to be observed (Figure 4.9e). To ensure this wasn't an off-target effect of CNO injection, a control experiment was completed using mice which had no DREADD expression. CNO injections following an equivalent day time fast had no net effect on 2-hour food intake of chow diet (Figure 4.10).

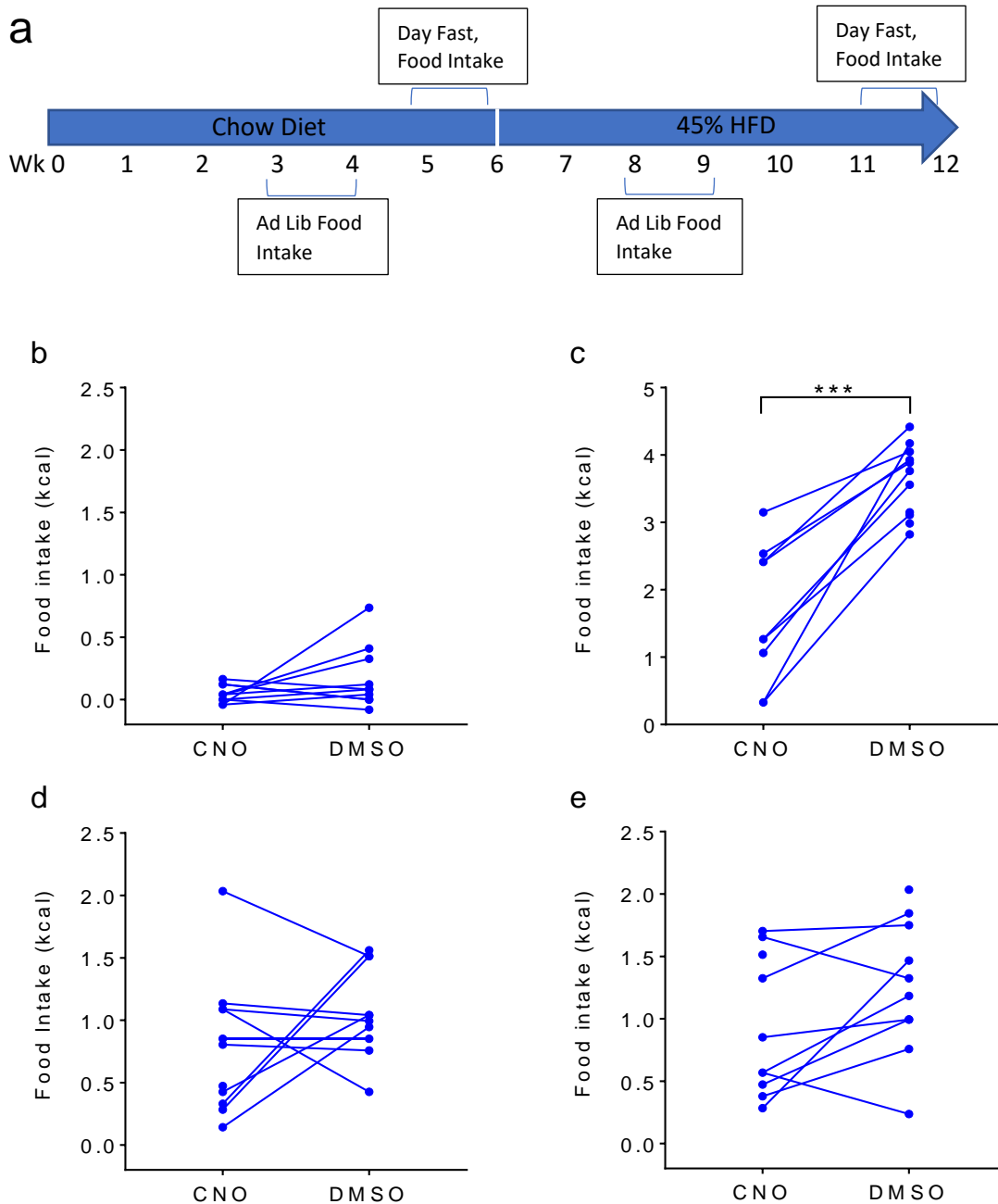


Figure 4.9 Effect of acute activation of hypothalamic GIPR neurons on food intake. (a) Schematic representation of GIPR activation study timeline. (b) 2 hour food intake of chow diet following injection of CNO or DMSO to mice fed ad libitum. Food intake was measured in the light cycle. (c) 2 hour food intake of chow diet following injection of CNO or DMSO to mice which had been fasted for up to 10 hours during the day. Food intake was measured in the dark cycle. (d) 2 hour food intake of 45% HFD following injection of CNO or DMSO to mice fed ad libitum. Food intake was measured in the dark cycle. (e) 2 hour food intake of 45% HFD following injection of CNO or DMSO to mice which had been fasted for up to 10 hours during the day. Food intake was measured in the dark cycle. All experiments were performed on mice that had received an ICV injection of AAV-hSyn-DIO-hM3D(Gq)-mCherry meaning CNO administration activated the GIPR positive neurons in the hypothalamus. Statistical significance was assessed using a two-tailed t-test, *** $p<0.001$.

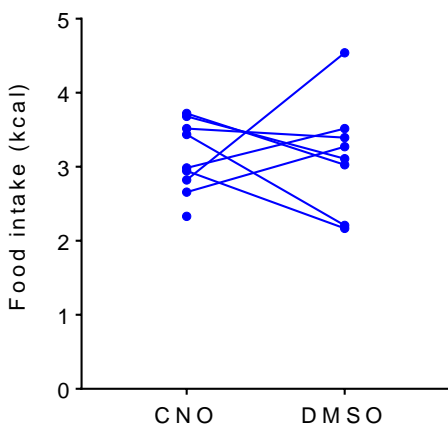


Figure 4.10 Negative control to determine off target effects of CNO on food intake. 2 hour food intake of chow diet following injection of CNO or DMSO to mice which had been fasted for up to 10 hours during the day. Food intake was measured in the dark cycle, and experiment was performed on mice which had not received an ICV injection of AAV-hSyn-DIO-hM3D(Gq)-mCherry.

At the end of the study, brains were harvested by perfusion fixation and stained for RFP alone or in combination with YFP to determine the AAV targeting success. Of the 11 mice used for the activation study, 4 of these were genotypically positive for either the EYFP or GCamp3, enabling colocalisation immunostaining experiments to be performed. Between bregma levels -1.22 mm and -1.58 mm, the average percentage of YFP positive cells targeted by the AAV was 11%. In contrast, the average percentage of off-target RFP positive cells was high at 83%. Between bregma levels -2.06 mm and -2.6 mm, the average percentage of targeted cells was 13%, and the average off-target percentage was 55%. In addition to this, of the 11 mice used for the study, 5 mice had RFP staining on only one side of the 3rd ventricle, suggesting one of the injectors could have become blocked within surgery.

The poor colocalisation of YFP and RFP positive cells raised concerns surrounding the cre-dependent integration of the AAV into neurons. Therefore, a set of control experiments were kindly performed by A. Adriaenssens. Gipr-Cre, Agouti-related peptide (AgRP)-Cre, and Cre negative mice underwent surgery for ICV injections of AAV-hSyn-DIO-hM3D(Gq)-mCherry. Following recovery, the brains were harvested by perfuse fixation, and then immunostained for YFP and/or RFP. Within the Gipr-Cre mice, the average percentage of targeted cells was 19%, and the average off-target percentage was 36% (Figure 4.11a). AgRP is known to be localised to the arcuate nucleus [345]. Although colocalisation experiments could not be performed on the AgRP-Cre mice, due to a lack of fluorescent reporter carried in the Rosa26 locus, staining of AgRP-Cre mice for RFP revealed the AAV was only found in the arcuate nucleus region (Figure 4.11b). The most important observation was that no RFP staining was

observed in the cre negative control mouse, showing that AAV integration was dependent on cre expression (Figure 4.11c).

Overall, the immunostaining results here mean conclusions surrounding the effect of GIPR activation on food intake should be made with caution. Further investigation will be required to understand the role of hypothalamic GIPR.

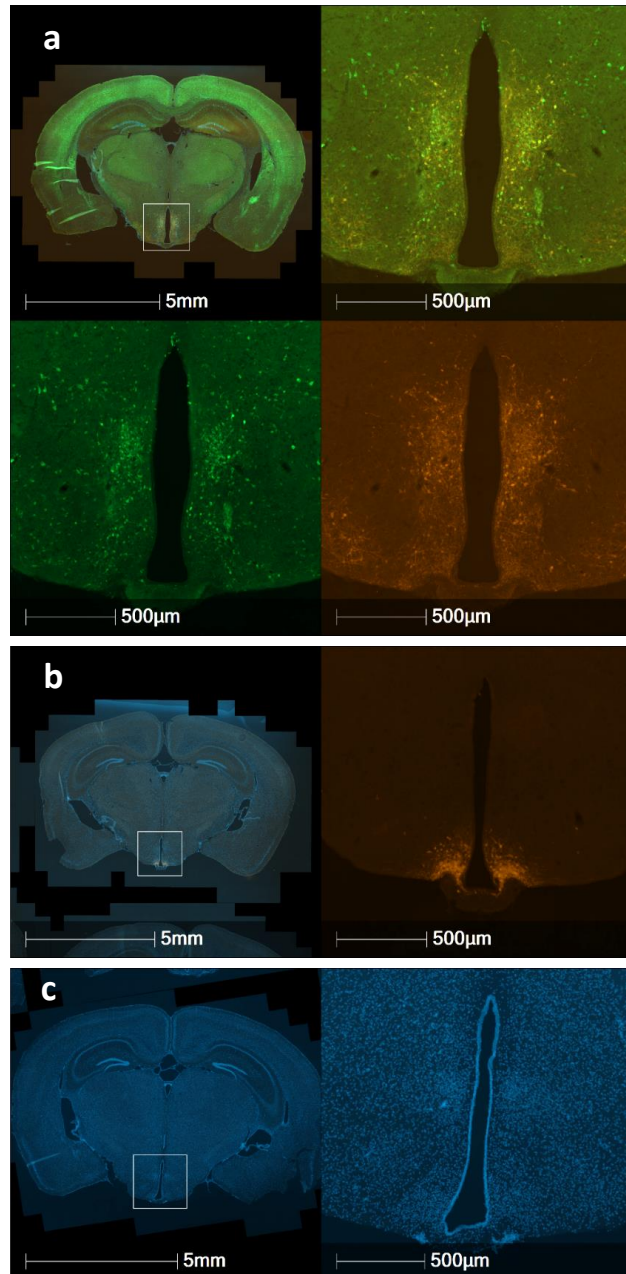


Figure 4.11 Immunostaining of Gipr-Cre, AgRP-Cre, and Cre negative brains injected with AAV-hSyn-DIO-hM3D(Gq)-mCherry. (a) Example image of Gipr-Cre brain slice stained for YFP (green, representing GIPR), and RFP (orange, representing AAV). (b) Example image of AgRP-Cre brain slice stained for RFP (orange, representing AAV). (c) Example image of Cre negative brain slice stained for RFP (orange, representing AAV). All sections also stained with Hoescht as a nuclear stain, the area surrounding the third ventricle is magnified in the right-hand column.

4.5 Discussion

4.5.1 Use of Gipr-Cre mice for GIPR localisation

The Gipr-Cre mouse model used here relies on a lineage tracing approach, in which one copy of the Gipr promoter drives Cre recombinase expression, enabling the expression of a fluorescent reporter protein (Figure 4.1). The result of this is that GIPR expressing cells are fluorescently labelled, and can be identified without the use of GIPR antibodies, which for the purpose of immunostaining seem to be limited and poorly validated.

Hence, with this novel transgenic mouse model we could identify GIPR expressing cells in both the periphery, and central nervous system. The limitation however, is that the lineage tracing approach means that cells which have expressed GIPR transiently, or within the course of development, will also produce the fluorescent reporter protein. To ensure GIPR expression, one useful step would have been to perform qPCR alongside immunostaining, though often levels of the mRNA are extremely low and can be hard to detect by qPCR, aside from in pancreatic tissue where GIPR is highly expressed.

Within the pancreas, GIPR was expressed in the α and β cells of the islets, and acinar tissue in a heterogenous pattern (Figure 4.2). Despite GIPR expression in δ cells not being investigated by colocalisation with somatostatin (Sst), it has previously been shown that GIPR is ubiquitously expressed in pancreatic islets, with equal expression in α , β , and δ cells [346]. Even without this Sst containing data we were able to conclude that reporter expression in the pancreas was as expected for the GIPR, suggesting that the novel transgenic mouse model accurately detects GIPR expression.

The heterogenous expression of GIPR in the acinar tissue was initially unexpected. However, studies from the 1980's and 1990's show that GIP stimulates release of pancreatic lipase, colipase and amylase, which are produced in the exocrine acinar tissue [347, 348]. In addition to this, the acinar tissue is known to be a heterogenous population of cells [349, 350]. These previous studies could explain why GIPR expression was observed in a heterogenous pattern in acinar tissue.

GIPR expression is also important within the adipose tissue, though the exact underlying functions of the GIPR in adipocytes remain unclear. *In vitro* studies using mammalian cell lines and human adipocytes show that GIP increases lipoprotein lipase (LPL) expression and activity, triglyceride (TG) accumulation, and GLUT4 expression at the plasma membrane [176, 181, 351]. Adipose specific GIPR knockout ($GIPR^{adipo-/-}$) mice, driven by a *mouse adipocyte protein 2 (aP2)-Cre* line, gain less weight on HFD compared to wild-type mice, suggesting protection from HFD induced obesity [185]. *aP2* encodes fatty-acid binding protein 4 (FABP4) which has a less specific pattern of expression than originally thought, with expression also found in macrophages [352, 353]. However, *GIPR* is not detected in

macrophages, and despite the potential caveats of GIPR^{adipo-/-} mice, the importance of GIPR in adipose tissue has been clearly demonstrated [185]. In a different experimental setting, GIPR expression driven by the *aP2* promoter on a GIPR knockout background increased weight gain on HFD, preventing the protection from HFD induced obesity [354].

Staining of brown and white adipose tissue showed scattered GIPR positive adipocytes (Figure 4.3a, b), which provided further confirmation that the Gipr-Cre transgenic mouse line was successfully labelling GIPR positive cells. Within the white adipose tissue, some of the GIPR positive adipocytes appeared to be multilocular, which may indicate beiging of the inguinal white adipose tissue. To determine whether this is the case, it could be useful to stain adjacent sections with haematoxylin and eosin for histological analysis of the tissue.

GIP is produced and secreted by K cells in the duodenum, therefore expression of GIPR in the duodenum could indicate the presence of local signalling pathways for GIP. GIPR expression was found in very few epithelial cells, with more cells appearing GIPR positive in the centre of the villi (Figure 4.3c).

Several of the epithelial GIPR positive cells co-stained with a 5-HT antibody, suggesting the expression of GIPR in gut enterochromaffin (EC) cells. This observation is supported by recent qPCR analysis of EC cells, which showed GIPR is enriched in both small intestinal and colonic EC cells [355]. The main role of these EC cells is to secrete 5-HT. This 5-HT produced in the periphery is unable to cross the blood-brain barrier, and the majority is taken up by platelets for use in blood clotting [356]. The 5-HT also has other gastrointestinal functions such as peristalsis, perception of pain, nausea and is thought to be involved in the regulation of metabolism [59-62]. Despite this the regulation of 5-HT secretion is poorly understood. The withstanding hypothesis is that 5-HT secretion is regulated by dietary nutrients and microbial metabolites [357, 358].

Recent findings suggest that the EC cells are not directly regulated by dietary nutrients, as there is a lack of expression of the main nutrient receptors. Instead, the expression of GLP1R in colonic EC cells, combined with the observation that GLP-1 stimulates 5-HT secretion, has led to the suggestion that EC cell nutrient sensing is indirect via GLP-1 producing enteroendocrine L-cells [355]. The colocalisation of GIPR and 5-HT in the duodenum could be used to suggest a similar mechanism for indirect EC cell nutrient sensing in the small intestine via GIP producing K-cells. Further studies to investigate GIP stimulated 5-HT secretion would be needed to confirm this hypothesis.

The GIPR positive cells in the centre of the villi colocalised with vimentin immunostaining, used as a marker for cells of mesenchymal origin. GIPR expression within mesenchymal cells was a new finding

of this study, which can be compared to GLP2R expression in sub-epithelial myofibroblasts, a cell-type of mesenchymal origin [198]. Before proposing a role for GIPR within the mesenchymal cells, confirmation of GIPR presence in this cell type by analysis of the RNA is required. GIPR expression within the nodose ganglia (Figure 4.3d) was also a new finding of this study, which again needs to be confirmed by RNA analysis.

4.5.2 Central expression of GIPR

The Gipr-Cre mouse model not only allowed the study of GIPR in peripheral tissues, we were also able to demonstrate GIPR expression throughout the brain (Figure 4.4 and 4.5). GIPR expression was detected in several regions of the brain, some of which were in line with previous findings. Observation of GIPR expression in the olfactory bulb, defined areas of the cortex, the LSD, and hippocampus gave confidence that the mouse model was accurately detecting GIPR expression as GIPR had previously been detected in these regions using *in situ* hybridisation [149, 161].

Immunostaining with the YFP antibody to detect GIPR expression produced images of higher resolution than those previously published, meaning the location of GIPR in further areas of interest could be characterised. Here, for the first time, GIPR expression was identified within hypothalamic nuclei, in particular in the Arc and DMD. GIPR expression was also found in the BST region, the PV, DG and the AP. No comment can be made upon the level of GIPR expression, because once cre-recombinase excises the ‘floxed’ stop codon in the reporter gene construct, the fluorescent reporters are under control of a constitutively active promoter. Immunostaining of the fluorescent reporter means that low and high levels of GIPR expression would both be easily detected at the same level. Lower limits of detection using this new mouse model could be used to explain why we were able to detect GIPR expression in several brain regions for the first time here.

When comparing GIPR expression to GLP1R expression in the brain, there are a number of areas in which expression appears to overlap. For example, both GLP1R and GIPR expression were observed in the SFO, CA3 of the hippocampus, Arc, and AP [94, 359]. Of particular interest is the expression in the Arc and AP; when considering the function of these regions, both are thought to be important in controlling food intake and energy expenditure [336]. With respect to the role of GIPR in obesity, central GIPR in these regions may play a role. A series of experiments have been performed here with the Gipr-Cre mouse model to further investigate the role of hypothalamic GIPR in control of food intake (discussed in section 4.5.3 and 4.5.4). In addition to these, it would be interesting to further characterise the role of the GIPR in the AP.

We have demonstrated GIPR expression in several locations within the brain, however as discussed earlier the Gipr-Cre model has limitations due to the lineage tracing nature of this approach.

Confirmation of *Gipr* expression in the brain using alternative methods will be essential to ensure the *Gipr-Cre* model is accurately reporting. However, GIPR antibodies for use in immunostaining are limited, and accurate qPCR of specific regions will be difficult. When EYFP positive cells were sorted from *Gipr-Cre* x *Rosa26-EYFP* mice, hypothalamic *Gipr* gene expression was detected in the EYFP positive population, and not in the negative population, although the levels of expression were extremely low compared to other neuronal and astrocyte gene markers.

One method to confirm GIPR expression at the time of immunostaining would be to stain with a Cre antibody, for example that produced by Novagen which has been used to specifically stain AAV-Cre [360]. A further way to infer GIPR expression would be to determine if the YFP expressing cells are activated by ICV infusion of GIP. Experimentally, this could be performed by co-staining for c-Fos expression and EYFP, as c-Fos is a marker for activated cells [361].

Obviously, a more in-depth characterisation of these GIPR positive cells would be useful to determine the cell-type and possible functions. One method for this is immunostaining and colocalisation analysis, which has been completed for GLP1R positive cells [94]. A number of cell-type specific markers can be used for this purpose, for example antibodies for glial fibrillary acidic protein immunostain astrocytes [362], antibodies for tyrosine hydroxylase immunostain catecholamine neurons [363], and parvalbumin neurons can be detected by antibodies for parvalbumin [364]. The main limitation of this technique is specificity and availability of antibodies.

An alternative method which has been used within the lab is flow cytometry to sort cells positive for the fluorescent reporter, followed by single cell RNA sequencing. This enables sequencing of over 1000 genes per cell, providing a better overview of GIPR positive cell-type. This approach is limited to a defined area, thus we have focused entirely on the hypothalamic population of GIPR positive cells. When this technique was used to characterise proopiomelanocortin (POMC) neurons from the arcuate, the clustering analysis revealed the POMC neurons are a highly heterogenous population [365]. When searching this dataset, GIPR expression was detected in 2 of the 163 neurons. Of these, one neuron was defined as a ‘canonical’ POMC neuron with high levels of the POMC gene, the other was an unknown cell-type with low levels of the POMC and AgRP genes [365].

A final stage for characterisation of the GIPR positive cells would be to determine what the neurons are projecting to using anterograde viral tracing vectors based on the herpes simplex virus [366]. Alternatively, retrograde viral tracing vectors based on the pseudorabies virus [367, 368] could be used to identify the neurons which project to the GIPR positive cells.

4.5.3 Hypothalamic GIPR ablation

Together, use of the Gipr-Cre mouse model with Cre-dependent AAV technology allowed for acute manipulation of hypothalamic GIPR positive cells. The hypothalamic GIPR positive cells were either ablated or activated, and the effects on food intake were monitored.

In previous studies, global GIPR knockout and adipose specific GIPR knockout gave protection from HFD induced obesity. The underlying mechanism for this is not clearly understood, one key difference between these studies is that global GIPR knockout increases energy expenditure, whereas adipose specific GIPR knockout has no effect on energy expenditure [182, 185]. We hypothesised that hypothalamic GIPR identified here may have a role in regulating either food intake or energy expenditure. To determine if hypothalamic GIPR knockout gives protection from HFD induced obesity, GIPR positive cells were ablated, and effects on body weight and food intake were monitored.

Overall, on both chow diet and 45% HFD, hypothalamic ablation of GIPR positive cells had no effect on body weight or food intake (Figure 4.6). This suggests the hypothalamic GIPR is less important for regulating GIP effects on obesity compared to the GIPR in adipose tissue. At the end of the experiment no differences were observed in fat mass, but lean mass was not measured (Figure 4.7). It would have been useful to also assess whole body composition, for example by using a non-invasive method of dual-energy X-ray absorptiometry (DEXA) or time domain nuclear magnetic resonance (TD-NMR) [369].

Food intake in all the ablation experiments was assessed over a 24-hour period, however retrospectively it could have been useful to measure leptin sensitivity over a shorter timeframe due to the half-life of leptin, which in C57/Bl6 mice is 49.5 minutes [370]. For comparison, when Yan *et al* assessed food intake after a leptin dose, a dose dependent decrease in 4-hour food intake was observed, whereas the magnitude of this effect was decreased when food intake was measured over 24-hours [371]. In this study, leptin was injected towards the end of the day before dark onset, which is also important to consider due to the nocturnal activity of mice.

It should be noted that over the course of the ablation experiments, we identified that the automated lighting within the mouse-holding room was faulty, and that the room was continuously light through to day 64 post-surgery. The issue was fixed for the experiments on HFD. This is a major confounding factor of this set of experiments, meaning that the circadian rhythm of the mice will have been disrupted throughout this study. Therefore, for any firm conclusions to be drawn, a repeat cohort is required.

A further factor for consideration when interpreting the body weight and food intake results of the ablation experiments is the degree of successful ablation. Only three of the mice from the ablation cohort had the EYFP fluorescent reporter, therefore these were the only mice which could be used in immunostaining for confirmation of GIPR ablation. Of these, only 2 of the 3 mice appeared to have decreased GIPR positive cells in the arcuate nucleus region (Figure 4.8; Table 4.1). For the remaining 6 mice within the ablation cohort, we have been unable to show whether GIPR ablation was successful. One option to prove ablation could have been to co-inject an EGFP encoding cre-dependent AAV to label the Cre positive cells in the reporter negative mice, this would be similar to the method used in the original paper that describes the use of AAV-flex-taCasp3-TEVp [340].

As it stands, we are unsure whether the GIPR cell ablation was successful throughout the ablation cohort, and consequently conclusions regarding the effect of hypothalamic GIPR ablation on food intake and body weight cannot be drawn. If repeated, it would be useful to have all Gipr-Cre mice genotypically positive for the fluorescent reporter gene.

4.5.4 Hypothalamic GIPR activation

Conversely to the GIPR ablation study, hypothalamic GIPR positive cells were acutely activated using DREADD technology, and effects on short-term food intake over a 2-hour window was measured. The use of DREADD technology is an increasingly popular technique for genetic manipulation of selected populations of neurons [372].

As briefly described earlier, the DREADD receptors have been designed so that they are specifically activated by CNO, an otherwise inert ligand [341]. However, over the course of our study, Gomez *et al* have shown that clozapine, a CNO metabolite [373, 374], binds with higher affinity to the DREADD receptors, accumulates over time, and more readily crosses the blood-brain barrier compared to CNO [375, 376]. Together, this suggests that following CNO injection, clozapine is the activating ligand of the DREADD receptors. The significance of this is currently unknown, but it should be noted that clozapine also has endogenous receptors which may be activated if clozapine concentrations are above the threshold [377]. Alternative DREADD agonists have not been characterised *in vivo*, thus the current recommendation is to continue using either CNO or clozapine for DREADD experiments with emphasis on the importance of negative control experiments in non-DREADD expressing animals [378].

In this study we found activation of hypothalamic GIPR positive cells by intraperitoneal injection of CNO led to decreased food intake of chow diet following a 10-hour day time fast (Figure 4.9c). The same experiment in non-DREADD expressing mice showed CNO had no effect on food intake (Figure 4.10). This is an intriguing observation which is in line with other rodent studies in which central

administration of GIP decreased food intake over 24 hours [332]. Additionally, transgenic overexpression of GIP leads to decreased food intake of low fat and high fat diet in the dark cycle [379]. However, together this data doesn't seem to fit with the knowledge that knockout of the GIPR protects from high fat diet induced obesity [182]. The contrasting data is rather confusing, clearly the role of central GIP in regulating food intake requires further investigation. One possibility is that rather than solely effecting food intake, GIP may play a role in determining food preference. This hypothesis stems from a recent publication in which it was found that although GIPR knockout mice are protected from weight gain on HFD, they are not protected from weight gain induced by high starch diet (HSD) [380].

When interpreting the results of our study, it is important to consider the immunostaining results which were used for confirmation of accurate targeting of the AAV. We identified a high percentage (55 – 83%) of off-target cells, positive for RFP but negative for YFP. This was improved in a separate control cohort of mice, with an average off-target percentage of 36% (Figure 4.11a). It should be noted that this counting was manual, meaning error could have accumulated due to uncertainty surrounding the threshold at which to count a 'positive' cell. Despite this, there was clearly a degree of AAV off-targeting observed. The reason for this off-targeting of the AAV is unclear, particularly as no RFP staining was observed in the Cre negative control, outruling the possibility of the AAV randomly integrating into cells in a cre-independent manner (Figure 4.11c). One possible reason is a difference in efficacy of the cre-dependent fluorescent reporter protein expression versus the cre-dependent incorporation of the AAV.

Prior to conclusions being drawn surrounding the effect of hypothalamic GIPR activation, the effects on food intake found here must first be confirmed in a second cohort. It is essential that within this second cohort all animals express a fluorescent reporter so that AAV targeting can be assessed in the whole group. Following this, it could be possible to investigated food preference using specially designed holding cages for the mice.

4.5.5 Summary

Within this chapter, a novel transgenic mouse line, Gipr-Cre, has been used to identify and characterise cells expressing the GIPR. Immunostaining of the pancreas and adipose tissue suggested that the model was successfully reporting GIPR positive cells. Additionally, GIPR was found sporadically in duodenal EC cells and sub-epithelial cells, nodose ganglia and in several regions of the brain.

Expression of GIPR in hypothalamic nuclei was of particular interest as this central brain region plays a role in the control of food intake and energy expenditure. Despite our efforts to characterise the role of GIPR positive cells within the hypothalamus, we are currently unable to conclude with high confidence that acute manipulation of these GIPR positive cells effects food intake.

Chapter 5. Characterisation of a GLP2R variant, D470N, associated with Type 2 Diabetes risk

5.1 Introduction

5.1.1 A missense variant in GLP2R is associated with citrulline levels and type 2 diabetes risk

Genome wide association studies (GWAS) have been successful in the identification of genetic variants robustly associated with metabolite levels and disease risk. In a GWAS of metabolite levels L. Lotta, C. Langenberg and colleagues found a common missense variant within GLP2R (Asp470Asn; D470N; rs17681684) that is strongly associated with higher circulating levels of citrulline ($n=30,940$; $p = 6.4e-22$), a biomarker of enterocyte mass [381].

Other GWAS studies have associated the same single nucleotide polymorphism (SNP) with increased fasting GIP levels ($p = 1.4e-9$), and a nominal association with slightly lower fasting glucose has also been identified ($p = 0.03$) [382]. In addition, a GWAS of type 2 diabetes recently identified a common variant associated with higher diabetes risk in high linkage disequilibrium with the citrulline-raising allele of D470N [383].

The functional effect of this GLP2R mutation is not known [382], however the pattern of association with citrulline levels suggests it might be a gain-of-function mutation, on the basis that greater signalling via GLP2R would result in greater enterocyte mass. We therefore aimed to characterise the functional effects of the D470N mutant on GLP2R signalling.

5.1.2 Function of intestinal GLP2R

GLP-2 is secreted from enteroendocrine L-cells in response to dietary nutrients, alongside GLP-1 [384]. The gastrointestinal functions include regulation of epithelial cell proliferation and apoptosis [202]. Activation of the GLP2R leads to a rapid expansion of the mucosal epithelium [214], which is thought to be related to increased intestinal absorption of carbohydrates, amino acids and lipids [203-205]. Other observed effects of GLP2R activation include decreased gastrointestinal motility [206], decreased gut permeability, increased intestinal barrier function [207, 208], and increased visceral blood flow [209, 210]. A detailed review of these functions, along with the possible underlying mechanisms can be found elsewhere [201].

There is contrasting evidence regarding the location of the GLP2R, with some groups arguing expression is found in 5-HT positive enterochromaffin cells within the epithelial lining of the intestine [194-196]. In contrast, other groups fail to detect GLP2R in epithelial cells. Using techniques including

qPCR, *in situ* hybridisation and receptor autoradiography these groups argue that GLP2R expression is either in subepithelial myofibroblasts or enteric neurons [197-200].

Despite the lack of understanding surrounding the location of GLP2R, the gastrointestinal functions of GLP-2 have been utilised therapeutically. A stabilised GLP-2 analogue, teduglutide, is approved for the treatment of short bowel syndrome, successfully reducing malabsorption-related consequences [385-387]. Clinical trials show that teduglutide may also be useful for treating patients with inflammatory bowel diseases such as Crohn's disease [388, 389]. Additionally, one group has suggested that GLP-2 has beneficial metabolic effects in a HFD setting [390, 391].

For the potential next generation of GLP-2 therapeutics, co-agonists are being developed. For example, a GLP-2/GLP-1 dual acting agonist has recently been produced and characterised *in vivo*, demonstrating the viability of modulating metabolic and intestinotrophic factors using a single molecule [392].

5.1.3 GLP2R signalling pathways

The GLP2R belongs to the class B family of GPCR's (as detailed in chapter 1), thus the canonical signalling pathway is mediated by $G_{\alpha s}$ and leads to an increase in cAMP [191]. Regarding G-protein independent pathways, GLP2R signalling via phosphorylation of ERK1/2 and phosphorylation of protein kinase B (known as Akt) has been observed in primary cultures of rodent enteric neurons. This phosphorylation is dependent upon phosphatidylinositol-3 kinase (PI3K), and downstream leads to an increase in vasoactive intestinal polypeptide (VIP) expression [192].

In addition to this, GLP2R over-expressing cell lines show β -arrestin 2 is recruited to the GLP2R upon activation, however the downstream role of β -arrestin 2 is unknown. Investigation has shown that β -arrestin 2 is not involved in agonist induced desensitisation of the GLP2R, nor the phosphorylation of ERK1/2 [193].

To characterise the effect of the D470N mutation within GLP2R, we investigated the effects on signalling via cAMP, β -arrestin 1, β -arrestin 2 and phosphorylation of ERK1/2 (P-ERK1/2).

5.2 Aims

Investigate the functional differences between wild-type (WT) GLP2R and the D470N mutant GLP2R by:

- a) Generation of D470N GLP2R mutant constructs using site-directed mutagenesis.
- b) Characterisation of canonical GLP2R signalling pathways via cAMP.
- c) Characterisation of alternative GLP2R signalling pathways via β -arrestin and P-ERK.

5.3 Methods

GLP-2 was diluted in 50% acetic acid to form a 1 mmol/l stock solution.

5.3.1 Molecular Biology

Firstly, an internal ribosome entry site (IRES) and venus gene segment was inserted downstream of the GLP2R cDNA sequence using Gibson cloning. The IRES-Venus fragment was amplified from a Glucagon(GCG)-IRES-Venus plasmid using PCR, with primers that had a 19-21 basepair overlap with *Xho1/Xba1* linearized GLP2R plasmid. The PCR product and linearized GLP2R plasmid were combined with Gibson cloning (New England Biolabs) which utilises 5' exonuclease, DNA polymerase and DNA ligase to assemble DNA in a one-step process. Reactions were incubated at 50°C for 60 minutes, and resultant cloning product was used to transform One Shot® OmniMAX™ 2 T1^R bacteria. DNA was harvested from the transformation products using the QIAprep® Spin miniprep kit, and successful cloning was confirmed using *Apa1* restriction digest together with DNA Sanger sequencing (SourceBioscience).

To generate the D470N mutant, a single point mutation was made in GLP2R-IRES-Venus in the pcDNA3.1 vector using the QuikChange Lightning Site-Directed Mutagenesis Kit (Agilent Technologies) according to the standard protocol (primers detailed in Appendix 2). One Shot® OmniMAX™ 2 T1^R bacteria (Invitrogen) were used for transformation of the mutant product, and DNA was harvested from resultant colonies using a QIAprep® Spin miniprep kit. DNA Sanger sequencing (SourceBioscience) was used to confirm successful mutagenesis.

5.3.2 HitHunter® cAMP Assay

To determine differences in cAMP signalling between wild-type GLP2R and Asp470Asn (D470N) GLP2R a HitHunter® cAMP assay was used. CHO K1 cells were seeded into white-bottomed 96 well plates at 20,000 cells/well. The following day, cells were transiently transfected with wild-type/mutant GLP2R constructs or control plasmid. 100 ng DNA was transfected per well using 1 µl lipofectamine 2000. The following day, cells were washed once with PBS, then incubated for 30 minutes at 37°C in PBS containing 0.5 mM IBMX ± ligand. Cellular cAMP levels were measured using HitHunter® cAMP assay according to the manufacturer's recommendations (DiscoveRx, Fremont, CA, USA). Briefly, antibody reagent and lysis solutions were added to the plate, then plates were incubated for 1 hour in the dark on a shaker. Enzyme solution was then added to the plates, and plates were incubated for a further hour in the dark on a shaker. After a final 3 hours at room temperature, luminescence was measured on a TopCount plate reader (PerkinElmer).

5.3.3 Nano-Glo® Live Cell Assay for Beta-Arrestin Measurements

Assay performed according to method described in chapter 3.

5.3.4 ERK1/2 Phosphorylation Analysis by Western Blotting

HEK293 cells were seeded into 6 well plates at 300,000 cells/well, and transfected the following day with wild-type or D470N mutant GLP2R expressing constructs using 2 µg DNA and 6 µl lipofectamine 2000 per well. 16-24 hours post transfection, media was replaced with OptiMEM reduced serum media and cells were incubated at 37°C for 2 hours prior to stimulation with 1 µM GLP-2. After 5, 10, 15, 30 or 60 minutes of treatment, cells were washed with ice-cold PBS, and lysed using RIPA lysis buffer (ThermoFisher Scientific) containing PhosSTOP™ and cOmplete™ protease inhibitors (Sigma-Aldrich). Samples were then centrifuged at 13,200 rpm for 10 minutes at 4°C, and the supernatant used for western blotting. The protein content was determined by bicinchoninic acid (BCA) assay (ThermoFisher Scientific) according to the manufacturer's protocol.

Samples were prepared for western blotting, by mixing with 10X Bolt™ Sample Reducing Agent and 4X Bolt™ LDS Sample Buffer, then heating samples to 85°C for 10 minutes. 8 µg of samples were loaded onto 4–15% precast polyacrylamide gels for electrophoresis at 150 V for 45 minutes, then transferred onto nitrocellulose membrane using the iBlot® Dry Blotting System iBlot (Life Technologies). Membranes were blocked for 1 hour using 5% (w/v) milk in tris-buffered saline (TBS) + 0.1% (v/v) Tween-20 (TBS-T). For protein detection, primary antibodies of interest (Appendix 4) diluted in 0.5% (w/v) milk TBS-T were incubated with membranes overnight at 4°C. After washing with TBS-T, goat anti-rabbit IgG HRP conjugated secondary antibody (1:2,500) was incubated with membranes in 1% (w/v) milk TBS-T for 1 hour. Proteins were detected with Pierce™ ECL Western Blotting Substrate (Thermo Scientific) and imaged with a Bio-Rad ChemiDoc Imaging System.

5.4 Results

5.4.1 Generation of D470N GLP2R mutant expressing constructs

To investigate the functional differences between WT GLP2R and the D470N mutant, first GLP2R expressing constructs were generated. Human GLP2R cDNA within the pcDNA3.1+ vector was purchased, and Gibson cloning was completed to insert an internal ribosome entry site (IRES) and venus gene downstream of the GLP2R sequence. Briefly, primers were designed for amplification of the IRES-Venus fragment from a GCG-IRES-Venus plasmid within the lab. The 5' end of each primer had a 19 – 21 basepair sequence complementary to the ends of *Xho1* and *Xba1* linearized GLP2R pcDNA3.1+ vector (Appendix 2). The amplified IRES-Venus fragment and linearized GLP2R vector were combined using Gibson cloning. Successful Gibson cloning products were determined by analysis by gel electrophoresis after an *Apa1* restriction digest, along with DNA Sanger sequencing.

Following this, QuikChange Lightning site directed mutagenesis was used to perform a single base change from GAC (encoding aspartic acid) to AAC (encoding asparagine) at amino acid position 470 (Figure 5.1a, b). Successful mutagenesis was confirmed by DNA Sanger sequencing (Figure 5.1c), and the successful products were scaled up for use in functional assays. The WT and mutant GLP2R constructs within the pcDNA3.1+ vector were used to assess signalling by cAMP and P-ERK.

To determine β-arrestin recruitment using NanoBiT® technology, an alternative vector was required for lower expression of GLP2R, and fusion of GLP2R to the Large BiT subunit of NanoBiT®. For this, GLP2R was cloned into the pBiT1.1_C[TK/LgBiT] vector using restriction cloning with *Xho1* and *EcoR1*, followed by quick ligation. DNA Sanger sequencing was then used for confirmation of successful cloning.

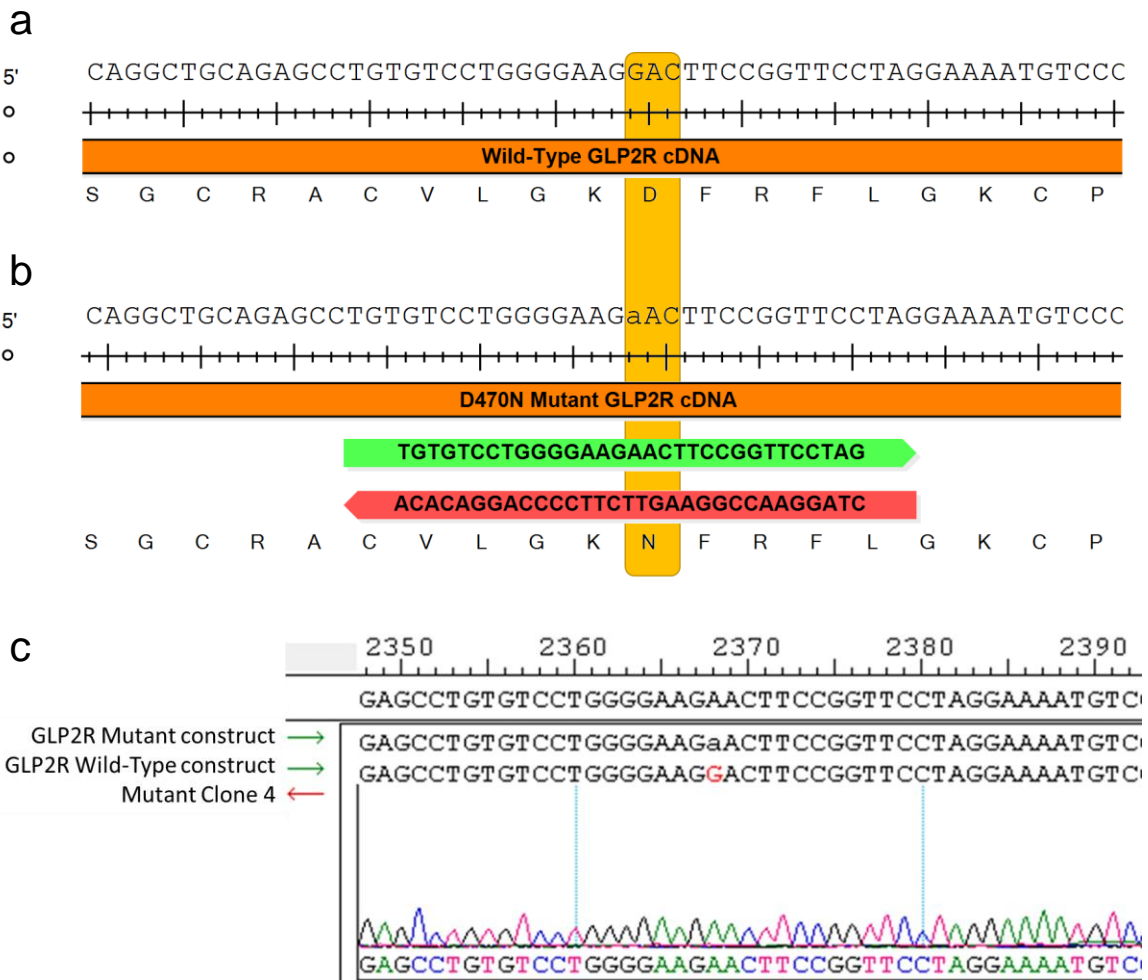


Figure 5.1 Schematic depicted wild-type and mutant GLP2R sequences. (a) Wild-type GLP2R sequence, amino acid targeted for mutation is highlighted in yellow. (b) Mutant GLP2R sequence, showing D470N mutation highlighted in yellow. Primers used to introduce the mutation using QuikChange Lightning Site-Directed Mutagenesis are depicted, forward primer shown in green, and reverse primer shown in red. (c) Sequence confirmation of successfully mutagenesis, chromatogram depicted for clone 4 which was then sequenced in full.

5.4.2 Comparison of WT and D470N GLP2R signalling via cAMP

After generation of WT and D470N GLP2R containing constructs, these were used to assess differences in WT and mutant GLP2R signalling. The initial signalling pathway to be assessed was $G_{\alpha s}$ signalling via cAMP. CHO K1 cells were transiently transfected with WT or mutant GLP2R constructs, then after 16 - 24 hours were treated with a dose response of GLP-2. cAMP levels were measured following 30 minutes of GLP-2 treatment, in an end-point lysis HitHunter® cAMP assay.

The presence of IRES-Venus within the GLP2R expressing vectors allowed transfection efficiency to be determined for each construct. Transfection efficiency was approximately 60 - 70%, with no differences between the WT and mutant constructs. Comparison of the GLP-2 dose-response in WT

and mutant GLP2R expressing cells revealed no significant differences in signalling, with an almost overlapping dose response curve (Figure 5.2).

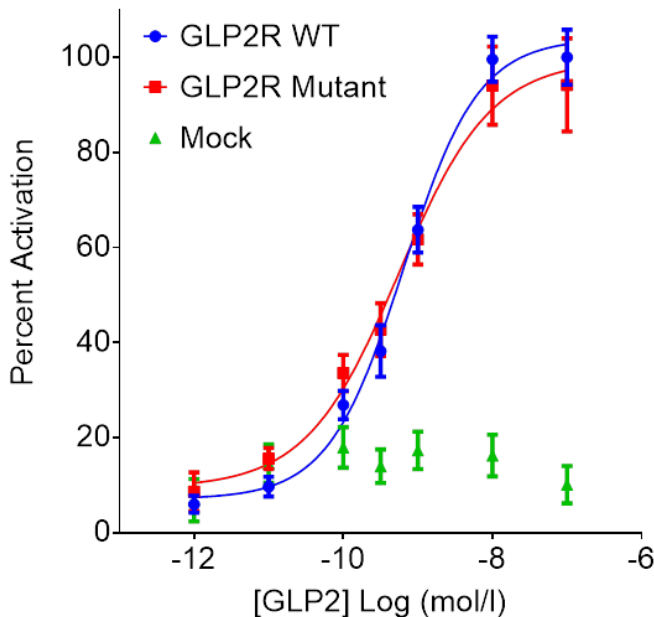


Figure 5.2 GLP-2 dose response curves in cAMP assay for GLP2R wild-type and mutant receptors. The dose response curves of cAMP stimulation by GLP-2 in CHO K1 cells transiently transfected with either GLP2R wild-type or mutant constructs. Data has been normalised to the wild-type maximal and minimal response, with 100% being GLP-2 maximal stimulation of the wild-type GLP2R, and 0% being wild-type GLP2R cells with buffer only. Data are mean \pm SEM ($n=4$).

5.4.3 Comparison of β -arrestin recruitment to the WT and D470N GLP2R

Aside from cAMP signalling, it is known that the WT GLP2R recruits β -arrestin 2 [193]. Therefore, following assessment of cAMP signalling, we investigated β -arrestin recruitment to the WT and mutant GLP2R. Both β -arrestin 1 and β -arrestin 2 recruitment were assessed using a Nano-Glo® live cell assay in transiently transfected HEK293 cells. Briefly, the recruitment of β -arrestin to GLP2R brings the large and small BiT subunit of NanoBiT® together, resulting in increased luciferase activity. The top concentrations from the GLP-2 dose response in the cAMP assay (1 – 100 nmol/l GLP-2) were chosen for stimulation of the GLP2R and observation of β -arrestin recruitment.

Both β -arrestin 1 and β -arrestin 2 were recruited to the WT GLP2R upon GLP-2 stimulation, in a dose-dependent manner (Figure 5.3a, c). The maximal luciferase activity for both β -arrestin 1 and β -arrestin 2 recruitment to the mutant GLP2R was significantly decreased when compared to the WT GLP2R, indicating the extent of β -arrestin recruitment was markedly decreased (Figure 5.3b, d). The example traces indicate that neither β -arrestin 1 or β -arrestin 2 were recruited to the mutant GLP2R upon stimulation with 1 nmol/l GLP-2, however the same concentration of GLP-2 induced β -arrestin

recruitment to the WT GLP2R (Figure 5.3). Overall there was a significant decrease in β -arrestin 1 and β -arrestin 2 recruitment to the D470N GLP2R mutant (Figure 5.4).

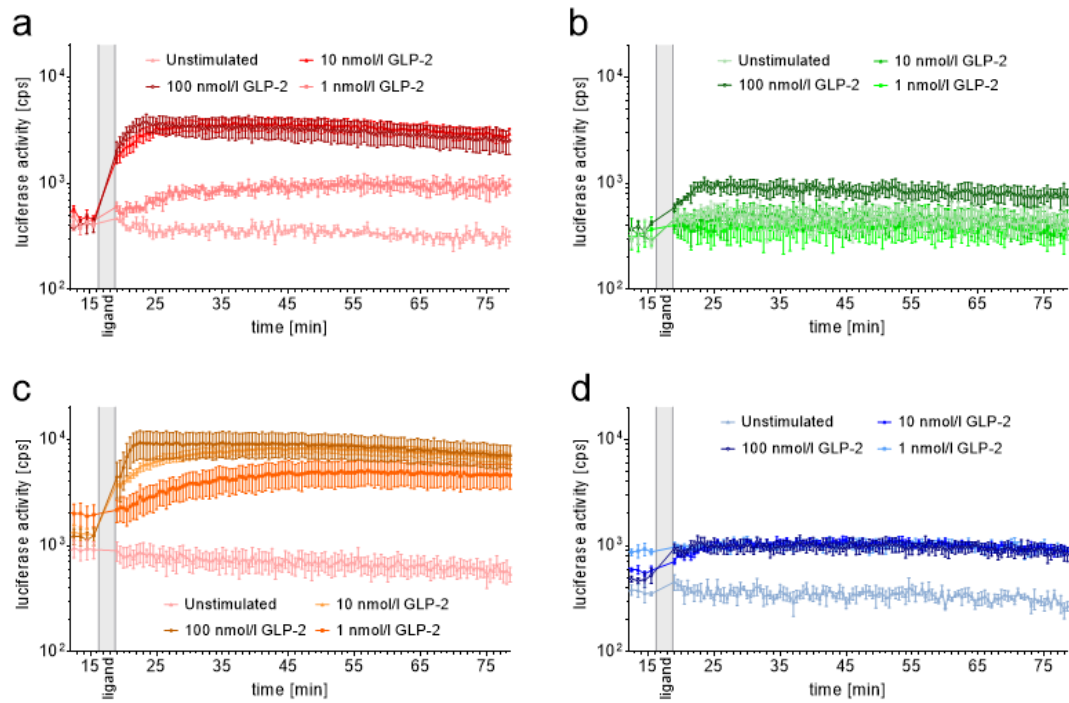


Figure 5.3 Example traces of GLP2R wild-type and mutant signalling via beta-arrestin 1 and beta-arrestin 2. Example real-time beta arrestin responses to a dose titration of GLP-2 are displayed for beta-arrestin 1 (a, b) for wild-type GLP2R (a) and D470N mutant GLP2R (b). Real time beta-arrestin responses are also displayed for beta-arrestin 2 (c, d) for wild-type GLP2R (c) and D470N mutant GLP2R (d). Data are from representative experiments, and are displayed as mean \pm SEM from 3 wells.

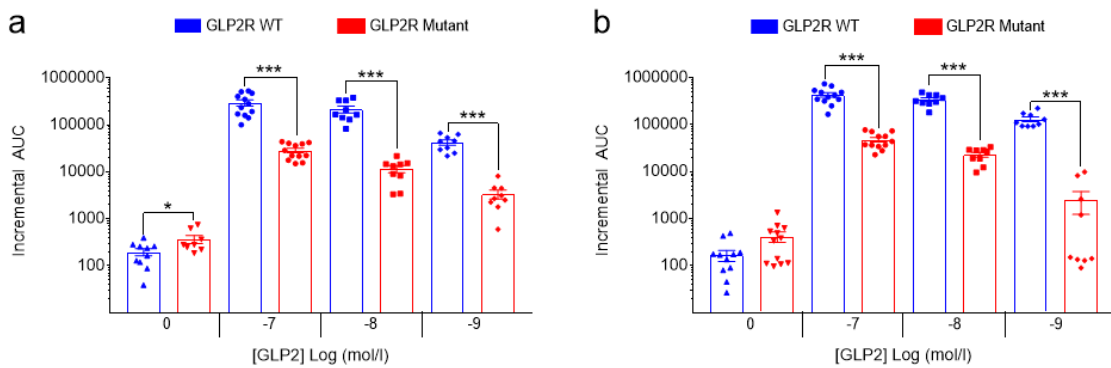


Figure 5.4 Summary of wild-type and mutant GLP2R beta-arrestin 1 and beta-arrestin 2 responses. Area under curve (AUC) summary data ($n=3-4$) displayed for beta-arrestin 1 recruitment (a) and beta-arrestin 2 recruitment (b). Individual data points are displayed, the presence of 2 populations within beta-arrestin 2 data is explained by a day-effect. AUC has been calculated using the 5 minutes prior to ligand addition as the baseline value. Data are mean \pm SEM. Normal distribution of \log_{10} transformed data was determined by the D'Agostino & Pearson normality test. Following this statistical significance was assessed by one-way ANOVA with post hoc Bonferroni test. *** $p<0.001$, * $p<0.05$.

5.4.4 Comparison of WT and D470N GLP2R signalling via P-ERK

Following the observation of decreased β-arrestin recruitment to the mutant GLP2R, we hypothesised that this would increase cell surface expression of the activated receptor, due to the generally accepted function of β-arrestin in promoting endocytosis [393].

We further hypothesised that this increased cell surface expression may lead to prolonged GLP2R signalling. As the D470N mutant GLP2R is associated with increased citrulline, and one of the main functions of the GLP2R is regulation of epithelial cell proliferation in the small intestine, we investigated signalling via P-ERK, a pathway known to be involved in modulating cell proliferation [394].

To determine signalling via P-ERK, transiently transfected HEK293 cells were used, and signalling was detected by western blotting of stimulated and unstimulated cell lysates, for P-ERK and total ERK. To test the hypothesis that the mutant GLP2R would have prolonged signalling, cells were stimulated with 1 μmol/l GLP-2 for varying lengths of time, and cell lysates were used for western blotting.

Initially, HEK293 cells transfected with GLP2R in the low expressing pBiT1.1_C[TK/LgBiT] vector were used for western blotting. However, stimulation with 1 μmol/l GLP-2 was not able to produce a P-ERK signal strong enough to be detected by western blotting. The bands observed were extremely faint, and unquantifiable above background (data not shown).

Therefore, HEK293 cells transfected with the WT or mutant GLP2R within the pcDNA3.1 backbone were used. Treatment with 1 μmol/l GLP-2 produced signalling via P-ERK which appeared to peak at 10 minutes for both the WT and mutant GLP2R (Figure 5.5). Upon observation of the western blots, no difference in the time-course of GLP-2 signalling via P-ERK could be seen between the WT and mutant GLP2R. To normalise and quantify the three independent western blots, the optical densities of bands were measured and expressed relative to optical density of beta-actin bands on the same western blot. P-ERK was then expressed relative to total ERK. This quantification confirmed that there was no difference in the time-course GLP-2 stimulated P-ERK signalling (Figure 5.6).

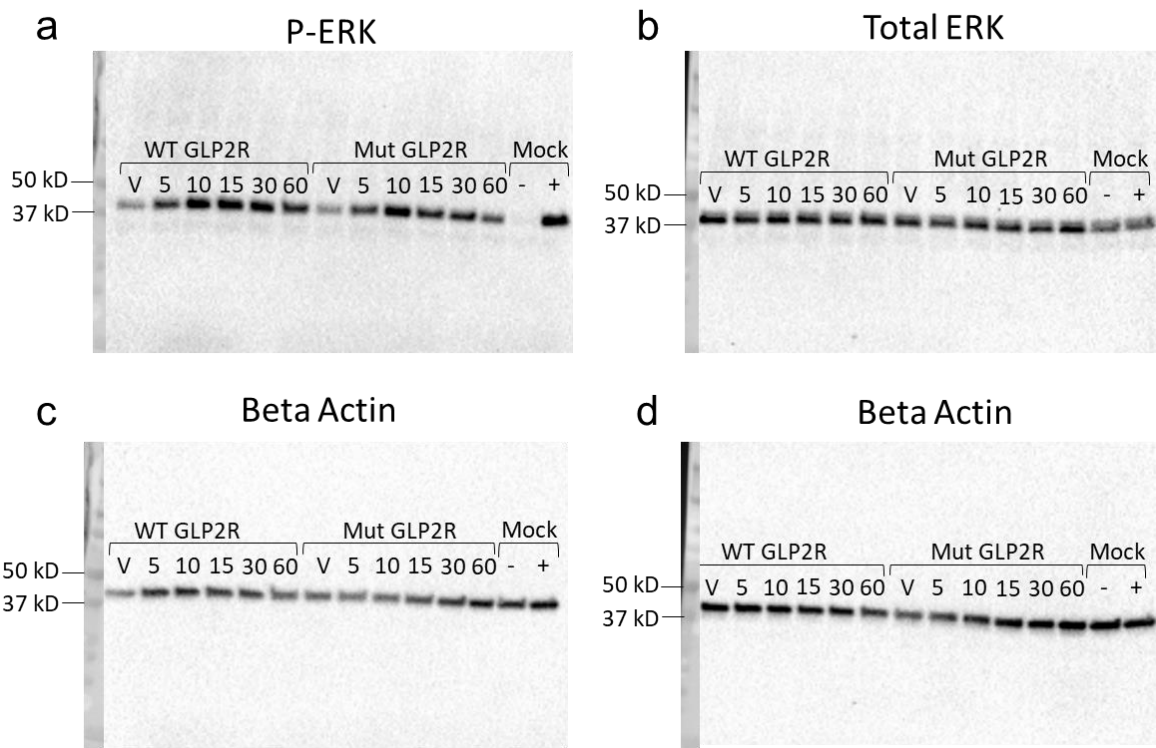


Figure 5.5 Western Blots demonstrating wild-type and mutant GLP2R signalling via P-ERK.
 Representative western blots of HEK293 cells transiently transfected with wild-type or mutant GLP2R constructs, and stimulated with 1 μ mol/l GLP-2 for the times indicated above bands. Mock transfected cells were transfected with empty pCDNA3.1, and either untreated, or treated with 1 ng/ml EGF. Blots are presented for P-ERK (a), total ERK (b), and beta-actin for the respective blots (c) and (d).

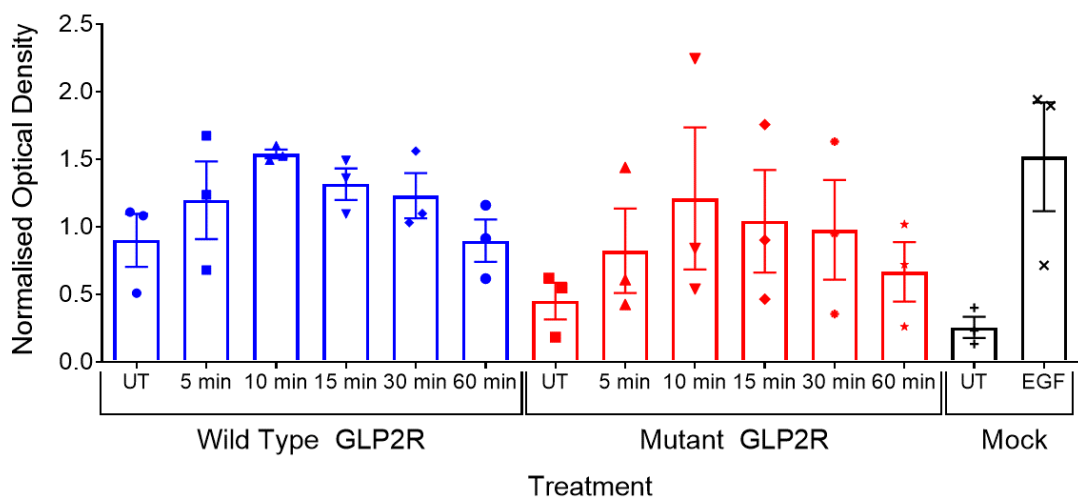


Figure 5.6 Quantification of western blots to compare wild-type and mutant GLP2R signalling via P-ERK.
 Densitometry was used to measure density of each band from 3 independent western blots, data are mean \pm SEM. Optimal density for each blot was normalised by dividing by beta-actin density. Following this normalised P-ERK intensity is expressed relative to total ERK intensity.

5.5 Discussion

5.5.1 Mutant GLP2R displays decreased β-arrestin recruitment

Upon investigation of WT and D470N mutant GLP2R downstream signalling pathways, no differences were observed in the canonical cAMP signalling or P-ERK signalling. However, we observed decreased β-arrestin recruitment to the D470N mutant GLP2R (Figure 5.3, 5.4).

We were able to demonstrate binding of both β-arrestin 1 and β-arrestin 2 to the WT GLP2R. It appears that this is the first report of GLP2R association with β-arrestin 1, with the β-arrestin 2 recruitment being in line with previous findings [193]. In comparison to the WT receptor, both β-arrestin 1 and β-arrestin 2 binding to the mutant GLP2R were decreased.

It is generally accepted that β-arrestins are involved in mediating endocytosis [393], though for GLP2R it seems this may not be the case. Deletion studies, in which different portions of the GLP2R C terminal tail were deleted have shown that this portion of the GLP2R is required for binding to β-arrestin 2. However, the truncated receptors still undergo agonist induced endocytosis, with a more rapid recovery of cell surface expression following endocytosis. This suggests β-arrestin 2 is not required for GLP2R endocytosis, a clathrin- and dynamin-independent, lipid-raft-dependent process [193, 395].

The function of β-arrestin 2 binding to the GLP2R is currently undefined. One suggestion is that GLP2R bound β-arrestin 2 regulates intracellular signalling and trafficking downstream of endocytosis [193]. The other β-arrestin, β-arrestin 1 may well be involved in regulating GLP2R endocytosis.

5.5.2 Consequences of decreased β-arrestin recruitment to the mutant GLP2R

To investigate the consequences of decreased β-arrestin recruitment to the mutant GLP2R, the time-course of ERK phosphorylation was assessed. No differences were observed between the WT and mutant GLP2R (Figure 5.5, 5.6).

Upon reflection, the optimal experimental conditions may not have been used to test the hypothesis that decreased β-arrestin recruitment would lead to increased cell surface expression of GLP2R, thus prolonged signalling via P-ERK. GLP2R was transfected into cells using a high expressing construct with a CMV promoter, which may overwrite any slight differences in surface expression produced by decreased β-arrestin recruitment. Perhaps a lower level of expression is required to observe any differences related to increased cell surface expression. However, detection of P-ERK by western blotting was not sensitive enough to allow for measurement of P-ERK in the lower expressing cells. Further optimisation of this technique may be required to increase sensitivity. Alternatively, one could look at cAMP signalling at different timepoints using the low expressing constructs. Though the P-ERK experiments suggest that decreased β-arrestin recruitment has no effect on prolonged GLP2R

activation, to confirm this cAMP signalling should be assessed as the better-defined signalling pathway of the GLP2R.

One possible reason to explain the P-ERK results could be related to the location of the endogenous GLP2R. P-ERK signalling is a well-known pathway for the control of proliferation [394], and GLP-2 stimulates P-ERK [192]. However, *in vivo*, if the GLP2R is expressed on enteric neurons rather than endothelial cells [197-200], one would hypothesise that GLP-2 has an indirect role in stimulating endothelial cell proliferation, indirect of P-ERK stimulation.

A potential mechanism for the proliferative actions of GLP-2 could be GLP2R activation on the enteric neurons leading to cAMP stimulation. Downstream, one could hypothesise this leads to release of an intermediate factor such as a growth factor, which then causes proliferation of the endothelial cells. Similar indirect effects of GLP-2 on intestinal growth have previously been reported, requiring insulin-like growth factor-I (IGF-I) [396]. Therefore, prolonged cAMP stimulation could be more relevant to the gain of function effect observed by increased citrulline in people with the D470N mutant.

Interestingly, progressive truncation of the C terminal tail of GLP2R reduces cell surface receptor expression, and decreases cAMP signalling. However, when the expression level of WT GLP2R is matched to the truncated GLP2R, the truncated forms of GLP2R produce more cAMP per receptor [193]. It appears that the GLP2R C-terminal tail responsible for β-arrestin recruitment in some way interferes with G_{αs} coupling. We hypothesize the failure of D470N GLP2R mutants to recruit β-arrestin may enhance or prolong cAMP signalling independently of cell surface receptor expression. In future experiments, the time-course of cAMP signalling in WT and mutant D470N GLP2R cells will be investigated.

5.5.3 Future investigations of the D470N mutant GLP2R

In addition to investigating the time course of cAMP signalling in WT and mutant GLP2R cells, the cell surface expression of the GLP2R could be assessed, along with any effects on the proliferative actions of GLP-2.

To assess cell surface expression, a labelled version of the GLP2R would need to be used. For example, a FLAG tag could be used, similar to in previous settings [193]. The combination of a FLAG tagged WT and mutant GLP2R with techniques such as immunostaining could be helpful for determining cell surface expression. Alternatively, the availability of GLP2R antibodies or fluorescently tagged GLP-2 could be useful for looking at GLP2R cell surface expression.

To determine effects of mutant GLP2R on the proliferative action of GLP-2 *in vitro* may be more difficult. Transiently transfected cell lines could be used in a scratch wound assay to assess

proliferation, however this is not necessarily the best model as it does not represent the endogenous setting. A cell line expressing endogenous levels of the GLP2R may be helpful, although this again does not represent the endogenous setting where GLP2R is likely on the enteric neurons rather than endothelial cells [197-200]. Perhaps biopsies from patients displaying the GLP2R mutation could be useful to assess intestinal morphology histologically, which would then give an indication of differences in proliferative actions of GLP-2.

5.5.4 Summary

In summary, the functional effects of the D470N mutation within GLP2R were characterised in a variety of downstream signalling assays. Interest in this mutant arose from GWAS studies in which the D470N GLP2R mutant was found to be associated with higher circulating citrulline levels (C. Langenberg and L. Lotta), and increased risk of type 2 diabetes.

Characterisation of D470N GLP2R, and comparison with the WT receptor showed there was no difference in cAMP signalling after 30 minutes stimulation with a dose response of GLP-2. The D470N GLP2R mutant had decreased β -arrestin recruitment, however the physiological effect of this is currently unknown and requires further investigation. No differences were observed in the time-frame of P-ERK signalling. As a next step possible differences in the time-course of cAMP signalling are to be assessed.

Chapter 6. General Discussion

6.1 Summary

The aims of this thesis focused on generation of tools to characterise the expression and function of gut hormone receptors in more depth. For this purpose, three parallel projects have been undertaken; an antagonistic antibody has been developed for GLP1R, a novel GIPR transgenic mouse model has been used to characterise GIPR expression, and mutant GLP2R expressing vectors have been generated to understand effects of a common missense mutation in the GLP2R associated with type 2 diabetes.

In this chapter, the overall results from each of the above projects are summarised and put into context with the wider field. The key findings are schematically depicted in figure 6.1. Alongside this, future directions and possible therapeutic implications are discussed.

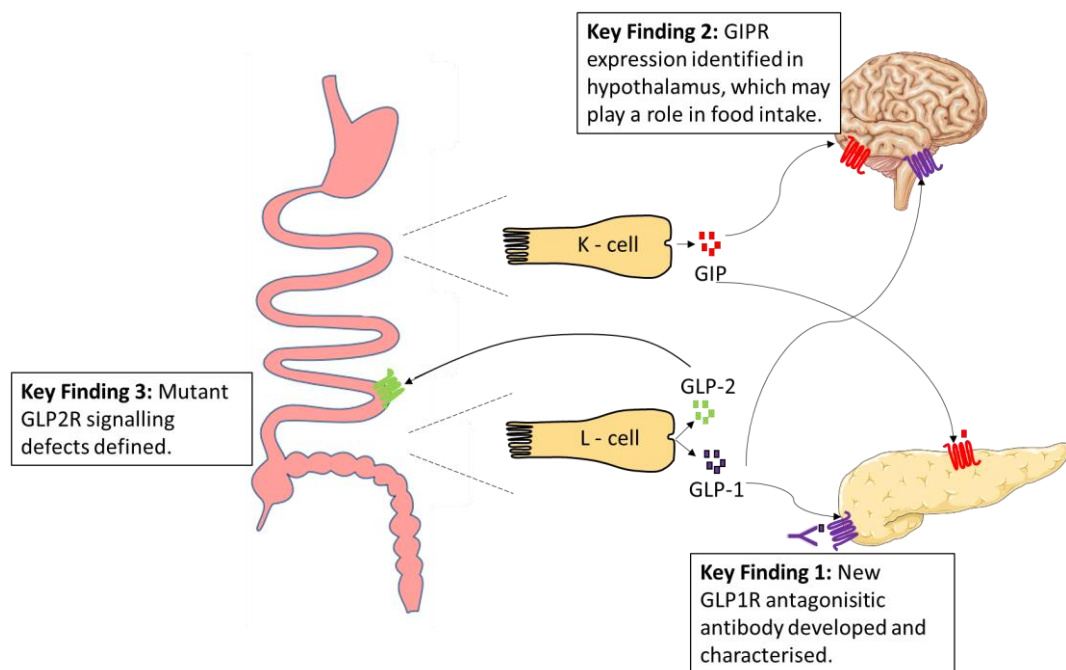


Figure 6.1 Summary of key findings throughout thesis. A schematic representation of key findings for research on the gut hormones GLP-1, GIP and GLP-2.

6.2 Glp1R0017 enables controlled blockade of the GLP1R over several days

In chapter 2, a new monoclonal antagonistic antibody for the GLP1R, Glp1R0017, was identified using naïve phage display libraries. Several studies have focused on the function of the GLP1R, due to its therapeutic importance in the treatment of type 2 diabetes [237]. Pharmacologically, the GLP1R has been studied using exendin 9-39 as a peptide antagonist for GLP1R [239]. However, questions have been raised surrounding the specificity of exendin 9-39 [121, 243, 244]. When considering the location

of the GLP1R, rather than using antibodies, a transgenic mouse model expressing fluorescent reporters downstream of the *Glp1r* promoter seems to give the most detailed characterisation of GLP1R [93]. The generation of Glp1R0017 provides a new tool for the field studying the function of GLP1R.

Upon characterisation of Glp1R0017, detailed in chapter 3, specificity for the GLP1R was confirmed, and cross-species reactivity was defined. Although we have indicated specificity of Glp1R0017 for GLP1R using overexpressing cell lines expressing closely related GPCR's, we cannot exclude potential interactions with unknown targets. Use of the INS-1 832/3 cell line to assess off-target effects of Glp1R0017 was limited upon discovery that GLP-1 is secreted from this cell line in the presence of 8.3 mmol/l glucose. To add to our research, it would be interesting to assess Glp1R0017 effects on glucose stimulated insulin secretion from isolated islets, however this would not necessarily enable us to assess off-target effects as there are claims that GLP-1 is secreted from α -cells within pancreatic islets [397].

Further characterisation, in an *in vivo* setting using a mouse model, showed that Glp1R0017 inhibits GLP-1 mediated incretin effects on glucose tolerance, and has an extended half-life in comparison to exendin 9-39 which may be beneficial in certain *in vivo* studies. In comparison to mAb3F52 and 7F38A2, two antibodies developed and characterised by Novo Nordisk during the course of this PhD [116, 252, 253], Glp1R0017 has the major advantage of having cross-species reactivity, likely due to the selection approach using both human GLP1R ECD and mouse GLP1R overexpressing cells as the target antigens.

6.2.1 Future directions for Glp1R0017

Glp1R0017 has been characterised in substantial detail within chapter 3, however more experiments can be thought of for further characterisation of the antibody. For example, western blotting is the method used previously, by Panjwani and colleagues, that showed a number of commercially available antibodies were unspecific for GLP1R [92]. The use of Glp1R0017 for western blotting of the GLP1R has not been detailed here, initial attempts using cell lysates from the mouse and human GLP1R overexpressing cell lines were unsuccessful with an absence of bands on the blots. Optimisation of this technique is required to determine if Glp1R0017 is able to detect GLP1R by western blotting. Other groups are interested in using Glp1R0017 for western blotting, and will hopefully be able to optimise this technique.

In vivo, following a short pharmacokinetic study we characterised Glp1R0017 effects on metabolism by using glucose tolerance tests. We found that Glp1R0017 dose-dependently reversed the actions of liraglutide on glucose tolerance, and decreased glucose tolerance in an OGTT in C57Bl6 wild-type mice.

Other published glucose tolerance studies also measure insulin levels to give a more complete picture of glucose metabolism. Retrospectively, it could have been interesting to measure insulin in our glucose tolerance tests. Additionally, to confirm that Glp1R0017 is specific for GLP1R in an *in vivo* setting, one could make use of the GLP1R knock-out model [294], and test the effects of Glp1R0017 in glucose tolerance.

It is hoped that Glp1R0017 provides a new tool to the field for answering currently unanswered questions surrounding GLP1R physiology. For example, Glp1R0017 is currently being used to assess the importance of GLP-1 in controlling glucose tolerance and weight loss following vertical sleeve gastrectomy in mice. The long half-life of Glp1R0017 means that a weekly injection is able to block the GLP1R, in comparison this study would be impossible using exendin 9-39 due to its short half-life. The GLP1R knock-out mouse would also not be suitable for this type of study as the mice are thought to have adaptations to the knock-out during the course of development, including compensatory increases in GIP secretion and responsiveness to GIP in terms of insulin secretion [398]. This form of experiment shows the key benefits of using a GLP1R antagonistic antibody to study GLP1R physiology, and will hopefully reveal new findings surrounding the importance of GLP-1 post bariatric surgery.

In the longer term one could postulate that a GLP1R antagonistic antibody, may be therapeutically beneficial for patients suffering from post-prandial hypoglycaemia. There are two main groups of patients which suffer with this; one being patients with “dumping syndrome” which often occurs in lean patients that undergo gastrectomy to treat cancer, the other group is patients with the metabolic disorder “post-bariatric hypoglycaemia” which occasionally happens in patients that have undergone bariatric surgery [242, 312]. Studies are currently ongoing using exendin 9-39 infusions, with promising results that GLP1R blockade is a potential therapeutic strategy for treating these patients. Using this previously published data it is exciting to hypothesise that a GLP1R antagonistic antibody may also be beneficial therapeutically, and the longer half-life may provide an important advantage in comparison to exendin 9-39.

6.3 GIPR transgenic mice reveal previously unknown central GIPR localisation

The GIPR is particularly interesting due to its possible role in the control of obesity which has been postulated from a range of studies in both mice and humans [182, 185, 328]. Prior to this study, the limited availability of GIPR antibodies meant that the majority of knowledge surrounding GIPR location was from early studies using *in situ* hybridisation and radioligand binding with low resolution [149, 161]. Here, in chapter 4, a new transgenic mouse model expressing fluorescent reporters downstream of the *Gipr* promoter was used to identify cells expressing the GIPR. This led to a more detailed description of GIPR location, particularly with regards to central expression of the GIPR.

The technique of using transgenic mouse models to label cells of interest has been used widely within the Gribble/Reimann lab, with focus on characterising either enteroendocrine cells [81] or cells expressing receptors for enteroendocrine hormones [93]. The GIPR transgenic mouse line can be directly compared with a GLP1R transgenic model previously used in the lab to characterise GLP1R expression [93]. Another line of interest relevant for this project is the GIP-cre mouse model, it will be interesting to compare the expression of GIP and GIPR [337]. When comparing these expression patterns, the percentage cre penetrance of both lines should be taken into account. Flow cytometry experiments using a GIP antibody and tdRFP labelled ‘GIP’ cells showed that the GIP-cre model only labels 60% of GIP positive K cells in the upper small intestine [337]. Unfortunately, due to the lack of suitable GIPR antibodies, we have been unable to assess the degree to which the GIPR transgenic mouse line successfully labels GIPR positive cells, which is a limitation to this study.

Here we have used the GIPR mouse model to assess GIPR location by immunohistochemistry, though this is not the only potential use of the model. The transgenic mice enable study of cells of interest using a variety of techniques including isolation of cells by flow cytometry followed by genomic analysis [399], and single-cell imaging [400, 401].

In peripheral tissues, we found that GIPR was present in pancreatic islets and exocrine acinar tissue. Expression of GIPR in the acinar tissue was initially unexpected, however a role for GIP in the regulation of digestive enzymes from acinar tissue has been previously suggested [347, 348]. GIPR was also found in both white and brown adipose tissue depots, which is in line with the knowledge that GIPR in adipose tissue is important for storage of fats and may play a role in the regulation of HFD induced obesity [176, 181, 185, 351]. In the duodenum, a population of epithelial GIPR positive cells appeared to be enterochromaffin cells. Most of the GIPR expression was found in cells in the centre of the villi, which are thought to be of mesenchymal origin. GIPR was also detected in the nodose ganglia, where a population of cells are also GLP1R positive. It could be interesting to see if the GIPR positive cells in the nodose ganglia are also GLP1R positive, which could now be performed with the use of Glp1R0017 described in chapters 3 and 4.

Clearly, there are still outstanding tissues for characterisation of GIPR expression or lack of. So far, each tissue assessed has had some form of GIPR expression, therefore it would be useful to find a completely GIPR negative tissue. GIPR expression in the liver is of particular interest, as the GIPR^{adipo-/-} mice have decreased liver volume and fat content but the reason for this is unknown [185]. Collaborators are also using our GIPR transgenic line to assess GIPR expression in the bones where GIP is thought to promote bone formation [402].

The most interesting results from the study of GIPR expression was the observation of GIPR in the hypothalamus, an area of the brain involved in the regulation of food intake. We tried to characterise the role of GIPR within the hypothalamus, however more investigation is required. The main observation was that upon activation of the GIPR positive hypothalamic cells there was a decrease in acute food intake of chow diet following a 10-hour day time fast.

6.3.1 Future directions for understanding GIPR biology using GIPR transgenic mice

The GIPR transgenic mouse model used here to label GIPR positive cells, adds to the field of GIPR research providing a new tool for studying GIPR localisation and the function of GIPR positive cells. As Gipr-Cre x Rosa26-GCamp3 mice have been bred within the lab, the techniques to study GIPR positive cells are not limited to immunostaining. GCamp3 is a fluorescent indicator of intracellular calcium, which combines calmodulin (a Ca^{2+} sensitive protein) with a modified GFP [293]. Combined with the advancements in hypothalamic neuronal culture [403], this means that the calcium responses of GIPR positive cells in primary neuronal cultures can be studied. This could be used in part to further characterise the function of hypothalamic GIPR neurons. Alternatively, rather than imaging individual neurons, one could utilise organotypic brain slice acute preparations or cultures [404, 405] in which the exact location of responding GIPR positive cells could be determined. These studies should be completed alongside further *in vivo* studies to understand the physiology of hypothalamic GIPR positive neurons.

As discussed earlier in chapter 4, the GIPR transgenic mouse model used in this study relies on a lineage tracing approach. Although this technique circumvents the need for antibodies to describe the location of GIPR positive cells, GIPR antibodies would have been useful for full validation of the transgenic mouse line. One possibility for future development would be to use an inducible system to label GIPR cells. For example, Cre-ERT2 and tetracycline-inducible expression systems ('Tet-on') are currently being investigated in the lab for labelling glucagon expressing cells and insulin-like peptide 5 expressing cells. Briefly, the Cre-ERT2 system requires the addition of tamoxifen for activation of Cre [406], and consequently the fluorescent reporter would only be present if cre was expressed at the time of tamoxifen injection. For the Tet-on system, expression of a reverse tetracycline transactivator (rtTA) is driven by the promoter of interest which activates tetracycline responsive elements (Tre) when bound to tetracycline, or doxycycline [407]. For labelling cells of interest, fluorescent reporters are under the control of Tre activation (e.g. Tre-GFP). Both of these methods would provide the advantage that the fluorescent reporters are only expressed in cells that transcribe the gene of interest during the time of treatment.

6.4 The common missense GLP2R mutation, D470N, has decreased β-arrestin binding

The third gut hormone receptor investigated here was the GLP2R. In contrast to GLP1R and GIPR, the GLP2R is not an incretin hormone receptor. GLP-2 is a gut hormone, related to GLP-1 in that it is processed from the same proglucagon gene, and is co-released from enteroendocrine L cells alongside GLP-1 [384]. The main gastrointestinal function of GLP-2 appears to be the regulation of epithelial cell proliferation and apoptosis [202, 214].

As the final part of this thesis, the functional implications of a common missense GLP2R mutation, D470N, associated with type 2 diabetes were investigated. For this purpose, site directed mutagenesis was used to mutate the GLP2R expressing construct. Mammalian cell lines were then transfected with either WT or mutant GLP2R, and signalling was investigated. The mutant GLP2R displayed decreased β-arrestin binding compared to the WT receptor, however there was no difference in cAMP signalling or the timecourse of ERK phosphorylation. The relevance of decreased β-arrestin binding is currently unknown.

6.4.1 Future directions of GLP2R research

The major next step for the GLP2R research project is to determine whether decreased β-arrestin binding to the mutant GLP2R results in any differences in the time course of cAMP signalling downstream of receptor activation. There is good evidence in the field that GLP2R activation stimulates growth factor release (e.g. IGF-1) from sub-epithelial cells in the intestinal wall, which regulate proliferation of the epithelial cell layer [396]. Rather than searching for possible changes in proliferation signals directly downstream of the mutant GLP2R, one can postulate that decreased β-arrestin binding would alter the time-course of primary cAMP signalling, which may affect growth factor release. In our findings there was no difference between the WT and mutant GLP2R accumulated cAMP response at 30 minutes, however a range of time points will now be investigated in more detail.

Therapeutically, without knowing the function of decreased β-arrestin binding to the mutant GLP2R, it is difficult to postulate whether type 2 diabetes patients with the mutant GLP2R should be treated any differently to patients with a WT GLP2R. Currently there are no treatments for type 2 diabetes solely based on the GLP2R, though there are some indications that GLP2 is beneficial for glucose metabolism in an obese state [408].

As an aside to research on the D470N GLP2R mutant, the Gribble/Reimann group could also contribute to the field of GLP2R research in which there is debate surrounding GLP2R location [194-200]. It would be particularly helpful to clarify if the GLP2R is expressed on enteric neurons or on enterochromaffin cells. Using the expertise within the lab a GLP2R lineage tracing transgenic mouse line, similar to the

Gipr-Cre model, could be generated circumventing the need to use GLP2R specific antibodies for studies of GLP2R location.

6.5 Overall therapeutic implications of gut hormone research

There has been a surge in interest surrounding gut hormone research in recent years, due to the success of targeting the enteroendocrine hormone GLP-1 for the treatment of type 2 diabetes [47]. Of increasing therapeutic interest is the use of unimolecular agonists that target multiple pathways simultaneously, which is in part based on the knowledge that gastric bypass surgery can cause the rapid resolution of type 2 diabetes [225]. It is known that this surgery does not simply alter one pathway, but triggers a range of physiological changes including an alteration of several gut hormones [231].

A lot of these dual agonists contain a central GLP-1 component due to the success of established GLP-1 mimetics as treatments. A variety of dual, and even triple agonists have been developed; unimolecular agonists targeting either 2 or 3 different pathways. Of relevance to the research carried out in this thesis are the GLP-1/GIP and GLP-1/GLP-2 dual peptides.

The GLP-1/GIP dual peptide is based upon the premise that both the GLP-1 and GIP components would target pancreatic β -cells increasing glucose stimulated insulin secretion, meaning lower doses of the GLP-1 receptor ligand would be required for the same efficacy on insulin secretion. The hypothesis followed that these lower doses would reduce any GLP-1 gastrointestinal side effects [48]. Concerns were initially raised as the role of GIP in regulating weight gain is unclear, with GIPR knockout animals being protected from HFD induced obesity [182]. However, the GLP-1/GIP dual peptide has proved successful in pre-clinical models with synergistic effects on body weight reduction and insulinotropic effects. The GLP-1/GIP dual peptide is now in clinical trials [232].

The GLP-1/GLP-2 dual peptide was developed to investigate whether the beneficial effects of GLP-1 agonism and GLP-2 agonism could be combined into a single molecule. Results show that the GLP-1/GLP-2 dual peptide can both improve glucose tolerance and increase gut volume, suggesting that the novel concept of combining GLP-1 and GLP-2 agonism could be used to treat both type 2 diabetes and short bowel syndrome [392]. However, our data showing the GLP2R polymorphism D470N is associated with increased enterocyte mass and increased risk of type 2 diabetes, questions whether a GLP-1/GLP-2 dual peptide which increases gut volume would be useful for treatment of type 2 diabetes.

In the development of these unimolecular dual acting peptides, the balance of agonism is often important. With regards to the research performed within this thesis, Glp1R0017 could be a useful

tool in the development of GLP-1 containing dual agonists to determine the importance of the GLP-1 component.

6.6 Conclusion

Together, the data presented in this thesis has demonstrated the applicability of biological and molecular tools for the characterisation of gut hormone receptors. A new antagonistic antibody targeting the GLP1R has been developed and characterised in depth, which is now available for use in collaborative projects to further understand GLP1R physiology. A new transgenic mouse model has been used to determine the location of cells expressing GIPR, and central GIPR expression was revealed which may play a role in the control of food intake. Finally, the signalling defects in a common missense GLP2R mutant, associated with type 2 diabetes, have been defined. It is hoped that the contributions made within this thesis will be helpful for further understanding gut hormone receptor physiology, which will be critical in the development of new therapeutics for type 2 diabetes.

7. References

1. Vella A and Camilleri M (2017) The Gastrointestinal Tract as an Integrator of Mechanical and Hormonal Response to Nutrient Ingestion. *Diabetes* 66: 2729-2737.
2. Hunt JN and Macdonald I (1954) The influence of volume on gastric emptying. *J Physiol* 126: 459-474.
3. Hunt JN (1983) Mechanisms and disorders of gastric emptying. *Annu Rev Med* 34: 219-229.
4. Park MI, Camilleri M, O'Connor H, et al. (2007) Effect of different macronutrients in excess on gastric sensory and motor functions and appetite in normal-weight, overweight, and obese humans. *Am J Clin Nutr* 85: 411-418.
5. Smith DK, Sarfeh J and Howard L (1983) Truncal vagotomy in hypothalamic obesity. *Lancet* 1: 1330-1331.
6. Lu KH, Cao J, Oleson S, et al. (2018) Vagus nerve stimulation promotes gastric emptying by increasing pyloric opening measured with magnetic resonance imaging. *Neurogastroenterol Motil* 30: e13380.
7. Sam AH, Troke RC, Tan TM and Bewick GA (2012) The role of the gut/brain axis in modulating food intake. *Neuropharmacology* 63: 46-56.
8. Berthoud HR and Neuhuber WL (2000) Functional and chemical anatomy of the afferent vagal system. *Auton Neurosci* 85: 1-17.
9. Affleck VS, Coote JH and Pyner S (2012) The projection and synaptic organisation of NTS afferent connections with presynaptic neurons, GABA and nNOS neurons in the paraventricular nucleus of the hypothalamus. *Neuroscience* 219: 48-61.
10. Baraboi ED, Michel C, Smith P, Thibaudeau K, Ferguson AV and Richard D (2010) Effects of albumin-conjugated PYY on food intake: the respective roles of the circumventricular organs and vagus nerve. *Eur J Neurosci* 32: 826-839.
11. Schwartz GJ (2006) Integrative capacity of the caudal brainstem in the control of food intake. *Philos Trans R Soc Lond B Biol Sci* 361: 1275-1280.
12. Konner AC, Klockener T and Bruning JC (2009) Control of energy homeostasis by insulin and leptin: targeting the arcuate nucleus and beyond. *Physiol Behav* 97: 632-638.
13. Broadwell RD and Brightman MW (1976) Entry of peroxidase into neurons of the central and peripheral nervous systems from extracerebral and cerebral blood. *J Comp Neurol* 166: 257-283.
14. Peruzzo B, Pastor FE, Blazquez JL, et al. (2000) A second look at the barriers of the medial basal hypothalamus. *Exp Brain Res* 132: 10-26.

15. Cone RD, Cowley MA, Butler AA, Fan W, Marks DL and Low MJ (2001) The arcuate nucleus as a conduit for diverse signals relevant to energy homeostasis. *Int J Obes Relat Metab Disord* 25 Suppl 5: S63-67.
16. Kalra SP, Dube MG, Pu S, Xu B, Horvath TL and Kalra PS (1999) Interacting appetite-regulating pathways in the hypothalamic regulation of body weight. *Endocr Rev* 20: 68-100.
17. Bouret SG, Draper SJ and Simerly RB (2004) Formation of projection pathways from the arcuate nucleus of the hypothalamus to hypothalamic regions implicated in the neural control of feeding behavior in mice. *J Neurosci* 24: 2797-2805.
18. Williams JA (2006) Regulation of pancreatic acinar cell function. *Curr Opin Gastroenterol* 22: 498-504.
19. Chandra R and Liddle RA (2009) Neural and hormonal regulation of pancreatic secretion. *Curr Opin Gastroenterol* 25: 441-446.
20. Roder PV, Wu B, Liu Y and Han W (2016) Pancreatic regulation of glucose homeostasis. *Exp Mol Med* 48: e219.
21. Briant L, Salehi A, Vergari E, Zhang Q and Rorsman P (2016) Glucagon secretion from pancreatic alpha-cells. *Ups J Med Sci* 121: 113-119.
22. Michael DJ, Ritzel RA, Haataja L and Chow RH (2006) Pancreatic beta-cells secrete insulin in fast- and slow-release forms. *Diabetes* 55: 600-607.
23. Rorsman P and Huisings MO (2018) The somatostatin-secreting pancreatic δ-cell in health and disease. *Nature Reviews Endocrinology* 14: 404-414.
24. Ekblad E and Sundler F (2002) Distribution of pancreatic polypeptide and peptide YY. *Peptides* 23: 251-261.
25. Wierup N, Svensson H, Mulder H and Sundler F (2002) The ghrelin cell: a novel developmentally regulated islet cell in the human pancreas. *Regul Pept* 107: 63-69.
26. Matschinsky FM, Glaser B and Magnuson MA (1998) Pancreatic beta-cell glucokinase: closing the gap between theoretical concepts and experimental realities. *Diabetes* 47: 307-315.
27. Ashcroft FM and Rorsman P (1989) Electrophysiology of the pancreatic beta-cell. *Prog Biophys Mol Biol* 54: 87-143.
28. Rorsman P (1997) The pancreatic beta-cell as a fuel sensor: an electrophysiologist's viewpoint. *Diabetologia* 40: 487-495.
29. Sano H, Kane S, Sano E, et al. (2003) Insulin-stimulated phosphorylation of a Rab GTPase-activating protein regulates GLUT4 translocation. *J Biol Chem* 278: 14599-14602.
30. Bolsoni-Lopes A and Alonso-Vale MI (2015) Lipolysis and lipases in white adipose tissue - An update. *Arch Endocrinol Metab* 59: 335-342.

31. Large V, Peroni O, Letexier D, Ray H and Beylot M (2004) Metabolism of lipids in human white adipocyte. *Diabetes Metab* 30: 294-309.
32. Lafontan M and Langin D (2009) Lipolysis and lipid mobilization in human adipose tissue. *Prog Lipid Res* 48: 275-297.
33. Cannon B and Nedergaard J (2004) Brown adipose tissue: function and physiological significance. *Physiol Rev* 84: 277-359.
34. Bartelt A and Heeren J (2014) Adipose tissue browning and metabolic health. *Nat Rev Endocrinol* 10: 24-36.
35. Klingenberg M (1999) Uncoupling protein--a useful energy dissipator. *J Bioenerg Biomembr* 31: 419-430.
36. Fenzl A and Kiefer FW (2014) Brown adipose tissue and thermogenesis. *Horm Mol Biol Clin Investig* 19: 25-37.
37. Lim S, Honek J, Xue Y, et al. (2012) Cold-induced activation of brown adipose tissue and adipose angiogenesis in mice. *Nat Protoc* 7: 606-615.
38. Klingenspor M (2003) Cold-induced recruitment of brown adipose tissue thermogenesis. *Exp Physiol* 88: 141-148.
39. Chartoumpekis DV, Habeos IG, Ziros PG, Psyrogiannis AI, Kyriazopoulou VE and Papavassiliou AG (2011) Brown adipose tissue responds to cold and adrenergic stimulation by induction of FGF21. *Mol Med* 17: 736-740.
40. Gunawardene AR, Corfe BM and Staton CA (2011) Classification and functions of enteroendocrine cells of the lower gastrointestinal tract. *Int J Exp Pathol* 92: 219-231.
41. Bayliss WM and Starling EH (1902) The mechanism of pancreatic secretion. *J Physiol* 28: 325-353.
42. Moore B (1906) On the treatment of Diabetus mellitus by acid extract of Duodenal Mucous Membrane. *Biochem J* 1: 28-38.
43. McIntyre N, Holdsworth CD and Turner DS (1964) New Interpretation of Oral Glucose Tolerance. *Lancet* 2: 20-21.
44. Elrick H, Stimmmer L, Hlad CJ, Jr. and Arai Y (1964) Plasma Insulin Response to Oral and Intravenous Glucose Administration. *J Clin Endocrinol Metab* 24: 1076-1082.
45. Kreymann B, Williams G, Ghatei MA and Bloom SR (1987) Glucagon-like peptide-1 7-36: a physiological incretin in man. *Lancet* 2: 1300-1304.
46. Dupre J, Ross SA, Watson D and Brown JC (1973) Stimulation of insulin secretion by gastric inhibitory polypeptide in man. *J Clin Endocrinol Metab* 37: 826-828.

47. Meier JJ (2012) GLP-1 receptor agonists for individualized treatment of type 2 diabetes mellitus. *Nat Rev Endocrinol* 8: 728-742.
48. Finan B, Ma T, Ottaway N, et al. (2013) Unimolecular dual incretins maximize metabolic benefits in rodents, monkeys, and humans. *Sci Transl Med* 5: 209ra151.
49. Rehfeld JF (1998) The new biology of gastrointestinal hormones. *Physiol Rev* 78: 1087-1108.
50. Patel YC (1999) Somatostatin and its receptor family. *Front Neuroendocrinol* 20: 157-198.
51. Krejs GJ (1986) Physiological role of somatostatin in the digestive tract: gastric acid secretion, intestinal absorption, and motility. *Scand J Gastroenterol Suppl* 119: 47-53.
52. Billing LJ, Smith CA, Larraufie P, et al. (2018) Co-storage and release of insulin-like peptide-5, glucagon-like peptide-1 and peptideYY from murine and human colonic enteroendocrine cells. *Mol Metab* 16: 65-75.
53. Boey D, Lin S, Karl T, et al. (2006) Peptide YY ablation in mice leads to the development of hyperinsulinaemia and obesity. *Diabetologia* 49: 1360-1370.
54. Batterham RL, Cowley MA, Small CJ, et al. (2002) Gut hormone PYY3-36 physiologically inhibits food intake. *Nature* 418: 650.
55. Grosse J, Heffron H, Burling K, et al. (2014) Insulin-like peptide 5 is an orexigenic gastrointestinal hormone. *Proc Natl Acad Sci U S A* 111: 11133-11138.
56. Muurahainen N, Kissileff HR, Derogatis AJ and Pi-Sunyer FX (1988) Effects of cholecystokinin-octapeptide (CCK-8) on food intake and gastric emptying in man. *Physiol Behav* 44: 645-649.
57. Kopin AS, Mathes WF, McBride EW, et al. (1999) The cholecystokinin-A receptor mediates inhibition of food intake yet is not essential for the maintenance of body weight. *J Clin Invest* 103: 383-391.
58. Anika MS (1982) Effects of cholecystokinin and caerulein on gastric emptying. *Eur J Pharmacol* 85: 195-199.
59. El-Merahbi R, Loffler M, Mayer A and Sumara G (2015) The roles of peripheral serotonin in metabolic homeostasis. *FEBS Lett* 589: 1728-1734.
60. Gregory RE and Ettinger DS (1998) 5-HT3 receptor antagonists for the prevention of chemotherapy-induced nausea and vomiting. A comparison of their pharmacology and clinical efficacy. *Drugs* 55: 173-189.
61. Savastano DM and Covasa M (2007) Intestinal nutrients elicit satiation through concomitant activation of CCK(1) and 5-HT(3) receptors. *Physiol Behav* 92: 434-442.
62. Bulbring E and Crema A (1958) Observations concerning the action of 5-hydroxytryptamine on the peristaltic reflex. *Br J Pharmacol Chemother* 13: 444-457.

63. Martin AM, Young RL, Leong L, et al. (2017) The Diverse Metabolic Roles of Peripheral Serotonin. *Endocrinology* 158: 1049-1063.
64. Itoh Z (1997) Motilin and clinical application. *Peptides* 18: 593-608.
65. Sekar R and Chow BK (2013) Metabolic effects of secretin. *Gen Comp Endocrinol* 181: 18-24.
66. Habib AM, Richards P, Cairns LS, et al. (2012) Overlap of endocrine hormone expression in the mouse intestine revealed by transcriptional profiling and flow cytometry. *Endocrinology* 153: 3054-3065.
67. Fothergill LJ, Callaghan B, Hunne B, Bravo DM and Furness JB (2017) Costorage of Enteroendocrine Hormones Evaluated at the Cell and Subcellular Levels in Male Mice. *Endocrinology* 158: 2113-2123.
68. Sjolund K, Sanden G, Hakanson R and Sundler F (1983) Endocrine cells in human intestine: an immunocytochemical study. *Gastroenterology* 85: 1120-1130.
69. Kieffer TJ and Habener JF (1999) The glucagon-like peptides. *Endocr Rev* 20: 876-913.
70. Trinh DK, Zhang K, Hossain M, Brubaker PL and Drucker DJ (2003) Pax-6 activates endogenous proglucagon gene expression in the rodent gastrointestinal epithelium. *Diabetes* 52: 425-433.
71. Yi F, Brubaker PL and Jin T (2005) TCF-4 mediates cell type-specific regulation of proglucagon gene expression by beta-catenin and glycogen synthase kinase-3beta. *J Biol Chem* 280: 1457-1464.
72. Rouille Y, Westermark G, Martin SK and Steiner DF (1994) Proglucagon is processed to glucagon by prohormone convertase PC2 in alpha TC1-6 cells. *Proc Natl Acad Sci U S A* 91: 3242-3246.
73. Holst JJ (2007) The physiology of glucagon-like peptide 1. *Physiol Rev* 87: 1409-1439.
74. Orskov C, Wettergren A and Holst JJ (1993) Biological effects and metabolic rates of glucagonlike peptide-1 7-36 amide and glucagonlike peptide-1 7-37 in healthy subjects are indistinguishable. *Diabetes* 42: 658-661.
75. Orskov C, Rabenholz L, Wettergren A, Kofod H and Holst JJ (1994) Tissue and plasma concentrations of amidated and glycine-extended glucagon-like peptide I in humans. *Diabetes* 43: 535-539.
76. Mentlein R, Gallwitz B and Schmidt WE (1993) Dipeptidyl-peptidase IV hydrolyses gastric inhibitory polypeptide, glucagon-like peptide-1(7-36)amide, peptide histidine methionine and is responsible for their degradation in human serum. *Eur J Biochem* 214: 829-835.
77. Deacon CF, Nauck MA, Toft-Nielsen M, Pridal L, Willms B and Holst JJ (1995) Both Subcutaneously and Intravenously Administered Glucagon-Like Peptide I Are Rapidly

- Degraded From the NH₂-Terminus in Type II Diabetic Patients and in Healthy Subjects. *Diabetes* 44: 1126-1131.
78. Baggio LL and Drucker DJ (2007) Biology of incretins: GLP-1 and GIP. *Gastroenterology* 132: 2131-2157.
79. Kuc RE, Maguire JJ, Siew K, et al. (2014) Characterization of [¹²⁵I]GLP-1(9-36), a novel radiolabeled analog of the major metabolite of glucagon-like peptide 1 to a receptor distinct from GLP1-R and function of the peptide in murine aorta. *Life Sciences* 102: 134-138.
80. Elahi D, Egan JM, Shannon RP, et al. (2008) GLP-1 (9–36) Amide, Cleavage Product of GLP-1 (7–36) Amide, Is a Glucoregulatory Peptide. *Obesity* 16: 1501-1509.
81. Gribble FM and Reimann F (2016) Enteroendocrine Cells: Chemosensors in the Intestinal Epithelium. *Annu Rev Physiol* 78: 277-299.
82. Foord SM, Bonner TI, Neubig RR, et al. (2005) International Union of Pharmacology. XLVI. G protein-coupled receptor list. *Pharmacol Rev* 57: 279-288.
83. Underwood CR, Garibay P, Knudsen LB, et al. (2010) Crystal structure of glucagon-like peptide-1 in complex with the extracellular domain of the glucagon-like peptide-1 receptor. *J Biol Chem* 285: 723-730.
84. Runge S, Thogersen H, Madsen K, Lau J and Rudolph R (2008) Crystal structure of the ligand-bound glucagon-like peptide-1 receptor extracellular domain. *J Biol Chem* 283: 11340-11347.
85. Jazayeri A, Rappas M, Brown AJH, et al. (2017) Crystal structure of the GLP-1 receptor bound to a peptide agonist. *Nature* 546: 254-258.
86. Song G, Yang D, Wang Y, et al. (2017) Human GLP-1 receptor transmembrane domain structure in complex with allosteric modulators. *Nature* 546: 312-315.
87. Zhang Y, Sun B, Feng D, et al. (2017) Cryo-EM structure of the activated GLP-1 receptor in complex with a G protein. *Nature* 546: 248-253.
88. Yang L, Yang D, de Graaf C, et al. (2015) Conformational states of the full-length glucagon receptor. *Nat Commun* 6: 7859.
89. Drucker DJ, Philippe J, Mojsov S, Chick WL and Habener JF (1987) Glucagon-like peptide I stimulates insulin gene expression and increases cyclic AMP levels in a rat islet cell line. *Proc Natl Acad Sci U S A* 84: 3434-3438.
90. Holz GG (2004) Epac: A new cAMP-binding protein in support of glucagon-like peptide-1 receptor-mediated signal transduction in the pancreatic beta-cell. *Diabetes* 53: 5-13.
91. Pobreja K, Mohd MA, Koole C, Wootten D and Furness SG (2014) Molecular mechanisms underlying physiological and receptor pleiotropic effects mediated by GLP-1R activation. *Br J Pharmacol* 171: 1114-1128.

92. Panjwani N, Mulvihill EE, Longuet C, et al. (2013) GLP-1 receptor activation indirectly reduces hepatic lipid accumulation but does not attenuate development of atherosclerosis in diabetic male ApoE(-/-) mice. *Endocrinology* 154: 127-139.
93. Richards P, Parker HE, Adriaenssens AE, et al. (2014) Identification and characterization of GLP-1 receptor-expressing cells using a new transgenic mouse model. *Diabetes* 63: 1224-1233.
94. Cork SC, Richards JE, Holt MK, Gribble FM, Reimann F and Trapp S (2015) Distribution and characterisation of Glucagon-like peptide-1 receptor expressing cells in the mouse brain. *Mol Metab* 4: 718-731.
95. Jensen CB, Pyke C, Rasch MG, Dahl AB, Knudsen LB and Secher A (2018) Characterization of the Glucagonlike Peptide-1 Receptor in Male Mouse Brain Using a Novel Antibody and In Situ Hybridization. *Endocrinology* 159: 665-675.
96. Fusco J, Xiao X, Prasad K, et al. (2017) GLP-1/Exendin-4 induces beta-cell proliferation via the epidermal growth factor receptor. *Sci Rep* 7: 9100.
97. Zhang L, Wang Y, Wang J, Liu Y and Yin Y (2015) Protein kinase C pathway mediates the protective effects of glucagon-like peptide-1 on the apoptosis of islet beta-cells. *Mol Med Rep* 12: 7589-7594.
98. Campbell JE and Drucker DJ (2013) Pharmacology, physiology, and mechanisms of incretin hormone action. *Cell Metab* 17: 819-837.
99. Li Y, Cao X, Li LX, Brubaker PL, Edlund H and Drucker DJ (2005) beta-Cell Pdx1 expression is essential for the glucoregulatory, proliferative, and cytoprotective actions of glucagon-like peptide-1. *Diabetes* 54: 482-491.
100. De Marinis YZ, Salehi A, Ward CE, et al. (2010) GLP-1 inhibits and adrenaline stimulates glucagon release by differential modulation of N- and L-type Ca²⁺ channel-dependent exocytosis. *Cell Metab* 11: 543-553.
101. de Heer J, Rasmussen C, Coy DH and Holst JJ (2008) Glucagon-like peptide-1, but not glucose-dependent insulinotropic peptide, inhibits glucagon secretion via somatostatin (receptor subtype 2) in the perfused rat pancreas. *Diabetologia* 51: 2263-2270.
102. Wettergren A, Schjoldager B, Mortensen PE, Myhre J, Christiansen J and Holst JJ (1993) Truncated GLP-1 (proglucagon 78-107-amide) inhibits gastric and pancreatic functions in man. *Dig Dis Sci* 38: 665-673.
103. Imeryuz N, Yegen BC, Bozkurt A, Coskun T, Villanueva-Penacarrillo ML and Ulusoy NB (1997) Glucagon-like peptide-1 inhibits gastric emptying via vagal afferent-mediated central mechanisms. *Am J Physiol* 273: G920-927.

104. Plamboeck A, Veedfald S, Deacon CF, et al. (2013) Characterisation of oral and i.v. glucose handling in truncally vagotomised subjects with pyloroplasty. *Eur J Endocrinol* 169: 187-201.
105. Hellstrom PM, Naslund E, Edholm T, et al. (2008) GLP-1 suppresses gastrointestinal motility and inhibits the migrating motor complex in healthy subjects and patients with irritable bowel syndrome. *Neurogastroenterol Motil* 20: 649-659.
106. Wettergren A, Wojdemann M, Meisner S, Stadil F and Holst JJ (1997) The inhibitory effect of glucagon-like peptide-1 (GLP-1) 7-36 amide on gastric acid secretion in humans depends on an intact vagal innervation. *Gut* 40: 597-601.
107. Tang-Christensen M, Larsen PJ, Goke R, et al. (1996) Central administration of GLP-1-(7-36) amide inhibits food and water intake in rats. *Am J Physiol* 271: R848-856.
108. Moreno C, Mistry M and Roman RJ (2002) Renal effects of glucagon-like peptide in rats. *Eur J Pharmacol* 434: 163-167.
109. Farah LX, Valentini V, Pessoa TD, Malnic G, McDonough AA and Girardi AC (2016) The physiological role of glucagon-like peptide-1 in the regulation of renal function. *Am J Physiol Renal Physiol* 310: F123-127.
110. Crajoinas RO, Oricchio FT, Pessoa TD, et al. (2011) Mechanisms mediating the diuretic and natriuretic actions of the incretin hormone glucagon-like peptide-1. *Am J Physiol Renal Physiol* 301: F355-363.
111. Carraro-Lacroix LR, Malnic G and Girardi AC (2009) Regulation of Na⁺/H⁺ exchanger NHE3 by glucagon-like peptide 1 receptor agonist exendin-4 in renal proximal tubule cells. *Am J Physiol Renal Physiol* 297: F1647-1655.
112. Muskiet MHA, Tonneijck L, Smits MM, et al. (2017) GLP-1 and the kidney: from physiology to pharmacology and outcomes in diabetes. *Nat Rev Nephrol* 13: 605-628.
113. Marso SP, Daniels GH, Brown-Frandsen K, et al. (2016) Liraglutide and Cardiovascular Outcomes in Type 2 Diabetes. *N Engl J Med* 375: 311-322.
114. Marso SP, Bain SC, Consoli A, et al. (2016) Semaglutide and Cardiovascular Outcomes in Patients with Type 2 Diabetes. *N Engl J Med* 375: 1834-1844.
115. Pfeffer MA, Claggett B, Diaz R, et al. (2015) Lixisenatide in Patients with Type 2 Diabetes and Acute Coronary Syndrome. *N Engl J Med* 373: 2247-2257.
116. Pyke C, Heller RS, Kirk RK, et al. (2014) GLP-1 receptor localization in monkey and human tissue: novel distribution revealed with extensively validated monoclonal antibody. *Endocrinology* 155: 1280-1290.
117. Baggio LL, Yusta B, Mulvihill EE, et al. (2018) GLP-1 Receptor Expression Within the Human Heart. *Endocrinology* 159: 1570-1584.

118. Kim M, Platt MJ, Shibasaki T, et al. (2013) GLP-1 receptor activation and Epac2 link atrial natriuretic peptide secretion to control of blood pressure. *Nat Med* 19: 567-575.
119. Gros R, You X, Baggio LL, et al. (2003) Cardiac function in mice lacking the glucagon-like peptide-1 receptor. *Endocrinology* 144: 2242-2252.
120. Ban K, Noyan-Ashraf MH, Hoefer J, Bolz SS, Drucker DJ and Husain M (2008) Cardioprotective and vasodilatory actions of glucagon-like peptide 1 receptor are mediated through both glucagon-like peptide 1 receptor-dependent and -independent pathways. *Circulation* 117: 2340-2350.
121. Ban K, Kim KH, Cho CK, et al. (2010) Glucagon-like peptide (GLP)-1(9-36)amide-mediated cytoprotection is blocked by exendin(9-39) yet does not require the known GLP-1 receptor. *Endocrinology* 151: 1520-1531.
122. Nikolaidis LA, Elahi D, Shen YT and Shannon RP (2005) Active metabolite of GLP-1 mediates myocardial glucose uptake and improves left ventricular performance in conscious dogs with dilated cardiomyopathy. *Am J Physiol Heart Circ Physiol* 289: H2401-2408.
123. Isbil-Buyukcoskun N and Gulec G (2004) Effects of intracerebroventricularly injected glucagon-like peptide-1 on cardiovascular parameters; role of central cholinergic system and vasopressin. *Regul Pept* 118: 33-38.
124. Baggio LL, Ussher JR, McLean BA, et al. (2017) The autonomic nervous system and cardiac GLP-1 receptors control heart rate in mice. *Mol Metab* 6: 1339-1349.
125. Turton MD, O'Shea D, Gunn I, et al. (1996) A role for glucagon-like peptide-1 in the central regulation of feeding. *Nature* 379: 69-72.
126. Meeran K, O'Shea D, Edwards CM, et al. (1999) Repeated intracerebroventricular administration of glucagon-like peptide-1-(7-36) amide or exendin-(9-39) alters body weight in the rat. *Endocrinology* 140: 244-250.
127. Barrera JG, D'Alessio DA, Drucker DJ, Woods SC and Seeley RJ (2009) Differences in the central anorectic effects of glucagon-like peptide-1 and exendin-4 in rats. *Diabetes* 58: 2820-2827.
128. Sisley S, Gutierrez-Aguilar R, Scott M, D'Alessio DA, Sandoval DA and Seeley RJ (2014) Neuronal GLP1R mediates liraglutide's anorectic but not glucose-lowering effect. *J Clin Invest* 124: 2456-2463.
129. Secher A, Jelsing J, Baquero AF, et al. (2014) The arcuate nucleus mediates GLP-1 receptor agonist liraglutide-dependent weight loss. *J Clin Invest* 124: 4473-4488.
130. Burmeister MA, Ayala JE, Smouse H, et al. (2017) The Hypothalamic Glucagon-Like Peptide 1 Receptor Is Sufficient but Not Necessary for the Regulation of Energy Balance and Glucose Homeostasis in Mice. *Diabetes* 66: 372-384.

131. Nakagawa A, Satake H, Nakabayashi H, et al. (2004) Receptor gene expression of glucagon-like peptide-1, but not glucose-dependent insulinotropic polypeptide, in rat nodose ganglion cells. *Auton Neurosci* 110: 36-43.
132. Vahl TP, Tauchi M, Durler TS, et al. (2007) Glucagon-like peptide-1 (GLP-1) receptors expressed on nerve terminals in the portal vein mediate the effects of endogenous GLP-1 on glucose tolerance in rats. *Endocrinology* 148: 4965-4973.
133. Takeda J, Seino Y, Tanaka K, et al. (1987) Sequence of an intestinal cDNA encoding human gastric inhibitory polypeptide precursor. *Proc Natl Acad Sci U S A* 84: 7005-7008.
134. Buchan AM, Polak JM, Capella C, Solcia E and Pearse AG (1978) Electronimmunocytochemical evidence for the K cell localization of gastric inhibitory polypeptide (GIP) in man. *Histochemistry* 56: 37-44.
135. Tseng CC, Boylan MO, Jarboe LA, Williams EK, Sunday ME and Wolfe MM (1995) Glucose-dependent insulinotropic peptide (GIP) gene expression in the rat salivary gland. *Mol Cell Endocrinol* 115: 13-19.
136. Jepeal LI, Fujitani Y, Boylan MO, Wilson CN, Wright CV and Wolfe MM (2005) Cell-specific expression of glucose-dependent-insulinotropic polypeptide is regulated by the transcription factor PDX-1. *Endocrinology* 146: 383-391.
137. Suzuki K, Harada N, Yamane S, et al. (2013) Transcriptional regulatory factor X6 (Rfx6) increases gastric inhibitory polypeptide (GIP) expression in enteroendocrine K-cells and is involved in GIP hypersecretion in high fat diet-induced obesity. *J Biol Chem* 288: 1929-1938.
138. Ugleholdt R, Poulsen ML, Holst PJ, et al. (2006) Prohormone convertase 1/3 is essential for processing of the glucose-dependent insulinotropic polypeptide precursor. *J Biol Chem* 281: 11050-11057.
139. Kieffer TJ, McIntosh CH and Pederson RA (1995) Degradation of glucose-dependent insulinotropic polypeptide and truncated glucagon-like peptide 1 in vitro and in vivo by dipeptidyl peptidase IV. *Endocrinology* 136: 3585-3596.
140. Deacon CF, Nauck MA, Meier J, Hucking K and Holst JJ (2000) Degradation of endogenous and exogenous gastric inhibitory polypeptide in healthy and in type 2 diabetic subjects as revealed using a new assay for the intact peptide. *J Clin Endocrinol Metab* 85: 3575-3581.
141. Vilsboll T, Krarup T, Deacon CF, Madsbad S and Holst JJ (2001) Reduced postprandial concentrations of intact biologically active glucagon-like peptide 1 in type 2 diabetic patients. *Diabetes* 50: 609-613.
142. Vollmer K, Holst JJ, Baller B, et al. (2008) Predictors of incretin concentrations in subjects with normal, impaired, and diabetic glucose tolerance. *Diabetes* 57: 678-687.

143. Elliott RM, Morgan LM, Tredger JA, Deacon S, Wright J and Marks V (1993) Glucagon-like peptide-1 (7-36)amide and glucose-dependent insulinotropic polypeptide secretion in response to nutrient ingestion in man: acute post-prandial and 24-h secretion patterns. *J Endocrinol* 138: 159-166.
144. Cleator IGM and Gourlay RH (1975) Release of immunoreactive gastric inhibitory polypeptide (IR-GIP) by oral ingestion of food substances. *The American Journal of Surgery* 130: 128-135.
145. Meier JJ and Nauck MA (2004) Clinical endocrinology and metabolism. Glucose-dependent insulinotropic polypeptide/gastric inhibitory polypeptide. *Best Pract Res Clin Endocrinol Metab* 18: 587-606.
146. Sykes S, Morgan LM, English J and Marks V (1980) Evidence for preferential stimulation of gastric inhibitory polypeptide secretion in the rat by actively transported carbohydrates and their analogues. *J Endocrinol* 85: 201-207.
147. Parker HE, Habib AM, Rogers GJ, Gribble FM and Reimann F (2009) Nutrient-dependent secretion of glucose-dependent insulinotropic polypeptide from primary murine K cells. *Diabetologia* 52: 289-298.
148. Yamane S, Harada N and Inagaki N (2016) Mechanisms of fat-induced gastric inhibitory polypeptide/glucose-dependent insulinotropic polypeptide secretion from K cells. *J Diabetes Investig* 7 Suppl 1: 20-26.
149. Usdin TB, Mezey E, Button DC, Brownstein MJ and Bonner TI (1993) Gastric inhibitory polypeptide receptor, a member of the secretin-vasoactive intestinal peptide receptor family, is widely distributed in peripheral organs and the brain. *Endocrinology* 133: 2861-2870.
150. Gelling RW, Wheeler MB, Xue J, et al. (1997) Localization of the Domains Involved in Ligand Binding and Activation of the Glucose-Dependent Insulinotropic Polypeptide Receptor. *Endocrinology* 138: 2640-2643.
151. Wheeler MB, Gelling RW, Hinke SA, et al. (1999) Characterization of the Carboxyl-terminal Domain of the Rat Glucose-dependent Insulinotropic Polypeptide (GIP) Receptor: A ROLE FOR SERINES 426 AND 427 IN REGULATING THE RATE OF INTERNALIZATION. *Journal of Biological Chemistry* 274: 24593-24601.
152. Parthier C, Kleinschmidt M, Neumann P, et al. (2007) Crystal structure of the incretin-bound extracellular domain of a G protein-coupled receptor. *Proc Natl Acad Sci U S A* 104: 13942-13947.
153. Hoare SR (2005) Mechanisms of peptide and nonpeptide ligand binding to Class B G-protein-coupled receptors. *Drug Discov Today* 10: 417-427.

154. Ding W-G and Gromada J (1997) Protein Kinase A-Dependent Stimulation of Exocytosis in Mouse Pancreatic β -Cells by Glucose-Dependent Insulinotropic Polypeptide. *Diabetes* 46: 615-621.
155. McIntosh CH, Widenmaier S and Kim SJ (2012) Glucose-dependent insulinotropic polypeptide signaling in pancreatic beta-cells and adipocytes. *J Diabetes Investig* 3: 96-106.
156. Miki T, Minami K, Shinozaki H, et al. (2005) Distinct Effects of Glucose-Dependent Insulinotropic Polypeptide and Glucagon-Like Peptide-1 on Insulin Secretion and Gut Motility. *Diabetes* 54: 1056-1063.
157. Al-Sabah S, Al-Fulaij M, Shaaban G, et al. (2014) The GIP receptor displays higher basal activity than the GLP-1 receptor but does not recruit GRK2 or arrestin3 effectively. *PLoS One* 9: e106890.
158. Ehses JA, Pelech SL, Pederson RA and McIntosh CHS (2002) Glucose-dependent Insulinotropic Polypeptide Activates the Raf-Mek1/2-ERK1/2 Module via a Cyclic AMP/cAMP-dependent Protein Kinase/Rap1-mediated Pathway. *Journal of Biological Chemistry* 277: 37088-37097.
159. Campbell JE, Ussher JR, Mulvihill EE, et al. (2016) TCF1 links GIPR signaling to the control of beta cell function and survival. *Nat Med* 22: 84-90.
160. Widenmaier SB, Ao Z, Kim SJ, Warnock G and McIntosh CH (2009) Suppression of p38 MAPK and JNK via Akt-mediated inhibition of apoptosis signal-regulating kinase 1 constitutes a core component of the beta-cell pro-survival effects of glucose-dependent insulinotropic polypeptide. *J Biol Chem* 284: 30372-30382.
161. Kaplan AM and Vigna SR (1994) Gastric inhibitory polypeptide (GIP) binding sites in rat brain. *Peptides* 15: 297-302.
162. Prasad K, Koizumi M, Tulachan S, et al. (2011) The expression and function of glucose-dependent insulinotropic polypeptide in the embryonic mouse pancreas. *Diabetes* 60: 548-554.
163. Marcos AB, Forner S, Martini AC, et al. (2016) Temporal and Regional Expression of Glucose-Dependent Insulinotropic Peptide and Its Receptor in Spinal Cord Injured Rats. *J Neurotrauma* 33: 261-268.
164. Ravn P, Madhurantakam C, Kunze S, et al. (2013) Structural and pharmacological characterization of novel potent and selective monoclonal antibody antagonists of glucose-dependent insulinotropic polypeptide receptor. *J Biol Chem* 288: 19760-19772.
165. Xie D, Cheng H, Hamrick M, et al. (2005) Glucose-dependent insulinotropic polypeptide receptor knockout mice have altered bone turnover. *Bone* 37: 759-769.

166. Nauck MA, Bartels E, Orskov C, Ebert R and Creutzfeldt W (1992) Lack of effect of synthetic human gastric inhibitory polypeptide and glucagon-like peptide 1 [7-36 amide] infused at near-physiological concentrations on pentagastrin-stimulated gastric acid secretion in normal human subjects. *Digestion* 52: 214-221.
167. Faivre E, Gault VA, Thorens B and Holscher C (2011) Glucose-dependent insulinotropic polypeptide receptor knockout mice are impaired in learning, synaptic plasticity, and neurogenesis. *J Neurophysiol* 105: 1574-1580.
168. Gault VA and Holscher C (2008) Protease-resistant glucose-dependent insulinotropic polypeptide agonists facilitate hippocampal LTP and reverse the impairment of LTP induced by beta-amyloid. *J Neurophysiol* 99: 1590-1595.
169. Gasbjerg LS, Gabe MBN, Hartmann B, et al. (2018) Glucose-dependent insulinotropic polypeptide (GIP) receptor antagonists as anti-diabetic agents. *Peptides* 100: 173-181.
170. Kim SJ, Nian C, Widenmaier S and McIntosh CH (2008) Glucose-dependent insulinotropic polypeptide-mediated up-regulation of beta-cell antiapoptotic Bcl-2 gene expression is coordinated by cyclic AMP (cAMP) response element binding protein (CREB) and cAMP-responsive CREB coactivator 2. *Mol Cell Biol* 28: 1644-1656.
171. Friedrichsen BN, Neubauer N, Lee YC, et al. (2006) Stimulation of pancreatic beta-cell replication by incretins involves transcriptional induction of cyclin D1 via multiple signalling pathways. *J Endocrinol* 188: 481-492.
172. Chia CW, Carlson OD, Kim W, et al. (2009) Exogenous glucose-dependent insulinotropic polypeptide worsens post prandial hyperglycemia in type 2 diabetes. *Diabetes* 58: 1342-1349.
173. Beck B and Max JP (1983) Gastric inhibitory polypeptide enhancement of the insulin effect on fatty acid incorporation into adipose tissue in the rat. *Regul Pept* 7: 3-8.
174. Wasada T, McCorkle K, Harris V, Kawai K, Howard B and Unger RH (1981) Effect of gastric inhibitory polypeptide on plasma levels of chylomicron triglycerides in dogs. *J Clin Invest* 68: 1106-1107.
175. Ebert R, Nauck M and Creutzfeldt W (1991) Effect of exogenous or endogenous gastric inhibitory polypeptide (GIP) on plasma triglyceride responses in rats. *Horm Metab Res* 23: 517-521.
176. Kim SJ, Nian C and McIntosh CH (2007) Activation of lipoprotein lipase by glucose-dependent insulinotropic polypeptide in adipocytes. A role for a protein kinase B, LKB1, and AMP-activated protein kinase cascade. *J Biol Chem* 282: 8557-8567.

177. Kim SJ, Nian C and McIntosh CH (2007) Resistin is a key mediator of glucose-dependent insulinotropic polypeptide (GIP) stimulation of lipoprotein lipase (LPL) activity in adipocytes. *J Biol Chem* 282: 34139-34147.
178. Eckel RH, Fujimoto WY and Brunzell JD (1979) Gastric inhibitory polypeptide enhanced lipoprotein lipase activity in cultured preadipocytes. *Diabetes* 28: 1141-1142.
179. Knapper JM, Puddicombe SM, Morgan LM and Fletcher JM (1995) Investigations into the actions of glucose-dependent insulinotropic polypeptide and glucagon-like peptide-1(7-36)amide on lipoprotein lipase activity in explants of rat adipose tissue. *J Nutr* 125: 183-188.
180. Mead JR, Irvine SA and Ramji DP (2002) Lipoprotein lipase: structure, function, regulation, and role in disease. *J Mol Med (Berl)* 80: 753-769.
181. Kim SJ, Nian C and McIntosh CH (2010) GIP increases human adipocyte LPL expression through CREB and TORC2-mediated trans-activation of the LPL gene. *J Lipid Res* 51: 3145-3157.
182. Miyawaki K, Yamada Y, Ban N, et al. (2002) Inhibition of gastric inhibitory polypeptide signaling prevents obesity. *Nat Med* 8: 738-742.
183. Starich GH, Bar RS and Mazzaferri EL (1985) GIP increases insulin receptor affinity and cellular sensitivity in adipocytes. *Am J Physiol* 249: E603-607.
184. Mohammad S, Ramos LS, Buck J, Levin LR, Rubino F and McGraw TE (2011) Gastric inhibitory peptide controls adipose insulin sensitivity via activation of cAMP-response element-binding protein and p110beta isoform of phosphatidylinositol 3-kinase. *J Biol Chem* 286: 43062-43070.
185. Joo E, Harada N, Yamane S, et al. (2017) Inhibition of Gastric Inhibitory Polypeptide Receptor Signaling in Adipose Tissue Reduces Insulin Resistance and Hepatic Steatosis in High-Fat Diet-Fed Mice. *Diabetes* 66: 868-879.
186. Ugleholdt R, Zhu X, Deacon CF, Orskov C, Steiner DF and Holst JJ (2004) Impaired intestinal proglucagon processing in mice lacking prohormone convertase 1. *Endocrinology* 145: 1349-1355.
187. Drucker DJ (2002) Gut adaptation and the glucagon-like peptides. *Gut* 50: 428-435.
188. Drucker DJ, Shi Q, Crivici A, et al. (1997) Regulation of the biological activity of glucagon-like peptide 2 in vivo by dipeptidyl peptidase IV. *Nat Biotechnol* 15: 673-677.
189. Venneti KC and Hewage CM (2011) Conformational and molecular interaction studies of glucagon-like peptide-2 with its N-terminal extracellular receptor domain. *FEBS Lett* 585: 346-352.
190. Kelley LA and Sternberg MJ (2009) Protein structure prediction on the Web: a case study using the Phyre server. *Nat Protoc* 4: 363-371.

191. Munroe DG, Gupta AK, Kooshesh F, et al. (1999) Prototypic G protein-coupled receptor for the intestinotrophic factor glucagon-like peptide 2. *Proceedings of the National Academy of Sciences* 96: 1569-1573.
192. de Heuvel E, Wallace L, Sharkey KA and Sigalet DL (2012) Glucagon-like peptide 2 induces vasoactive intestinal polypeptide expression in enteric neurons via phosphatidylinositol 3-kinase-gamma signaling. *Am J Physiol Endocrinol Metab* 303: E994-1005.
193. Estall JL, Koehler JA, Yusta B and Drucker DJ (2005) The Glucagon-like Peptide-2 Receptor C Terminus Modulates β -Arrestin-2 Association but Is Dispensable for Ligand-induced Desensitization, Endocytosis, and G-protein-dependent Effector Activation. *Journal of Biological Chemistry* 280: 22124-22134.
194. Yusta B, Huang L, Munroe D, et al. (2000) Enteroendocrine localization of GLP-2 receptor expression in humans and rodents. *Gastroenterology* 119: 744-755.
195. Guan X, Karpen HE, Stephens J, et al. (2006) GLP-2 receptor localizes to enteric neurons and endocrine cells expressing vasoactive peptides and mediates increased blood flow. *Gastroenterology* 130: 150-164.
196. Nelson DW, Sharp JW, Brownfield MS, Raybould HE and Ney DM (2007) Localization and activation of glucagon-like peptide-2 receptors on vagal afferents in the rat. *Endocrinology* 148: 1954-1962.
197. Bjerknes M and Cheng H (2001) Modulation of specific intestinal epithelial progenitors by enteric neurons. *Proc Natl Acad Sci U S A* 98: 12497-12502.
198. Orskov C, Hartmann B, Poulsen SS, Thulesen J, Hare KJ and Holst JJ (2005) GLP-2 stimulates colonic growth via KGF, released by subepithelial myofibroblasts with GLP-2 receptors. *Regul Pept* 124: 105-112.
199. Pedersen J, Pedersen NB, Brix SW, et al. (2015) The glucagon-like peptide 2 receptor is expressed in enteric neurons and not in the epithelium of the intestine. *Peptides* 67: 20-28.
200. Korner M, Rehmann R and Reubi JC (2012) GLP-2 receptors in human disease: high expression in gastrointestinal stromal tumors and Crohn's disease. *Mol Cell Endocrinol* 364: 46-53.
201. Drucker DJ and Yusta B (2014) Physiology and Pharmacology of the Enteroendocrine Hormone Glucagon-Like Peptide-2. *Annual Review of Physiology* 76: 561-583.
202. Drucker DJ, Erlich P, Asa SL and Brubaker PL (1996) Induction of intestinal epithelial proliferation by glucagon-like peptide 2. *Proceedings of the National Academy of Sciences* 93: 7911-7916.
203. Scott RB, Kirk D, MacNaughton WK and Meddings JB (1998) GLP-2 augments the adaptive response to massive intestinal resection in rat. *Am J Physiol* 275: G911-921.

204. Hsieh J, Longuet C, Maida A, et al. (2009) Glucagon-Like Peptide-2 Increases Intestinal Lipid Absorption and Chylomicron Production via CD36. *Gastroenterology* 137: 997-1005.e1004.
205. Meier JJ, Nauck MA, Pott A, et al. (2006) Glucagon-Like Peptide 2 Stimulates Glucagon Secretion, Enhances Lipid Absorption, and Inhibits Gastric Acid Secretion in Humans. *Gastroenterology* 130: 44-54.
206. Nagell CF, Wettergren A, Pedersen JF, Mortensen D and Holst JJ (2004) Glucagon-like peptide-2 inhibits antral emptying in man, but is not as potent as glucagon-like peptide-1. *Scandinavian Journal of Gastroenterology* 39: 353-358.
207. Benjamin MA, McKay DM, Yang P-C, Cameron H and Perdue MH (2000) Glucagon-like peptide-2 enhances intestinal epithelial barrier function of both transcellular and paracellular pathways in the mouse. *Gut* 47: 112-119.
208. Cani PD, Possemiers S, Van de Wiele T, et al. (2009) Changes in gut microbiota control inflammation in obese mice through a mechanism involving GLP-2-driven improvement of gut permeability. *Gut* 58: 1091-1103.
209. Guan X, Stoll B, Lu X, et al. (2003) GLP-2-mediated up-regulation of intestinal blood flow and glucose uptake is nitric oxide-dependent in TPN-fed piglets 1. *Gastroenterology* 125: 136-147.
210. Bremholm L, Hornum M, Henriksen BM, Larsen S and Holst JJ (2009) Glucagon-like peptide-2 increases mesenteric blood flow in humans. *Scandinavian Journal of Gastroenterology* 44: 314-319.
211. Henriksen DB, Alexandersen P, Hartmann B, et al. (2007) Disassociation of bone resorption and formation by GLP-2: a 14-day study in healthy postmenopausal women. *Bone* 40: 723-729.
212. Henriksen DB, Alexandersen P, Hartmann B, et al. (2009) Four-month treatment with GLP-2 significantly increases hip BMD: a randomized, placebo-controlled, dose-ranging study in postmenopausal women with low BMD. *Bone* 45: 833-842.
213. de Heer J, Pedersen J, Orskov C and Holst JJ (2007) The alpha cell expresses glucagon-like peptide-2 receptors and glucagon-like peptide-2 stimulates glucagon secretion from the rat pancreas. *Diabetologia* 50: 2135-2142.
214. Brubaker PL, Izzo A, Hill M and Drucker DJ (1997) Intestinal function in mice with small bowel growth induced by glucagon-like peptide-2. *Am J Physiol* 272: E1050-1058.
215. Au A, Gupta A, Schembri P and Cheeseman CI (2002) Rapid insertion of GLUT2 into the rat jejunal brush-border membrane promoted by glucagon-like peptide 2. *Biochem J* 367: 247-254.

216. Dash S, Xiao C, Morgantini C, Connelly PW, Patterson BW and Lewis GF (2014) Glucagon-like peptide-2 regulates release of chylomicrons from the intestine. *Gastroenterology* 147: 1275-1284 e1274.
217. Lee J, Koehler J, Yusta B, et al. (2017) Enteroendocrine-derived glucagon-like peptide-2 controls intestinal amino acid transport. *Mol Metab* 6: 245-255.
218. Yu C, Jia G, Jiang Y, et al. (2014) Effect of Glucagon-like Peptide 2 on Tight Junction in Jejunal Epithelium of Weaned Pigs through MAPK Signaling Pathway. *Asian-Australas J Anim Sci* 27: 733-742.
219. Bahrami J, Longuet C, Baggio LL, Li K and Drucker DJ (2010) Glucagon-like peptide-2 receptor modulates islet adaptation to metabolic stress in the ob/ob mouse. *Gastroenterology* 139: 857-868.
220. Maleckas A, Venclauskas L, Wallenius V, Löroth H and Fändriks L (2015) Surgery in the treatment of type 2 diabetes mellitus. *Scandinavian Journal of Surgery* 104: 40-47.
221. Zimmet PZ (1999) Diabetes epidemiology as a tool to trigger diabetes research and care. *Diabetologia* 42: 499-518.
222. Colditz GA, Willett WC, Rotnitzky A and Manson JE (1995) Weight gain as a risk factor for clinical diabetes mellitus in women. *Annals of Internal Medicine* 122: 481-486.
223. Chan JM, Rimm EB, Colditz GA, Stampfer MJ and Willett WC (1994) Obesity, Fat Distribution, and Weight Gain as Risk Factors for Clinical Diabetes in Men. *Diabetes Care* 17: 961-969.
224. Cho YM (2014) A Gut Feeling to Cure Diabetes: Potential Mechanisms of Diabetes Remission after Bariatric Surgery. *Diabetes Metab J* 38: 406-415.
225. Buchwald H, Avidor Y, Braunwald E, et al. (2004) Bariatric surgery: a systematic review and meta-analysis. *JAMA* 292: 1724-1737.
226. O'Keefe SJ, Buchman AL, Fishbein TM, Jeejeebhoy KN, Jeppesen PB and Shaffer J (2006) Short bowel syndrome and intestinal failure: consensus definitions and overview. *Clin Gastroenterol Hepatol* 4: 6-10.
227. Buchman AL, Scolapio J and Fryer J (2003) AGA technical review on short bowel syndrome and intestinal transplantation. *Gastroenterology* 124: 1111-1134.
228. Thompson JS, Rochling FA, Weseman RA and Mercer DF (2012) Current management of short bowel syndrome. *Curr Probl Surg* 49: 52-115.
229. Martin-Timon I, Sevillano-Collantes C, Segura-Galindo A and Del Canizo-Gomez FJ (2014) Type 2 diabetes and cardiovascular disease: Have all risk factors the same strength? *World J Diabetes* 5: 444-470.

230. Green BD, Flatt PR and Bailey CJ (2006) Dipeptidyl peptidase IV (DPP IV) inhibitors: A newly emerging drug class for the treatment of type 2 diabetes. *Diab Vasc Dis Res* 3: 159-165.
231. Knop FK and Taylor R (2013) Mechanism of metabolic advantages after bariatric surgery: it's all gastrointestinal factors versus it's all food restriction. *Diabetes Care* 36 Suppl 2: S287-291.
232. Finan B, Clemmensen C and Muller TD (2015) Emerging opportunities for the treatment of metabolic diseases: Glucagon-like peptide-1 based multi-agonists. *Mol Cell Endocrinol* 418 Pt 1: 42-54.
233. Rouch JD and Dunn JC (2017) New insights and interventions for short bowel syndrome. *Curr Pediatr Rep* 5: 1-5.
234. Kim ES and Keam SJ (2017) Teduglutide: A Review in Short Bowel Syndrome. *Drugs* 77: 345-352.
235. Jeppesen PB, Sanguinetti EL, Buchman A, et al. (2005) Teduglutide (ALX-0600), a dipeptidyl peptidase IV resistant glucagon-like peptide 2 analogue, improves intestinal function in short bowel syndrome patients. *Gut* 54: 1224-1231.
236. Tappenden KA, Edelman J and Joelsson B (2013) Teduglutide enhances structural adaptation of the small intestinal mucosa in patients with short bowel syndrome. *J Clin Gastroenterol* 47: 602-607.
237. Drucker DJ and Nauck MA (2006) The incretin system: glucagon-like peptide-1 receptor agonists and dipeptidyl peptidase-4 inhibitors in type 2 diabetes. *Lancet* 368: 1696-1705.
238. Ussher JR and Drucker DJ (2012) Cardiovascular biology of the incretin system. *Endocr Rev* 33: 187-215.
239. Raufman JP, Singh L and Eng J (1991) Exendin-3, a novel peptide from *Heloderma horridum* venom, interacts with vasoactive intestinal peptide receptors and a newly described receptor on dispersed acini from guinea pig pancreas. Description of exendin-3(9-39) amide, a specific exendin receptor antagonist. *J Biol Chem* 266: 2897-2902.
240. Kimura H, Ogawa Y, Fujimoto H, et al. (2018) Evaluation of (18)F-labeled exendin(9-39) derivatives targeting glucagon-like peptide-1 receptor for pancreatic beta-cell imaging. *Bioorg Med Chem* 26: 463-469.
241. Ng CM, Tang F, Seeholzer SH, Zou Y and De Leon DD (2018) Population pharmacokinetics of exendin-(9-39) and clinical dose selection in patients with congenital hyperinsulinism. *Br J Clin Pharmacol* 84: 520-532.
242. Craig CM, Liu LF, Deacon CF, Holst JJ and McLaughlin TL (2017) Critical role for GLP-1 in symptomatic post-bariatric hypoglycaemia. *Diabetologia* 60: 531-540.

243. Gault VA, O'Harte FP, Harriott P, Mooney MH, Green BD and Flatt PR (2003) Effects of the novel (Pro3)GIP antagonist and exendin(9-39)amide on GIP- and GLP-1-induced cyclic AMP generation, insulin secretion and postprandial insulin release in obese diabetic (ob/ob) mice: evidence that GIP is the major physiological incretin. *Diabetologia* 46: 222-230.
244. Wheeler MB, Gelling RW, McIntosh CH, Georgiou J, Brown JC and Pederson RA (1995) Functional expression of the rat pancreatic islet glucose-dependent insulinotropic polypeptide receptor: ligand binding and intracellular signaling properties. *Endocrinology* 136: 4629-4639.
245. Jo M and Jung ST (2016) Engineering therapeutic antibodies targeting G-protein-coupled receptors. *Experimental & Molecular Medicine* 48: e207.
246. Bazarsuren A, Grauschof U, Wozny M, et al. (2002) In vitro folding, functional characterization, and disulfide pattern of the extracellular domain of human GLP-1 receptor. *Biophys Chem* 96: 305-318.
247. Smith GP (1985) Filamentous fusion phage: novel expression vectors that display cloned antigens on the virion surface. *Science* 228: 1315-1317.
248. Lloyd C, Lowe D, Edwards B, et al. (2009) Modelling the human immune response: performance of a 1011 human antibody repertoire against a broad panel of therapeutically relevant antigens. *Protein Eng Des Sel* 22: 159-168.
249. McCafferty J, Griffiths AD, Winter G and Chiswell DJ (1990) Phage antibodies: filamentous phage displaying antibody variable domains. *Nature* 348: 552-554.
250. Kabat EA and Wu TT (1991) Identical V region amino acid sequences and segments of sequences in antibodies of different specificities. Relative contributions of VH and VL genes, minigenes, and complementarity-determining regions to binding of antibody-combining sites. *J Immunol* 147: 1709-1719.
251. Barderas R, Desmet J, Timmerman P, Meloen R and Casal JI (2008) Affinity maturation of antibodies assisted by in silico modeling. *Proc Natl Acad Sci U S A* 105: 9029-9034.
252. Lehtonen J, Schaffer L, Rasch MG, Hecksher-Sorensen J and Ahnfelt-Ronne J (2015) Beta cell specific probing with fluorescent exendin-4 is progressively reduced in type 2 diabetic mouse models. *Islets* 7: e1137415.
253. Hennen S, Kodra JT, Soroka V, et al. (2016) Structural insight into antibody-mediated antagonism of the Glucagon-like peptide-1 Receptor. *Sci Rep* 6: 26236.
254. Payne AS, Ishii K, Kacir S, et al. (2005) Genetic and functional characterization of human pemphigus vulgaris monoclonal autoantibodies isolated by phage display. *J Clin Invest* 115: 888-899.

255. Dubel S, Stoevesandt O, Taussig MJ and Hust M (2010) Generating recombinant antibodies to the complete human proteome. *Trends Biotechnol* 28: 333-339.
256. Garet E, Cabado AG, Vieites JM and Gonzalez-Fernandez A (2010) Rapid isolation of single-chain antibodies by phage display technology directed against one of the most potent marine toxins: Palytoxin. *Toxicon* 55: 1519-1526.
257. Griffiths AD, Malmqvist M, Marks JD, et al. (1993) Human anti-self antibodies with high specificity from phage display libraries. *EMBO J* 12: 725-734.
258. Bradbury AR, Sidhu S, Dubel S and McCafferty J (2011) Beyond natural antibodies: the power of in vitro display technologies. *Nat Biotechnol* 29: 245-254.
259. Schier R, Bye J, Apell G, et al. (1996) Isolation of high-affinity monomeric human anti-c-erbB-2 single chain Fv using affinity-driven selection. *J Mol Biol* 255: 28-43.
260. Yang WP, Green K, Pinz-Sweeney S, Briones AT, Burton DR and Barbas CF, 3rd (1995) CDR walking mutagenesis for the affinity maturation of a potent human anti-HIV-1 antibody into the picomolar range. *J Mol Biol* 254: 392-403.
261. Boder ET, Midelfort KS and Wittrup KD (2000) Directed evolution of antibody fragments with monovalent femtomolar antigen-binding affinity. *Proc Natl Acad Sci U S A* 97: 10701-10705.
262. Batista FD and Neuberger MS (1998) Affinity dependence of the B cell response to antigen: a threshold, a ceiling, and the importance of off-rate. *Immunity* 8: 751-759.
263. Hu D, Hu S, Wan W, et al. (2015) Effective Optimization of Antibody Affinity by Phage Display Integrated with High-Throughput DNA Synthesis and Sequencing Technologies. *PLoS One* 10: e0129125.
264. Kang AS, Jones TM and Burton DR (1991) Antibody redesign by chain shuffling from random combinatorial immunoglobulin libraries. *Proc Natl Acad Sci U S A* 88: 11120-11123.
265. Wu H, Beuerlein G, Nie Y, et al. (1998) Stepwise in vitro affinity maturation of Vitaxin, an alphav beta3-specific humanized mAb. *Proc Natl Acad Sci U S A* 95: 6037-6042.
266. Ulrich HD, Patten PA, Yang PL, Romesberg FE and Schultz PG (1995) Expression studies of catalytic antibodies. *Proc Natl Acad Sci U S A* 92: 11907-11911.
267. Deng SJ, MacKenzie CR, Hirama T, et al. (1995) Basis for selection of improved carbohydrate-binding single-chain antibodies from synthetic gene libraries. *Proc Natl Acad Sci U S A* 92: 4992-4996.
268. Boder ET and Wittrup KD (1997) Yeast surface display for screening combinatorial polypeptide libraries. *Nat Biotechnol* 15: 553-557.
269. Cherf GM and Cochran JR (2015) Applications of Yeast Surface Display for Protein Engineering. *Methods Mol Biol* 1319: 155-175.

270. Hanes J, Schaffitzel C, Knappik A and Pluckthun A (2000) Picomolar affinity antibodies from a fully synthetic naive library selected and evolved by ribosome display. *Nat Biotechnol* 18: 1287-1292.
271. Thakkar S, Nanaware-Kharade N, Celikel R, Peterson EC and Varughese KI (2014) Affinity improvement of a therapeutic antibody to methamphetamine and amphetamine through structure-based antibody engineering. *Sci Rep* 4: 3673.
272. Clark LA, Boriack-Sjodin PA, Eldredge J, et al. (2006) Affinity enhancement of an in vivo matured therapeutic antibody using structure-based computational design. *Protein Sci* 15: 949-960.
273. Koole C, Reynolds CA, Mobreec JC, Hick C, Sexton PM and Sakmar TP (2017) Genetically encoded photocross-linkers determine the biological binding site of exendin-4 peptide in the N-terminal domain of the intact human glucagon-like peptide-1 receptor (GLP-1R). *J Biol Chem* 292: 7131-7144.
274. Thorens B (1992) Expression cloning of the pancreatic beta cell receptor for the gluco-incretin hormone glucagon-like peptide 1. *Proc Natl Acad Sci U S A* 89: 8641-8645.
275. Montrose-Rafizadeh C, Avdonin P, Garant MJ, et al. (1999) Pancreatic glucagon-like peptide-1 receptor couples to multiple G proteins and activates mitogen-activated protein kinase pathways in Chinese hamster ovary cells. *Endocrinology* 140: 1132-1140.
276. Litosch I (2016) Decoding Galphaq signaling. *Life Sci* 152: 99-106.
277. Hawes BE, van Biesen T, Koch WJ, Luttrell LM and Lefkowitz RJ (1995) Distinct pathways of Gi- and Gq-mediated mitogen-activated protein kinase activation. *J Biol Chem* 270: 17148-17153.
278. Budd DC, Willars GB, McDonald JE and Tobin AB (2001) Phosphorylation of the Gq/11-coupled m3-muscarinic receptor is involved in receptor activation of the ERK-1/2 mitogen-activated protein kinase pathway. *J Biol Chem* 276: 4581-4587.
279. Thompson A and Kanamarlapudi V (2015) Agonist-induced internalisation of the glucagon-like peptide-1 receptor is mediated by the Galphaq pathway. *Biochem Pharmacol* 93: 72-84.
280. Zhang H, Sturchler E, Zhu J, et al. (2015) Autocrine selection of a GLP-1R G-protein biased agonist with potent antidiabetic effects. *Nat Commun* 6: 8918.
281. Freedman NJ and Lefkowitz RJ (1996) Desensitization of G protein-coupled receptors. *Recent Prog Horm Res* 51: 319-351; discussion 352-313.
282. Luttrell LM, Roudabush FL, Choy EW, et al. (2001) Activation and targeting of extracellular signal-regulated kinases by beta-arrestin scaffolds. *Proc Natl Acad Sci U S A* 98: 2449-2454.

283. Sonoda N, Imamura T, Yoshizaki T, Babendure JL, Lu JC and Olefsky JM (2008) Beta-Arrestin-1 mediates glucagon-like peptide-1 signaling to insulin secretion in cultured pancreatic beta cells. *Proc Natl Acad Sci U S A* 105: 6614-6619.
284. Jorgensen R, Martini L, Schwartz TW and Elling CE (2005) Characterization of glucagon-like peptide-1 receptor beta-arrestin 2 interaction: a high-affinity receptor phenotype. *Mol Endocrinol* 19: 812-823.
285. Quoyer J, Longuet C, Broca C, et al. (2010) GLP-1 mediates antiapoptotic effect by phosphorylating Bad through a beta-arrestin 1-mediated ERK1/2 activation in pancreatic beta-cells. *J Biol Chem* 285: 1989-2002.
286. Jones B, Buenaventura T, Kanda N, et al. (2018) Targeting GLP-1 receptor trafficking to improve agonist efficacy. *Nature Communications* 9: 1602.
287. Dupre J, Behme MT and McDonald TJ (2004) Exendin-4 normalized postcibal glycemic excursions in type 1 diabetes. *J Clin Endocrinol Metab* 89: 3469-3473.
288. Drucker DJ (2018) Mechanisms of Action and Therapeutic Application of Glucagon-like Peptide-1. *Cell Metab* 27: 740-756.
289. Waser B, Blank A, Karamitopoulou E, Perren A and Reubi JC (2015) Glucagon-like-peptide-1 receptor expression in normal and diseased human thyroid and pancreas. *Mod Pathol* 28: 391-402.
290. Skov J (2014) Effects of GLP-1 in the kidney. *Rev Endocr Metab Disord* 15: 197-207.
291. Naylor J, Suckow AT, Seth A, et al. (2016) Use of CRISPR/Cas9-engineered INS-1 pancreatic beta cells to define the pharmacology of dual GIPR/GLP-1R agonists. *Biochem J* 473: 2881-2891.
292. Luche H, Weber O, Nageswara Rao T, Blum C and Fehling HJ (2007) Faithful activation of an extra-bright red fluorescent protein in "knock-in" Cre-reporter mice ideally suited for lineage tracing studies. *Eur J Immunol* 37: 43-53.
293. Zariwala HA, Borghuis BG, Hoogland TM, et al. (2012) A Cre-dependent GCaMP3 reporter mouse for neuronal imaging in vivo. *J Neurosci* 32: 3131-3141.
294. Scrocchi LA, Brown TJ, MaClusky N, et al. (1996) Glucose intolerance but normal satiety in mice with a null mutation in the glucagon-like peptide 1 receptor gene. *Nat Med* 2: 1254-1258.
295. Nikolaev VO, Bunemann M, Hein L, Hannawacker A and Lohse MJ (2004) Novel single chain cAMP sensors for receptor-induced signal propagation. *J Biol Chem* 279: 37215-37218.
296. Kuhre RE, Wewer Albrechtsen NJ, Hartmann B, Deacon CF and Holst JJ (2015) Measurement of the incretin hormones: glucagon-like peptide-1 and glucose-dependent insulinotropic peptide. *J Diabetes Complications* 29: 445-450.

297. Hohmeier HE, Mulder H, Chen G, Henkel-Rieger R, Prentki M and Newgard CB (2000) Isolation of INS-1-derived cell lines with robust ATP-sensitive K⁺ channel-dependent and -independent glucose-stimulated insulin secretion. *Diabetes* 49: 424-430.
298. Asfari M, Janjic D, Meda P, Li G, Halban PA and Wollheim CB (1992) Establishment of 2-mercaptoethanol-dependent differentiated insulin-secreting cell lines. *Endocrinology* 130: 167-178.
299. Marchetti P, Lupi R, Bugliani M, et al. (2012) A local glucagon-like peptide 1 (GLP-1) system in human pancreatic islets. *Diabetologia* 55: 3262-3272.
300. Piro S, Mascali LG, Urbano F, et al. (2014) Chronic exposure to GLP-1 increases GLP-1 synthesis and release in a pancreatic alpha cell line (alpha-TC1): evidence of a direct effect of GLP-1 on pancreatic alpha cells. *PLoS One* 9: e90093.
301. Hughes P, Marshall D, Reid Y, Parkes H and Gelber C (2007) The costs of using unauthenticated, over-passaged cell lines: how much more data do we need? *Biotechniques* 43: 575, 577-578, 581-572 *passim*.
302. Heppner KM, Kirigiti M, Secher A, et al. (2015) Expression and distribution of glucagon-like peptide-1 receptor mRNA, protein and binding in the male nonhuman primate (*Macaca mulatta*) brain. *Endocrinology* 156: 255-267.
303. Liu L, Stadheim A, Hamuro L, et al. (2011) Pharmacokinetics of IgG1 monoclonal antibodies produced in humanized *Pichia pastoris* with specific glycoforms: a comparative study with CHO produced materials. *Biologicals* 39: 205-210.
304. Pamir N, Lynn FC, Buchan AM, et al. (2003) Glucose-dependent insulinotropic polypeptide receptor null mice exhibit compensatory changes in the enteroinsular axis. *Am J Physiol Endocrinol Metab* 284: E931-939.
305. Preitner F, Ibberson M, Franklin I, et al. (2004) Gluco-incretins control insulin secretion at multiple levels as revealed in mice lacking GLP-1 and GIP receptors. *J Clin Invest* 113: 635-645.
306. Biggs EK, Gribble FM and Reimann F (2017) Scaling it down: new in vitro tools to get the balance right. *Biochem J* 474: 47-50.
307. Dirksen C, Jorgensen NB, Bojsen-Moller KN, et al. (2012) Mechanisms of improved glycaemic control after Roux-en-Y gastric bypass. *Diabetologia* 55: 1890-1901.
308. Rhee NA, Vilsboll T and Knop FK (2012) Current evidence for a role of GLP-1 in Roux-en-Y gastric bypass-induced remission of type 2 diabetes. *Diabetes Obes Metab* 14: 291-298.
309. Knop FK (2009) Resolution of type 2 diabetes following gastric bypass surgery: involvement of gut-derived glucagon and glucagonotropic signalling? *Diabetologia* 52: 2270-2276.

310. Ye J, Hao Z, Mumphrey MB, et al. (2014) GLP-1 receptor signaling is not required for reduced body weight after RYGB in rodents. *Am J Physiol Regul Integr Comp Physiol* 306: R352-362.
311. Salehi M, Prigeon RL and D'Alessio DA (2011) Gastric bypass surgery enhances glucagon-like peptide 1-stimulated postprandial insulin secretion in humans. *Diabetes* 60: 2308-2314.
312. Mine S, Sano T, Tsutsumi K, et al. (2010) Large-scale investigation into dumping syndrome after gastrectomy for gastric cancer. *J Am Coll Surg* 211: 628-636.
313. Roberts GP, Kay RG, Howard J, Hardwick RH, Reimann F and Gribble FM (2018) Gastrectomy with Roux-en-Y reconstruction as a lean model of bariatric surgery. *Surg Obes Relat Dis*
314. Salehi M, Gastaldelli A and D'Alessio DA (2014) Blockade of glucagon-like peptide 1 receptor corrects postprandial hypoglycemia after gastric bypass. *Gastroenterology* 146: 669-680 e662.
315. Lord K and De Leon DD (2013) Monogenic hyperinsulinemic hypoglycemia: current insights into the pathogenesis and management. *Int J Pediatr Endocrinol* 2013: 3.
316. De Leon DD, Li C, Delson MI, Matschinsky FM, Stanley CA and Stoffers DA (2008) Exendin-(9-39) corrects fasting hypoglycemia in SUR-1-/ mice by lowering cAMP in pancreatic beta-cells and inhibiting insulin secretion. *J Biol Chem* 283: 25786-25793.
317. Calabria AC, Li C, Gallagher PR, Stanley CA and De Leon DD (2012) GLP-1 receptor antagonist exendin-(9-39) elevates fasting blood glucose levels in congenital hyperinsulinism owing to inactivating mutations in the ATP-sensitive K⁺ channel. *Diabetes* 61: 2585-2591.
318. Nauck MA, Heimesaat MM, Orskov C, Holst JJ, Ebert R and Creutzfeldt W (1993) Preserved incretin activity of glucagon-like peptide 1 [7-36 amide] but not of synthetic human gastric inhibitory polypeptide in patients with type-2 diabetes mellitus. *J Clin Invest* 91: 301-307.
319. Meier JJ, Gallwitz B, Siepmann N, et al. (2003) Gastric inhibitory polypeptide (GIP) dose-dependently stimulates glucagon secretion in healthy human subjects at euglycaemia. *Diabetologia* 46: 798-801.
320. Christensen M, Calanna S, Sparre-Ulrich AH, et al. (2015) Glucose-dependent insulinotropic polypeptide augments glucagon responses to hypoglycemia in type 1 diabetes. *Diabetes* 64: 72-78.
321. Gasbjerg LS, Christensen MB, Hartmann B, et al. (2018) GIP(3-30)NH₂ is an efficacious GIP receptor antagonist in humans: a randomised, double-blinded, placebo-controlled, crossover study. *Diabetologia* 61: 413-423.
322. Asmar M, Asmar A, Simonsen L, et al. (2017) The Gluco- and Liporegulatory and Vasodilatory Effects of Glucose-Dependent Insulinotropic Polypeptide (GIP) Are Abolished by an Antagonist of the Human GIP Receptor. *Diabetes* 66: 2363-2371.

323. Brøns C, Jensen CB, Storgaard H, et al. (2009) Impact of short-term high-fat feeding on glucose and insulin metabolism in young healthy men. *The Journal of Physiology* 587: 2387-2397.
324. Falko JM, Crockett SE, Cataland S and Mazzaferri EL (1975) Gastric inhibitory polypeptide (GIP) stimulated by fat ingestion in man. *J Clin Endocrinol Metab* 41: 260-265.
325. Flatt PR, Bailey CJ, Kwasowski P, Swanston-Flatt SK and Marks V (1983) Abnormalities of GIP in spontaneous syndromes of obesity and diabetes in mice. *Diabetes* 32: 433-435.
326. Creutzfeldt W, Ebert R, Willms B, Frerichs H and Brown JC (1978) Gastric inhibitory polypeptide (GIP) and insulin in obesity: Increased response to stimulation and defective feedback control of serum levels. *Diabetologia* 14: 15-24.
327. Bailey CJ, Flatt PR, Kwasowski P, Powell CJ and Marks V (1986) Immunoreactive gastric inhibitory polypeptide and K cell hyperplasia in obese hyperglycaemic (ob/ob) mice fed high fat and high carbohydrate cafeteria diets. *Acta Endocrinol (Copenh)* 112: 224-229.
328. Møller CL, Vistisen D, Færch K, et al. (2016) Glucose-Dependent Insulinotropic Polypeptide Is Associated With Lower Low-Density Lipoprotein But Unhealthy Fat Distribution, Independent of Insulin: The ADDITION-PRO Study. *The Journal of Clinical Endocrinology & Metabolism* 101: 485-493.
329. Harada N, Yamada Y, Tsukiyama K, et al. (2008) A novel GIP receptor splice variant influences GIP sensitivity of pancreatic beta-cells in obese mice. *Am J Physiol Endocrinol Metab* 294: E61-68.
330. Halaas JL, Gajiwala KS, Maffei M, et al. (1995) Weight-reducing effects of the plasma protein encoded by the ob gene. *Science* 269: 543-546.
331. Ambati S, Duan J, Hartzell DL, Choi YH, Della-Fera MA and Baile CA (2011) GIP-dependent expression of hypothalamic genes. *Physiol Res* 60: 941-950.
332. NamKoong C, Kim MS, Jang BT, Lee YH, Cho YM and Choi HJ (2017) Central administration of GLP-1 and GIP decreases feeding in mice. *Biochem Biophys Res Commun* 490: 247-252.
333. Blouet C, Jo YH, Li X and Schwartz GJ (2009) Mediobasal hypothalamic leucine sensing regulates food intake through activation of a hypothalamus-brainstem circuit. *J Neurosci* 29: 8302-8311.
334. Pinchuk IV, Mifflin RC, Saada JI and Powell DW (2010) Intestinal mesenchymal cells. *Curr Gastroenterol Rep* 12: 310-318.
335. Powell DW, Pinchuk IV, Saada JI, Chen X and Mifflin RC (2011) Mesenchymal cells of the intestinal lamina propria. *Annu Rev Physiol* 73: 213-237.
336. Waterson MJ and Horvath TL (2015) Neuronal Regulation of Energy Homeostasis: Beyond the Hypothalamus and Feeding. *Cell Metab* 22: 962-970.

337. Svendsen B, Pais R, Engelstoft MS, et al. (2016) GLP1- and GIP-producing cells rarely overlap and differ by bombesin receptor-2 expression and responsiveness. *J Endocrinol* 228: 39-48.
338. Gray DC, Mahrus S and Wells JA (2010) Activation of specific apoptotic caspases with an engineered small-molecule-activated protease. *Cell* 142: 637-646.
339. Atasoy D, Aponte Y, Su HH and Sternson SM (2008) A FLEX switch targets Channelrhodopsin-2 to multiple cell types for imaging and long-range circuit mapping. *J Neurosci* 28: 7025-7030.
340. Yang CF, Chiang MC, Gray DC, et al. (2013) Sexually dimorphic neurons in the ventromedial hypothalamus govern mating in both sexes and aggression in males. *Cell* 153: 896-909.
341. Armbruster BN, Li X, Pausch MH, Herlitze S and Roth BL (2007) Evolving the lock to fit the key to create a family of G protein-coupled receptors potently activated by an inert ligand. *Proc Natl Acad Sci U S A* 104: 5163-5168.
342. Krashes MJ, Koda S, Ye C, et al. (2011) Rapid, reversible activation of AgRP neurons drives feeding behavior in mice. *J Clin Invest* 121: 1424-1428.
343. Ferguson SM, Eskenazi D, Ishikawa M, et al. (2011) Transient neuronal inhibition reveals opposing roles of indirect and direct pathways in sensitization. *Nat Neurosci* 14: 22-24.
344. Alexander GM, Rogan SC, Abbas AI, et al. (2009) Remote control of neuronal activity in transgenic mice expressing evolved G protein-coupled receptors. *Neuron* 63: 27-39.
345. Ollmann MM, Wilson BD, Yang Y-K, et al. (1997) Antagonism of Central Melanocortin Receptors in Vitro and in Vivo by Agouti-Related Protein. *Science* 278: 135-138.
346. DiGruccio MR, Mawla AM, Donaldson CJ, et al. (2016) Comprehensive alpha, beta and delta cell transcriptomes reveal that ghrelin selectively activates delta cells and promotes somatostatin release from pancreatic islets. *Mol Metab* 5: 449-458.
347. Sjodin L and Conlon TP (1984) Effects of gastric inhibitory polypeptide on dispersed pancreatic acinar cells from the guinea pig. *Acta Physiol Scand* 122: 79-84.
348. Duan RD and Erlanson-Albertsson C (1992) Gastric inhibitory polypeptide stimulates pancreatic lipase and colipase synthesis in rats. *Am J Physiol* 262: G779-784.
349. Jeraldo TL, Coutu JA, Verdier PA, McMillan PN and Adelson JW (1996) Fundamental cellular heterogeneity of the exocrine pancreas. *J Histochem Cytochem* 44: 215-220.
350. Bendayan M, Roth J, Perrelet A and Orci L (1980) Quantitative immunocytochemical localization of pancreatic secretory proteins in subcellular compartments of the rat acinar cell. *J Histochem Cytochem* 28: 149-160.
351. Song DH, Getty-Kaushik L, Tseng E, Simon J, Corkey BE and Wolfe MM (2007) Glucose-dependent insulinotropic polypeptide enhances adipocyte development and glucose uptake in part through Akt activation. *Gastroenterology* 133: 1796-1805.

352. Makowski L, Boord JB, Maeda K, et al. (2001) Lack of macrophage fatty-acid-binding protein aP2 protects mice deficient in apolipoprotein E against atherosclerosis. *Nat Med* 7: 699-705.
353. Lee KY, Russell SJ, Ussar S, et al. (2013) Lessons on conditional gene targeting in mouse adipose tissue. *Diabetes* 62: 864-874.
354. Ugleholdt R, Pedersen J, Bassi MR, et al. (2011) Transgenic rescue of adipocyte glucose-dependent insulinotropic polypeptide receptor expression restores high fat diet-induced body weight gain. *J Biol Chem* 286: 44632-44645.
355. Lund ML, Egerod KL, Engelstoft MS, et al. (2018) Enterochromaffin 5-HT cells - A major target for GLP-1 and gut microbial metabolites. *Mol Metab* 11: 70-83.
356. De Clerck F, Somers Y and Van Gorp L (1984) Platelet-vessel wall interactions in hemostasis: implication of 5-hydroxytryptamine. *Agents Actions* 15: 627-635.
357. Reigstad CS, Salmonson CE, Rainey JF, 3rd, et al. (2015) Gut microbes promote colonic serotonin production through an effect of short-chain fatty acids on enterochromaffin cells. *FASEB J* 29: 1395-1403.
358. Yano JM, Yu K, Donaldson GP, et al. (2015) Indigenous bacteria from the gut microbiota regulate host serotonin biosynthesis. *Cell* 161: 264-276.
359. Merchenthaler I, Lane M and Shughrue P (1999) Distribution of pre-pro-glucagon and glucagon-like peptide-1 receptor messenger RNAs in the rat central nervous system. *J Comp Neurol* 403: 261-280.
360. Polex-Wolf J, Lam BY, Larder R, et al. (2018) Hypothalamic loss of Snord116 recapitulates the hyperphagia of Prader-Willi syndrome. *J Clin Invest* 128: 960-969.
361. Morgan JI and Curran T (1986) Role of ion flux in the control of c-fos expression. *Nature* 322: 552-555.
362. Sofroniew MV and Vinters HV (2010) Astrocytes: biology and pathology. *Acta Neuropathol* 119: 7-35.
363. Weihe E, Depboylu C, Schutz B, Schafer MK and Eiden LE (2006) Three types of tyrosine hydroxylase-positive CNS neurons distinguished by dopa decarboxylase and VMAT2 co-expression. *Cell Mol Neurobiol* 26: 659-678.
364. Mascagni F, Muly EC, Rainnie DG and McDonald AJ (2009) Immunohistochemical characterization of parvalbumin-containing interneurons in the monkey basolateral amygdala. *Neuroscience* 158: 1541-1550.
365. Lam BYH, Cimino I, Polex-Wolf J, et al. (2017) Heterogeneity of hypothalamic pro-opiomelanocortin-expressing neurons revealed by single-cell RNA sequencing. *Mol Metab* 6: 383-392.

366. Zeng W-B, Jiang H-F, Gang Y-D, et al. (2017) Anterograde monosynaptic transneuronal tracers derived from herpes simplex virus 1 strain H129. *Molecular Neurodegeneration* 12: 38.
367. Pomeranz LE, Ekstrand MI, Latcha KN, Smith GA, Enquist LW and Friedman JM (2017) Gene Expression Profiling with Cre-Conditional Pseudorabies Virus Reveals a Subset of Midbrain Neurons That Participate in Reward Circuitry. *J Neurosci* 37: 4128-4144.
368. Pickard GE, Smeraski CA, Tomlinson CC, et al. (2002) Intravitreal injection of the attenuated pseudorabies virus PRV Bartha results in infection of the hamster suprachiasmatic nucleus only by retrograde transsynaptic transport via autonomic circuits. *J Neurosci* 22: 2701-2710.
369. Halldorsdottir S, Carmody J, Boozer CN, Leduc CA and Leibel RL (2009) Reproducibility and accuracy of body composition assessments in mice by dual energy x-ray absorptiometry and time domain nuclear magnetic resonance. *Int J Body Compos Res* 7: 147-154.
370. Ahrén B, Baldwin RM and Havel PJ (2000) Pharmacokinetics of human leptin in mice and rhesus monkeys. *International Journal Of Obesity* 24: 1579.
371. Yan J, Mei FC, Cheng H, et al. (2013) Enhanced leptin sensitivity, reduced adiposity, and improved glucose homeostasis in mice lacking exchange protein directly activated by cyclic AMP isoform 1. *Mol Cell Biol* 33: 918-926.
372. Gaykema RP, Newmyer BA, Ottolini M, et al. (2017) Activation of murine pre-proglucagon-producing neurons reduces food intake and body weight. *J Clin Invest* 127: 1031-1045.
373. Jann MW, Lam YW and Chang WH (1994) Rapid formation of clozapine in guinea-pigs and man following clozapine-N-oxide administration. *Arch Int Pharmacodyn Ther* 328: 243-250.
374. MacLaren DAA, Browne RW, Shaw JK, et al. (2016) Clozapine N-Oxide Administration Produces Behavioral Effects in Long-Evans Rats: Implications for Designing DREADD Experiments. *eneuro* 3:
375. Cremers TI, Flik G, Hofland C and Stratford RE, Jr. (2012) Microdialysis evaluation of clozapine and N-desmethylclozapine pharmacokinetics in rat brain. *Drug Metab Dispos* 40: 1909-1916.
376. Gomez JL, Bonaventura J, Lesniak W, et al. (2017) Chemogenetics revealed: DREADD occupancy and activation via converted clozapine. *Science* 357: 503-507.
377. Selent J, Lopez L, Sanz F and Pastor M (2008) Multi-receptor binding profile of clozapine and olanzapine: a structural study based on the new beta2 adrenergic receptor template. *ChemMedChem* 3: 1194-1198.
378. Mahler SV and Aston-Jones G (2018) CNO Evil? Considerations for the Use of DREADDs in Behavioral Neuroscience. *Neuropsychopharmacology* 43: 934.

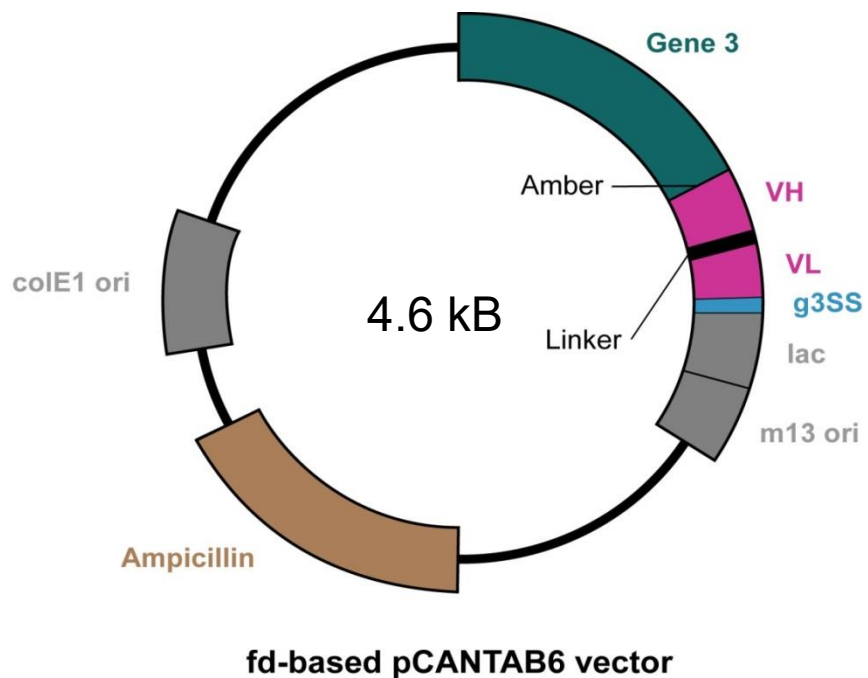
379. Kim SJ, Nian C, Karunakaran S, Clee SM, Isales CM and McIntosh CH (2012) GIP-overexpressing mice demonstrate reduced diet-induced obesity and steatosis, and improved glucose homeostasis. *PLoS One* 7: e40156.
380. Maekawa R, Ogata H, Murase M, et al. (2018) Glucose-dependent insulinotropic polypeptide is required for moderate high fat diet, but not high carbohydrate diet-induced weight gain. *Am J Physiol Endocrinol Metab*
381. Crenn P, Coudray-Lucas C, Thuillier F, Cynober L and Messing B (2000) Postabsorptive plasma citrulline concentration is a marker of absorptive enterocyte mass and intestinal failure in humans. *Gastroenterology* 119: 1496-1505.
382. Almgren P, Lindqvist A, Krus U, et al. (2017) Genetic determinants of circulating GIP and GLP-1 concentrations. *JCI Insight* 2:
383. Scott RA, Scott LJ, Magi R, et al. (2017) An Expanded Genome-Wide Association Study of Type 2 Diabetes in Europeans. *Diabetes* 66: 2888-2902.
384. Drucker DJ (2001) Minireview: The Glucagon-Like Peptides. *Endocrinology* 142: 521-527.
385. Jeppesen PB (2012) Teduglutide, a novel glucagon-like peptide 2 analog, in the treatment of patients with short bowel syndrome. *Therapeutic Advances in Gastroenterology* 5: 159-171.
386. Jeppesen PB, Pertkiewicz M, Messing B, et al. (2012) Teduglutide Reduces Need for Parenteral Support Among Patients With Short Bowel Syndrome With Intestinal Failure. *Gastroenterology* 143: 1473-1481.e1473.
387. Ukleja A, To C, Alvarez A and Lara LF (2018) Long-Term Therapy With Teduglutide in Parenteral Support-Dependent Patients With Short Bowel Syndrome: A Case Series. *JPEN J Parenter Enteral Nutr*
388. Buchman AL, Katz S, Fang JC, Bernstein CN, Abou-Assi SG and Teduglutide Study G (2010) Teduglutide, a novel mucosally active analog of glucagon-like peptide-2 (GLP-2) for the treatment of moderate to severe Crohn's disease. *Inflamm Bowel Dis* 16: 962-973.
389. Kocher B, Long MD, Shelton E, et al. (2017) Safety and Efficacy of Teduglutide (Gattex) in Patients With Crohn's Disease and Need for Parenteral Support Due to Short Bowel Syndrome-associated Intestinal Failure. *J Clin Gastroenterol* 51: 508-511.
390. Baldassano S, Rappa F, Amato A, Cappello F and Mule F (2015) GLP-2 as Beneficial Factor in the Glucose Homeostasis in Mice Fed a High Fat Diet. *J Cell Physiol* 230: 3029-3036.
391. Baldassano S, Amato A, Caldara GF and Mule F (2016) Glucagon-like peptide-2 treatment improves glucose dysmetabolism in mice fed a high-fat diet. *Endocrine* 54: 648-656.
392. Wismann P, Pedersen SL, Hansen G, et al. (2018) Novel GLP-1/GLP-2 co-agonists display marked effects on gut volume and improves glycemic control in mice. *Physiol Behav*

393. Ferguson SSG (2001) Evolving Concepts in G Protein-Coupled Receptor Endocytosis: The Role in Receptor Desensitization and Signaling. *Pharmacological Reviews* 53: 1-24.
394. Mebratu Y and Tesfaigzi Y (2009) How ERK1/2 activation controls cell proliferation and cell death: Is subcellular localization the answer? *Cell Cycle* 8: 1168-1175.
395. Estall JL, Yusta B and Drucker DJ (2004) Lipid Raft-dependent Glucagon-like Peptide-2 Receptor Trafficking Occurs Independently of Agonist-induced Desensitization. *Molecular Biology of the Cell* 15: 3673-3687.
396. Dubé PE, Rowland KJ and Brubaker PL (2008) Glucagon-Like Peptide-2 Activates β -Catenin Signaling in the Mouse Intestinal Crypt: Role of Insulin-Like Growth Factor-I. *Endocrinology* 149: 291-301.
397. Fava GE, Dong EW and Wu H (2016) Intra-islet glucagon-like peptide 1. *J Diabetes Complications* 30: 1651-1658.
398. Pederson RA, Satkunarajah M, McIntosh CH, et al. (1998) Enhanced glucose-dependent insulinotropic polypeptide secretion and insulinotropic action in glucagon-like peptide 1 receptor -/- mice. *Diabetes* 47: 1046-1052.
399. Reimann F, Habib AM, Tolhurst G, Parker HE, Rogers GJ and Gribble FM (2008) Glucose sensing in L cells: a primary cell study. *Cell Metab* 8: 532-539.
400. Psichas A, Glass LL, Sharp SJ, Reimann F and Gribble FM (2016) Galanin inhibits GLP-1 and GIP secretion via the GAL1 receptor in enteroendocrine L and K cells. *Br J Pharmacol* 173: 888-898.
401. Emery EC, Diakogiannaki E, Gentry C, et al. (2015) Stimulation of GLP-1 secretion downstream of the ligand-gated ion channel TRPA1. *Diabetes* 64: 1202-1210.
402. Seino Y and Yabe D (2013) Glucose-dependent insulinotropic polypeptide and glucagon-like peptide-1: Incretin actions beyond the pancreas. *J Diabetes Investig* 4: 108-130.
403. Heeley N, Kirwan P, Darwish T, et al. (2018) Rapid sensing of l-leucine by human and murine hypothalamic neurons: Neurochemical and mechanistic insights. *Mol Metab* 10: 14-27.
404. Humpel C (2015) Organotypic brain slice cultures: A review. *Neuroscience* 305: 86-98.
405. Holt MK, Llewellyn-Smith IJ, Reimann F, Gribble FM and Trapp S (2017) Serotonergic modulation of the activity of GLP-1 producing neurons in the nucleus of the solitary tract in mouse. *Mol Metab* 6: 909-921.
406. Feil R, Wagner J, Metzger D and Chambon P (1997) Regulation of Cre recombinase activity by mutated estrogen receptor ligand-binding domains. *Biochem Biophys Res Commun* 237: 752-757.
407. Gossen M, Freundlieb S, Bender G, Muller G, Hillen W and Bujard H (1995) Transcriptional activation by tetracyclines in mammalian cells. *Science* 268: 1766-1769.

408. Amato A, Baldassano S and Mulè F (2016) GLP2: an underestimated signal for improving glycaemic control and insulin sensitivity. *Journal of Endocrinology* 229: R57-R66.

8. Appendix

Appendix 1 – Plasmid Map for pCantab6



Appendix 2– Primer Details

Primers for V fragment cloning into IgG expression vectors	
AF16 (for V _H)	CTCTCCACAGGC GCGCACTCCGAGGTGCAGCTGGTGCAG
RH100 (for V _H)	CGAGACGGTGACCGTGGTCCC
AF31 (for V _L)	CTCTCCACAGGC GTGCACTCCCAGTCTGTGCTGACTCAGCC
AF26 (for V _L)	CTATTCCCTAATTAAGTTAGATCTATTCTGACTCACCTAGGACG GTGACCTTGGTCCCTCC
GLP2R Cloning Primers	
GLP2R_IRESVenus_GibsonF	GGAAGAGAGTGAGATCTAGCGCTGCTAGCCACCGTAC
GLP2R_IRESVenus_GibsonR	GGGTTAAACGGGCCCTCTAGTTACTTGTACAGCTC
GLP2R_D470N_SDM_F	TGTGT CCTGGGG AAGAAC TCCGGT CCTAG
GLP2R_D470N_SDM_R	CTAGGAACCGGAAGTTCTCCCCAGGACACA
GLP2R_Barr_Xho1_Rev	CACCGCTCGAGGCGATCTCACTCTTCCAG
GLP2R Sequencing Primers	
pcDNA3.1+_1_F	GACGGATCGGGAGATCTCCC
pcDNA3.1+_2_F	GTTCCC ATAGTAACGCCAATAGGG
GLP2R_1_F	GGCTCAGTACAAACAGGCATGTC
GLP2R_2_F	CGCGCAACTACATCCACATGAAC
GLP2R_3_F	GAGGACCCATGATGCTCTGT
GLP2R_4_F	GAAGGCTGAGCTCGGAAATAC
IRES_1_F	gcggctagtactccggattgc
IRES_2_F	ggctgcttatggtgacaat
Venus_1_F	ggcatcaaggccaacctcaag
pcDNA3.1+_3	GCATCGCATTGTCTGAGTAGGTG
pcDNA3.1+_4	CGCCCTGATAGACGGTTTCG
pcDNA3.1+_5	GTCAGCAACCATA GTCCC GC
pcDNA3.1+_6	CAGCTGTGCTCGACGTTGTAC
pcDNA3.1+_7	GGCCGCTTTCTGGATT CATC
pcDNA3.1+_8	GGGATCTCATGCTGGAGTTCTC
pcDNA3.1+_9	CGCAGGAAAGAACATGTGAGC
pcDNA3.1+_10	GCGCCTTATCCGGTA ACTATCG
pcDNA3.1+_11	GTGAGGCACCTATCTCAGCGATC
pcDNA3.1+_12	CTGAGAATAGTGTATCGGGCGAC

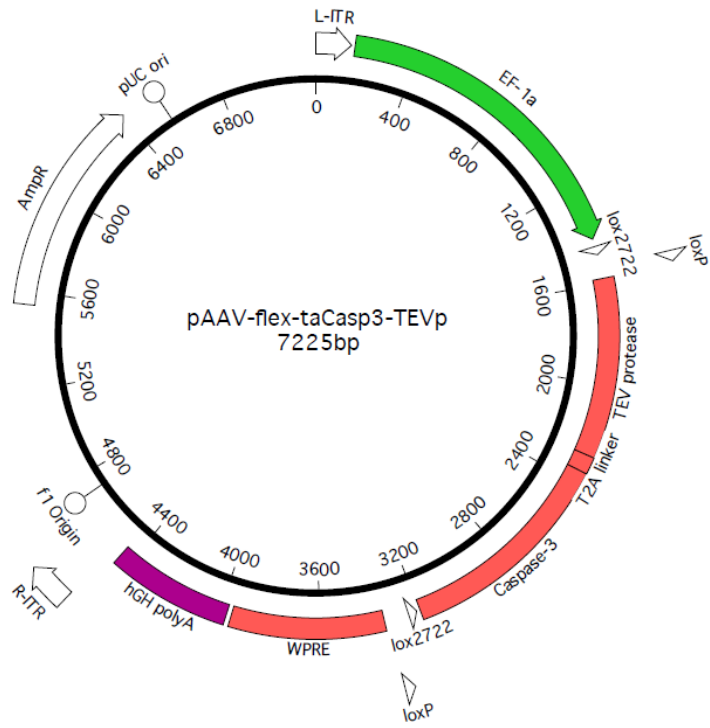
Appendix 3 – Cell Seeding Densities for cAMP HTRF Assay

Cell Line	Plating density (cells/ml)	Plating density (cells/well)
Mouse GLP1R (CHO mGLP1 clone A10)	8e ⁵	4000
Human GLP1R (CHO K1 3xVIP c2.6GLP-1)	2e ⁵	1000
Rat GLP1R (CHO/Flp In rat GLP1)	16e ⁵	8000
Cyno GLP1R (CHO Jump In cyno GLP-1R)	2e ⁵	1000
Dog GLP1R (CHO dog GLP1 clone B9)	8e ⁵	4000
Mouse GIPR (HEK 293s mouse GIPR)	3e ⁵	1500
Human GIPR (CHO K1 hGIPR low expressing pool C3)	4e ⁵	2000
Human GLP2R (HEK293s pcDNA3 hGLP2R cB12)	3e ⁵	1500
Mouse GCGR (CHO K1 Jump In mGR 5:1)	8e ⁵	4000
Human GCGR (CHO K1 3xVIP c2.6 hGR C12)	1e ⁵	500
Rat GCGR (CHO K1 2.6 RGR C8)	4e ⁵	2000

Appendix 4 – Antibody Details

	Dilution	Source
dsRed	1/1,000 – 1/500	Clontech, #632496
GFP	1/1,000	Abcam #5450
Insulin	1/100	Abcam, #7842
Proglucagon	1/100	Santa Cruz, #sc-7782
Serotonin (5-HT)	1/10,000	Immunostar, #20080
Vimentin	1/200	Abcam, #92547
Phospho-p44/42 MAPK (Erk1/2) (Thr202/Tyr204)	1/1,000 – 1/500	Cell Signalling, #9101
p44/42 MAPK (Erk1/2) (137F5)	1/1,000	Cell Signalling, #4695
B-actin	1/10,000	Abcam, #8227

Appendix 5 – AAV-flex-taCasp3-TEVp plasmid map



Appendix 6 – AAV-hSyn-DIO-hM3D(Gq)-mCherry plasmid map

